

0 1 2 4 3 3 3 0

**LA-UR-93-866**

Issued: March 1993

**Proceedings of the  
Muon Collider Workshop**

**February 22, 1993  
LAMPF Auditorium**

**Los Alamos**

**Los Alamos National Laboratory  
Los Alamos, New Mexico 87545**

*This work was supported by the U.S. Department of Energy, Office of Energy Research.*

*These papers are printed as submitted by the authors.*

*An Affirmative Action/Equal Opportunity Employer*

*This report was prepared as an account of work sponsored by an agency of the United States Government. Neither the United States Government nor any agency thereof, nor any of their employees, makes any warranty, express or implied, or assumes any legal liability or responsibility for the accuracy, completeness, or usefulness of any information, apparatus, product, or process disclosed, or represents that its use would not infringe privately owned rights. Reference herein to any specific commercial product, process, or service by trade name, trademark, manufacturer, or otherwise, does not necessarily constitute or imply its endorsement, recommendation, or favoring by the United States Government or any agency thereof. The views and opinions of authors expressed herein do not necessarily state or reflect those of the United States Government or any agency thereof.*

# MUON COLLIDER WORKSHOP

22 February 1993  
LAMPF Auditorium

## CONTENTS

<b>Attendees.....</b>	<b>1</b>
<b>Agenda.....</b>	<b>3</b>
<b>Physics of <math>\mu^+\mu^-</math> Collider.....</b> David Cline, UCLA	<b>5</b>
<b>Muon Collider - Possibilities &amp; Challenges.....</b> David Neuffer, CEBAF	<b>27</b>
<b>Summary of NAPA Workshop &amp;.....</b> <b>Electrons as Source of Muons</b> William Barletta, UCLA	<b>73</b>
<b>Comments on 2-GeV Protons.....</b> Henry A. Thiessen, LANL	<b>115</b>
<b>2-GeV Protons as Source of Muons.....</b> James Langenbrunner, University of Minnesota	<b>117</b>
<b>Combined Ionization and Stochastic Cooling.....</b> Alessandro Ruggiero	<b>131</b>
<b>Proton Storage Ring with Intensity Greater than.....</b> <b>Space Charge Limit</b> Vadim Dudnikov, BINP	<b>141</b>
<b>Muon Collider Work at Novosibirsk.....</b> Gregory Silvestrov, BINP	<b>163</b>
<b>Comments on Polarized Muons.....</b> Henry A. Thiessen, LANL	<b>243</b>
<b>Muon Source.....</b> Mikhail Grachev, INR	<b>245</b>

# MUON COLLIDER WORKSHOP

22 February 1993  
LAMPF Auditorium

## Attendees

William Bartetta  
Lawrence Berkeley  
Laboratory  
One Cyclotron Road  
Berkeley, CA 94720  
(510) 486-5048

T. S. Bhatia  
USDOE  
ER-224  
Germantown  
Washington, DC 20585  
(301) 903-5228

Paul Channell  
Los Alamos National  
Laboratory  
AT-7, MS H829  
Los Alamos, NM 87545  
(505) 665-0955

David Cline  
UCLA  
Department of Physics  
405 Hilgard Ave.  
Los Angeles, CA 90024-1547  
(310) 825-1673

Vadim Dudnikov  
Budker Inst. of Nuclear  
Physics  
Russia Academia of Sciences  
Siberian Branch  
Novosibirsk, Russia  
7-3832-35-7268

Mikhail Grachev  
Institute of Nuclear Research  
60th October Anniversary  
Prospect 7A  
Moscow 117312, Russia  
7-095-334-0186

Cy Hoffman  
Los Alamos National  
Laboratory  
MP-DO, MS H844  
Los Alamos, NM 87545  
(505) 667-5876

Robert Jameson  
Los Alamos National  
Laboratory  
AT-DO, MS H811  
Los Alamos, NM 87545  
(505) 665-2275

Glen R. Lambertson  
Lawrence Berkeley  
Laboratory  
One Cyclotron Road  
MS 71-259  
Berkeley, CA 94720  
(510) 486-7205

James Langenbrunner  
University of Minnesota  
1024 Osage Circle  
Santa Fe, NM 87501  
(505) 982-3943

David Neuffer  
CEBAF  
MS 12-A2  
12000 Jefferson Ave  
Newport News, VA 23612  
(804) 249-7613

Alessandro Ruggiero  
Brookhaven National  
Laboratory  
Building 1005-S  
Upton, NY 11973  
(516) 282-4997

Stan Schriber  
Los Alamos National  
Laboratory  
AT-DO, MS H811  
Los Alamos, NM 87545  
(505) 667-5634

Gregory Silvestrov  
Budker Inst. of Nuclear  
Physics  
Russia Academia of Sciences  
Siberian Branch  
Novosibirsk, Russia  
7-3832-35-7268

George Swain  
Los Alamos National  
Laboratory  
MP-14, MS H847  
Los Alamos, NM 87545  
(505) 667-4433

H. Arch Thiessen  
Los Alamos National  
Laboratory  
MP-14, MS H847  
Los Alamos, NM 87545  
(505) 667-8991

Tai-Sen Wang  
Los Alamos National  
Laboratory  
AT-7, MS H825  
Los Alamos, NM 87545  
(505) 667-3183

John Zumbro  
Los Alamos National  
Laboratory  
MP-14, MS H847  
Los Alamos, NM 87545  
(505) 665-1009

**MUON COLLIDER WORKSHOP**

**22 February 1993  
LAMPF Auditorium**

**AGENDA**

9:30	David Cline	Physics of $\mu^+\mu^-$ Collider
10:30	COFFEE	
10:45	David Neuffer	Muon Collider - Possibilities & Challenges
11:45	William Barletta	Summary of Napa Workshop
12:30	LUNCH	
1:30	William Barletta	Electrons as Source of Muons
1:55	Henry A.Thiessen	Comments on 2 GeV Protons
2:00	James Langenbrunner	2 GeV Protons as Source of Muons
2:15	Alessandro Ruggiero	Combined Ionization and Stochastic Cooling
3:00	COFFEE	
3:30	Vadim Dudnikov	Proton Storage Ring with Intensity Greater than Space Charge Limit
4:00	Gregory Silvestrov	Muon Collider Work at Novosibirsk
4:25	Henry A. Thiessen	Comments on Polarized Muons
4:30	Mikhail Grachev	Muon Source
5:00	Group Discussion	

0 1 2 4 0 3 7 5

**Physics of  $\mu^+\mu^-$  Collider**

**David Cline**

**UCLA**

# $\mu\mu$ COLLIDER PHYSICS

FEB 22, 93

LANL

D. CLINE

UCLA

- (1) Search For the Higgs Boson (Std Model)
  - $t$  Quark Connection
  - Cabibbo angle calculations
  - cross section /  $\Gamma$  for  $\mu\mu \rightarrow H$
- (2) Strategy for Search for Massive Higgs
  - Comparison with LHC/SSC
  - Difficulty of Search for  $H \rightarrow \gamma\gamma$  at SSC -
- (3) Higgs Search - Min. Just -
  - Increased Complexity
  - Possible weakness of insensitivity
- (4)  $t$  Quark Physics at  $e\mu\mu$  Colliders

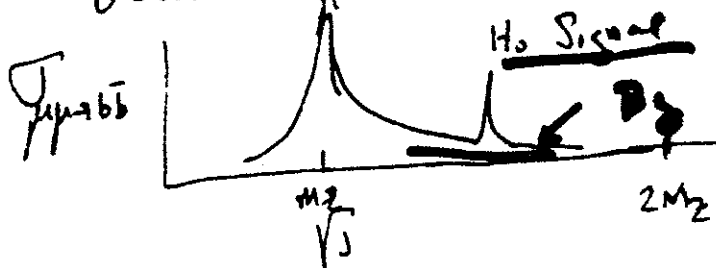
(2)

ADVANTAGES of  $\mu^+\mu^-$  COLLIDER

1)  $\sigma_{\mu\mu \rightarrow H^0} \sim \left(\frac{M_H}{M_e}\right)^2 \times \sigma_{e^+e^-}$

FOR  $M_H \leq 2M_Z$  ;  $M_H > M_Z$   
 $H^0 \rightarrow b\bar{b}$  ; HENCE  $H^0 \rightarrow b\bar{b}$

Observe an enhancement in  $b\bar{b}$  cross section



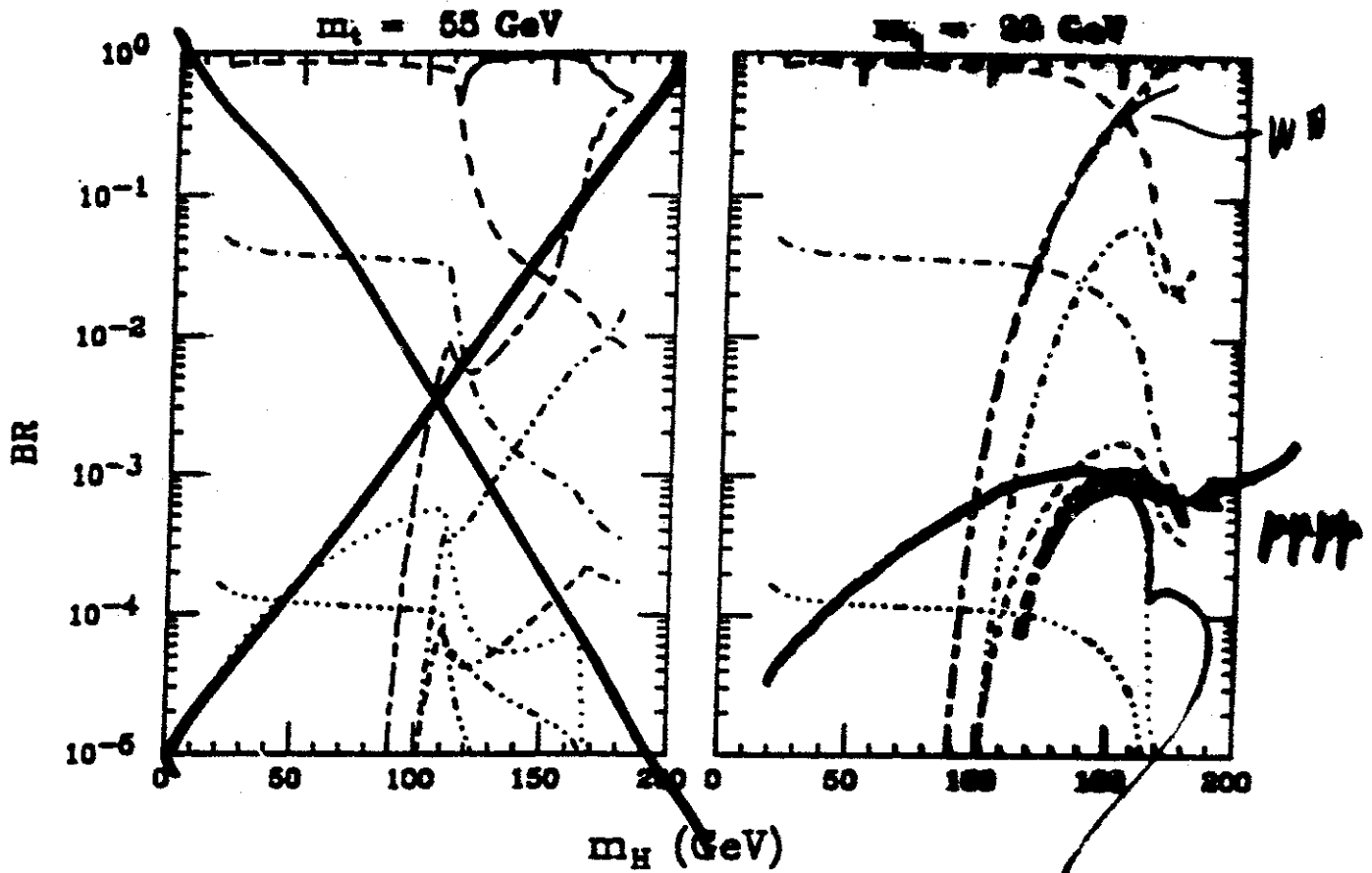
2)  $\Gamma_H$  is SMALL -  $\sim 1 \text{ keV}$  - CLEAR  
LARGE S/B<sub>g</sub> FOR  $M_H > 160 \text{ GeV}$

3) BUT - Search for Higgs requires a  
 variation in  $\sqrt{s}$  to find the narrow  
Resonance! - This is an important  
 and crucial constraint on the  $\mu\mu$  collider

!!

# DOMINANT DECAY $H_0 \rightarrow b\bar{b}$

Higgs Branching Ratios  
3 Generations, SM W only



$H_0 \rightarrow \gamma\gamma$

$BR \sim 10^{-3} - 10^{-4}$

HADRON MACHINES MUST USE

RARE DECAYS  $H_0 \rightarrow \gamma\gamma / \mu\mu (\mu\mu)$

WITH CARE

# ARGUMENTS FOR A LOW MASS H

## ANALYTICAL STATEMENT

G KANE  
- Review Review -

It was shown over a decade ago<sup>13)</sup> that for a Standard Model Higgs boson the effect of such a requirement gave an upper limit on  $M_h$  that was dependent on the value of  $M_t$  (because if  $M_t > M_W$  then the top quark Yukawa coupling affects the equation for the Higgs self-coupling  $\lambda$ , and  $M_h \sim \sqrt{\lambda}$ ). One can summarize the results very approximately in mnemonic form by saying either  $2M_t > M_h > 2(M_t - M_W)$  or the apparent unification of forces is a meaningless accident. Any planning for future detectors or colliders that uses a Standard Model Higgs boson with mass outside of this range should provide strong justification for doing so.

(Why are we bullying the SSC)

ALSO  $V^2$  THEOREM -

$W_L W_L$  SCATTERING NOT

LIKE  $\pi\pi$  - WE MAY

LEARN NOTHING FROM

THIS EVEN UP TO  $\sim 8$  TEV

~~XXXXXXXXXX~~  
CABIBBO et al

Bounds on  $m_{\nu^c}$  as a function of  $m_t$

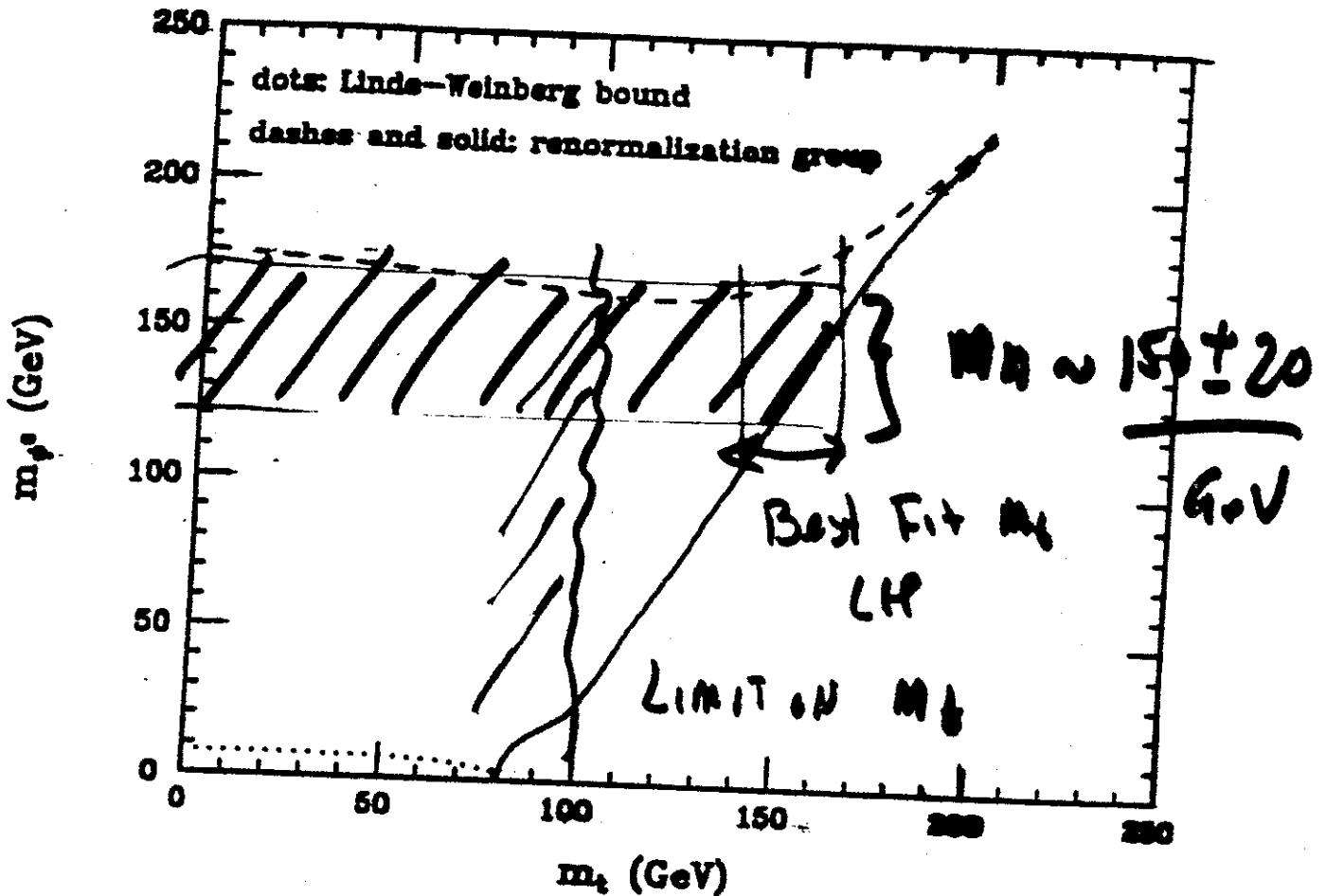
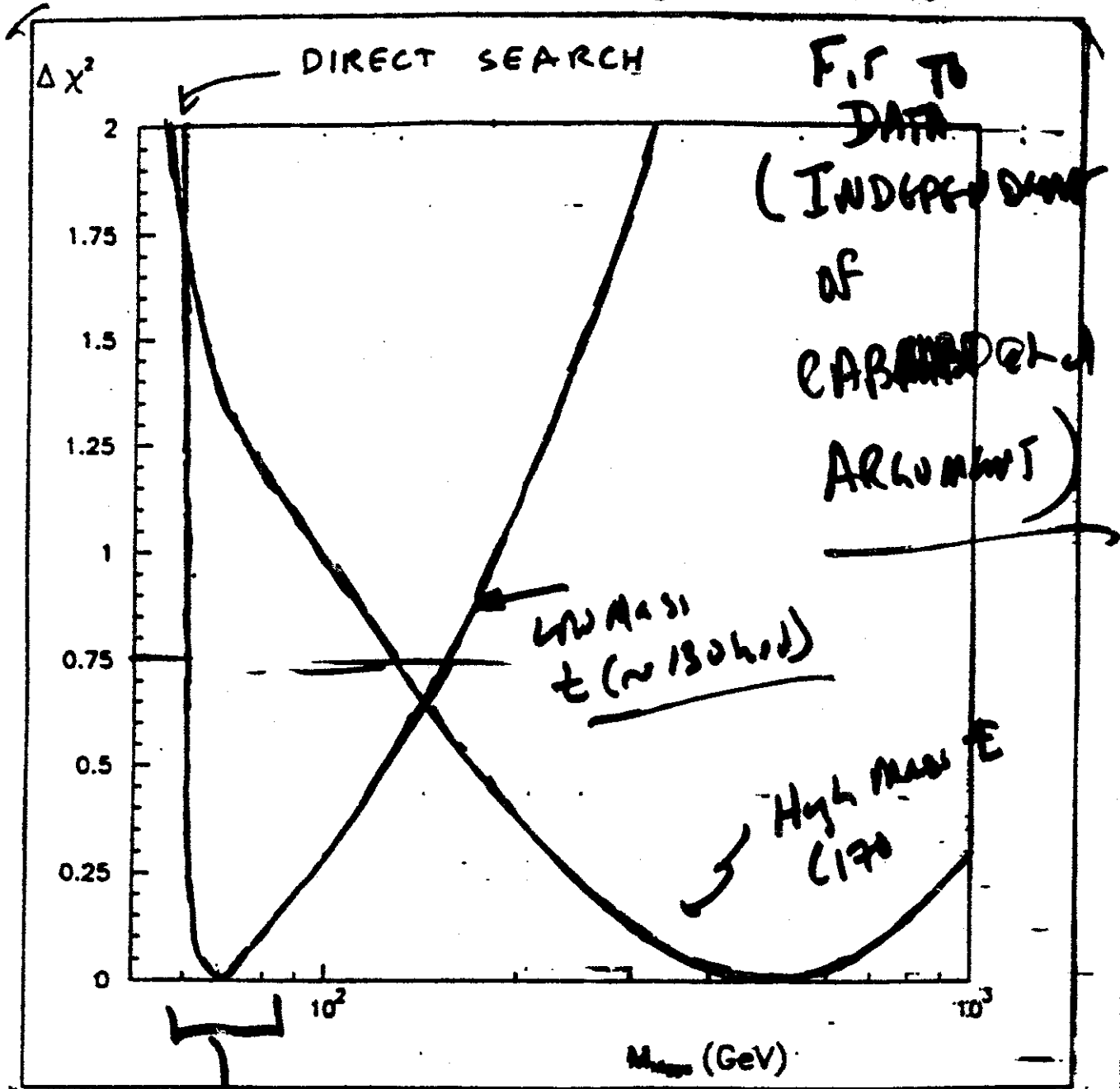


Figure 2.16 Upper and lower bounds on  $m_{\nu^c}$  as a function of  $m_t$ , coming from the requirement of a perturbative theory at all energy scales from  $s$  to  $M_U$ . This figure is taken from ref. 76, where  $M_U$  is taken to be the grand unification scale  $M_U \simeq 10^{16}$  GeV and  $\sin^2 \theta_W \simeq 0.2$ . Three generations of quarks and leptons have been assumed.

Actual



IF  $M_\tau < 150$  GeV  
 THEN  $M_H \lesssim 2M_\tau$

$$\sigma_{\mu\mu \rightarrow H} \sim \tilde{\kappa} \frac{\Gamma_{\mu\mu} \Gamma_{b\bar{b}}}{(s - M_H)^2 + \Gamma_H^2/4}$$

$\hookrightarrow b\bar{b}$

$$\approx 4 \tilde{\kappa} \left( \frac{\Gamma_{\mu\mu}}{\Gamma_H} \right) \left( \frac{\Gamma_{b\bar{b}}}{\Gamma_H} \right) \times \frac{1}{3} \quad \text{for color}$$

$$\left( \frac{M_{\mu}^2}{M_{b}^2} \right) \sim \frac{1}{2500}$$

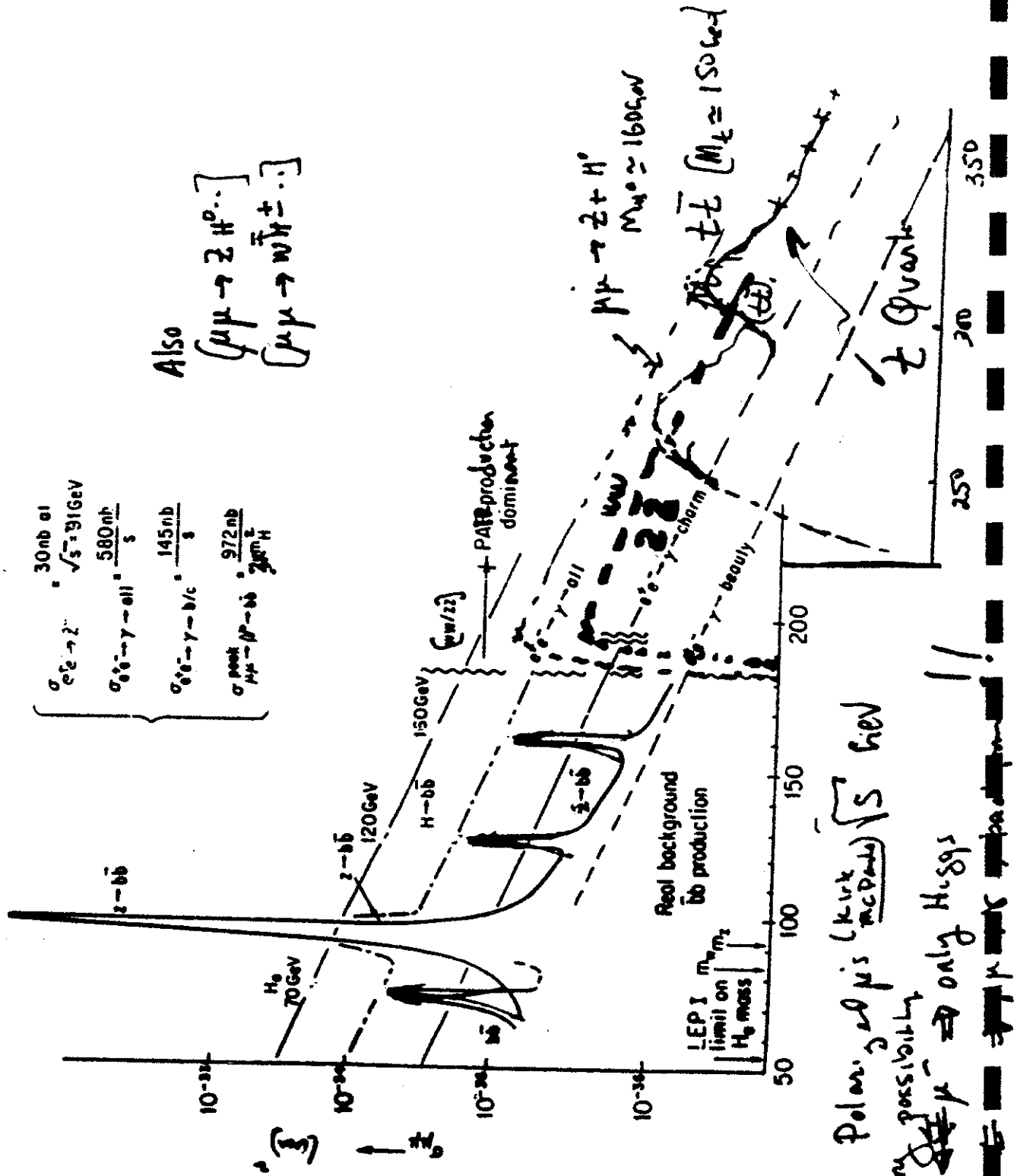
$$\approx 10^{-34} \text{ cm}^2 \text{ at } M_H = 100 \text{ GeV}$$

$$\approx 4 \times 10^{-35} \text{ cm}^2 \text{ at } M_H = 150 \text{ GeV}$$

$$\text{AREA} \sim \int_{dE > \Gamma_H} \sigma \, dE \sim 4\pi^2 \frac{\Gamma_{\mu\mu} \Gamma_{b\bar{b}}}{M_H^2 \Gamma_H}$$

$$\sim \frac{1}{2} \pi \tilde{\kappa}^2 (\Gamma_{\mu\mu})$$

$$\approx 10^{-34} \text{ cm}^2 \text{ GeV at } M_H = 150 \text{ GeV}$$



Note - For Polarized  $\mu$ s ( $K_{\mu\mu}$   $\mu$   $\mu$ )  $\sqrt{s}$  GeV  
 an interesting possibility  
 $\mu^+ \mu^- \rightarrow \text{only } H, S_1$  !!

0 1 2 4 0 9 0 4

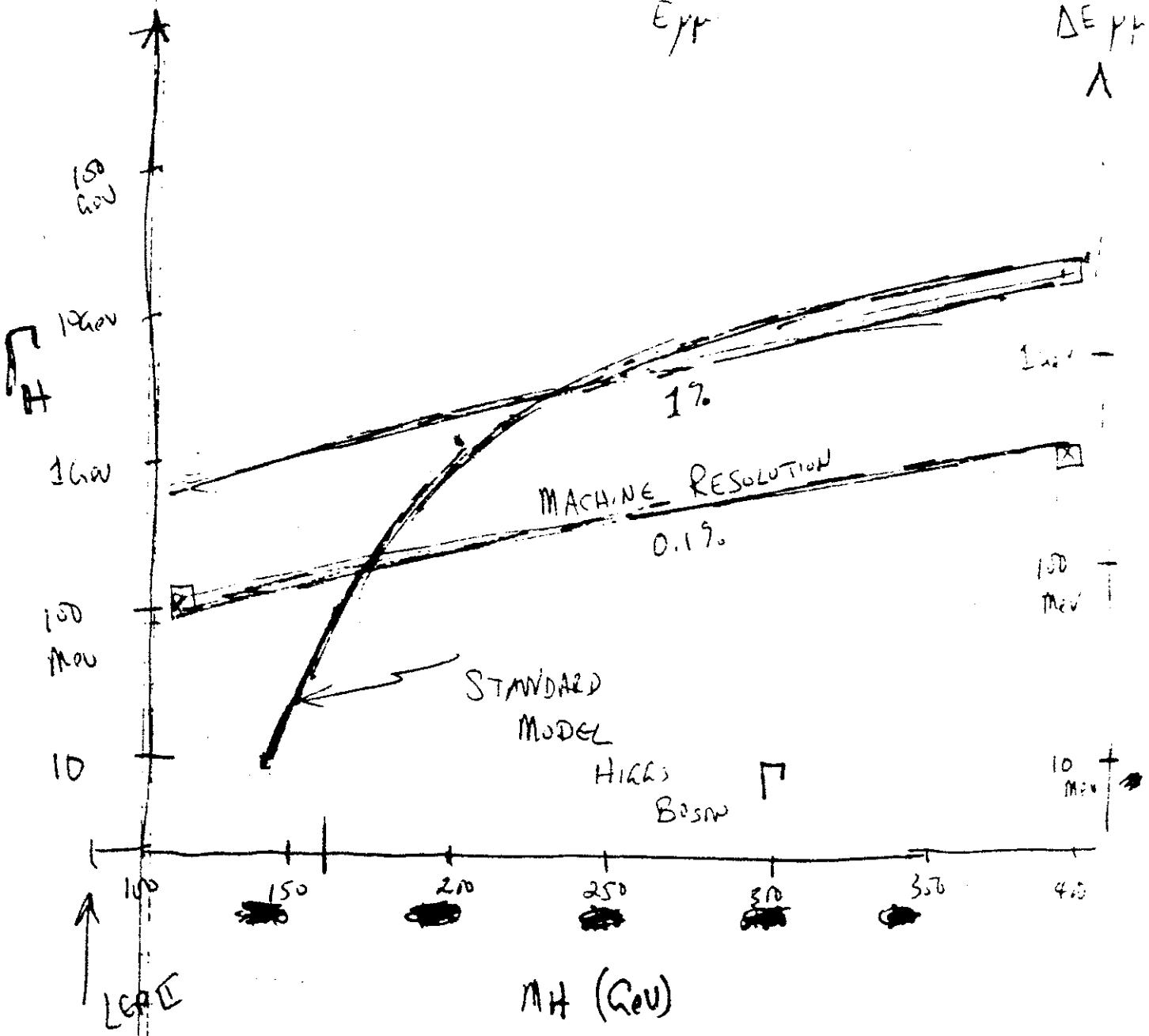
3 1 2 1 3 9 3 5

200 x 200 = 400

$\mu\mu$  Collider

$$1 + \frac{\Delta E}{E_{pp}} \approx 10^{-3}$$

$\Delta E_{pp}$   
 $\Lambda$





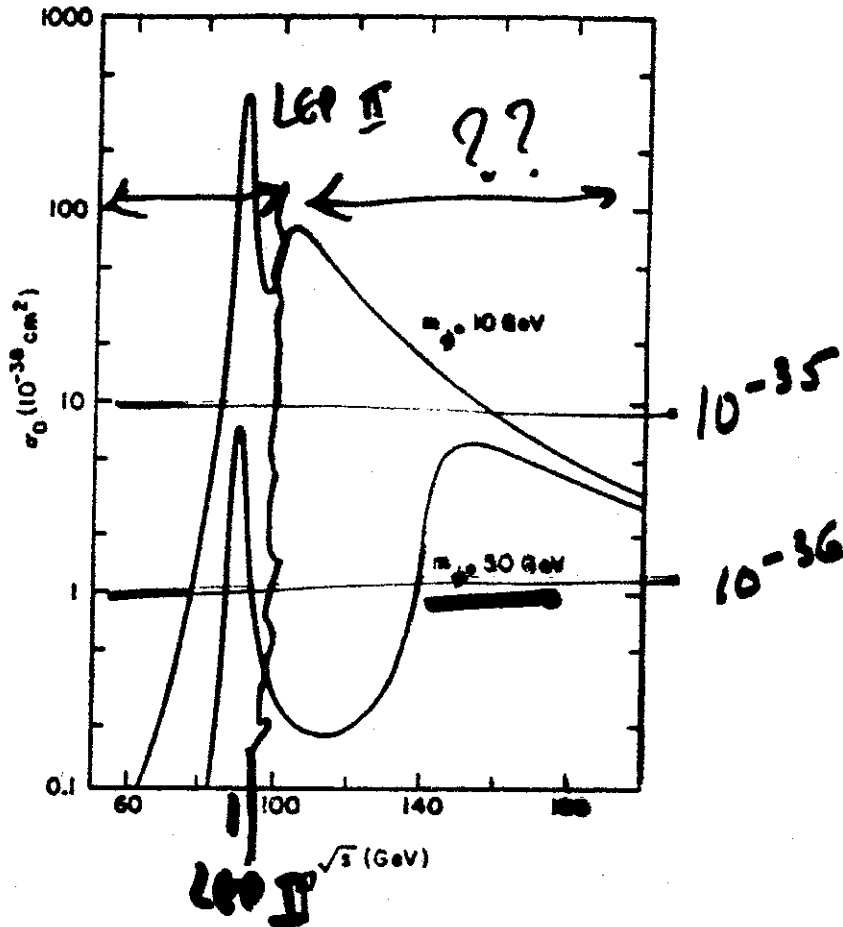


Figure 3.22 Cross section for  $e^+e^- \rightarrow \mu^+\mu^-\phi^0$  as a function of  $\sqrt{s}$ , for  $m_{\phi^0} = 10$  and  $50$  GeV. Parameter choices are  $m_Z = 90$  GeV,  $\Gamma_Z = 2.5$  GeV, and  $\sin^2 \theta_W = 0.22$ , from ref. 117.

Search For H0 to 50 GeV - TRIUMF

- Beyond very difficult.

Current LEP limit ~ 55 GeV  
 ( $4 \times 10^6 z$ )

J Sjogvist

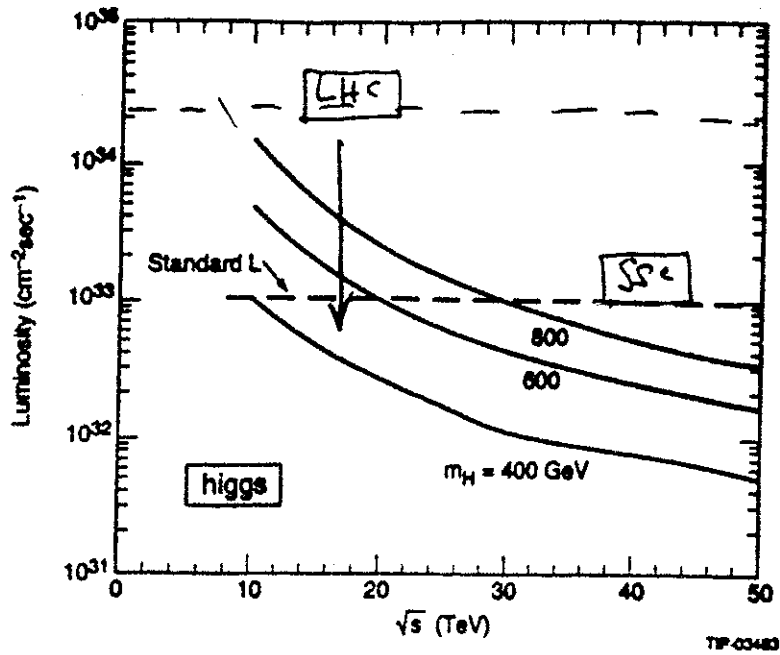


Figure 1. Luminosity required to produce in one year 20 Standard-Model Higgs bosons that decay to four charged leptons ( $e, \mu$ ) as a function of c.m. energy. (mass of  $t$  quark = 85 GeV.) Results are shown for Higgs masses of 400, 600 and 800 GeV.

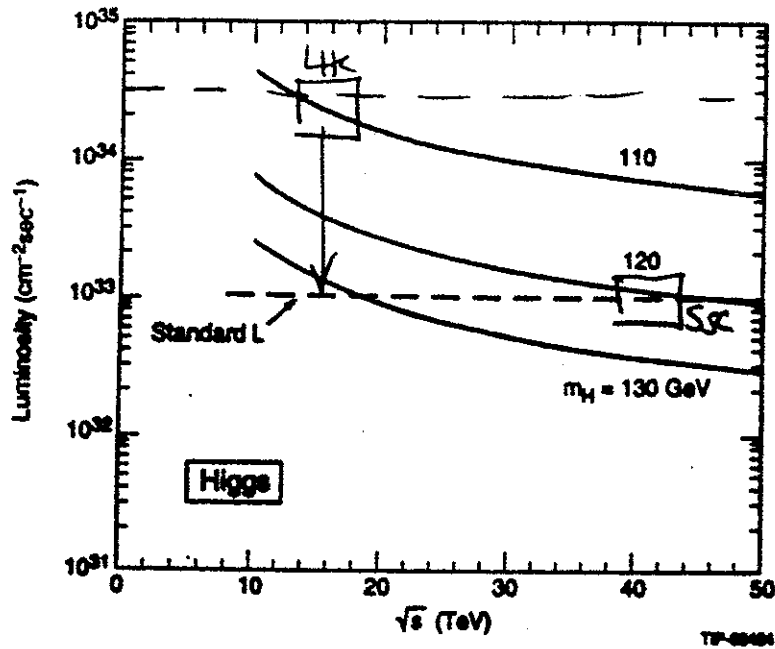


Figure 2. Luminosity required to produce in one year 40 intermediate mass Higgs bosons that decay into four charged leptons ( $e, \mu$ ) as a function of c.m. energy. (Mass of  $t$  quark = 85 GeV.) Results are shown for Higgs masses of 110, 120 and 130 GeV.

resolution suggests that other modes suffering less background would be more suitable for the SDC design.

Associated production of Higgs with a  $W$  or  $t$  quark gives an additional lepton tag that assists with triggering and significantly reduces the background. Figure 37 shows the efficiency for detection of  $t\bar{t} + H \rightarrow l\gamma\gamma + X$  vs.  $p_t$  and  $\eta$ . The analysis requires  $p_t > 20$  and  $|\eta| < 2.5$  for the lepton and both photons. The dotted (solid) curves are for  $M = 80$  (160) GeV, with four curves for  $\eta$  coverage of 1.5, 2.0, 2.5, 3.0. Several classes of background have been considered in this process. These include two-photon backgrounds  $W + \gamma\gamma$ ,  $b\bar{b} + \gamma\gamma$ ,  $t\bar{t} + \gamma\gamma$ ; QED radiative decays  $W$ ,  $Z + \gamma\gamma$ , and leptons faking  $\gamma$  in  $Z + \gamma$ ; backgrounds with one real  $\gamma$  and one misidentified jet ( $t\bar{t} + \gamma$ ); and backgrounds where both photons arise from misidentified jets. Figure 38 shows the resulting estimated background vs. Higgs mass. Figure 39 shows the signal and background for associated light Higgs production with signals at 80, 100, 120, 140, and 160 GeV. Note that the right-hand scale shows the number of events expected; the curves are generated with large statistics. This signal can be confirmed by SDC after several years' running.

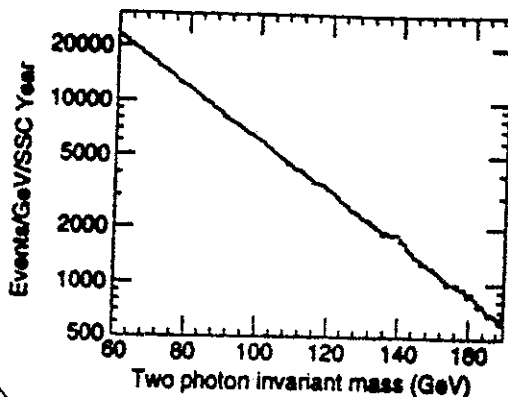


Figure 35. The two-photon invariant mass distribution including the signals from Higgs bosons with masses of 80, 100, 120, 140, and 160 GeV. The background includes only the irreducible backgrounds arising from the  $q\bar{q} \rightarrow \gamma\gamma$  and  $g\bar{g} \rightarrow \gamma\gamma$  processes.

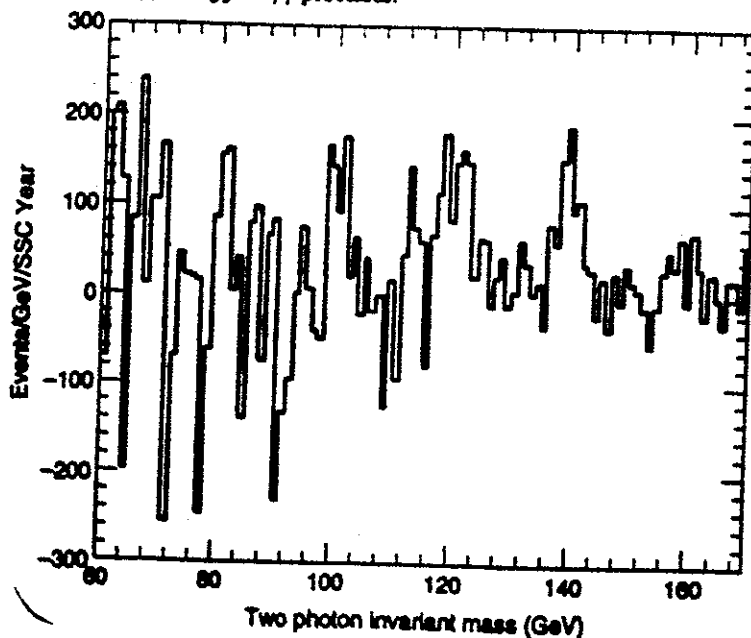
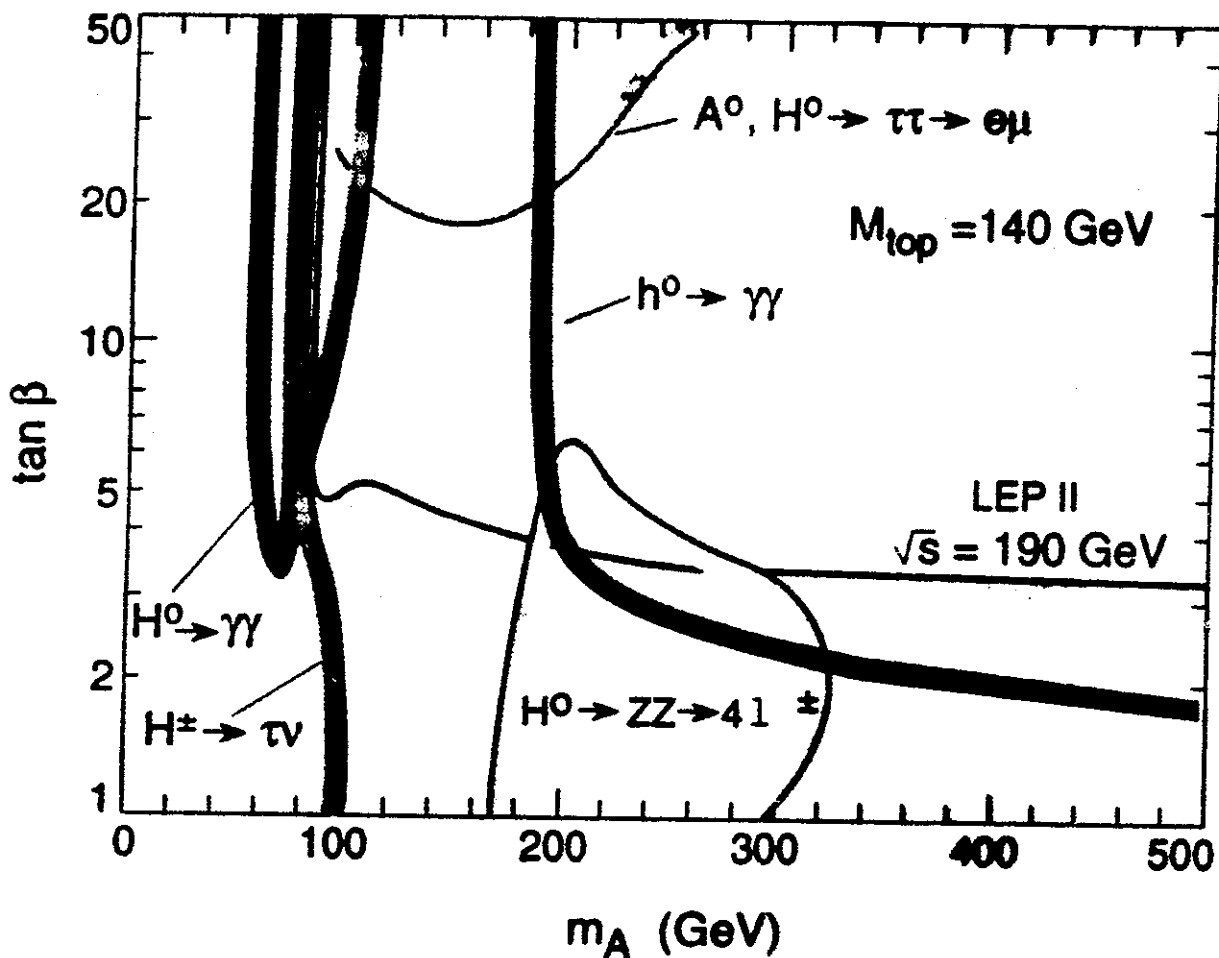


Figure 36. The expected signals from Higgs bosons with masses of 80, 100, 120, 140, and 160 GeV. The irreducible backgrounds displayed in Figure 35 have been statistically subtracted using an exponential fit to the background shape. The baseline calorimeter performance has been assumed.

TP-03488

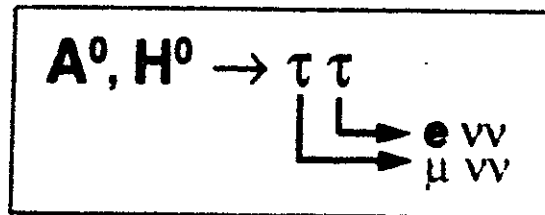
## Search Regions in SUSY Parameter Space

- $5\sigma$  contours
- $h^0, H^0 \rightarrow \gamma\gamma$  and  $H^0 \rightarrow 4l^\pm$  for  $10^5 \text{ pb}^{-1}$
- $A^0, H^0 \rightarrow \tau\tau$  and  $H^\pm \rightarrow \tau\nu$  for  $10^4 \text{ pb}^{-1}$



# MSSM Neutral Higgs

- $\tau\tau$  decays of  $A^0, H^0$  allow exploration of this region  $\tan \beta \geq 15, 100 \leq m_A \leq 200$  GeV
- Channel studied:



- For  $m_{A,H} \geq 120$  GeV  $m_H \approx m_A$  ( $\tan \beta > 10$ )
- Selection cuts
  - Isolated  $e$  and  $\mu$
  - Number of hard hadronic jets  $\leq 1$
- Reconstruct the  $\nu$ s by assuming  $m_\tau = 0$ , if  $e$ - $\mu$  not collinear;
  - $\Rightarrow$  Reconstruct  $\tau\tau$  effective mass  $m_{\tau\tau}$ 
    - For  $10^{33} \text{ cm}^{-2} \text{ s}^{-1} / 10^4 \text{ pb}^{-1}$  signal clearly visible with  $\geq 5 \sigma$  for  $\tan \beta > 20, 100 \leq m_{A,H} \leq 200$  GeV
- Backgrounds considered:
  - $t\bar{t}$  - dominant  $m_{\tau\tau} > 150$  GeV
  - $b\bar{b}$  - dominant  $m_{\tau\tau} < 150$  GeV
  - $Z/DY \rightarrow \tau\tau$  important at  $m_{\tau\tau} \sim 100$  GeV
  - $WW$  negligible

The nature of SUSY models was outlined in a previous section. As was shown, evidence for supersymmetry would first be seen in relatively high-rate gluino production. Once SUSY is seen there, a more complicated Higgs sector would naturally be expected. The richer Higgs spectrum predicted in such models is a considerable experimental challenge to disentangle from the data. Extensive work with detailed detector simulations on the SUSY Higgs sector has not yet been carried out by the community. In the SDC case, decay modes of  $\gamma\gamma$ ,  $ZZ^*$ , or  $ZZ$ , and top decay to charged Higgs have been studied. (Recall that for the two-doublet SUSY Higgs case, there are five physical Higgs bosons,  $h^0$ ,  $H^0$ ,  $A^0$ , and  $H^\pm$ .) The two free parameters are taken to be  $M_A$  and  $\tan\beta$ , where  $\beta$  is the ratio of the vacuum expectation values for the two Higgs doublets.

The branching ratios for neutral Higgs decays to  $\gamma\gamma$  are shown in Figure 47, where the solid curve is for  $h^0$  and the dotted (dashed) curve is for  $H^0$  ( $A^0$ ). For large values of  $M_A$ ,  $h^0 \rightarrow \gamma\gamma$  is observable. For small  $\tan\beta$ ,  $A^0 \rightarrow \gamma\gamma$  should be observable. Figure 48 shows the branching ratios for neutral Higgs to  $ZZ$ . Again, the solid curve is for  $h^0$ , and the dotted (dashed) curve is for  $H^0$  ( $A^0$ ). For large values of  $\tan\beta$ ,  $H^0 \rightarrow ZZ$  is observable. For small values of  $\tan\beta$ ,  $H^0 \rightarrow ZZ$  is observable. Studies of  $\text{top} \rightarrow H^\pm b$  have shown that the charged Higgs can be seen for all values of  $\tan\beta > 0.1$  via the  $c\bar{s}$  and  $\tau\nu_\tau$  decay modes.

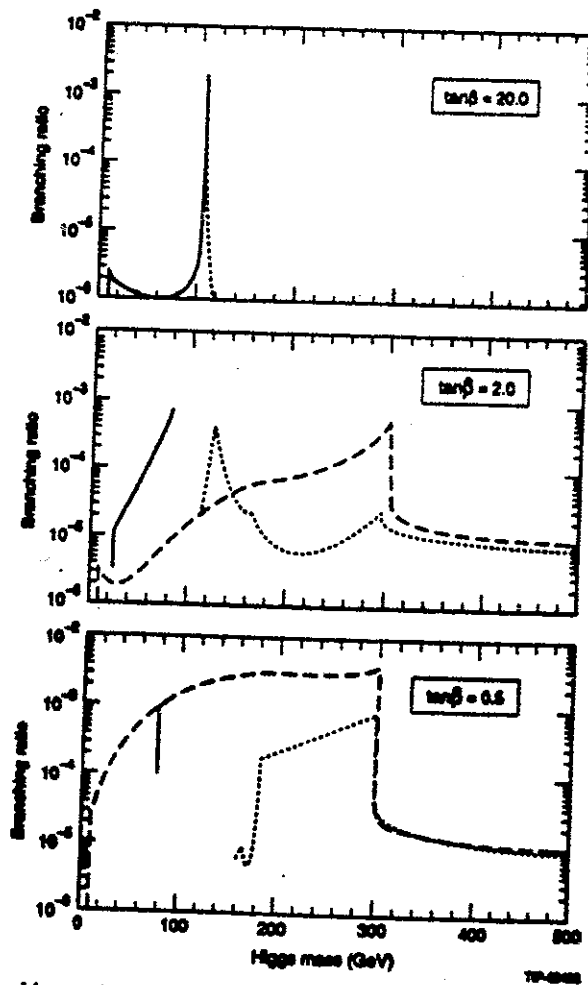


Figure 47. The branching ratios for the decay of the neutral Higgs bosons in the MSSM to the  $\gamma\gamma$  final state, assuming  $M_{\text{top}} = 150$  GeV. The solid curve is for the  $h^0$ , the dotted curve is for the  $H^0$ , and the dashed curve is for the  $A^0$ . The three different plots are for  $\tan\beta = 0.5, 2,$  and  $20$ .

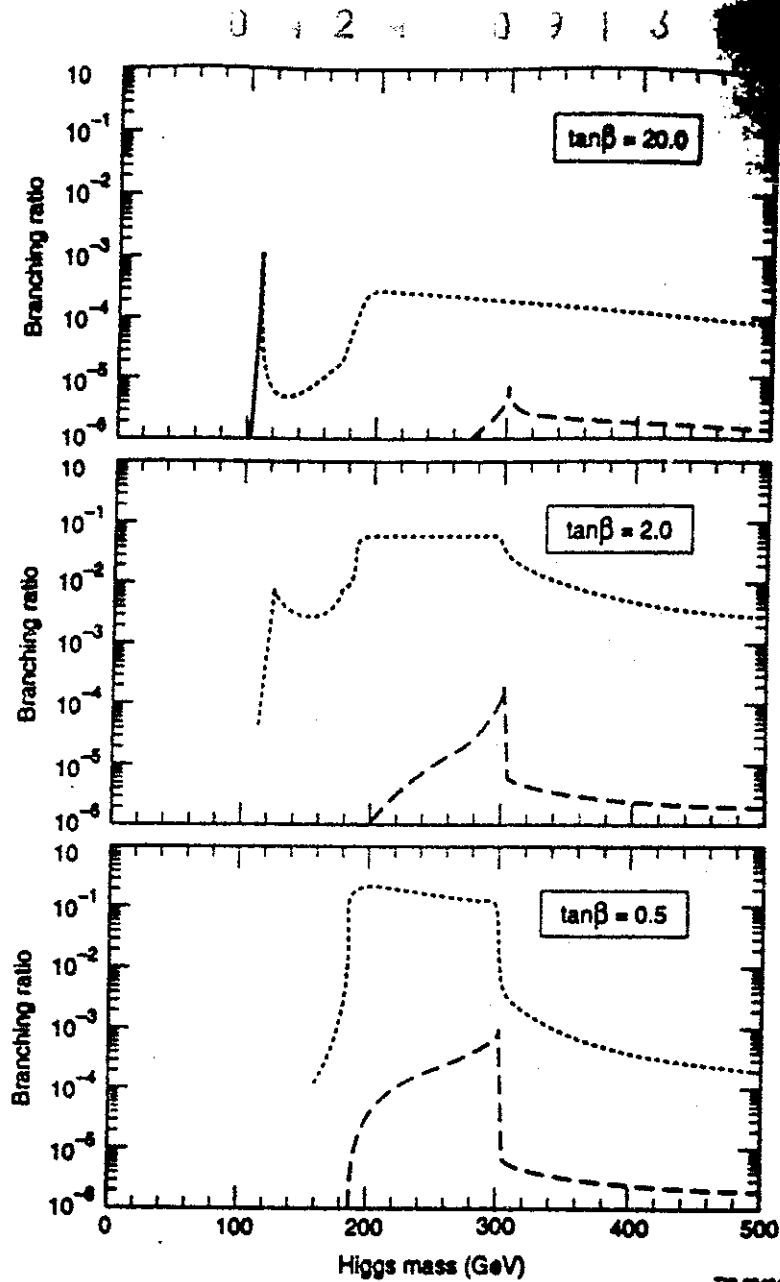


Figure 48. The branching ratios for the decay of the neutral Higgs bosons in the MSSM to the  $ZZ$  or  $ZZ^*$  final state, assuming  $M_{\text{top}} = 150$  GeV. The solid curve is for the  $A^0$ , the dotted curve is for the  $H^0$ , and the dashed curve is for the  $A^0$ . The three different plots are for  $\tan\beta = 0.5, 2,$  and  $20$ .

Assuming 3-5 years at SSC design luminosity, the experimental situation can be summarized for SDC by the following comments. For small  $M_A$ ,  $h^0$  is observable at LEP-II, and  $t \rightarrow H^\pm b$  is observable at SSC. For moderate  $M_A$  and small  $\tan\beta$ ,  $h^0$  is observable at LEP-II, and  $H^0 \rightarrow ZZ$ ,  $t \rightarrow H^\pm b$  are observable at SSC. For moderate  $M_A$  and large  $\tan\beta$ , none of the Higgs bosons may be observable in  $ZZ$  or  $\gamma\gamma$ . For large  $M_A$ ,  $h^0 \rightarrow \gamma\gamma$  is observable at SSC.

Clearly, the experimental situation needs further work and clarification within the context of realistic detector models. Tau decays and  $b$  tagging may provide some of the tools necessary to further extend the parameter range over which a viable search may be carried out.

NOTE -  $8.3 \times 10^9$  \$  
and no Higgs<sup>23</sup> DISCOVERY

0 1 2 4 0 9 1 4

CAN WE REACH

$10^{31} \text{ cm}^{-2} \text{ s}^{-1}$

Two Ref - Liliham

SRINISKI

- AIP - 1980

The muon colliding beam experiments will also be accessible /58,1V. For this purpose it is required to accelerate the cooled muon beams in the linear accelerator up to the required energy and make them collide in the sections with very strong focusing in a special ring with magnetic field as high as possible in order to increase the number of collisions during the life-time of the muons. Evaluations have shown that this way would enable one to achieve the satisfactory luminosity of the order  $10^{31} \text{ cm}^{-2} \text{ s}^{-1}$  at energies of hundreds GeV.

Madison Cong.

D Newcomb  
Acc. P.

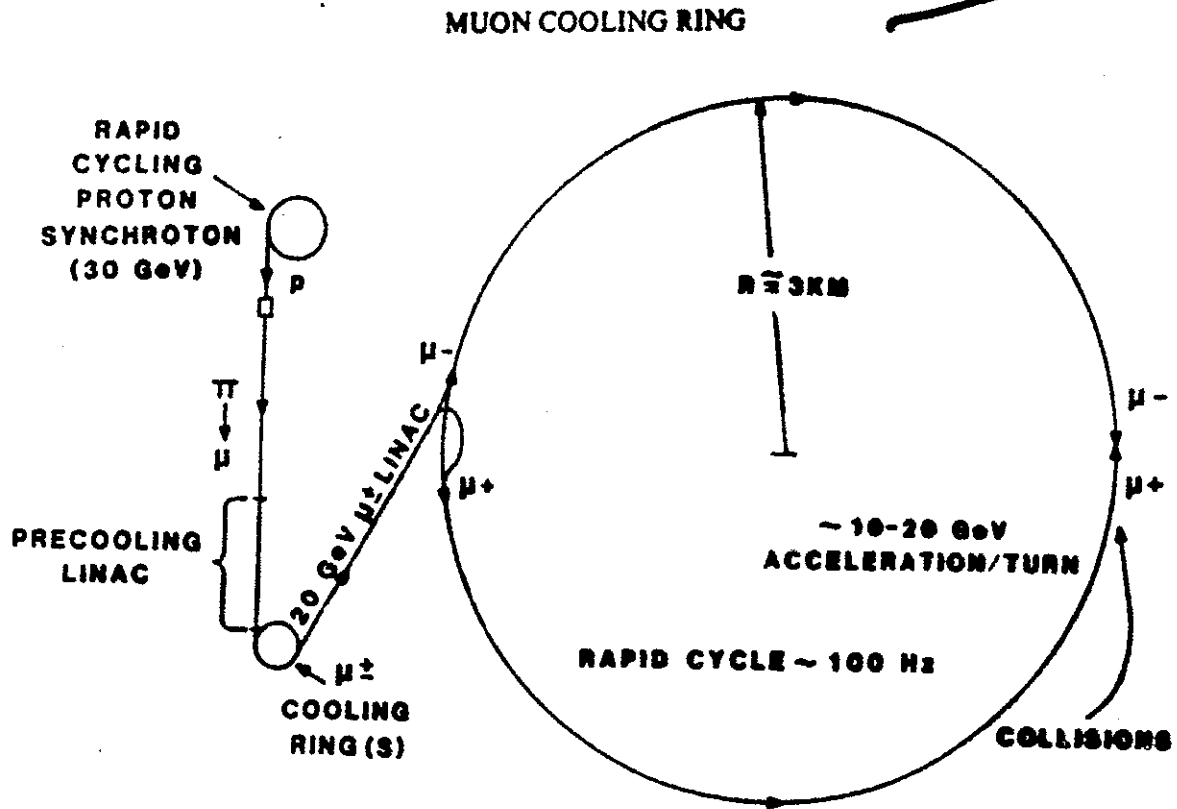


FIGURE 9 (1 TeV  $\mu$  rapid cycling synchrotron)

$L \sim 10^{33} \text{ ??}$

GOAL OF THIS MEET TO DETERMINE  
WHAT COLS COULD BE UNDER OPTIMAL

# SUMMARY

1) THERE IS GROWING EVIDENCE  
 THAT THE STO HIGGS IS  
 BELOW  $2M_Z$

2) SUSY HIGGS - 3 HIGGS - ONE NEAR  
 $M_Z$  (POSSIBLY UP TO  $\sim 150$  GeV)  
 - EXTREMELY HARD TO DETECT - MAY NEED  
 $\mu\mu$  AND HADRON MACHINES TO BE CERTAIN

3) HADRON MACHINES CAN SEARCH FOR  
 THESE HIGGS PROVIDED

(a)  $\sigma_{\text{prod}} \geq 10^5 \text{ pb (LHC)}$

(b) THE BR FOR  $H \rightarrow \mu\mu$  IS  
 SMALL ENOUGH

BOTH POSSIBILITIES ARE EXTREMELY DIFFICULT!!

4) A  $\mu\mu$  COLLIDER WITH  $\mathcal{L} \sim 10^{30} \text{ cm}^{-2} \text{ s}^{-1}$  ] NEED  
 OPERATING BETWEEN 100 - 180 GeV  
 COULD DISCOVER THIS HIGGS - THIS COULD BE  
 THE MOST IMPORTANT DISCOVERY IN 2000 +

0 1 2 4 0 9 1 7

## **Muon Collider - Possibilities & Challenges**

**David Neuffer**

**CEBAF**

## $\mu^+ - \mu^-$ Colliders - Possibilities and Challenges \*

David V. Neuffer

CEBAF, 12000 Jefferson Avenue, Newport News VA 23606

### Abstract

The current status of the  $\mu^+ - \mu^-$  collider concept is reviewed and discussed. In a reference scenario, a high-intensity pulsed proton accelerator (of K-factory class) produces large numbers of secondary  $\pi$ 's in a nuclear target, which produce muons by decay. The muons are collected and cooled (by "ionization cooling") to form high-intensity bunches that are accelerated to high energy collisions. High luminosity  $\mu^+ - \mu^-$  and  $\mu^- - p$  colliders at TeV or higher energy scales may be possible. Challenges in implementing the scenario are described. Possible variations and changes in muon production, accumulation, and collisions are discussed; further innovations and improvements are encouraged.

### Introduction

Current and planned highest energy colliders are hadronic proton-(anti)proton ( $p-p$  or  $p-\bar{p}$ ) colliders or electron-positron ( $e^+ - e^-$ ) colliders, and both approaches have significant difficulties in extension to higher energies. Hadrons are composite objects; so only a small fraction of the total energy participates in a collision, and this fraction decreases with increasing energy. Also, production of new particle states is masked by a large background of nonresonant hadronic events; identification of new physics becomes increasingly difficult with increasing energy. Leptonic ( $e^+ - e^-$ ) colliders have had the advantage of providing simple, single-particle interactions with little background. However, extension to higher energies is limited in energy, luminosity, and resolution by radiative effects (synchrotron radiation in circular colliders, beam-beam radiation and pair creation in linear colliders). At very high energies, the collisions are no longer point-like, because of the radiative background.

However, this radiation scales inversely as the fourth power of the lepton mass. Thus, we can extend the high-quality features of  $e^+ - e^-$  colliders to much higher energies by colliding higher mass leptons such as muons. The  $\mu^+ - \mu^-$  collider concept has been suggested, and is described in some detail in references (1, 2, 3, 4), and an example is displayed graphically in Figure 1. In those initial concepts, a high-intensity multi-GeV hadron accelerator beam produces pions from a hadronic target, and muons are obtained from  $\pi$ -decay. The  $\mu^+$ 's and  $\mu^-$ 's are accumulated and cooled by ionization cooling, and then accelerated (in linacs and/or synchrotrons)

\* Work supported by Department of Energy contract #DE-AC05-84ER40150

to high energies for high-energy collisions in a storage ring. The process is repeated at a rate matched to the high-energy muon lifetime to obtain potentially high luminosities.

Since the initiation of the muon collider concept, some subsequent developments have increased interest in the possibility of muon colliders, and recent progress in related fields may increase their potential capabilities.

In high energy physics (HEP), plans for the current generation of high-energy facilities are now reasonably well established. The next HEP devices are to be high-energy (8–20 TeV) p-p colliders (SSC and/or LHC), to be followed by an  $e^+e^-$  linear collider (up to 0.5 TeV per beam). It is now possible to begin serious consideration of projects to follow these, such as a  $\mu^+-\mu^-$  collider. The current generation of HEP devices includes large components (injectors, tunnels, storage rings, linacs) and technology (high-gradient linacs, low- $\beta^*$  optics, large-bandwidth stochastic cooling, etc.) which may be incorporated into a muon collider. This generation has also pushed back the frontiers of federal funding by more than an order of magnitude, and that greatly extends the potential scope of a muon collider.

Development of high-intensity accelerator concepts (for KAON factories, or accelerator transmutation of waste, or tritium production, or for  $\mu$ -catalyzed fusion) can also provide methods and facilities for improved  $\mu$  production, collection and cooling.

Recent studies of  $e^+e^-$  linear colliders show that that approach appears to be limited in energy or luminosity at the TeV scale by beamstrahlung radiation effects. This calls for a "new paradigm" in extension to higher energies;<sup>5</sup> possibly including a  $\mu^+-\mu^-$  collider option. Also the next frontier in HEP appears to be in understanding the "Higgs sector", the generation of masses. The greater direct coupling of muons to the Higgs sector (by  $(m_\mu/m_e)^2$ ) may provide an important incentive for developing  $\mu^+-\mu^-$  colliders, possibly in the energy-specific form of a Higgs-resonance "factory".

In this paper we present an overview of possible high-energy  $\mu^+-\mu^-$  colliders for the  $\mu^+-\mu^-$  workshop (Napa, CA, 12/1992), following the concepts previously presented in the references (1–4). In this overview, we will identify some of the critical problems in implementing the scenario, suggest some possible variations and improvements, and, hopefully, inspire some further directions for innovation and invention from the participants and other readers.

### $\mu$ -Production

A critical problem in  $\mu^+ - \mu^-$  colliders is the production and collection of adequate numbers of muons. The critical difficulties are the large initial phase-space volume of the muons (since they are produced as secondary or tertiary products of high-energy collisions) and the fact that muons decay, with a lifetime of  $2.2 \times 10^{-6} \gamma$  s decay time. ( $\gamma$  is the usual kinetic factor ( $E_\mu/m_\mu$ )). The problem is to obtain, compress, and use sufficient muons before decay.

We will first consider as a baseline reference a high-energy hadronic (HEH) muon source of the type described in references (1, 2, 4): a medium-energy high-intensity hadron accelerator beam is transported onto a high-density target to produce GeV-energy  $\pi$ 's, and the  $\pi$ 's are confined in a transport channel where they decay to produce  $\mu$ 's, which are collected, compressed, and accelerated. In this section, the baseline HEH source is described, and guidelines for optimization and improvement are suggested. Variations and alternative approaches are then mentioned; these include a low energy (GeV-scale) " $\pi$ -factory" beam, possibly producing surface muon beams, or an  $e^-$ -beam producing  $\mu^+ - \mu^-$  pairs by photoproduction.

Production of large numbers of muons in the baseline scenario is not difficult. Hadronic interactions of the beam with the target produce large numbers of  $\pi$ 's, and almost all of these  $\pi$ 's decay by producing a muon plus a neutrino. The difficult problem of optimizing production and collection for maximal  $\mu$  intensity is not yet solved; however, some guidelines may be obtained from approximate calculations. A first estimate of  $\pi^\pm$  production in proton-hadron collisions may be obtained using known and calculated particle spectra, such as the empirical formulae of Wang<sup>6</sup>:

$$\frac{d^2 N}{dP d\Omega} = AP_p X(1-X)e^{-ax^c - DP_p} \frac{\text{pions}}{\text{sr-GeV/c}} / \text{interacting proton} \quad (1)$$

where  $P_p$  is the incident proton momentum,  $X = P_\pi/P_p$  is the pion/proton momentum ratio,  $P_\pi$  is the pion transverse momentum and  $A = 2.385$  (1.572),  $B = 3.558$  (5.732),  $C = 1.333$  (1.333), and  $D = 4.727$  (4.247) for positive (negative) pions. In this formula, pions are produced with a mean transverse momentum of  $\sim D^{-1}$  or  $\sim 0.2$  GeV. Also, if  $P_\pi/P_p \ll 1$ , pion production is nearly independent of proton energy, and pion production within a given momentum bite ( $\Delta P_\pi/P_p$ ) is nearly constant. If the Wang model is accurate, an optimal  $\pi$ -source may be obtained from a medium energy proton beam (20–50 GeV) which collides into a nuclear target, followed by strong-focusing optics which collects secondaries ( $P_\pi$  acceptance  $\sim 0.2$  GeV) and a strong-focusing transport line for  $\pi - \mu \nu$  decay. Small spot sizes on the

production target and small beam sizes in the transport line are desired to minimize  $\pi$  and  $\mu$  emittance. High momentum acceptance ( $\delta P/P > \pm 10\%$ ) is desired for maximal production. Economy would favor lower energies.

Figure 2 displays a possible configuration for  $\mu^+$  or  $\mu^-$  production. A 40 GeV proton beam is focussed (possibly with a Li lens) onto a 5 cm W target to a mm-scale spot, producing  $\pi$ 's, which are captured by the following optics, which is designed to accept 2 GeV  $\pi$ 's at angles up to  $\theta_T = 100$  mrad ( $P_i < 0.3$  GeV/c). This optics is approximated by a 2.0 cm radius Li lens of 10 cm length centered 15 cm downstream from the target center. The capture optics is to be followed by a strong-focussing transport of  $\sim 1$   $\pi$  decay length ( $\sim 110$ m at 2 GeV), which maintains a mean betatron function of 1m. The resulting muons are inserted into a muon accumulator system for cooling and acceleration.

According to the Wang model, this outline system would produce and accept 0.12 (0.08)  $\pi$ 's/(GeV/c)/interacting proton. This must be multiplied by a target efficiency factor  $\eta_T = 0.4$  (the probability that an incident proton produces an exiting  $\pi$ ), and by the momentum acceptance width (0.4 GeV/c for  $\pm 10\%$  acceptance), to obtain the number of  $\pi$ 's accepted in the decay channel per primary proton (0.019/0.012  $\pi^+/\pi^-$ ).

In the decay channel,  $\pi$ -decay ( $\pi \rightarrow \mu \nu$ ) produces  $\mu$ 's within a uniform energy distribution (between 0.57 and 1.0  $E_\pi$ ) and with a maximum transverse momentum of 29.8 MeV/c. With 63% ( $1/e$ ) of the  $\pi$ 's decaying and  $\sim 40\%$  of the product  $\mu$ 's within the transport acceptance, we find  $\sim 0.005$  (0.0033)  $\mu^+$  ( $\mu^-$ ) per primary proton are delivered to the  $\mu$ -collector.

The transverse emittance is determined by the  $\pi$ -production phase space, and the  $\pi$ -decay phase-space. The transverse emittance from  $\pi$ -production from a thin target is of order  $r_T \theta_T$  or  $2.5 \times 10^{-4}$  m-rad at 2 GeV, if the primary beam size on the target,  $r_T$ , is 0.0025m. (For a thick target, the projected source size ( $\sim l_T \theta_T/2$ , where  $l_T$  is the target length) must be included in  $r_T$ . In our example the projected source is similar to the target size.) The  $\pi$ -decay increases emittance by  $\sim \beta \theta_d^2/2$ , where  $\beta$  is the mean decay-line betatron function and  $\theta_d$  is the maximum decay angle. With  $\theta_d = P_i/P_\mu = 0.02$  and  $\beta = 1$ m in our reference case, an emittance  $\epsilon_t$  of  $\sim 2 \times 10^{-4}$  m-rad at 1.5 GeV is obtained from the decay line. For this example, the total transverse emittance would be  $< 4 \times 10^{-4}$  m-rad ( $6 \times 10^{-3}$  m-rad normalized), and could be somewhat reduced by further optimizations.

This reference case is oversimplified. The problems of separating primary  $p$ 's from secondary  $\pi^+$  and  $\pi^-$  beams, and separating the  $\pi$  beams from each other are not addressed; the actual optics will be more interesting. The parameters are not

optimized, and the production estimates are not very accurate. The calculations do not include  $\pi$ 's (and  $\mu$ 's) from secondary interactions. For  $E_p \ll E_p$ , secondary and cascade production could be large. However,  $\mu$ -decay from source to collider will reduce the final number (by  $\sim 2\times$ ). The calculations do show that an HEH source can obtain  $\geq 10^{-3}$   $\mu$ 's per primary proton, and that is adequate for a high-luminosity collider. This result is in agreement with an independent analysis of Noble.<sup>7</sup> It is possible that improvements, acceptance increases, and optimization could conceivably increase this to the  $10^{-2}$  level, but probably not much greater.

The HEH scenario has been motivated from a high-energy physics bias, and imitates  $\bar{p}$  source methods.  $\pi$ -production also occurs in low-energy hadronic (LEH) " $\pi$ -factories", from GeV/nucleon protons or deuterons, at a level of  $\sim 0.5 \pi/p$ . For  $\mu$ -collider use, a compressor ring would be needed to combine the proton(deuteron) linac beams into sub- $\mu$ s pulses. The  $\pi$ 's are produced at the 100 MeV energy level, where they can be stopped in an absorber to produce 29 MeV/c  $\mu$ 's, which will lose further energy in the absorber. (Stopping times are at ns levels; the  $\mu$ -lifetime at rest is 2.2 $\mu$ s.) (Nagamine has proposed extracting such slow muons in a high-intensity surface muon source.<sup>8</sup>) An LEH source can produce large numbers of  $\mu$ 's with low energy and momentum spread, which may require little or no further cooling, and the LEH source could be preferable to an HEH source. The difficulty is in extracting sufficient  $\mu$ 's in a small phase-space volume which are suitable for acceleration in a  $\mu^+ - \mu^-$  collider. The problem of calculating and optimizing  $\mu$  production in an LEH configuration is unsolved; it is an important challenge for the reader.

Another possible  $\mu$ -source can be obtained by colliding multi-GeV  $e^-$  beams into a hadronic target; bremsstrahlung would produce  $\mu^+ - \mu^-$  pairs by photoproduction, but not as frequently as  $e^+ - e^-$  pairs. Obtaining the  $\mu$ 's through pair production avoids the phase-space dilution of  $\pi$ -decay; however  $\mu$ -production does not seem to be as copious as in a hadronic source. An optimized calculated comparison has not yet been made.

The best possible  $\mu$ -source is not yet identified or developed. It may follow some of the ideas suggested in this section, with added improvements and innovations, or it may be dramatically different. That development is an important challenge for the workshop.

#### $\mu$ -Cooling, and Combination

The  $\mu$ 's are produced in a relatively large phase-space volume which must be compressed to obtain high-luminosity collisions. Most of the needed compression is obtained from adiabatic damping; acceleration from GeV-scale  $\mu$  collection to TeV-

scale collisions reduces phase-space by  $\sim 10^9$  ( $10^3$  per dimension). Additional phase-space reduction can be obtained by "ionization cooling" of muons (" $\mu$ -cooling"), which is described in some detail in references (1,2,3), and is conceptually similar to radiation damping. In this section we first describe transverse  $\mu$ -cooling. Longitudinal cooling and bunch combination, and muon survival and acceleration are then discussed.

The basic mechanism of transverse  $\mu$ -cooling is quite simple, and is shown graphically in figure 3. Muons passing through a material medium lose energy (and momentum) through ionization interactions. The losses are parallel to the particle motion, and therefore include transverse and longitudinal momentum losses; the transverse energy losses reduce (normalized) emittance. Reacceleration of the beam (in rf cavities) restores only longitudinal energy. The combined process of ionization energy loss plus rf reacceleration reduces transverse momentum and hence reduces transverse emittance. However, the random process of multiple scattering in the material medium increases the emittance.

The equation for transverse cooling can be written in a differential-equation form as:

$$\frac{de_{\perp}}{dz} = -\frac{dE_{\mu}}{E_{\mu}} e_{\perp} + \frac{\beta^* d\langle\theta_{rms}^2\rangle}{2 dz} \quad (2)$$

where  $e_{\perp}$  is the (unnormalized) transverse emittance,  $dE_{\mu}/dz$  is the absorber energy loss per cooler transport length  $z$ ,  $\beta^*$  is the betatron function in the absorber and  $\theta_{rms}$  is the mean accumulated multiple scattering angle in the absorber. Note that  $dE_{\mu}/dz = f_A dE_{\mu}/ds$ , where  $f_A$  is the fraction of the transport length occupied by the absorber, which has an energy absorption coefficient of  $dE_{\mu}/ds$ . Also the multiple scattering can be estimated from:

$$\frac{d\langle\theta_{rms}^2\rangle}{dz} = \frac{f_A}{L_R} \left(\frac{0.014}{E_{\mu}}\right)^2 \quad (3)$$

where  $L_R$  is the material radiation length and  $E_{\mu}$  is in GeV. (The differential-equation form assumes the cooling system is formed from small alternating absorber and reaccelerator sections; a similar difference equation would be appropriate if individual sections are long.)

If the parameters are constant, equations 2 and 3 may be combined to find a minimum cooled (unnormalized) emittance of

$$e_{\perp} = \frac{(0.014)^2}{2E_{\mu}} \frac{\beta^*}{L_R \frac{dE_{\mu}}{ds}} \quad (4)$$

or, when normalized

$$e_{N\perp} = e_{\perp} \gamma = \frac{(0.014)^2}{2m_{\mu} c^2} \frac{\beta^*}{L_R \frac{dE_{\mu}}{ds}} \quad (5)$$

(All energies are in GeV.)

Avoiding longitudinal phase-space dilution implies cooling at  $E_{\mu} \geq 0.3$  GeV, and economy implies cooling at relatively low energies (since cooling by  $e^{-1}$  requires  $E_{\mu}$  energy loss and recovery).  $E_{\mu} = 0.5-1.5$  GeV seems reasonable. Cooling can be obtained in either linacs (possibly using recirculation lines) or storage rings. Multiple stages can be used to optimize cooling scenarios. The important constraint is that cooling must be completed within a muon lifetime, which can be expressed as  $\sim 300 \bar{B}$  (T) turns in a storage ring, where  $\bar{B}$  is the mean bending field, or as a length  $L_{\mu} = 660 \gamma$  meters of path length. This constraint is surmountable.

Some guidelines for optimal cooling may be obtained from equations 2-5. They indicate that it is desirable to obtain small  $\beta^*$  (strong focusing) at the absorber. It is also desirable to have materials with large  $L_R dE/ds$ .  $L_R dE/ds$  is largest for light elements (0.1 GeV for Li, Be but  $\sim 0.01$  GeV for W, Pb) indicating the desirability of light absorbers. However, the need for small  $\beta^*$  and the depth of focus constraint that a (non-focusing) absorber section must be less than  $2\beta^*$  would favor large  $dE/ds$  (heavy) absorbers. A conducting light-metal absorber (Li, Be, Al) can also be a continuously focusing lens, which could then be arbitrarily long while maintaining small  $\beta^*$ . With current technology, lenses maintaining  $\beta^* < 1$  cm appear possible.

With  $\beta^* = 1$  cm, and  $L_R dE/ds = 0.1$  GeV, a normalized emittance of  $e_{N\perp} = 10^{-2} \beta^* = 10^{-4}$  m-rad is obtained as a reasonable goal for transverse cooling. Some improvements may be possible; the reader may develop ideas for optimal implementation.

Longitudinal (energy-spread) cooling is also possible, if the energy loss increases with increasing energy. The energy loss function for muons,  $dE/ds$ , is rapidly decreasing (heating) with energy for  $E_{\mu} < 0.3$  GeV, but is slightly increasing

(cooling) for  $E_\mu > 0.3$  GeV. This natural dependence can be enhanced by placing a wedge-shaped absorber at a "non-zero dispersion" region where position is energy-dependent (see figure 4). Longitudinal cooling is limited by statistical fluctuations in the number and energy of muon-atom interactions. An equation for energy cooling is:

$$\frac{d(\Delta E)^2}{dz} = -2 \frac{\partial \frac{dE_\mu}{dz}}{\partial E_\mu} (\Delta E)^2 + \frac{dE_\mu}{dz} I \quad (6)$$

where  $I$  is the mean energy exchange ( $\sim 12Z$  eV), and the derivative with energy combines natural energy dependence with dispersion-enhanced dependence. An expression for this enhanced cooling derivative is:

$$\frac{\partial \frac{dE_\mu}{dz}}{\partial E_\mu} = f_A \left( \frac{dE_\mu}{ds} \right)_0 + f_A \frac{dE_\mu}{ds} \frac{d\delta}{dx} \frac{\eta}{E_\mu \delta_0} \quad (7)$$

where  $\eta$  is the dispersion at the absorber,  $\delta$  and  $d\delta/dx$  are the thickness and tilt of the absorber. Note that using a wedge absorber for energy cooling will reduce transverse cooling; the sum of transverse and longitudinal cooling rates is invariant. From eqs. 6 and 7, cooling of 1 GeV  $\mu$  energy spreads to  $\Delta E/E \leq 0.005$  is possible. An rf buncher plus compressor arc (or synchrotron oscillations) can use this reduced energy spread to reduced bunch length.

The major problem in longitudinal space derives from the mismatch between the initial bunch structure of the  $\mu$ -source and the desired  $\mu$ -collider bunch configuration. The primary proton beam from a rapid-cycling synchrotron (RCS) would consist of  $\sim 100$ – $200$  bunches, while compression to one (or a few)  $\mu$ -collider bunches is desired. Phase-space manipulations will be needed.

Bunch combination procedures could include:

1. **Proton-bunch Overlap:** Before extraction from the RCS, the proton bunches can be compressed with a lower harmonic (or sideband) rf system to provide spatially overlapping bunches (with different momenta) on the target. Since target spot sizes need not be very small and  $\pi$ -production is not energy-dependent, a broad primary energy spread can be accepted at the target, with no degradation of  $\pi$ -production. Combination by at least a factor of 10 should be obtainable. A separate extraction-

energy proton compressor ring for the rf bunch manipulations may be desired.

2. Non-Liouvillian "Stochastic Injection"<sup>9</sup>: Bunch-combination without phase-space dilution can occur during  $\pi$ -decay, as in "stochastic injection" into a  $\mu$ -storage ring, as shown in figure 5. In this process a train of  $\pi$ -bunches from a hadronic target, is injected into a decay channel, which is also a zero-dispersion straight-section of a  $\mu$ -storage ring. The  $\pi$ -bunch spacing is matched to the storage ring period (or a low harmonic). The injected  $\pi$ 's are not in the acceptance of the ring; the ring accepts lower-energy particles and, in particular, those  $\mu$ 's from  $\pi$ -decay in the straight section that are within that acceptance. Successive  $\pi$ -bunch arrivals are timed to overlap an accumulated  $\mu$ -bunch. The  $\pi$ -lifetime is  $\approx 1\%$  of the  $\mu$ -lifetime, and is naturally matched for decay within the first-turn decay channel, while permitting multiple turn accumulation. At reasonable parameters,  $\mu$ 's from 10—30  $\pi$ -bunches can be accumulated in a single bunch, without large  $\mu$ -decay losses. (The storage ring can also be used for cooling the accumulated  $\mu$ 's.)

3. Beam Cooling with Bunch Combination: Transverse or energy cooling of  $\mu$ -bunches can compress beams to a degree where bunches can be stacked together, using conventional Liouvillian bunch-combination optics. The stacked bunch can then be further cooled to a phase-space volume  $\leq$  the previous cooled single-bunch size. The process can continue through further stacking and cooling steps. The process adds the complications of multiple beam-combination transport lines and optics; however, combinations of many bunches (10—100) could be obtained.

Some combination of these three (plus other to-be-developed) methods can be used to reduce the number of  $\mu$  bunches to a few enhanced-intensity bunches. (The first two procedures are complementary: proton bunch stacking combines nearby bunches while stochastic injection more naturally combines widely spaced bunches.) Ionization cooling can then be used for further compression, in bunch-length or energy spread, for optimal collider use.

### Acceleration and Collider Scenarios

Cooled and compressed  $\mu$  bunches can be used in high-energy high-luminosity colliders. In this section, we describe some potential scenarios. We use as a reference case a 1 TeV per beam  $\mu^+ - \mu^-$  collider (2 TeV in the center-of-mass), as this is the energy scale where the  $\mu^+ - \mu^-$  collider may begin to be preferable to  $e^+ - e^-$  colliders. Table 1 shows a reference case, with relatively conservative choices of parameters.

1. Linac-Storage Ring - This scenario is displayed graphically in Figure 1, and this is probably the highest-luminosity case.  $\mu^+ - \mu^-$  bunches from the collector/cooler

are both accelerated to full energy in a high-gradient linac to 1 TeV, where both bunches are injected into a superconducting storage ring for high-energy collisions at low- $\beta_0$  interaction points. The  $\mu$  beam lifetime is  $\sim 300 B$  turns, where  $B$  is the mean bending field in T.  $B = 8T$ , implying 2400 turns, is currently achievable. The main difficulty is the relatively large cost of the full-energy TeV linac.

2. Linac-Linac collider - As in  $e^+e^-$  linear colliders,  $\mu$  bunches from opposing linacs can collide. This scenario loses the luminosity magnification obtained from multiple collisions in a storage ring, which is permitted by the long  $\mu$  lifetime. It also requires two full-energy linacs, and a TeV storage ring is cheaper than a TeV linac. However, an existing  $e^+e^-$  linear collider could be modified to obtain  $\mu^+-\mu^-$  collisions, with the addition of a  $\mu$ -source.

3. Rapid-cycling Synchrotron Collider - At 1 TeV, the  $\mu$  lifetime has increased to 0.021s, and the lifetime increase with energy is sufficient to permit acceleration in a rapid-cycling synchrotron with acceptable losses. Figure 6 shows the basic components: a  $\mu$ -source injected into a  $\sim 20$ – $50$  GeV linac followed by a rapid cycling synchrotron with 20 km circumference ( $B = 1T$ ). Acceleration from injection to full energy in  $\sim 50$ – $100$  turns could follow a 60–120 Hz waveform followed by  $\sim 0.02$ s at fixed field for collisions or, for higher luminosity, transfer to a fixed-field (8T) collider ring. Luminosity would be naively expected to be about an order of magnitude smaller than in the linac-storage ring scenario.

4. The  $\mu$ -p Collider - A  $\mu^+-\mu^-$  collider can also be operated as a  $\mu^-$ -p collider with both  $\mu$  and p beams at full energy. High luminosity would be relatively easily obtained because only one beam ( $\mu$ ) is unstable and diffuse. This is a probable initial and debugging operating mode for a storage ring  $\mu^+-\mu^-$  collider. Revolution frequencies of equal energy  $\mu$  and p beams would be naturally mismatched because of unequal speeds. They can be rematched by displacing the beams in energy and using the ring nonisochronicity.<sup>2</sup> The required energy displacement is

$$\frac{\delta E}{E} = \gamma_T^2 \left( \frac{1}{2\gamma_p^2} - \frac{1}{2\gamma_\mu^2} \right) \quad (8)$$

where  $\gamma_T$  is the ring transition-gamma. At reference parameters ( $E_\mu = 1$  TeV,  $\gamma_T = 30$ )  $\delta E/E = 0.0005$  is required.

5. Physics-Opportunity Colliders - A resonance, such as a new Z particle or a Higgs particle, may exist or be predicted in  $\mu^+-\mu^-$  collisions. At such a resonance, a lower luminosity and/or lower energy collider could still provide extremely important physics. Such a collider would be a simplified form of the baseline high-luminosity

models, possibly with  $\mu$ -sources using existing accelerators, omitting  $\mu$ -cooling, and/or using existing storage rings for collisions. Such a facility would, of course, provide excellent training for a high-energy high-luminosity collider.

### Luminosity Possibilities and Constraints

Using the previously discussed techniques, high luminosity can be obtained in a  $\mu^+ - \mu^-$  collider. The luminosity is given by the equation:

$$L = \frac{f_C N^+ N^-}{4\pi\sigma^2} = \frac{f_C N^+ N^-}{4\pi\beta_0 \epsilon_{\perp}} \quad (9)$$

where  $N^+$ ,  $N^-$  are the number of  $\mu^+$ ,  $\mu^-$  per colliding bunch,  $f_C$  is the frequency of bunch collisions,  $\sigma^2$  is the colliding beam size,  $\beta^0$  is the betatron function at the collision point and  $\epsilon_{\perp} = \epsilon_N/\gamma$  is the transverse emittance. In a storage-ring collider,  $f_C = f_0 n_B n_S$ , where  $f_0$  is the system cycling rate,  $n_B$  is the number of bunches, and  $n_S$  is the number of turns of storage per cycle.

This formula is applied to a reference TeV  $\mu^+ - \mu^-$  collider (Table 1). The parameters we use include  $N^+ = N^- = 10^{11}$  (which can be obtained assuming a modest production rate of  $10^3 \mu/p$  from  $10^{14}$  proton high-energy pulses),  $n_B = 1$ ,  $f_0 = 30$  Hz, and  $n_S = 1200$  turns storage. With  $\epsilon_N = 10^{-4}$  m-rad ( $\epsilon_{\perp} = 10^{-8}$ ) from  $\beta^0 = 1$  cm and  $\beta_0 = 1$  mm ( $\sigma = 3 \mu\text{m}$ ), we obtain a respectable baseline luminosity of  $L = 3 \times 10^{32}$ .

Note that the above parameter set is relatively modest, and improvements in some of the parameters (i. e.,  $N^+$ ,  $N^-$ ,  $\sigma$ ) by up to an order of magnitude are conceivable. However, reliable accomplishment of high luminosity in a novel and complicated facility which uses unstable particles and has several difficult design components will still not be easy.

Luminosity in a  $\mu^+ - \mu^-$  collider ring may be expected to be limited by the beam-beam interaction. Since long-term stability is not needed, the allowable beam-beam tune shift should be somewhat greater than the  $e^+ - e^-$  storage limit of  $\Delta\nu < -0.05$ . The tune shift is given by

$$\Delta\nu = \frac{N r_{\mu} \beta_0}{4\pi\gamma\sigma^2} \quad (10)$$

where  $r_{\mu} = 1.363 \times 10^{-17}$  m. At the baseline parameters  $\Delta v = 0.001$ ; luminosity would have to be increased dramatically for the beam-beam limit to be significant.

A  $\mu^+ - \mu^-$  collider has substantial beam power requirements, particularly in the primary proton beam. In the reference case, the requirements are  $10^{14}$  40 GeV protons at 30 Hz, which implies 20 MW beam power. This is an order of magnitude above present facilities, but is the same magnitude as proposed K-factories. (The high-energy  $\mu$  beams themselves require only 0.32MW.) More efficient  $\mu$ -production may be desirable (obtaining more  $\mu/p$ , using lower energy p's or a LEH source). However a high-luminosity high-energy  $\mu^+ - \mu^-$  collider is a successor to SSC or TLC-size facilities, and on that scale, a K-factory type source is small. An even higher intensity source could be affordable.

A significant difficulty in a storage ring is that  $\mu$ 's decay ( $\mu \rightarrow e\nu\nu$ ), and decay electrons at  $\sim 0.3$  TeV will hit the walls of the storage ring. At the reference parameters, with half the  $\mu$ 's decaying during storage, we find 50 kW of  $\sim 0.3$  TeV electrons will be deposited evenly within a narrow strip on the inner wall of the ring. The ring must be designed to accept this.

The obtainable luminosity  $L$  is expected to increase with increasing end point energy  $E_{\mu}$ , as the  $\mu$  lifetime increases and the emittance and energy spreads are adiabatically damped. As discussed in reference (4), the beam size ( $\sigma^2$ ) at collision should decrease as  $E_{\mu}^{-2}$ , as both  $\beta^*$  and  $e_t$  can decrease. Cycle time would increase; however, the longer cycle time could permit accumulation of successive rapid-cycling proton pulses to obtain magnified-intensity  $\mu$ -bunches. The net effect is that  $N^+$  and  $N^-$  increase as  $E_{\mu}$  and  $f_c$  is reduced by  $E_{\mu}^{-1}$ . In all,  $L$  naturally increases as  $E_{\mu}^3$ . (Costs increase linearly with  $E_{\mu}$ .) This scaling would be expected to dominate until the  $E_{\mu} = 100-1000$  TeV region, where  $\mu$  synchrotron-radiation excludes  $\mu$  storage-ring colliders.

### Summary

In this paper, we have introduced concepts which show the promise of the development of high-luminosity TeV-scale  $\mu^+ - \mu^-$  colliders. These initial concepts need considerable practical development. While key ingredients of a future facility have been introduced, further inventions and improvements are greatly desired. These concepts plus further developments must be integrated into a fully self-consistent design for a  $\mu^+ - \mu^-$  facility. The discussions at the first  $\mu^+ - \mu^-$  collider workshop at Napa, CA should elucidate the possibilities and set a basis for further development. Contributions and improvements from the workshop participants and other readers are encouraged. A functional  $\mu^+ - \mu^-$  collider will be obtained only through further innovation and development.

### Acknowledgments

I thank D. Cline, A. Ruggiero, J. D Biorken, S. Glashow, J. MacLachlan, H. A. Thiessen, R. Palmer and R. Noble (and any others I forgot) for important conversations contributing to the ideas expressed in this paper.

### References

1. D. Neuffer, *Particle Accelerators*, 14, 75 (1983).
2. D. Neuffer, *Proc. 12th Int. Conf. on High Energy Accelerators*, F. T. Cole and R. Donaldson, eds., 481 (1983).
3. E. A. Perevedentsev and A. N. Skrinsky, *Proc. 12th Int. Conf. on High Energy Accelerators*, F. T. Cole and R. Donaldson, eds., 485 (1983).
4. D. Neuffer, in *Advanced Accelerator Concepts*, AIP Conf. Proc. 156, 201 (1987).
5. M. Tigner, at *Third Int. Workshop on Adv. Accel. Concepts*, Port Jefferson, N. Y., to be published (1992).
6. C. L. Wang, *Phys Rev D9*, 2609 (1973) and *Phys. Rev. D10*, 3876 (1974).
7. R. Noble, at *Third Int. Workshop on Adv. Accel. Concepts*, Port Jefferson, N. Y., to be published (1992).
8. K. Nagamine, unpublished communication (1986).
9. D. Neuffer, *IEEE Trans. NS-28*, 2034 (1981).
10. D. Cline, unpublished communication (1992).

## Appendix

Since this report is appearing subsequent to the 1992 Napa  $\mu^+ - \mu^-$  Collider workshop, in this section, I am adding some initial impressions of the proceedings of the workshop.

D. Cline presented an interesting immediate application for a  $\mu^+ - \mu^-$  collider. There are theoretical reasons to believe that the Higgs boson might exist in the 90--180 GeV region, and that is an energy region at which only a  $\mu^+ - \mu^-$  Collider could obtain a clean observation of a Higgs boson. ( $\mu^+ - \mu^- \rightarrow H$  is favored because of the relatively large muon mass.) The observation would require luminosity greater than  $\sim 10^{29} \text{ cm}^{-2} \text{ s}^{-1}$ . Sample parameters with this luminosity goal are shown in Table 2. This relatively low-energy collider could be developed relatively inexpensively, possibly using existing facilities for major components, although it is unclear if any existing accelerator could deliver sufficient muon intensity. An important future goal is developing an optimal short-term path to this extremely important physics goal.

At the workshop, it was speculated that maximal muon production could be obtained from a hadronic (or leptonic) cascade source, possibly at a beam dump, rather than the single-interaction source outlined above. H. Thiessen suggested that the most efficient source may be a  $\sim 5$  GeV hadronic source. Serious target problems were noted for any high-intensity source. Further study/optimization is needed.

In beam cooling, the limitations on ionization cooling due to multiple scattering (described above) were discussed. It may be possible to have a muon source with initial emittance smaller than the multiple scattering limit, and therefore to avoid cooling.

The bunch combination/compression (see above) was identified as a key problem, particularly bunch length reduction to match small  $\beta^*$  optics. At multi-GeV energies, the muons will be relativistic and have no longitudinal motion within a linac. However, relativistic muon bunches can be compressed with an rf-induced energy tilt and transport through a bending arc (or ring). Scenario design/optimization is needed.

Although the workshop did not identify a clear path to a sufficient luminosity design, it did show important (and perhaps obtainable) physics goals, particularly the Higgs discovery opportunity. Future study goals, particularly in source design and scenario development, were identified, and the need for future workshop(s) after further development was suggested.

Figure 1. Overview of a linac-based  $\mu^+ - \mu^-$  collider, showing a hadronic accelerator, which produces  $\pi$ 's on a target, followed by a  $\pi$ -decay channel ( $\pi \rightarrow \mu \nu$ ) and  $\mu$ -cooling system, followed by a  $\mu$ -accelerating linac, feeding into a high-energy storage ring for  $\mu^+ - \mu^-$  collisions. (The linac could be replaced by a rapid-cycling ring, see Fig. 6).

Figure 2. Schematic view of  $\mu$ -production from  $\pi$ -decay, with  $\pi$ 's produced from hadrons. A high-energy hadronic beam is focussed onto a target; a collector lens(es) collects the resulting  $\pi$ 's into a strong-focussing "FODO" channel, where  $\pi$ -decay produces  $\mu$ 's for collider use.

Figure 3. Schematic view of transverse "ionization cooling." Energy loss in an absorber occurs parallel to the motion; therefore transverse momentum is lost with the longitudinal energy loss. Energy gain is longitudinal only; the net result is a decrease in transverse phase-space area.

Figure 4. Enhancement of energy cooling by using a wedge absorber placed in a non-zero dispersion region. The thickness of the absorber depends on transverse position ( $\Delta = \delta_0 + (d\delta/dx) x$ ), and the position at the absorber depends on the energy ( $x = \eta (AE/E)$ ), producing an enhanced energy dependence of energy loss, decreasing energy spread. Energy recovery in the accelerator is independent of energy. (Transverse cooling decreases with enhanced energy cooling.)

Figure 5. Schematic view of "stochastic injection" into a storage ring. A train of p-bunches produces  $\pi$ -bunches, which are injected into a storage ring for multi-turn stacking. The initial spacing is matched to a ring harmonic ( $h=2$  in the figure), so that following  $\pi$ -bunches overlap accumulated  $\mu$ 's from previous bunches.  $\pi$ -decays in the straight section which produce  $\mu$ 's within the ring acceptance add to the accumulation. (Note that the short but finite  $\pi$  lifetime is nearly optimally matched to make this scheme practical.)

Figure 6. Overview of a  $\mu^+ - \mu^-$  collider, with a rapid-cycling synchrotron for the primary accelerator. The figure shows a primary proton source, producing  $\pi$ 's on a target, which decay to  $\mu$ 's in a decay channel. After cooling and compression,  $\mu^+ - \mu^-$  bunches are accelerated in a linac and in a rapid-cycling synchrotron to full energy, where they are injected into a high-field storage ring for multi-turn collisions. For example, a 20-GeV linac feeding into a 20 GeV/turn (at 1.2 T) rapid-cycling synchrotron would produce 1 TeV  $\mu^+ - \mu^-$  beams with acceptable decay losses.

Table I Parameter List for TeV  $\mu^+ - \mu^-$  Collider  
(2 TeV Collisions)

<u>Parameter</u>	<u>Symbol</u>	<u>Value</u>
Energy	$E_{\mu\pm}$	1 TeV
Luminosity	$L$	$3 \cdot 10^{32} \text{ cm}^{-2}\text{s}^{-1}$
<u>HEH-Source Parameters</u>		
Proton energy	$E_p$	40 GeV
$P$ /pulse	$N_p$	$10^{14}$
Pulse rate	$f_0$	30 Hz
$\mu$ production efficiency	$\mu/p$	$10^{-3}$
<u>Collider Parameters</u>		
# $\mu^+/\mu^-$ per bunch	$N^\pm$	$10^{11}$
# bunches	$n_B$	1
Storage turns	$n_s$	1200
$\mu$ emittance	$\epsilon_\perp = \frac{\epsilon_N}{\gamma}$	$10^{-8} \text{ m-Rad}$
Interaction focus	$\beta_0$	1 mm
Beam size	$\sigma$	$3 \mu\text{m}$

Table II Parameter List for 100 GeV  $\mu^+ - \mu^-$  Collider

<u>Parameter</u>	<u>Symbol</u>	<u>Value</u>
Energy	$E_{\mu\pm}$	100 GeV
Luminosity	$L$	$10^{29} \text{ cm}^{-2}\text{s}^{-1}$
Pulse rate	$f_0$	10 Hz
Storage turns	$n_s$	1000
# bunches	$n_B$	10
# $\mu^+/\mu^-$ per bunch	$N^\pm$	$10^{10}$
$\mu$ -emittance	$\epsilon_\perp = \frac{\epsilon_N}{\gamma}$	$10^{-7} \text{ m-Rad}$
Interaction- $\beta$	$\beta^*$	1 cm
Beam size (at IR)	$\sigma$	30 mm

### μ LINAC-STORAGE RING SYSTEM

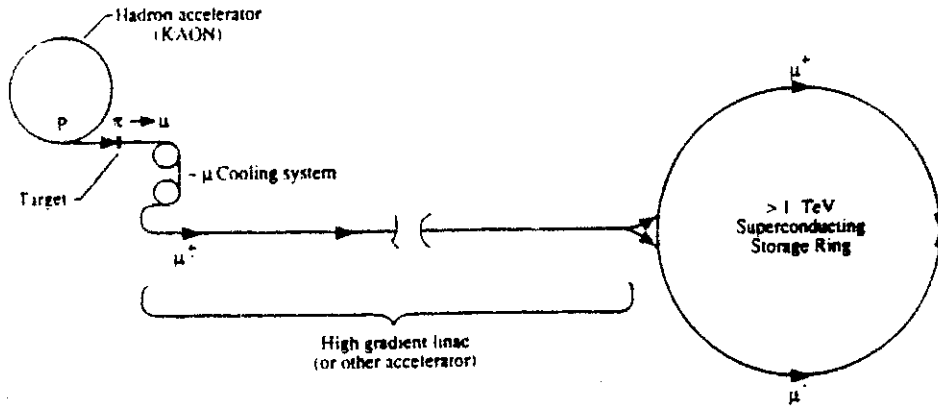


Figure 1. Overview of a linac-based  $\mu^+ - \mu^-$  collider, showing a hadronic accelerator, which produces  $\pi$ 's on a target, followed by a  $\pi$ -decay channel ( $\pi \rightarrow \mu \nu$ ) and  $\mu$ -cooling system, followed by a  $\mu$ -accelerating linac, feeding into a high-energy storage ring for  $\mu^+ - \mu^-$  collisions. (The linac could be replaced by a rapid-cycling ring, see Fig. 6).

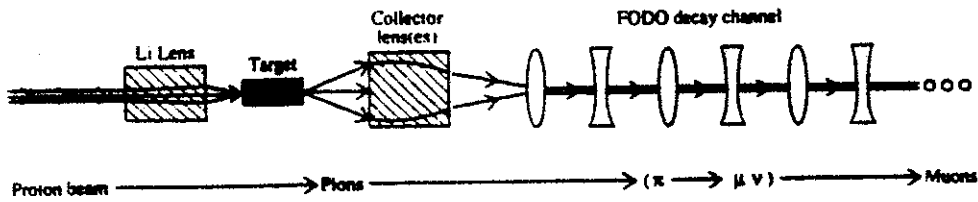


Figure 2. Schematic view of  $\mu$ -production from  $\pi$ -decay, with  $\pi$ 's produced from hadrons. A high-energy hadronic beam is focussed onto a target; a collector lens(es) collects the resulting  $\pi$ 's into a strong-focussing "FODO" channel, where  $\pi$ -decay produces  $\mu$ 's for collider use.

SKETCH OF TRANSVERSE "IONIZATION COOLING" PRINCIPLE

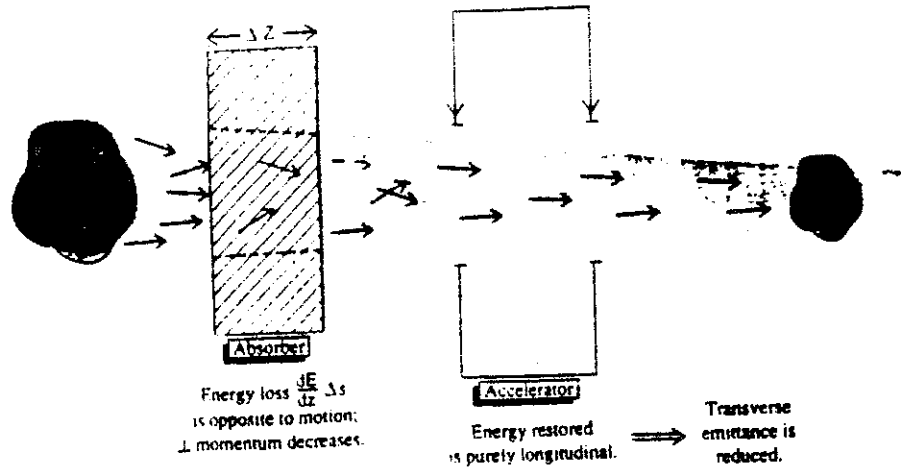


Figure 3. Schematic view of transverse "ionization cooling." Energy loss in an absorber occurs parallel to the motion; therefore transverse momentum is lost with the longitudinal energy loss. Energy gain is longitudinal only; the net result is a decrease in transverse phase-space area.

USE OF "WEDGE" ABSORBER TO ENHANCE ENERGY COOLING

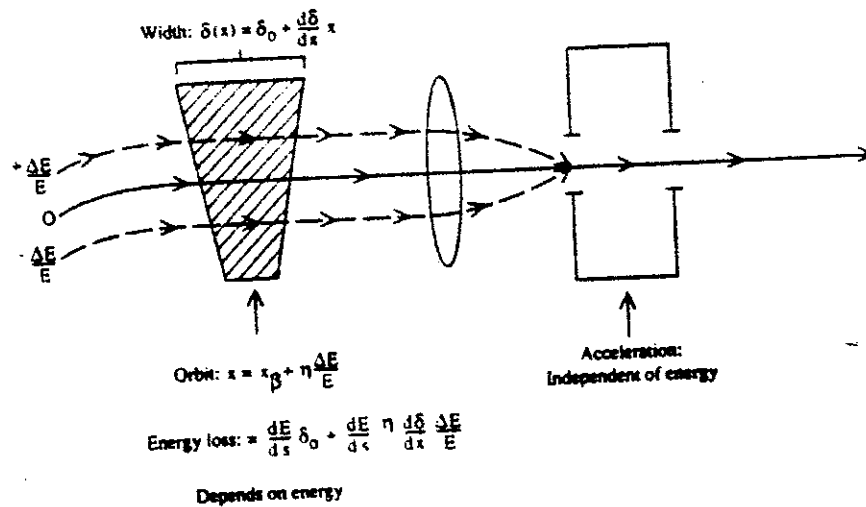


Figure 4. Enhancement of energy cooling by using a wedge absorber placed in a non-zero dispersion region. The thickness of the absorber depends on transverse position ( $\Delta = \delta_0 + (d\delta/dx) x$ ), and the position at the absorber depends on the energy ( $x = \eta (\Delta E/E)$ ), producing an enhanced energy dependence of energy loss, decreasing energy spread. Energy recovery in the accelerator is independent of energy. (Transverse cooling decreases with enhanced energy cooling.)

## SCHEMATIC VIEW OF "STOCHASTIC INJECTION"

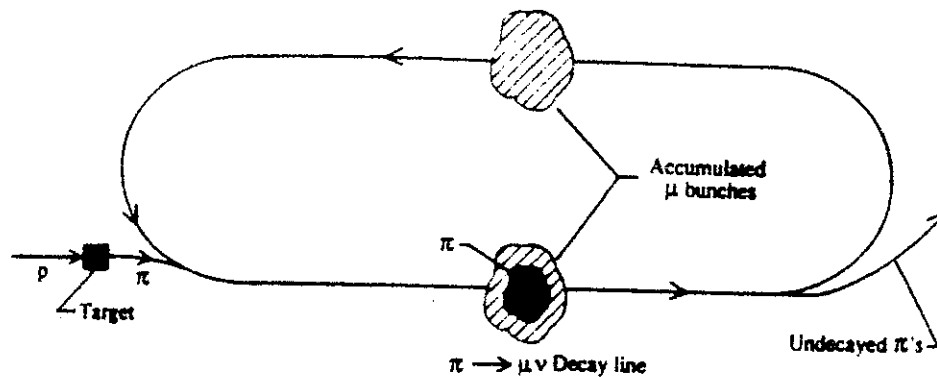


Figure 5. Schematic view of "stochastic injection" into a storage ring. A train of p-bunches produces  $\pi$ -bunches, which are injected into a storage ring for multi-turn stacking. The initial spacing is matched to a ring harmonic ( $h=2$  in the figure), so that following  $\pi$ -bunches overlap accumulated  $\mu$ 's from previous bunches, so that following  $\pi$ -bunches overlap accumulated  $\mu$ 's from previous bunches.  $\pi$ -decays in the straight section which produce  $\mu$ 's within the ring acceptance add to the accumulation. (Note that the short but finite  $\pi$  lifetime is nearly optimally matched to make this scheme practical.)

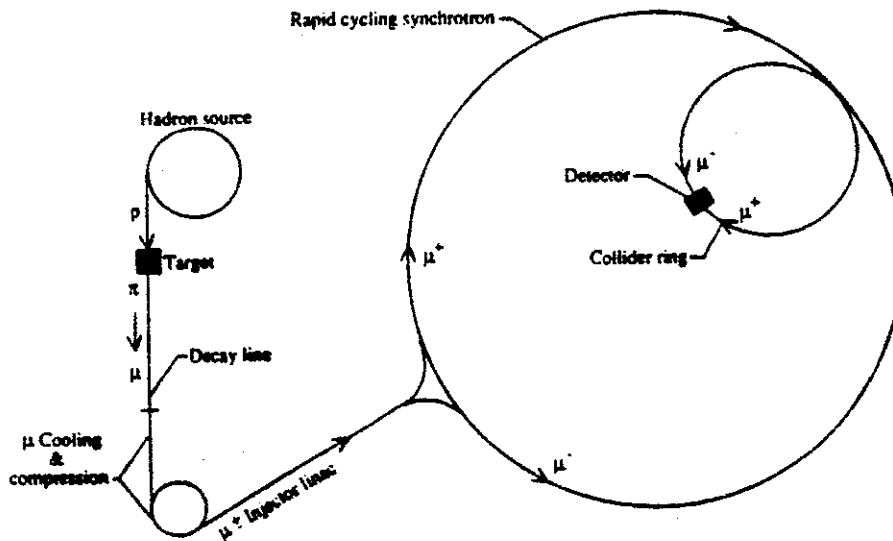


Figure 6. Overview of a  $\mu^+ - \mu^-$  collider, with a rapid-cycling synchrotron for the primary accelerator. The figure shows a primary proton source, producing  $\pi$ 's on a target, which decay to  $\mu$ 's in a decay channel. After cooling and compression,  $\mu^+ - \mu^-$  bunches are accelerated in a linac and in a rapid-cycling synchrotron to full energy, where they are injected into a high-field storage ring for multi-turn collisions. For example, a 20-GeV linac feeding into a 20 GeV/turn rapid-cycling synchrotron (at 1.2 T) would produce 1 TeV  $\mu^+ - \mu^-$  beams with acceptable decay losses.

$\mu^+ - \mu^-$  Colliders (93)

Possibilities

& Challenges

- D Newffer, CEBAF

# Outline

- I: Introduction
- II:  $\mu^\pm$  production & collection
- III:  $\mu^\pm$  cooling and compression
- IV: Acceleration / Collider scenarios
- V: Luminosity & constraints

for  $\mu^+ \mu^-$  Collider Workshop

- Motivation: TeV or 200 GeV
- Scenario Overview
- $\mu^\pm$  source
- $\mu^\pm$  cooling - stochastic, ionization
- bunch combination / multibunch
- Future Plans

## Motivation

I After SSC pp 20x20 T  
TLC ee 0.5 x 0.5

What? (Port Jefferson AAC works  
→  $e^+e^-$  limited by "radiation" effects

⇒  $\mu^+ \mu^-$  at many TeV?

II "Higgs Factory" D.Cline

$\mu^+ \mu^- \rightarrow H_0 \rightarrow b\bar{b}$

50 GeV  $\approx m_H \approx 200$  GeV

Theory:  
Cabibbo: If GUT and  $m_t < 2 M_Z$

then  $m_H < 2 M_Z$

Kane:  $2(M_1 - M_2) < m_H < 2 M_2$

2) If  $m_H > 2M_2$ , Higgs will  
 be easy to see at LHC/SSC  
 $H \rightarrow Z^+ Z^-$   $0.2 \lesssim m_H \lesssim 0.5 \text{ TeV}$

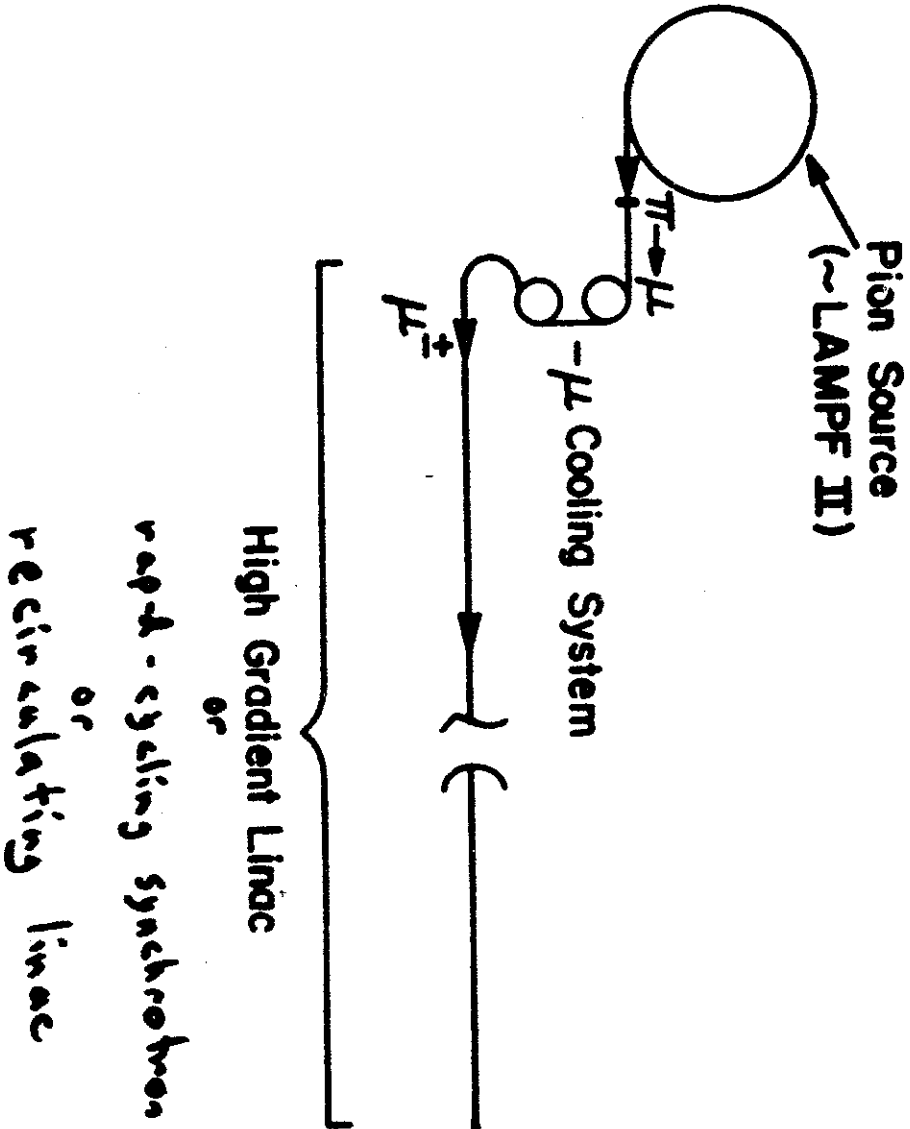
For  $m_H \lesssim 200 \text{ GeV}$ ,

$\mu^+ \mu^-$  collider is only "clean"  
 way of observing Higgs

need  $L_{\mu\mu} \gtrsim 10^{29} \text{ cm}^{-2} \text{ s}^{-1}$

# $\mu$ Lincac - Storage Ring System

0 1 2 4 1 9 1 2



$$N_{\mu} = \frac{300 \text{ B} (\text{T})}{\text{turns}}$$



Table I Parameter List for TeV  $\mu^+ - \mu^-$  Collider  
(2 TeV Collisions)

<u>Parameter</u>	<u>Symbol</u>	<u>Value</u>
Energy	$E_{\mu^\pm}$	1 TeV
Luminosity	$L$	$3 \cdot 10^{32} \text{ cm}^{-2}\text{s}^{-1}$
<u>HEH-Source Parameters</u>		
Proton energy	$E_p$	40 GeV
P/pulse	$N_p$	$10^{14}$
Pulse rate	$f_0$	30 Hz
$\mu$ production efficiency	$\mu/p$	$10^{-3}$
<u>Collider Parameters</u>		
# $\mu^+/\mu^-$ per bunch	$N^\pm$	$10^{11}$
# bunches	$n_B$	1
Storage turns	$n_s$	1200
$\mu$ emittance	$\epsilon_\perp = \frac{\epsilon_N}{\gamma}$	$10^{-6} \text{ m-Rad}$
Interaction focus	$\beta_0$	1 mm
Beam size	$\sigma$	$3 \mu\text{m}$

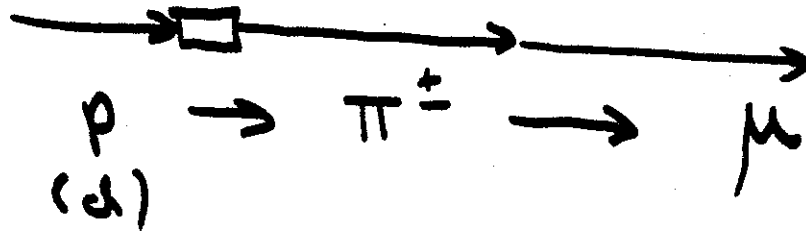
Table II Parameter List for 100 GeV  $\mu^+ - \mu^-$  Collider

<u>Parameter</u>	<u>Symbol</u>	<u>Value</u>
Energy	$E_{\mu^\pm}$	100 GeV
Luminosity	$L$	$4 \cdot 10^{29} \text{ cm}^{-2}\text{s}^{-1}$
Pulse rate	$f_0$	10 Hz $\rightarrow$ 100
Storage turns	$n_s$	1000
# bunches	$n_B$	10 $\rightarrow$ 4
# $\mu^+/\mu^-$ per bunch	$N^\pm$	$10^{10}$
$\mu$ -emittance	$\epsilon_\perp = \frac{\epsilon_N}{\gamma}$	$10^{-7} \text{ m-Rad}$
Interaction- $\beta$	$\beta^*$	1 cm
Beam size (at IR)	$\sigma$	30 $\mu\text{m}$ - $\mu$

# Baseline Scenario

— Muon Source:

High-Intensity Hadronic Accelerator

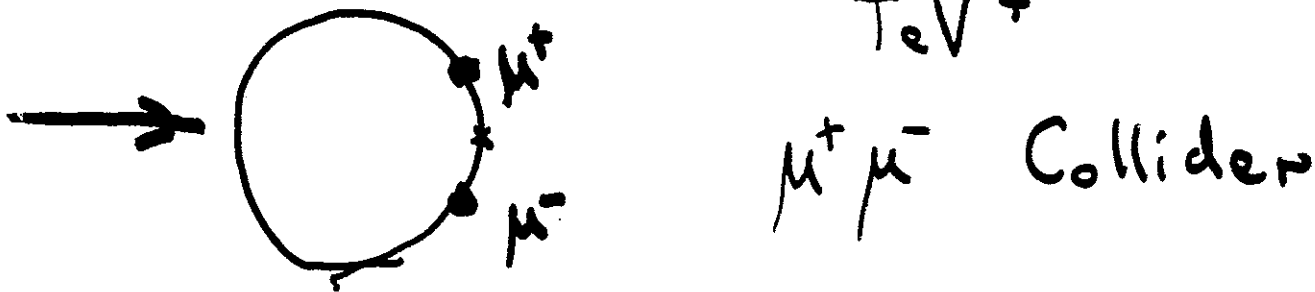


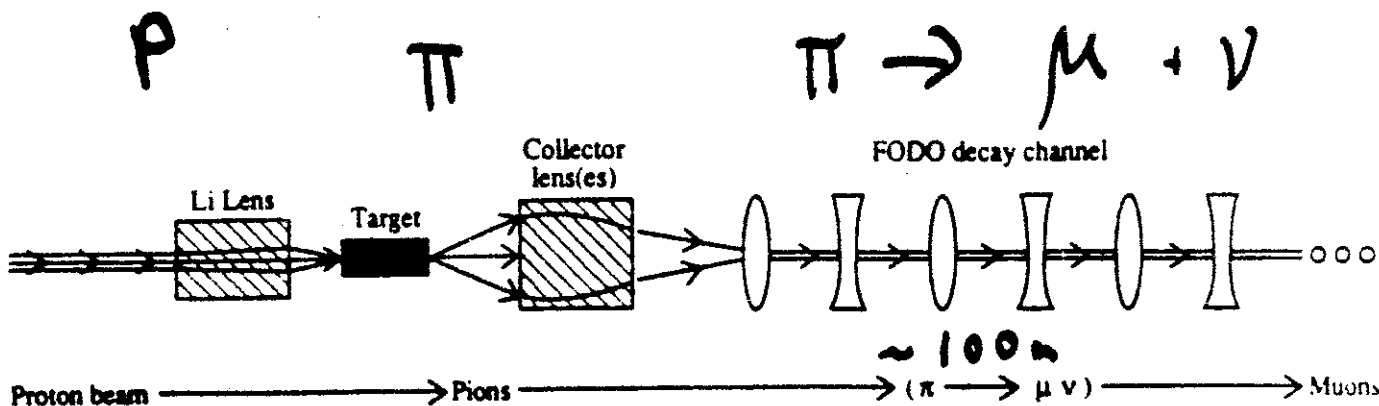
— μ Compression & damping



— Acceleration & collisions

Linac <sup>and/or</sup> Synchrotron  $\Rightarrow$  Collider Ring  
TeV<sup>+</sup>



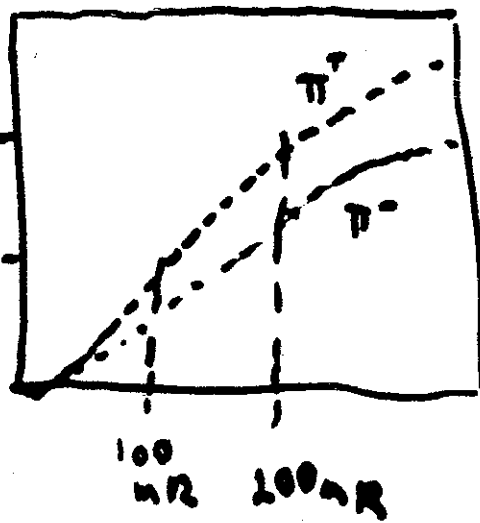


Example:

40 GeV p  $\rightarrow$  2 GeV  $\pi$

$\Rightarrow 0.1 - 0.2 \pi / \text{GeV-c/proton}$

$\pi$ -decay



Want  
 $P_{\pi} \sim 10^{-3}$



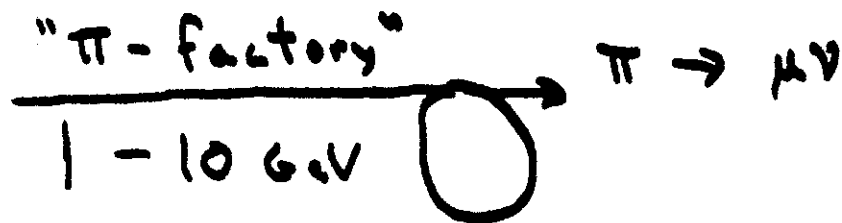
Assume  $\frac{\Delta E}{E} \sim \pm 5\%$

$\Rightarrow$  After many inefficiency factors

$\frac{N_{\mu^{\pm}}}{p} > 10^{-3}$   
 (Mob)

Other possible  $\mu$  sources

1. Lower Energy p/d source



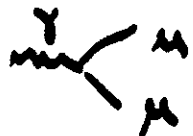
Nagamine-surface  $\mu$

Noble - acceptance difficult at  $E \rightarrow 0$

most efficient? 5 GeV? HAT

2.  $e^-$  photo production

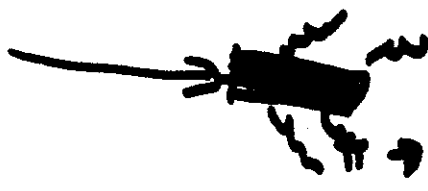
P. Chen / K. MacDonald - Compton back-scatter



to increase yield

3. Hadronic (or  $e^+e^-$ ) Cascade

$\rightarrow$   $\sim$  beam dump



many large initial phase-space  $\mu$ -possible

4. Something else!!

? Collect & Compress  $\mu$ 's  
for Collider use



(GeV) source

(TeV) Collider

- Adiabatic Damping  $\times 10^9$
- "ionization cooling"  $\times 10^{3-4}$
- "stochastic injection"  $\times 10$
- + bunching / optics  $\times 10$
- + other (ideas / improvements) !!
- stochastic cooling?

# 1. Emittance Sources

in  $\mu^+$  Collector

1. target size

$$\Delta E \sim r_T \theta_{\text{collect}}$$

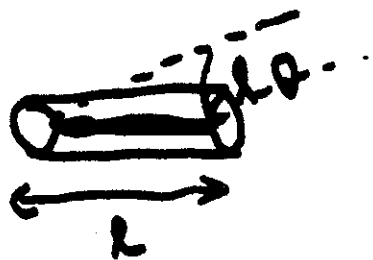
2mm  $\sim$  .1

Example (26)  $\mu^+$   
1.5 GeV

$$\Delta E \sim 10^{-4}$$

$$E_N \sim 1.5 \times 10^{-3}$$

2. depth of focus



$$\Delta E \sim \frac{r_T \theta^2}{2} E \sim 2 \times 10^{-4}$$

4cm W

$$E_N \sim 3 \times 10^{-3}$$

3.  $\pi$  decay



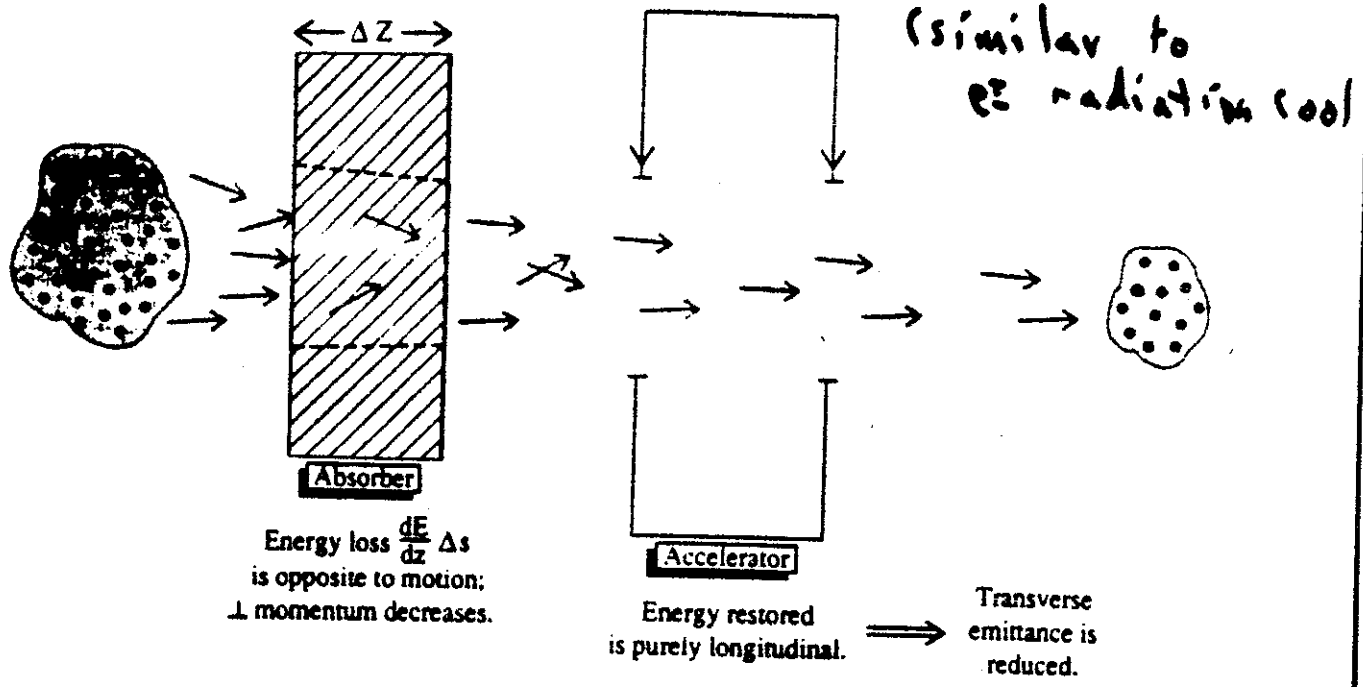
$$\Delta x \sim r_B \theta_{\text{decay}}$$

5mm  $p_{\perp} \sim 1.036 \text{ GeV}$   $E \sim 10^{-4}$   
 $E_N \sim 1.5 \times 10^{-3}$

\* ? ?

(Budker? O'Neill?)

SKETCH OF TRANSVERSE "IONIZATION COOLING" PRINCIPLE



$$\frac{d E_{\perp}}{d w} = - \frac{\int \frac{d E_{\perp}}{d z} E_{\perp}}{E_{\mu}} + \frac{\beta^*}{2} \Delta \theta^2$$

↑ cooling

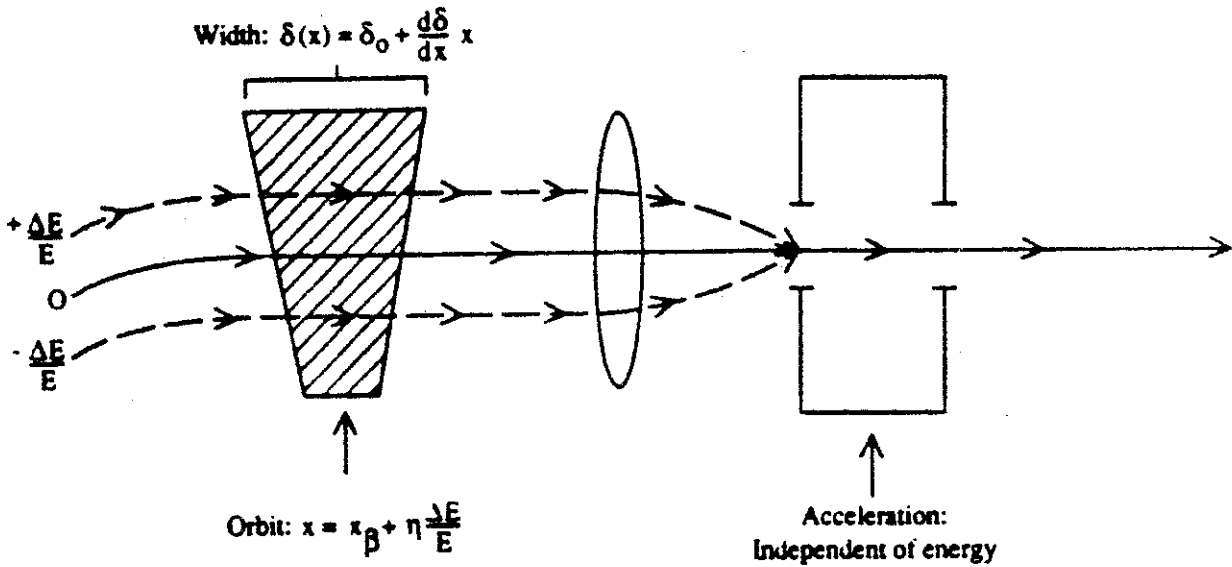
Limit

↑ Heating  
[multiple scattering]

$$E_{\perp, N} \rightarrow \frac{\beta^*}{2} (\Delta \theta)^2 E_{\mu} \gamma_{\mu} \rightarrow \underline{10^{-4} \text{ m-R?}}$$

# Energy Cooling also possible

USE OF "WEDGE" ABSORBER TO ENHANCE ENERGY COOLING



Energy loss:  $= \frac{dE}{ds} \delta_0 + \frac{dE}{ds} \eta \frac{d\delta}{dx} \frac{\Delta E}{E}$  (depends on Energy) mean  
loss

$$d \left\langle \frac{\Delta E^2}{\Delta \eta} \right\rangle = -2 \frac{\partial \left( \frac{dE}{ds} \right)}{\partial E_\mu} \Delta_s \langle \Delta E^2 \rangle + \frac{dE}{ds} \Delta_s$$

Cooling Heat

Energy Cooling  
Possible to  $\Delta E/E < 1\%$  (at 1 GeV  $\mu$ )

But

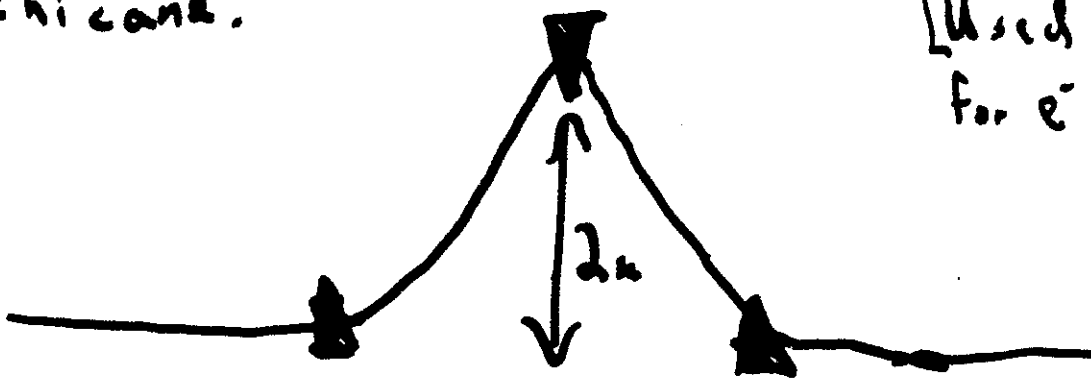
Longitudinal Bunch length reduction,  
Bunch combination needed



# Pulse Compression of Relativistic

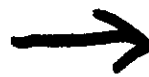
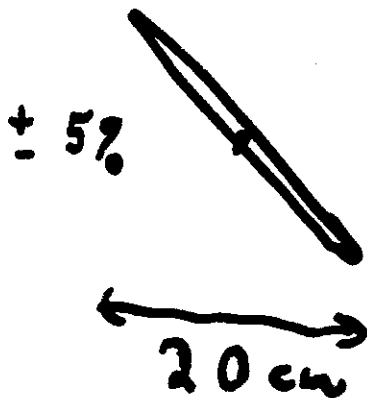
is possible!  
Simplest Example  
chicane:

[Used at CERN  
for  $e^-$  pulse comp.  
at 10 MeV]



path length depends on energy

$$MSL \sim \pi \theta \sim 2n \left( \frac{eas}{p} \right)$$



$$\frac{\Delta p}{p} \text{ comp}$$

ca?



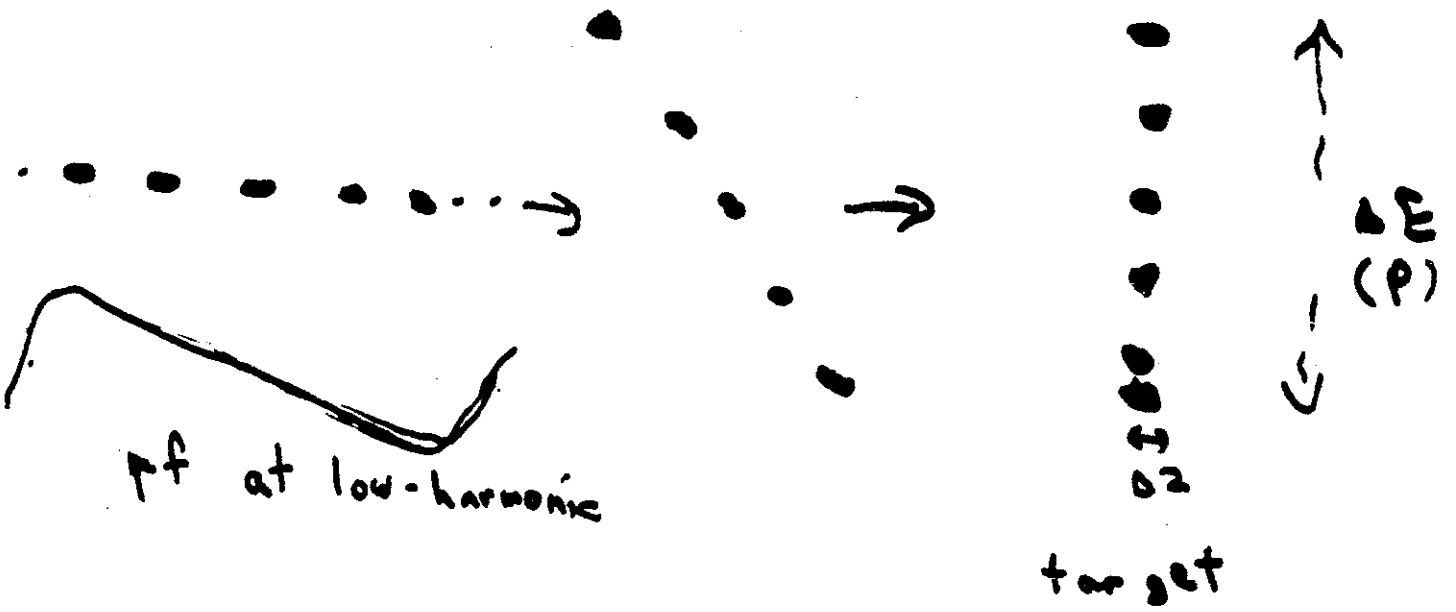
+ repeat

$$cn \rightarrow mn$$

# Bunch Combination Methods

p-ring  $h \approx 100 \rightarrow$

1) Bunch rotation in p-ring (Accumulat.)

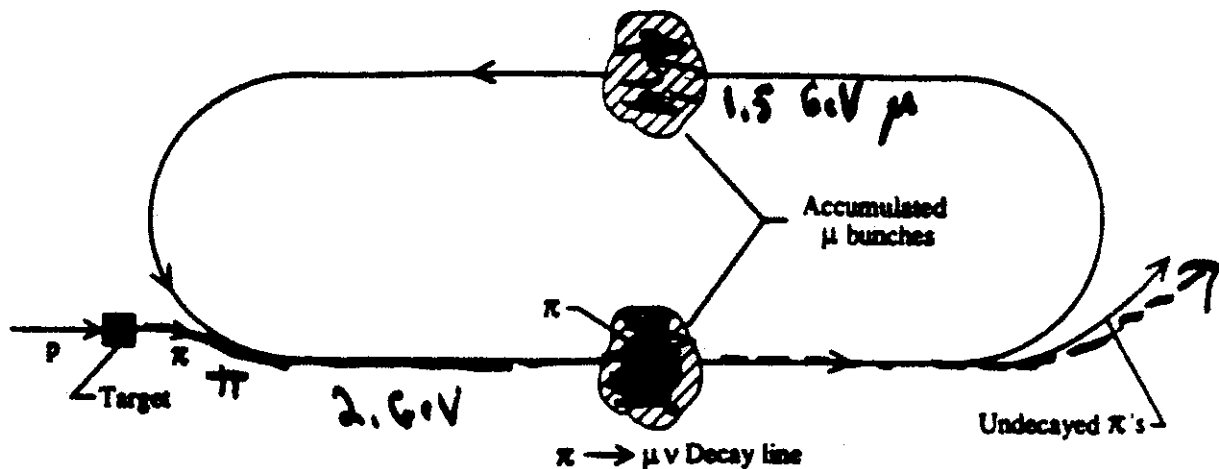


- combines nearby bunches

$x \approx 10$  possible

## 2) Stochastic Injection

SCHMATIC VIEW OF "STOCHASTIC INJECTION"



$\pi$ ' decay on top of circulating  $\mu$ 's

- multiturn stacking w no phase-space dilution
- complementary to p-bunch rotation

3) normal "Liouvillean" bunch combination

- combine w cooling to reduce phase space
- $\perp$  or  $\parallel$

4) Other Inventions?

## Parameter List for TeV $\mu^+\mu^-$ Collider

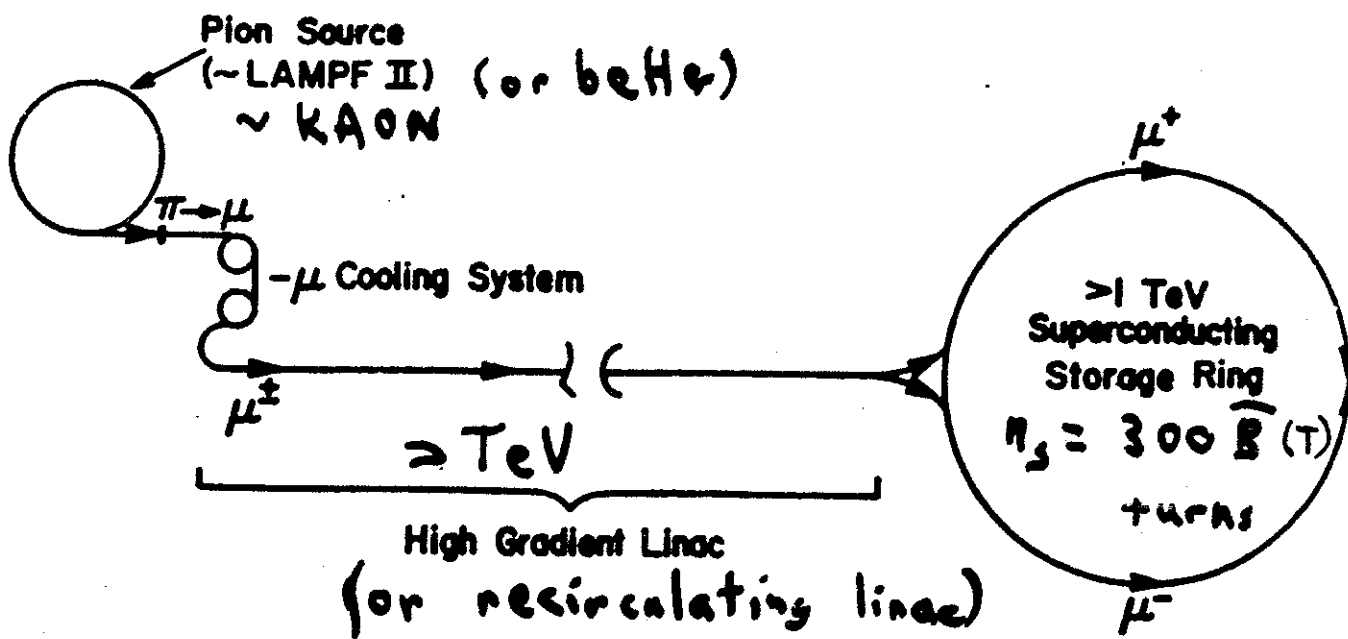
(2 TeV Collisions)

<u>Parameter</u>	<u>Symbol</u>	<u>Value</u>
Energy	$E_{\mu^\pm}$	1 TeV
Luminosity	$L$	$3 \cdot 10^{32} \text{ cm}^{-2}\text{s}^{-1}$
<u>HEH - Source Parameters</u>		
Proton energy	$E_p$	40 GeV } 20 MN
P/pulse	$N_p$	$10^{14}$
Pulse rate	$f_0$	30 Hz
$\mu$ production efficiency	$\mu/p$	<u><math>10^{-3}</math></u>
<u>Collider Parameters</u>		
# $\mu^+/\mu^-$ per bunch	$N^\pm$	$10^{11}$
# bunches	$n_B$	1
Storage turns	$n_s$	1200
$\mu$ emittance	$\epsilon_\perp = \frac{eN}{\gamma}$	$10^{-8} \text{ m-Rad}$
Interaction focus	$\beta_0$	1 mm
Beam size	$\sigma$	$3 \mu\text{m}$

clh[apd.neuffer]muonvg.tex, 12/7/92

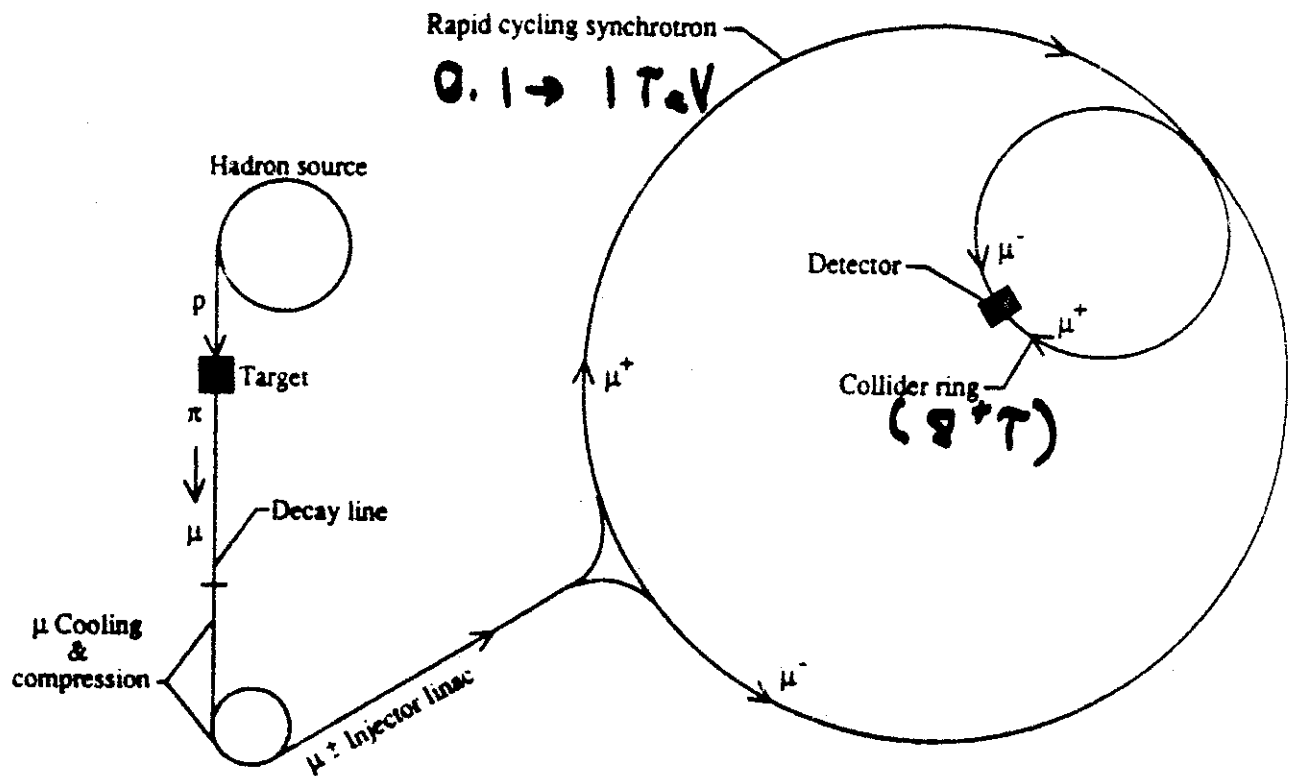
$$L = \frac{f_0 n_s N_b^+ N_b^- n_B}{4\pi \epsilon_\perp \beta_0}$$

# 1) $\mu$ Linac - Storage Ring System



- no decay loss in acceleration
- but
- large expense for TeV Linac
- \$

## 2) Rapid-Cycling Synchrotron Scenario



$\mu$  Lifetime = 300  $\bar{B}$  turns

Linac + ~ 30 turn acceleration in ring

→ Transfer to SC ring

Cheaper than linac-storage ring  
but more  $\mu$ -decay

## 3) 100 GeV "Higgs Factory"

Try to use existing facilities

- SLAC - ~ full energy linac, PEP  
tunnel  
(harder to make  $\mu$ 's  
from e's)

- LAMPF -  $\pi$  factory + linac upgrade  
+ compressor

Fermilab, BNL, CERN

(p's but not K-class intensity)

KAON - doesn't exist

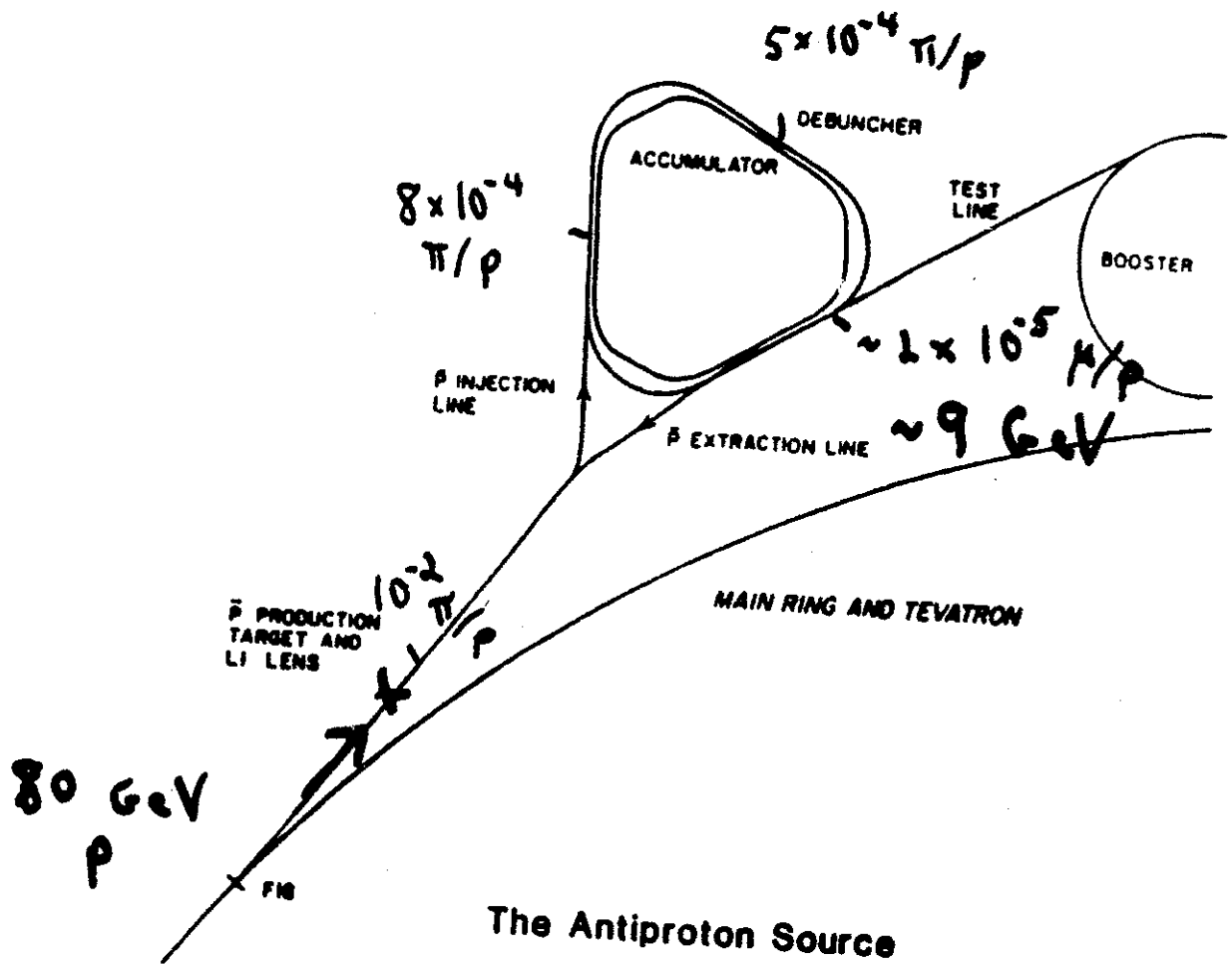
## Parameter List for 100-GeV

 $\mu^+\mu^-$  Collider

$$L = \frac{f_c N^+ N^-}{4\pi \sigma^2}$$

Parameter	Symbol	Value
Energy	$E_{\mu^\pm}$	100 GeV
Luminosity	$L$	$2 \cdot 10^{29} \text{ cm}^{-2} \text{ s}^{-1}$
Pulse-rate	$f_0$	100 Hz
Storage turns	$n_s$	1000
# bunches	$n_B$	2
# $\mu^+/\mu^-$ / bunch	$N^\pm$	$10^{10}$
$\mu$ -emittance	$e_\perp = \frac{E_N}{\gamma}$	$10^{-7} \text{ m-Rad}$
Interaction- $\beta$	$\beta^*$	1 cm
Beam-Size (at IR)	$a$	30 $\mu\text{m}$

Existing " $\mu^-$  accumulator"  $\approx$  Debuncher



The Antiproton Source

A. Bross, et al F N A L 92/357 (1992)  
C. Kim, W. Lee,

$\sim 2 \times 10^{-5} \mu / p$  accumulator

during  $\bar{p}$  production

$$\left[ \mu \approx \bar{p} \approx 2.5 \times 10^{-2} \pi \right]$$

Line designed for  $\bar{p}$  source  $\rightarrow$  cooler

Acceptance:  $\epsilon_{\perp} \sim 20 \pi \text{ mm-mr}$ ,  $\frac{\Delta p}{p} \sim \pm 2\%$

But

- $\pi$  losses large:  $10^{-2}/p \rightarrow 5 \times 10^{-4}/p$
- $\mu$  from  $\pi$  decay acceptance poor

$$A(\pi \rightarrow \mu) \sim .02 \mu/\pi \text{ (ring)}$$

$$\approx .01 \text{ (target transpo)}$$

$$\frac{2 \times 10^{-5} \mu}{p} \rightarrow ? 10^{-3} ?$$

- $\mu$  acceptance needs improvement

- Debuncher good benchmark for future scenarios

Not  $\mu^+ \mu^-$  Collider - ready  
 -  $\sim 80$  bunches  $\rightarrow ?$

$\mu^+ \mu^-$  Collider not impossible

but very difficult

feasible ingredients

but not a self-consistent,  
complete design

— need more ideas, inventions,  
improvements

$\mu^+$  source ?

collection, cooling ?

acceleration, collisions

Need more experiments on  $\mu^+$  source

+ ???

0 1 2 1 0 9 5 3

**Summary of NAPA Workshop  
Electrons as Source of Muons**

**William Barletta**

**UCLA**

## Characteristics of a high energy $\mu^+\mu^-$ collider based on electro-production of muons

William A. Barletta\* and Andrew M. Sessler†

January 9, 1993

**Abstract:** We analyze the design of an high energy  $\mu^+\mu^-$  collider based on electro-production of muons. We derive an expression for the luminosity in terms of analytic formulae for the electron-to-muon conversion efficiency and the electron beam power on the production target. On the basis of studies of self-consistent sets of collider parameters under "realistic" ("optimistic") assumptions about available technology with beam cooling, we find the luminosity limited to  $10^{27} \text{ m}^{-2}\text{s}^{-1}$  ( $10^{28} \text{ cm}^{-2}\text{s}^{-1}$ ). We also identify major technological innovations that will be required before  $\mu^+\mu^-$  colliders can offer sufficient luminosity ( $10^{30} \text{ cm}^{-2}\text{s}^{-1}$ ) for high energy physics research.

### 1. Introduction

Many physicists consider that the recent determinations of lower bounds for the mass of the top meson reinforce arguments that a Standard Model Higgs should have a mass less than twice the mass of the Z. This consideration has led to renewed interest in muon colliders as an ideal means of probing the mass range from  $m_Z$  to  $2m_Z$ . More generally, a muon collider with center-of-mass energy in the range of 200 to 400 GeV has the potential to produce very large numbers of Higgs particles because of the enhanced (vis á vis electrons) muon coupling to the Higgs. For such a collider to have maximum discovery potential the luminosity should be  $\geq 10^{30} \text{ cm}^{-2}\text{s}^{-1}$  [1]. As the muon is an unstable particle, the muons must be generated as secondary beams from either a proton beam or an electron beam striking a production target. The muons that emerge from the target must then be gathered and accelerated rapidly to high energy, at which point they can be injected into a storage ring collider with superconducting magnets.

This paper analyses the possibility of using electro-production to generate the muon beams. The chief advantage of producing the muons with an electron beam from a high energy, linear accelerator is that the bunches of muons are naturally formed with a short bunch length ( $< 1 \text{ cm}$ ) for acceleration to the desired high energy in a subsequent linear accelerator. As the muons will retain their short bunch length in the collider, a low  $\beta$  interaction region can be employed. This scheme is illustrated in Fig. 1.

---

\* Work performed under the auspices of the Lawrence Livermore National Laboratory under contract W-7405-eng-48.

† Work performed under the auspices of the Lawrence Berkeley Laboratory under contract DE-AC03-76SF00098.

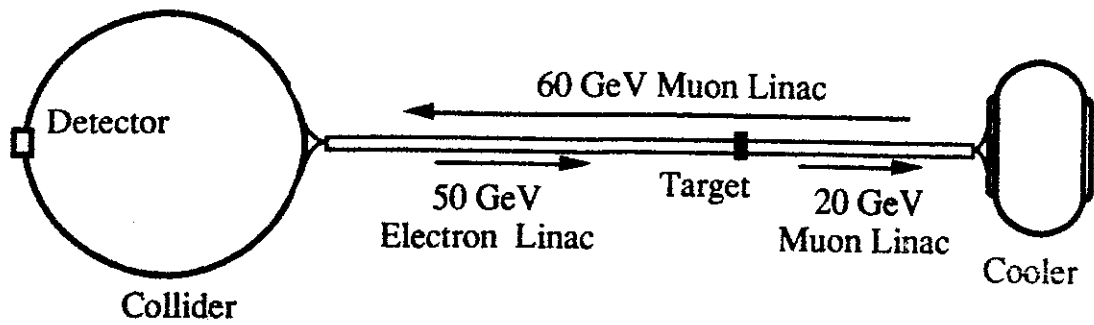


Figure 1. The scheme for a  $\mu^+\mu^-$  collider using electro-production.

2. Electro-production

Muons can be produced by an electron beam via two classes of processes, 1)  $\mu^+\mu^-$  pair production and 2) photo-production of  $\pi$ 's and K's, which subsequently decay into muons. It is known experimentally [2] that the cross-section for pair production is much more than an order of magnitude greater than that for process (2). Consequently, in the discussion that follows we will consider only pair production.

To estimate the muon pair production from an electron beam of energy,  $E_e$ , incident upon a thick target of atomic number  $Z$ , one can use the expression from Nelson [3] based on approximation A of shower theory.  $F$  is number of muons per electron produced at an angle  $\geq \phi$  with respect to the incident electron beam;

$$\frac{dF}{dE}(E_e, E, \phi) = \frac{1}{(2\pi)^2} \frac{m^2}{\mu^2} \frac{0.572 E_e \eta}{\mu^2 \ln(183 Z^{-1/3})} 2 \ln(\gamma_\mu) \times \left\{ (1 - v^2) - 0.33 [1 - 4v^3(1 - 0.75v)] \eta [1 + \lambda^2] \right\} \tag{1}$$

where  $m$  = electron mass,  $\mu$  = muon mass,  $E$  = energy of the muon at the production target,  $\gamma_\mu = E/\mu$  at the production target,  $v = E/E_e$ ,  $\lambda = \gamma^2 \phi^2$ , and  $\eta = (1+\lambda)^{-2}$ . Eq. (1) is known to overestimate the muon pair production by a factor of  $\approx 2$ .

The number of muons per electron accepted in an angle  $\leq \phi$ , in a momentum bite of  $\pm \Delta p/p$  at a muon energy  $E$  is

$$A_\mu = \left[ \frac{dF}{dE}(E_e, E, 0) - \frac{dF}{dE}(E_e, E, \phi) \right] E \frac{2 \Delta p}{p} \tag{2}$$

From eq. (2) it is immediately obvious that one will prefer to accept muons with a large value of  $E/E_e$  rather than with a small  $E/E_e$  as long as the function  $dF/dE$  is relatively flat in

energy. For small muon production angles this condition obtains for the energy range,  $0.2 < E/E_e < 0.8$ . The same consideration also argues that one should choose a large initial electron beam energy. Figures 2a) and 2b) display plots of eq. (2) for a low energy and a high energy production option respectively.

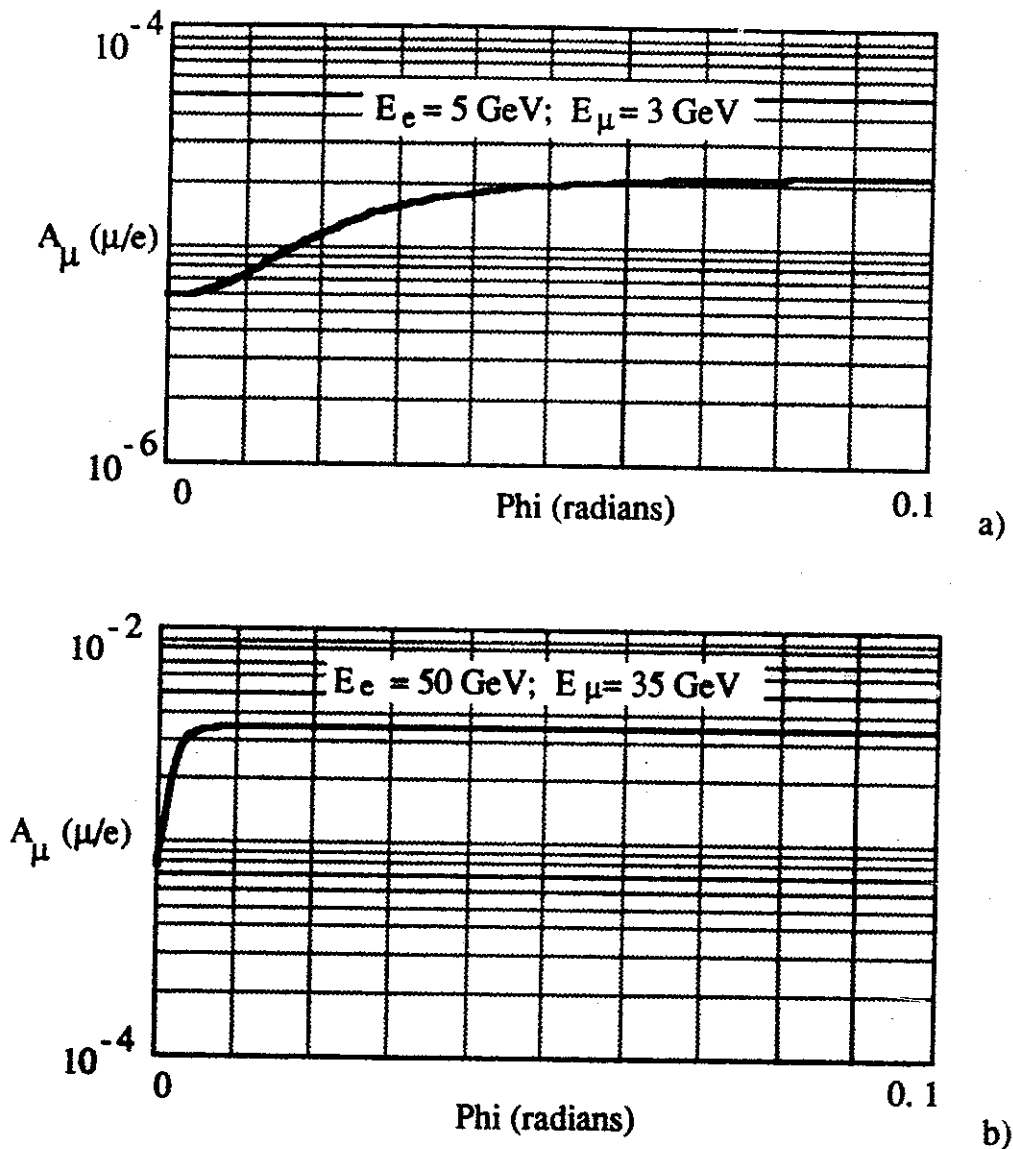


Figure 2. Number of  $\mu$  pairs per  $e^-$  accepted at an angle  $\leq \phi$  for a) a 5 GeV electron beam with  $E_\mu = 3$  GeV and b) a 50 GeV electron beam with  $E_\mu = 35$  GeV.

At the front surface of the production target the electron beam can be focused to a spot of radius,  $r_b \approx 1$  mm. The muons will, however, appear to originate from a somewhat larger spot with a size given by the radial extent of the electromagnetic shower at a depth

corresponding to the shower maximum, which occurs approximately six radiation lengths ( $6 X_0$ ) inside the target. The radiation length,  $X_0$ , for tungsten is 3 mm; hence the shower maximum will occur at  $\approx 20$  mm, and a tungsten target 30 mm long will yield almost the entire thick target conversion to muons.

At the depth corresponding to the shower maximum the primary electron beam will have suffered a mean scattering angle of

$$\Theta^2 = \left( \frac{0.028 \text{ GeV}}{E_e} \right)^2 \left( \frac{6 X_0}{X_0} \right), \quad (3)$$

which will induce a radial spread of  $6X_0\Theta$  in the primary beam. Actually in a high Z target, the shower will spread by an amount roughly double this value. Hence, the shower radius can be approximated by

$$r_{sh} = \left( r_b^2 + (12 \Theta X_0)^2 \right)^{1/2}. \quad (4)$$

At production the geometrical emittance,  $\epsilon(E)$ , of the muon beam of energy,  $E$ , accepted into an angle  $\phi_{accept}$  will be

$$\epsilon(E) = \frac{\epsilon_{n,prod}}{\gamma_{prod}} = r_{sh} \phi_{accept}, \quad (5)$$

where  $\epsilon_{n,prod}$  is the normalized emittance at production.

To increase the muon production efficiency one might consider alternate techniques of photo-production. The production process consists of two steps: 1) conversion of the electron energy into photons and 2) muon pair production from the photons. Rather than using bremsstrahlung, one might employ synchrotron radiation as the conversion process. Synchrotron radiation conversion could either take place in a crystal or in a plasma [4], which has an obvious advantage of being more amenable to high average power operation.

The choice of synchrotron radiation conversion is unlikely to increase the rate of muon production as the mean photon energy is lower for the synchrotron radiation photons than for the bremsstrahlung photons. The synchrotron radiation photons are more numerous, but only at low energies for which muon pair production is not energetically allowed. The angular distribution of the muons produced will be dominated by the spread of angles of the electrons in the primary beam as the average electron angle will be significantly larger than  $\gamma^{-1}$ .

The pair production rate in crystals is known experimentally [5] to be larger than in amorphous materials due to the coherent field effects. For photons of 100 GeV, the coherent production is a few times the Bethe-Heitler rate; however, for 20 GeV photons this effect increases pair production by only 10%. As the mean energy of bremsstrahlung photons is  $\approx 20\%$  of the incident beam energy, pair production in a crystal will not significantly enhance the muon yield for a 100 GeV per beam collider. Hence, in the analysis that follows we restrict our attention to the use of a conversion bremsstrahlung production target.

### 3. Ionization cooling

In designing a collider one will inevitably seek a means of having as low an emittance as possible for the beams. One suggested means of cooling the muons (Fig. 3) is to pass the beam through a succession of alternating slabs of material (ionization cells) and rf-accelerating sections. In the ionization cells each of the muons gives up momentum along its particular trajectory, thereby losing transverse and longitudinal momentum. In the accelerating sections the longitudinal momentum is restored to the beam. Thus the transverse emittance of the beam is reduced in a manner analogous to radiation damping.

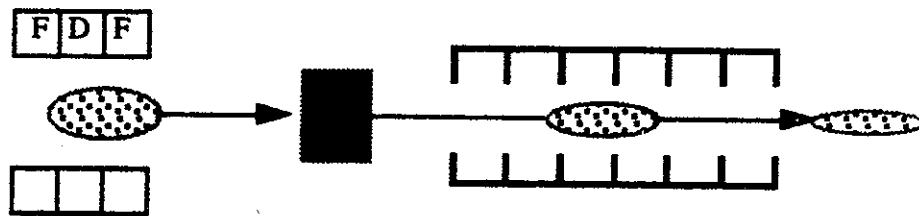


Figure 3. Schematic of the basic components of an ionization cooling array: a strong lens to focus the beam, the ionization medium in which the particles lose both transverse and longitudinal momentum, and an accelerating structure to restore the longitudinal momentum of the beam.

Neuffer [6] has showed that the ionization cooling of the transverse emittance is limited by beam heating due to multiple Coulomb scattering. If the transverse cooling is performed at an energy,  $E_c$ , using a medium for which the radiation length is  $X_R$  and the ionization loss rate is  $dE/dx$ , then the equilibrium, normalized emittance will be

$$\epsilon_{eq,n} = \frac{\beta_{cool}}{2} \frac{(14 \text{ MeV})^2}{m_{\mu} c^2 \left( X_R \frac{dE}{dx} \right)}, \quad (6)$$

where  $\beta_{cool}$  is the value of the beta function in the scattering medium. From eq. (6) it follows that efficient cooling requires that one employ a very strong focusing system that brings the beam to a symmetric waist of small radius in the ionization medium. For high energy muons traversing a medium of density  $\rho$  (g/cm<sup>3</sup>), of atomic number  $Z$ , and of atomic weight,  $A$ , the ionization loss rate can be approximated [7] by

$$\frac{dE}{dx} = \frac{D Z \rho}{A \beta^2} \left\{ \ln \left( \frac{2 m_e \gamma^2 \beta^2 c^2}{I} - \beta^2 \right) \right\}, \quad (7)$$

where  $\beta = v/c$ ,  $D = 0.307$  and  $I = 16 Z^{0.9}$  eV. For materials with  $Z \geq 6$ , the radiation length may be approximated by

$$X_R(\text{cm}) = \frac{716.4 A}{\rho Z (Z + 1) \ln (287 Z^{-1/2})}. \quad (8)$$

Multiplying eq. (7) and (8), one observes that the product ( $X_R dE/dx$ ) is independent of the density of the ionization medium and is greatest for small values of  $Z$ . Hence, low  $Z$  media will be preferred over high  $Z$  media for ionization cooling. The length of the scattering medium in any individual ionization cell will have to be limited to  $\beta_{cool}/2$ .

As the momentum bite of the selected muons will be relatively large, one should consider using optics with second order chromatic corrections to focus the beam onto the ionization targets as otherwise the spot size will be unacceptably large. The focusing system may be a strong quadrupole triplet. Brown [8] has suggested a focal system that is suitable for scaling calculations. In this triplet transverse dimensions are scaled by a factor  $a_q$ , which is the aperture (radius) of the first quadrupole of the triplet; longitudinal dimensions are scaled by the "ideal" focal length,  $f^*$ ,

$$f = \left( \frac{a_q}{B_q} (B\rho) \right)^{1/2}, \quad (9)$$

where  $B_q$  is the pole tip field in the first quadrupole, and  $(B\rho)$  is the magnetic rigidity of the beam. For a beam of momentum  $p$ ,

$$B (T) \rho (m) = 3.3 p (\text{GeV}/c) c. \quad (10)$$

The optical invariants of this particular triplet design are incorporated into the scaling equations that follow; the geometry the design is illustrated in Fig. 4,

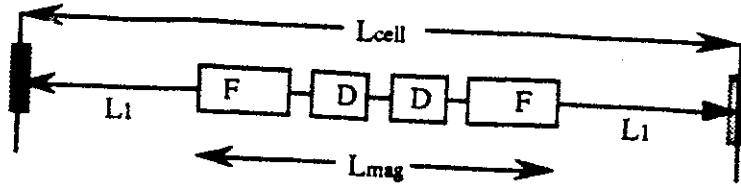


Figure 4. Schematic of the triplet optics of an ionization cooling cell; the disks of the ionizing medium are shaded and have a half width of  $\beta_{cool}/4$ .

The free space from the focus to the first quadrupole,  $L_1$ , is  $1.36 f$ ; the length of the triplet,  $L_{mag}$ , is  $3.13 f$  and the length of the cooling cell,  $l_{cell}$  is  $5.85 f$ . Without chromatic correction the value of  $\beta_{cool}$  for a beam with fractional momentum spread  $\sigma_p (= \Delta p/p)$  is given by

$$\beta_{cool} = 5.92 \sigma_p f. \tag{11}$$

With second order chromatic correction of the focusing optics the beta function can be reduced to

$$\beta_{cool} = 74.0 (B\rho) \left( \frac{a_q}{f B_q} \right) \sigma_p^2. \tag{12}$$

In the analysis that follows we chose the corrected optics described by eq. (12). As the cooling disks have a length,  $\beta_{cool}/2$ , each cooling cell produces an energy loss of  $e_{cell}$ , limited to

$$e_{cell} = \frac{\beta_{cool}}{2} \frac{dE}{dx}. \tag{13}$$

In optimizing the production/cooling scenario for the muon collider, one can now choose both the energy of muon production,  $E_\mu$ , and the energy at which the cooling is performed,  $E_c$ . Note that although the equilibrium emittance of eq. (6) does not depend explicitly on the cooling energy, the choice of  $E_\mu$ ,  $E_c$ , and the momentum acceptance will determine  $\sigma_p$  and thereby  $\beta_{cool}$  in the cooling lattice. Thus the choice of  $E_c$  will determine the transverse cooling coefficient,  $C_\mu$ , via

$$C_\mu = \frac{\epsilon_{n,prod}}{\epsilon_{eq,n}} = \frac{\tau_{sh} \phi_{accept} \gamma_{prod}}{\epsilon_{eq,n}}. \tag{14}$$

The choice of  $E_\mu$  will also influence the number of muons per bunch that are available to be injected into the collider as some of the muons will decay as they traverse

the cooling lattice. If energy is replaced during the cooling process by accelerator cells with an average accelerating gradient  $G$ , the total path length in the cooling lattice,  $L_{cool}$ , will be

$$L_{cool} = \frac{E_c}{F_c} \left( \frac{L_{cell}}{e_{cool}} + \frac{1}{G} \right) \ln(C_\mu) . \quad (15)$$

In eq. (15)  $F_c$  is the overall packing fraction of the ionization and acceleration cells in the cooler lattice.  $F_c$  accounts for pumping ports, flanges, diagnostics, bending magnets, and sextupoles in the cooling lattice. If the number of muons per bunch is injected into the cooling lattice is  $N_\mu$ , then the number of muons per bunch available for injection into the collider will be

$$N_\mu^* = N_\mu \exp \left( - \frac{L_{cool}}{c \tau_\mu \gamma_c} \right) , \quad (16)$$

where  $\tau_\mu$  is the muon lifetime at rest, and  $\gamma_c$  is  $E_c/m_\mu c^2$ .

Longitudinal cooling of the beam would allow smaller values of  $\beta_{cool}$  and consequently lower equilibrium emittances. Such reduction of the momentum spread can be accomplished by two means: 1) adiabatic damping by accelerating the muons prior to transverse cooling and 2) ionization cooling either in the transverse damper or in a separate damping structure. If the longitudinal cooling were limited to the ionization damping in the zero-dispersion cells of the transverse damper described above, the amount of acceleration,  $A_\mu$ , needed [4] to reduce the momentum spread by a factor  $1/e$  would be

$$A_\mu = E_c \left( \frac{\frac{dE}{dx}}{E_c \frac{\partial^2 E}{\partial E_\mu \partial x}} \right) \approx 5E_c . \quad (17)$$

If the longitudinal cooling is done in a dispersive section, the energy spread might be reduced by  $1/e$  with as little as  $2E_c$  of total energy exchange.

As computed from eq. (16), the path length of the muons in the cooler will typically be tens of kilometers, even if the packing fraction of the cooling lattice is large. A large packing fraction in conjunction with a high muon energy imply that the transverse emittance cooler should be constructed in the form of a recirculating linac such as CEBAF with high field bending magnets in the arcs and with as much as a few GeV per turn of acceleration in the straight, cooling sections.

At injection into the cooler the transverse emittance and the momentum spread of the muon beam will be large. Consequently the apertures of the quadrupoles in the cooling straights must be relatively large. One may envision a more effective form of cooler in which the emittance is reduced by an order of magnitude before injection into a final cooler which can have stronger, smaller aperture quadrupoles. As the value of  $\beta_{\text{cool}}$  can be much smaller in the second cooler, the equilibrium emittance could be much smaller than achievable in a single cooling ring. In such a scheme there is no need to duplicate the cost of the high field, dipole arcs. Rather the two coolers can share common arcs in a 2-in-1 arrangement illustrated in Fig. 5. The choice of straight-through or by-pass paths for the cooling stages can be selected to minimize the total path length of the muons in the coolers.

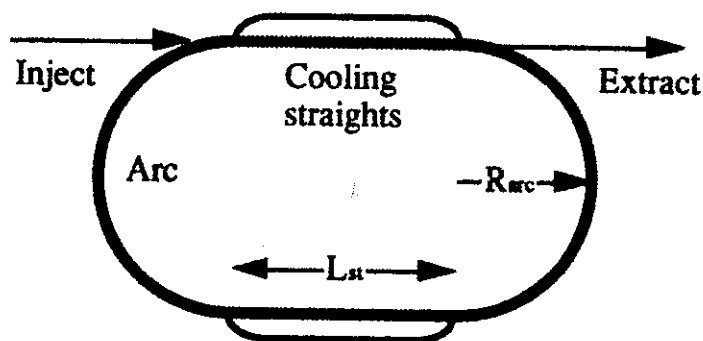


Figure 5. A 2-in-1 muon cooling ring. Transverse coolers are in each of the straight sections. The gray sections have large aperture quadrupoles for the first stage of cooling; the black straights have stronger, small aperture quadrupoles.

In the cooling ring the total length of the cooling cells plus re-acceleration cavities is  $2L_{\text{st}}P_c$  where  $P_c$  is the packing fraction of ionization cells plus accelerator cells in the straight sections. As the overall packing fraction,  $F_c$ , is just  $[2L_{\text{st}}P_c (2\pi R_{\text{arc}} + 2L_{\text{st}})^{-1}]$ , the number of cooling cells,  $N_c$  is related to the average dipole field in the bends,  $\langle B_d \rangle$  and the accelerating field,  $G$ , by

$$N_c = F_c \frac{2\pi \langle B_d \rangle}{G} \left[ 1 - \frac{F_c}{P_c} \right]^{-1} \left[ l_{\text{cell}} + \frac{e_{\text{cell}}}{G} \right]^{-1}. \quad (18)$$

Hence, the rf-system of the cooling ring must supply  $N_c e_{\text{cell}}$  volts per turn. In damping the emittance of the muons by a factor  $C_\mu$ , the muons must execute  $[E_c N_c e_{\text{cell}}^{-1} \ln C_\mu]$  turns.

#### 4. Collider considerations

The number of muons per bunch,  $N_\mu^*$ , that circulate in the collider will be determined by the production efficiency,  $A_\mu$ , by the charge,  $N_e$  in the electron bunch that strikes the production target, and by the path length through the cooling lattice. The number of electrons per bunch will be limited by the beam loading in the linac and by the design of the electron gun. The present SLAC gun (thermionic) produces bunches of 10 nC. If the electron beam emittance is not critical, the charge in the electron bunch can be raised to 20 to 30 nC. Bunches with as much as 50 nC may be produced with a photo-cathode gun, but such a large charge would lead to large beam loading and complications from the beam-breakup instability in an S-band linear accelerator

The electron bunches will be produced in a macropulse of duration,  $\tau_e$ , which is chosen to match the circulation period of the muons in the storage ring collider (Fig. 1). If the average dipole field in the ring is 3 T and if the muon energy is 100 GeV, then the circulation period will be 2  $\mu$ s;

$$\tau_e = 2 \mu\text{s} \left( \frac{3 \text{ T}}{B_{\text{ave}}} \right) \left( \frac{E_\mu}{100 \text{ GeV}} \right). \quad (19)$$

If the number of bunches per macropulse is  $N_b$ , then the frequency of collisions in the collider will be

$$f_{\text{coll}} = \frac{N_b}{\tau_e}. \quad (20)$$

To maintain the muon population in the collider the linac must be pulsed at a frequency of  $\tau_\mu^{-1}$ , where  $\tau_\mu$  is the muon lifetime as seen in the laboratory; at 100 GeV,  $\tau_\mu = 2$  ms. Hence, the duty factor of the linac will be  $\tau_e/\tau_\mu$ . The average power of the electron beam on the muon production target is, therefore,

$$P_{\text{beam}} = q \frac{N_b N_e}{\tau_e} \frac{\tau_e}{\tau_\mu} E_e = q \frac{N_b N_e}{\tau_\mu} E_e, \quad (21)$$

where  $q$  is the electron charge.

The peak luminosity of the collider with muons with a geometrical emittance,  $\epsilon$ , can be written as

$$L = \frac{N_\mu^{*2} f_{\text{coll}}}{4\pi \epsilon \beta^*}, \quad (22)$$

where  $\gamma = E_\mu/\mu$  and  $\beta^*$  is the value of the beta function at the collision point. Combining eq. (5), (16), (20) and (22), and evaluating the average luminosity of a collider of repetition rate, R, we obtain the following expression for the average luminosity of the collider ,

$$\langle L \rangle = \frac{A_\mu^2 N_e^2 N_b \gamma C_\mu}{4\pi \tau_{sh} \phi_{accept} \beta^* \tau_e} \left( \frac{\gamma}{\gamma_{prod}} \right) \exp\left( -\frac{2 L_{cool}}{c \tau_\mu \gamma_c} \right) \left[ 1 - \exp\left( -\frac{2}{\tau_\mu \gamma R} \right) \right] \left( \frac{\tau_\mu \gamma R}{2} \right), \quad (21)$$

The factor,  $\gamma/\gamma_{prod}$  implies that maximizing the luminosity argues for accepting the muons into the muon linac at an energy somewhat lower than the energy which maximizes  $A_\mu$ . The factor,  $C_\mu$ , accounts for the possibility of cooling the muons; if no transverse cooling is used,  $C_\mu = 1$  and  $L_{cool} = 0$ . At 100 GeV a reasonable value of  $\beta^*$  can be assumed to be 1 cm, although smaller values are possible, limited by the muon bunch length and by the design of the detector. Hence, the length of the muon bunch should be less than 1 cm. Such a short pulse is assured, if the length of the electron beam pulses are  $\approx 0.5$  cm.

### 5. Examples and parametric dependences

One now has a complete set of equations with which to maximize the luminosity of the muon collider as a function of the electron beam power incident on the production target and other system characteristics. As a first step in examining parametric dependences, we formulate a "realistic", baseline scenario that does not employ cooling of the muon beam.

The CLIC group at CERN [9] has developed a design concept for a high power positron production target to operate at 500 to 750 kW, more than an order of magnitude greater than presently operating designs. For the "realistic", baseline scenario assume that this target design can be realized at 0.5 MW. Using a 50 GeV electron beam with 20 nC per bunch and one bunch per macropulse, one can produce muon bunches of  $\approx 0.1$  nC at 29 GeV with an acceptance of  $\pm 3\%$  in the capture section of the muon linac. The geometrical emittance of the muon beam at 29 GeV will be  $5 \pi$  mm-mrad. If the average dipole field in the collider is 3 T, the revolution period will be  $2 \mu s$ . Hence, the collision frequency will be  $\approx 0.5$  MHz. Then for  $\beta^*$  equal to 1 cm, the luminosity of the muon collider at 100 GeV will be  $\approx 2 \times 10^{26} \text{ cm}^{-2} \text{ s}^{-1}$ . This scenario, which we will use as a base case for parametric studies, is summarized as Column 1 in the Table 1 along with a more optimistic case without cooling (Column 3).

The improvements to the "realistic" and "optimistic" cases that would obtain from damping the transverse emittance of the muons via ionization cooling are shown in Columns 2 and 4 respectively. A far more optimistic scenario (Column 5), which also

requires several technological inventions including considerable cooling of the muon beam, is discussed in Sec. 6. In all the examples with beam cooling the ionization media are beryllium disks of thickness of  $\beta_{\text{cool}}/2$ . The beam is re-accelerated in rf-cavities with rf-cavities operating with an average accelerating gradient of 17 MeV/m.

The effect of the choice of the electron beam energy on the production efficiency can be seen in Fig. 6, which displays the maximum luminosity versus the electron beam energy for the realistic scenario. In this calculation the number of electron bunches is varied to keep the beam power on the muon production target fixed at 0.5 MW. The momentum acceptance is fixed at  $\pm 3\%$ ; however, the value of muon energy accepted and the angular spread of muons accepted is varied so as to maximize the luminosity. As can be seen from eq. (2) and (22), the optimum acceptance energy will be a large fraction of the beam energy as the luminosity is quadratic in the conversion efficiency.

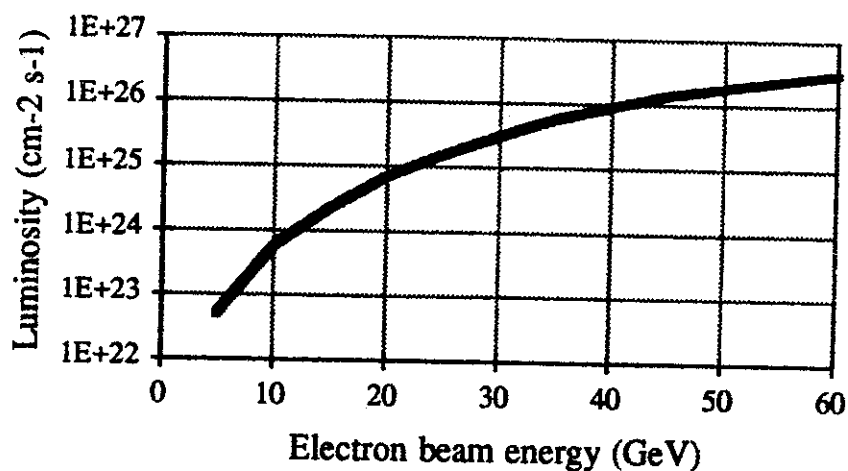


Figure 6. The variation of collider luminosity with energy of the electron beam at the production target in the "realistic" scenario. The beam power is fixed at 0.5 MW.

The scenarios employing production of muons at high initial energy (20 to 30 GeV) achieve relatively high luminosity at the expense of producing a muon beam with a relatively large ( $\approx 1\%$ ) momentum spread at the interaction point. If a much lower spread, say  $\pm 0.1\%$  were required for physics reasons, then the accepted muon energy,  $E_{\text{accept}}$ , would have to be reduced to  $\approx 5$  GeV. The luminosity is still maximized by maximizing the electron beam energy. Making this change in  $E_{\text{accept}}$  to the "realistic" scenario reduces the luminosity to  $\approx 6 \times 10^{24} \text{ cm}^{-2} \text{ s}^{-1}$ . As transverse cooling is accompanied by damping of the momentum spread, this consideration is not as severe in the scenarios with beam cooling.

The optimum energy for accepting the muons in the absence of cooling is 29 GeV. If instead we employ an ionization cooler, the optimum acceptance energy would be reduced to 21 GeV; a curve of the luminosity versus muon acceptance energy for the "realistic scenario" is given in Fig. 7. In this calculation cooling energy has been optimized, but limited to  $\leq 40$  GeV.

Somewhat surprisingly, the higher the energy at which the muons are cooled, the higher the final luminosity. The reason is that the adiabatic damping of the energy spread permits a much smaller value of  $\beta_c$ . If an initial stage of ionization cooling were employed to reduce the energy spread, the optimum energy at which transverse cooling is performed could shift to a lower value. In the "realistic" example, the traverse cooling by a factor of 48 at 40 GeV requires an energy exchange of only  $3.8 E_c$ . From eq.(17) one expects a slight improvement in  $C_\mu$  from the damping of the energy spread in the zero-dispersion cells. Adding ionization cells in the dispersive sections of the ring as suggested in Ref. 6 could improve the luminosity significantly.

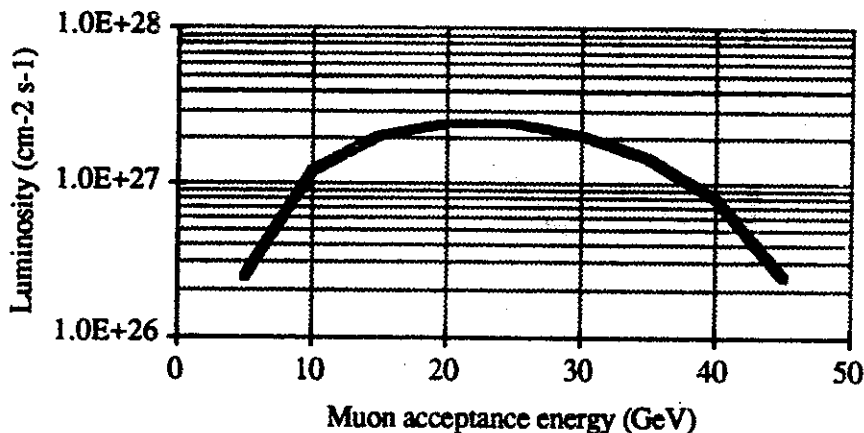


Figure 7. Luminosity as a function of muon acceptance energy for the "realistic" scenario with ionization cooling

Figure 8 illustrates the variation in luminosity for the "realistic" scenario with longitudinal cooling accompanying the transverse emittance damping. In this calculation cooling is done at the muon acceptance energy, 21 GeV so that no additional adiabatic reduction in energy spread is included. The field strength and aperture of the cooling channel optics is kept fixed. The decrease in luminosity as the cooling factor increases beyond six comes from the decay of the muon population as the transverse cooling path length increases to allow the beam to reach the equilibrium emittance.

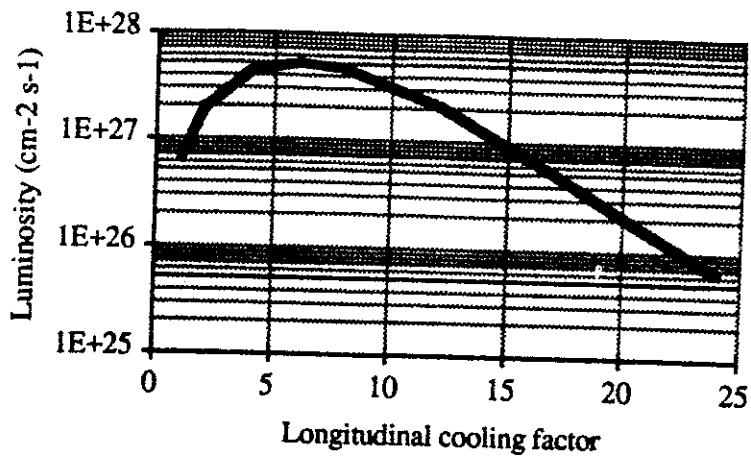


Figure 8. Luminosity variation with longitudinal cooling for the "realistic" scenario

As the muons must remain in the cooling lattice for hundreds of microseconds, it may not be possible to maintain an accelerating gradient of 17 MeV/m as assumed in the examples of Table 1. The consequence of reducing the gradient to allow for a lower power accelerating system in the cooling ring is displayed in Fig. 9. The degradation of the luminosity becomes especially large as the gradient falls below 10 MeV/m. As the number of muons in the ring is small, the beam loading in the cooling ring will be very small. One might consider the use of superconducting rf-cavities to keep rf-power requirements relatively small. Whether the superconducting cavities can function in the presence of radiation from the muon decay is uncertain.

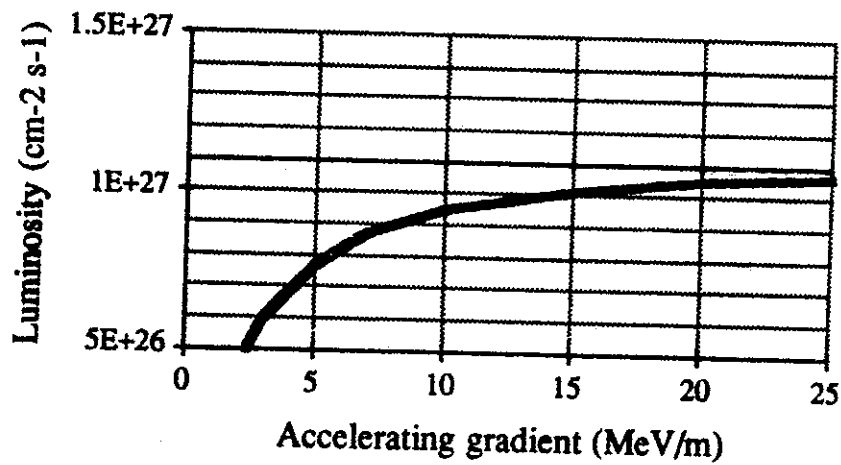


Figure 9. Luminosity versus accelerating field in the cooling ring for the "realistic" scenario of Table 1.

A second characteristic of the ionization cooling lattice that can have a strong effect on the final luminosity of the collider is the packing fraction,  $F_c$ , of the ionization cells plus the rf-cavities in the cooling ring. Fig. 10 illustrates the variation of luminosity with  $F_c$  for the "realistic" case with cooling.

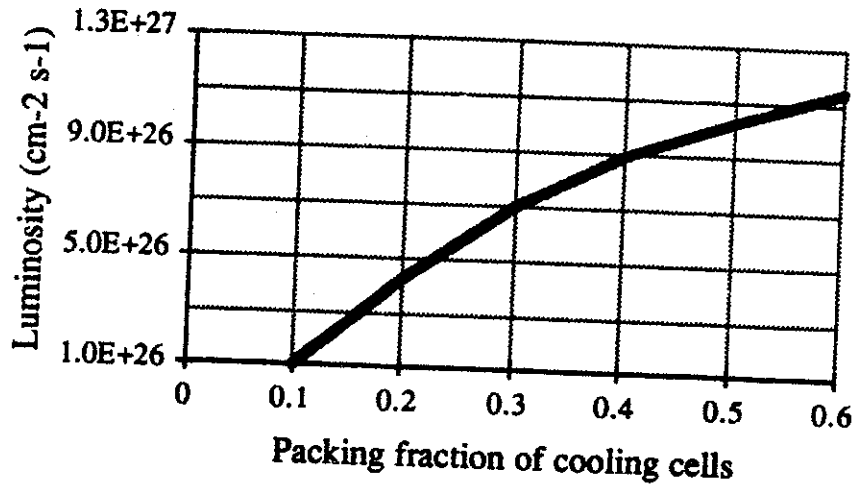


Figure 10. Luminosity versus packing fraction of ionization cells and re-acceleration cavities in the cooling ring for the "realistic" scenario of Table 1.

Applying eq. (7) through eq. (17) to calculate the characteristics of a cooling system, we find that the luminosity varies with choice of the ionizing medium as shown in Fig. 11. Although the product  $X_{RD}E/dx$  is independent of density, the luminosity is sensitive to the density of the ionizing medium as the energy lost per cell depends on the density and thickness of the medium. For each of the points in Fig. 11 the appropriate density has been used. From this examination we confirm that the preferred ionization media are beryllium disks.

If one were to design the muon collider with a broader energy reach, for example from 100 to 500 GeV center of mass energy, one would hope to realize a higher luminosity at the higher energies as the geometrical emittance is reduced by adiabatic damping. The scaling of the luminosity, as shown in Fig. 12, is slower than linear. The calculation of Fig. 12 is based on the "Needs invention" scenario of Table 1, with  $\beta^*$  reduced to 0.3 cm.

In this scenario the momentum spread of the beams is largest at the lowest energy. Unfortunately, the width of a standard model Higgs is expected to be a rapidly increasing function of the Higgs mass with a value of  $1 \text{ GeV}/c^2$  for  $m_H = 100 \text{ GeV}/c^2$ . If the momentum spread were reduced at the lower energies to allow for a fine scan of the range from 100 to 200 GeV, the luminosity would fall off much more precipitously.

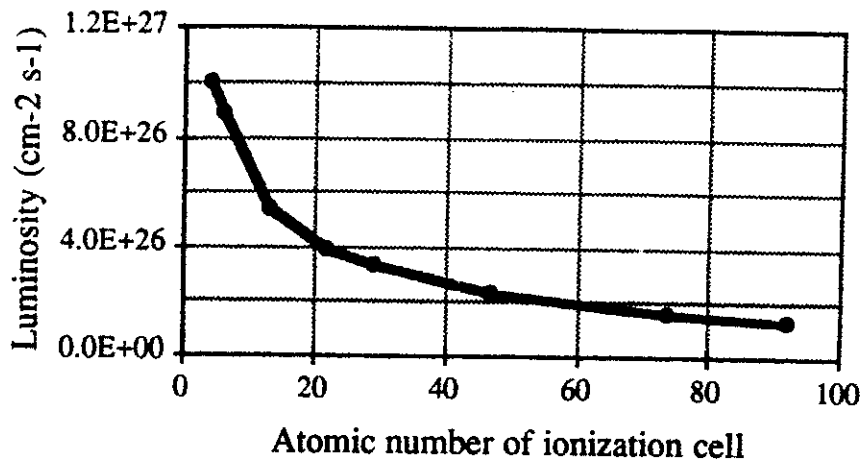


Figure 11. Variation of luminosity with the choice of ionizing medium

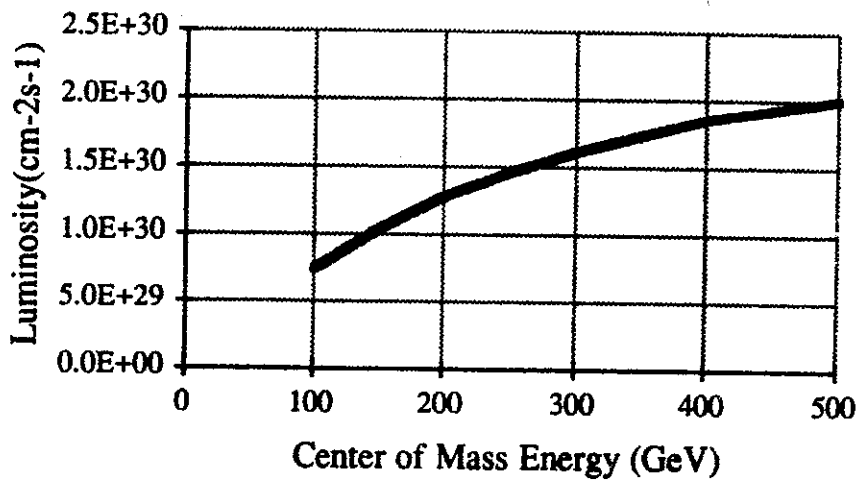


Figure 12. Variation of luminosity with energy for a 250 GeV x 250 GeV muon collider with  $\beta^* = 0.3$  cm.

### 6. Prospects and Conclusions

To obtain a muon collider with a luminosity of  $10^{30}$   $\text{cm}^{-2}\text{s}^{-1}$ , as desired for studies of the Higgs, one must adopt an extremely optimistic scenario (Column 5 of Table 1) that includes several technological innovations (indicated by a dagger). Perhaps the easiest of these advances may be the development of very strong, precision dipoles that would enable one to design a relatively small storage ring collider with a dipole field of 6 T averaged over the entire ring.

Continuing advances in the technology of electron guns with photo-cathodes suggest that one may be able to obtain 50 nC bunches of electrons for injection in a S-band structure. Accelerating multiple bunches of such high charge in a S-band structure also presents difficulties. For a 50 nC, 15 ps bunch, the single-bunch beam loading in a SLAC structure operating at 20 MeV/m would be  $\approx 20\%$ . As the bunches in the macropulse are separated by hundreds of meters, multi-bunch beam breakup is not a problem. However, a head-to-tail momentum variation of 4 % will be required for BNS damping of the single bunch, transverse, head-to-tail instability. Once this systematic variation is removed at the end of the electron linac, one would be left with a  $\pm 1.5\%$  spread that must be handled by the focusing optics at the production target.

Extending the conceptual design of the CERN production target to a reliable, 5 MW design is likely to be very difficult. Of particular difficulty will be finding suitable accelerator components that can withstand the extremely high radiation environment near the target. Note that the highest power, production target in operation is the 33 kW positron production target at SLAC.

It is likely that the greatest challenge to the designer will be to find an efficient scheme for cooling the muon beam at a high initial energy. In scenarios that include beam cooling in a storage ring the momentum bite must be chosen to be consistent with the acceptance of the cooling lattice. As it should be possible to design a lattice with an acceptance of  $\pm 2\%$ , cooling the muons at very high energy allows accepting a large momentum bite at the production target.

An idea of the scope of the project can be had by observing that in the realistic case the collider ring has a circumference of  $\approx 690$  meters while the cooler rings (one each for the  $\mu^+$  and  $\mu^-$ ) have circumferences of  $\approx 490$  m. Operating with a gradient of 17 MeV/m, the electron linac would be 3 km long while the 20 GeV muon linac would have a length of 1.32 km. A clever design may be possible in which these same linacs could be used to accelerate the muons from the cooler ring up to the full 100 GeV per beam of the collider. In this case the major cost of the project would be the 70 GeV of S-band linac. The major complexity and technological risk is in the lattices of the cooling rings which use very high field, superconducting quadrupoles and dipoles.

In conclusion, one sees that even with optimistic assumptions, it is difficult to envision a high energy  $\mu^+\mu^-$  collider which employs electro-production of muons functioning with a luminosity  $> 10^{27} \text{ cm}^{-2}\text{s}^{-1}$ . While the possibility of an electron-beam-driven muon collider with a luminosity  $\approx 10^{30} \text{ cm}^{-2}\text{s}^{-1}$  cannot be ruled out, it would require major advances in several of the primary constituent technologies. The areas for innovations include superconducting dipoles and quadrupoles, multi-kiloampere electron

beam sources, and multi-megawatt muon production targets. Most critically, efficient means of both transverse and longitudinal cooling of the muon beams at high energy must be found and demonstrated, if suitably high luminosity is to be achieved.

#### References:

- [1] Cline, D. B., Opening presentation at the Workshop on High Energy Muon Colliders, Napa, California, December, 1992
- [2] Nelson, W. R., Case, K. R., and Svensson, G. K, *Nuc. Inst. and Meth.*, 120, (1974) 413
- [3] Nelson, W. R., *Nuc. Inst. and Meth.*, 66 (1968) 293
- [4] Barletta, W. A. and Sessler, A. M. "Radiation from Fine Self-focussed Beams at High Energy" in High Gain, High Power Free Electron Lasers, (Bonifacio, De Salvo-Souza, & Pellegrini, ed.), Elsevier Scientific Publishers (North Holland), 1989
- [5] Belkacem, A., et al., "Experimental study of pair creation and radiation in Ge crystals at ultra-relativistic energies", in Relativistic Channeling, (Carrigan and Ellison, ed.), Plenum Press, Nato ASI Series B, Vol. 165
- [6] Neuffer, D., *Particle Accelerators*, 14, (1983) 75
- [7] Particle Data Group, *Phys. Rev.*, D45 Part 2 (1992)
- [8] Brown, K., Private communication as reported in Palmer, R., "Interdependence of Parameters for TeV Linear Colliders", *Proceedings of Workshop on New Developments in Particle Accelerator Techniques*, Orsay, (June, 1987)
- [9] Sievers, P., *Proceedings of the Workshop on Heavy Quark Factories*, Courmayeur, Italy, December, 1987

Table 1. Characteristics of a 100 GeV  $\times$  100 GeV muon collider using electro-production. The repetition rate in all cases is 500 Hz. For multiple rings,  $B_q$ ,  $a_q$ ,  $\beta_{cool}$  refer to the second ring. The quantities with daggers require technological inventions

	"Realistic" no cooling	"Realistic" with cooling	"Optimistic" no cooling	"Optimistic" with cooling	Needs inventions
<b>Production</b>					
$E_e$ (GeV)	50	50	50	50	50
$P_{beam}$ (MW)	0.5	0.5	2	2	5 <sup>†</sup>
$N_e$ (nC)	20	20	30	30	50 <sup>†</sup>
$E_{eccent}$ (GeV)	29	21	29	22	25
$(\Delta p/p)_\mu$ (%)	$\pm 3$	$\pm 3$	$\pm 4$	$\pm 4$	$\pm 8$
$N_\mu$ (nC)	0.1	0.1	0.2	0.18	0.6
$\epsilon_n$ ( $\pi$ m-rad)	$1.95 \times 10^{-3}$	$2.2 \times 10^{-3}$	$1.95 \times 10^{-3}$	$2.2 \times 10^{-3}$	$3.0 \times 10^{-3}$
<b>Cooler</b>					
$E_{cool}$ (GeV)	—	40	—	45	100 <sup>†</sup>
Number of rings	0	1	0	1	2
$F_{cool}$	—	0.5	—	0.5	0.6
$\langle B_q \rangle$ in arcs	—	4.5	—	4.5	4.5
$V_{ring}$ (GeV/turn)	—	0.95	—	1.2	3.2
$C_{ring}$ (m)	—	491	—	553	1840
$(B_q$ (T), $a_q$ (cm))	—	(4, 1.5)	—	(6, 1.2)	(8 <sup>†</sup> , 0.5)
$\beta_{cool}$ (cm)	—	1.3	—	1.5	0.4
$\epsilon_{n,eq}$ ( $\pi$ m-rad)	$1.7 \times 10^{-3}$	$5.7 \times 10^{-5}$	$1.9 \times 10^{-3}$	$7.4 \times 10^{-5}$	$1.6 \times 10^{-5}$
$C_\mu$	1	38	1	28	136
<b>Collider</b>					
$N_\mu^*$ (nC)	0.1	0.068	0.2	0.14	0.35
$N_{bunch}$	1	1	2	2	2
$B_{ave}$ (T)	3	3	4.5	4.5	6 <sup>†</sup>
$C_{collider}$ (m)	690	690	460	460	345
$f_{coll}$ (MHz)	0.5	0.5	1.33	1.33	2
$\beta^*$ (cm)	1	1	1	1	0.4
$(\Delta E/E)_{collider}$ (%)	$\pm 0.9$	$\pm 0.8$	$\pm 1.3$	$\pm 1.0$	$\pm 0.6$
$\langle L \rangle$ ( $\text{cm}^{-2}\text{s}^{-1}$ )	$1.5 \times 10^{26}$	$9.5 \times 10^{26}$	$7.1 \times 10^{26}$	$8.6 \times 10^{27}$	$1.0 \times 10^{30}$

## Why is the preceding "solution" absurd?

• Temperature of beam with  $\epsilon_{n,eq} = 1.8 \times 10^{-16} \pi \text{ m-rad}$   
is  $\ll 1 \text{ }^\circ\text{K}$

• Beam cannot be colder than temperature of pick-ups,  
kickers, and electronics,  $T_f$

• At pickups and kickers, assume the beta function is  $\beta_f$ .  
 $\implies$  minimum normalized emittance is

$$\epsilon_{n,min} = \beta_f \frac{2 k T_f}{m_\mu c^2}$$

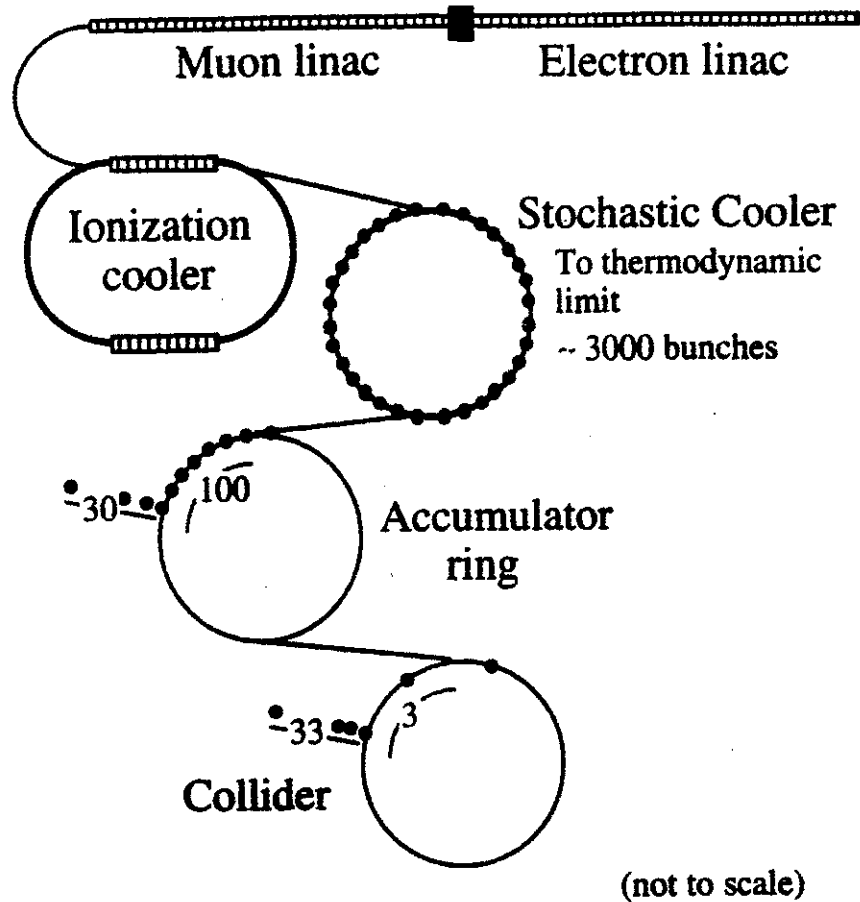
•  $T_f = 4.2 \text{ }^\circ\text{K}$ ,  $\beta_f = 1.2 \text{ cm}$   $\implies \epsilon_{n,min} \approx 10^{-12} \pi \text{ m-rad}$

$\implies$  Luminosity in preceding example is limited to

$$\langle L \rangle \approx 10^{27} \text{ cm}^{-2} \text{ s}^{-1}$$

• **This is not so far from what is needed. Is some invention possible?**

## Trading $f_{\text{coll}}$ for $N$ raises luminosity to required level



- This technique should yield  $\langle L \rangle$  as high as  $10^{31} \text{ cm}^{-2} \text{ s}^{-1}$
- Power on production target is not critical

## Summary & Conclusions

---

- Electro-production is competitive with proton production
- To attain  $\langle L \rangle = 10^{30} \text{ cm}^{-2} \text{ s}^{-1}$  muon colliders will require highly effective cooling of the muons
  - a) Ionization cooling
  - b) Stochastic cooling
- Ionization cooling scenario is extremely optimistic; needs several technological innovations
  - Very high power production targets
  - High charge (50 nC) injectors
  - Difficult beam control in electron linac
  - Very strong, high precision dipoles & quadrupoles
  - ====> Little “headroom”
- Stochastic cooling implies many bunches with  $N_b \sim 10^3$ 
  - Favors low  $E_\mu$  &  $\epsilon_0$  via tight cuts on  $\phi$  &  $\Delta p/p$
  - Adiabatically damping  $\rightarrow \Delta p/p < \pm 0.1\%$
  - Requires very low noise, cold electronics
  - Fast transfer & stacking of bunches
  - ==> Little “headroom”

## Scope of the project

---

- Assume the practicality of design scenarios.
- “Realistic” scenario → minimum scope.
  - Collider ring has a circumference  $\approx 690$  meters
  - Complex, cooler rings (for  $\mu^+$  &  $\mu^-$ ) are  $\approx 490$  m
  - 3 km long S-band electron linac (50 GeV)
  - $\geq 1.3$  km muon linac ( $\geq 20$  GeV) muon linac
  - Clever design may use same linacs to accelerate the muons from cooler to full 100 GeV per beam
- Major cost is 70 GeV of S-band linac
  - Large reduction through use of existing facility
- Major complexity / technological risk are cooling rings
  - must use high field, superconducting quadrupoles & dipoles (and in the stochastic cooler, octupoles).

## Epitome

---

- Given optimistic assumptions, it is difficult to envision a high energy ( $\geq 100$  GeV)  $\mu^+\mu^-$  collider which employs electro-production of muons with  $\langle L \rangle > 10^{27} \text{ cm}^{-2}\text{s}^{-1}$ .
  
- A muon collider with  $\langle L \rangle \approx 10^{30} \text{ cm}^{-2}\text{s}^{-1}$  cannot be ruled out. It would require major advances in several of the primary constituent technologies.
  - Superconducting magnets
  - Multi-kiloampere electron beam sources
  - Multi-megawatt muon production targets
  - Low noise feedback electronics for stochastic cooling
  - Efficient transfer & stacking schemes
  
- Efficient means of transverse & longitudinal of cooling the muon beams must be found and demonstrated, if suitably high luminosity is to be achieved.



**Fermi National Accelerator Laboratory**

FERMILAB-Pub-92/357

**Measurement of the Circulating Muon Flux  
in the Fermilab Debuncher Ring**

A. Bross, M. Gormely, C. Kim, S. O'Day, H. Park

*Fermi National Accelerator Laboratory  
P.O. Box 500, Batavia, Illinois 60510*

Y. Ho, W. Lee, E. Mannel

*Columbia University  
538 W. 120th Street, New York, New York 10027*

M. Murtagh

*Brookhaven National Laboratory  
Upton, New York, 11973*

December 1992

*Submitted to Nuclear Instruments and Methods*

### **Disclaimer**

*This report was prepared as an account of work sponsored by an agency of the United States Government. Neither the United States Government nor any agency thereof, nor any of their employees, makes any warranty, express or implied, or assumes any legal liability or responsibility for the accuracy, completeness, or usefulness of any information, apparatus, product, or process disclosed, or represents that its use would not infringe privately owned rights. Reference herein to any specific commercial product, process, or service by trade name, trademark, manufacturer, or otherwise, does not necessarily constitute or imply its endorsement, recommendation, or favoring by the United States Government or any agency thereof. The views and opinions of authors expressed herein do not necessarily state or reflect those of the United States Government or any agency thereof.*

## MEASUREMENT OF THE CIRCULATING MUON FLUX IN THE FERMILAB DEBUNCHER RING

A. Bross<sup>a</sup>, M. Gormely<sup>a</sup>, Y. Ho<sup>b</sup>, C. Kim<sup>a</sup>, W. Lee<sup>b</sup>, E. Mannel<sup>b</sup>, M. Murtagh<sup>c</sup>,  
S. O'Day<sup>a</sup>, H. Park<sup>a</sup>

<sup>a</sup>Fermi National Accelerator Laboratory, P.O. Box 500, Batavia, IL 60510

<sup>b</sup>Columbia University, 538 West 120th Street, New York, NY 10027

<sup>c</sup>Brookhaven National Laboratory, Upton, NY 11973

### Abstract

Using a novel experimental technique, we have measured the flux of pions, electrons, muons, and antiprotons which are injected into and circulate in the Fermilab Debuncher ring. The experimental technique relied upon the use of a non-destructive, rf pickup to measure the bunch structure of the beam on a turn-by-turn basis. The measured muon to antiproton ratio is  $\frac{\mu^-}{\bar{p}} = 1.0 \pm 0.2$ , and the ratio of muons to protons on target is  $\frac{\mu^-}{p_{OT}} = 2.0 \pm 0.4 \times 10^{-5}$ .

*Submitted to Nuclear Instruments and Methods*

$2 \times 10^{15} \rightarrow$  can probably  
increase to  $\sim 10^{16}$   
 $2 \times 10^{13} \mu/p \sim 80$  bunches

# 1 Introduction

To date, the only operational  $\mu$  storage rings have been those built to obtain measurements of the  $\mu$  (g-2) factor.[1, 2] However, the existence of a high energy  $\mu$  storage ring would make it possible to produce an intense beam of  $\nu_e$ 's of sufficient energy to open new opportunities in  $\nu_e$  physics and provide the means to explore, in detail,  $\nu_e \rightarrow \nu_\tau$  and  $\nu_e \rightarrow \nu_\mu$  mixing. The storage ring approach to these studies is very attractive for several reasons: flux normalization can be very precise; the neutrino energy spectrum is very well understood; and backgrounds should be very small and precisely calculable. It has been pointed out[3] that the Fermilab Debuncher might function as an efficient  $\mu$  storage ring.

The Fermilab  $p$  source includes a high-intensity target station, transport beam lines (AP-1 through AP-4), the Debuncher ring, and the Accumulator ring, Figure 1. The Debuncher ring is a 9 GeV storage ring with a circumference of 505 meters. The Debuncher's primary purpose is to reduce, by bunch rotation, the large momentum spread of the  $p$  beam coming from the production target. It also uses stochastic cooling to reduce the transverse emittance of the beam. The  $p$ 's are stacked and stored in the Accumulator prior to injection into the Main Ring. During normal collider running, the Debuncher accepts negative secondaries which originate at the  $p$  production target and are transported through the AP-2 beam line. Secondaries whose phase space coordinates lie within the momentum acceptance [8.9 GeV/c  $\pm$  2%] and transverse admittance [ $A(x) = A(y) = 25\text{mm} \times \text{mrad}$ ] of the Debuncher ring are injected and captured in the Debuncher. The particle composition of the first-turn beam in the Debuncher is dominated by  $\pi$ 's, but it contains  $e$ 's,  $p$ 's, and  $\mu$ 's as well.

10 GeV/c

# 2 Experimental

To estimate the  $\mu$  flux which is captured in the Debuncher, we use a mixture of experimental data coupled with relatively straight-forward calculations. During normal collider running,  $\pi$  fluxes have been measured at a variety of locations which are shown in Figure 2. The measurements in the AP-2 transfer line, at quads 704, 728, and 733, were made using ion chambers IC-704, IC-728, and IC-733, respectively, while at location D102 in the Debuncher ring, the measurement technique used a non-destructive rf pickup which is sensitive to, and relies upon, the bunch structure of the beam. The measured  $\pi$  fluxes (per  $10^{12}$  protons on

$$\frac{L}{B}$$

$$p^+ = 2.7 \text{ MeV}$$

$$5 \times 10^{-3} \text{ GeV}$$

target) are summarized in Table 1.

$$10^{-5}$$

Table 1: Measured  $\pi$  Flux (per  $10^{12}$  protons on target) at Various Locations

Location	$\pi$ Flux $\pm 20\%$ ( $\times 10^6$ particles)
IC-704	100.
IC-728	8.7
IC-733	8.3
D102	5.2

$$500m$$

$$2 \times 10^7$$

$$\rightarrow 10^9 - 10^{10}$$

$$5.2 \times 10^{-4} \text{ } \mu/\pi$$

To determine the  $\mu/\pi$  ratio at injection into the Debuncher, we have used the ray tracing program DECAY TURTLE and lattice function calculations to simulate  $\pi$  production and the subsequent decay and transport of  $\pi$ 's and  $\mu$ 's. The simulation considers only  $\pi$ 's produced within a transverse emittance of  $22\pi \text{ mm}^2\text{mrad}$  and discards any  $\pi$  or  $\mu$  which strikes a magnet pole tip or any  $\pi$  or  $\mu$  whose momentum lies outside the momentum acceptance of the Debuncher ( $\delta P/P = \pm 2\%$ ). Using this simulation, we have calculated the number of  $\pi$ 's and  $\mu$ 's which are injected onto the closed orbit of the Debuncher, and obtain:

$$5.2 \times 10^{-4} \quad 2 \times 10^{-5} \quad (\mu/\pi) \text{ Injected into Debuncher} = .018.$$

After three turns (one  $\pi$  lifetime = 1 turn), one finds:

$$(\mu\text{'s (total captured)})/(\pi\text{'s (injected into Debuncher)}) = .025.$$

Then, in order to calculate the ratio of the total number of  $\mu$ 's captured in the Debuncher to the number of protons on target, one uses the number of  $\pi$ 's measured at IC-728 and corrects this number ( $8.7 \times 10^6$ ) by the fraction (0.88) of  $\pi$ 's that decay between IC728 and the injection point. Thus the predicted number of  $\mu$ 's captured is  $0.025 \times 0.88 \times 8.7 \times 10^6 = 1.9 \times 10^7$ , and we have:

$$\frac{\mu\text{'s Captured in Debuncher}}{\text{Protons on Target}} = 1.9 \times 10^{-6}.$$

Since the typical  $\bar{p}/(\text{protons on target})$  ratio during normal collider operations is  $(1.8 \pm 0.2) \times 10^{-6}$ , we predict that  $\mu/\bar{p} \simeq 1$  in the Debuncher.

We have also used the rf pickup to make a "direct" measurement of the flux of  $\mu$ 's in the Debuncher by measuring the bunch structure of the beam on a turn-by-turn basis. The beam arrives in the Debuncher, at the location of the pickup (D102), in 84 narrow bunches ( $\sigma_t \approx 1$  nsec) with a bunch spacing of about 18 nsec. At this point, the fast particles ( $\pi$ 's,  $\mu$ 's and  $e$ 's) are separated from the slow particles ( $\bar{p}$ 's) by about 8 nsec, since the distance between the target and D102 is approximately 455 m. Hence,  $\pi$ 's,  $\mu$ 's and  $e$ 's can be distinguished from  $\bar{p}$ 's by looking at the time structure of the output from the rf pickup. As the beam circulates in the Debuncher, the  $\bar{p}$ 's are retarded in time with respect to the  $\pi$ 's,  $\mu$ 's and  $e$ 's by approximately 9 ns (or about  $\frac{1}{2}$  of a bunch spacing) for each revolution. Therefore, after 1 turn, the  $\bar{p}$ 's are delayed approximately 1 bunch spacing with respect to the  $\pi$ 's,  $\mu$ 's and  $e$ 's.  $\bar{p}$  bunch 1 is in time with bunch 2 of the  $\pi$ 's,  $\mu$ 's and  $e$ 's,  $\bar{p}$  bunch 2 is in time with bunch 3 of the  $\pi$ 's,  $\mu$ 's and  $e$ 's, etc. After turn 2, the  $\bar{p}$ 's are retarded another 9 ns with respect to the fast particles and are again separated in time. Therefore, only for the odd turns are the  $\bar{p}$ 's separated from the fast particles. The  $\pi$ 's decay in a few turns ( $\gamma\tau_\pi \approx 1$  turn), while the electrons spiral into the low energy edge of the machine, due to the emission of synchrotron radiation, and are completely lost after 14 turns. After turn number 14, the only particles left are  $\mu$ 's and  $\bar{p}$ 's.

The results of turn-by-turn measurements made in 1987[4] are summarized in Figure 3. In these data, there is no indication of a signal representing circulating  $\mu$ 's - which are expected to be the only fast particles remaining beyond turn number 14. The absence of a "bunched"  $\mu$  signal for turn 15, however, is not necessarily an indication that there are no  $\mu$ 's in the debuncher. This can be understood by calculating the  $\mu$  debunching time:

$$T_D = \frac{(\Delta T)_{rf}}{\eta \frac{dP}{P}}$$

For  $\mu$ 's,  $\eta = .017$  and  $T_D = 27.6 \mu\text{sec}$  (17 turns). Thus the  $\mu$ 's are completely debunched after 17 turns and, consequently, induce no signal on the rf pickup. We have checked the rate at which  $\mu$ 's debunch by performing a simulation which uses the longitudinal difference equations to study the bunch shape as a function of turn number in the Debuncher. The results, shown in Figure 4 for a bunch injected ( $N=1$ ) with  $\Delta t = \pm 0.5$  nsec and  $\delta P/P = \pm 2.0\%$ , illustrate the rate at which the injected  $\mu$ 's debunch and indicate complete debunching

in 15 - 17 turns. The rf pickup technique is thus not sensitive to circulating  $\mu$ 's in turns beyond turn 14.

An examination of Figure 4 suggests that it is straightforward to measure the bunched  $\mu$  signal by killing the electrons in the beam prior to injection into the Debuncher and then measuring the number of fast particles on turns 5 - 11 using the rf pickup. The most appealing method for killing the electrons is to insert a lead radiator at the end of the AP-2 transport line. Between the last two quadrupoles in this line (IQ32 and IQ33), the betatron amplitudes are reasonably small (4 m - 8 m), and the emittance blowup of the  $\mu$  bunches due to multiple scattering should be small.

We have studied the effectiveness of radiator thicknesses of 0.25, 0.50, and 1.0 radiation lengths on removing electrons from the beam at the end of the AP-2 transport line. The program EGS was used to determine the energy of the leading (maximum energy) electron exiting the radiator for electrons of energy 9.0 GeV incident on the radiator. (The simulation was also checked analytically using a formula from Tsai.[5] The results are shown in Figure 5. If we impose an 8.7 GeV cut on the electron energy for it to be captured in the Debuncher, then, for radiator thicknesses of 0.25, 0.50, and 1.0 radiation length, 40%, 11%, and 0.15%, respectively, of the incident electrons will survive the cut. We have chosen to use a radiator thickness of 1 radiation length in order to guarantee that electrons do not contribute to our  $\mu$  signal.

### 3 Results

Our measurements were performed, parasitic to the running of E-760, during the 1991 Fermilab Fixed Target run. A one radiation length lead absorber was inserted into the AP-2 transport line, completely eliminating electrons from the beam. We used a Tektronix DSA 602 digital sampling analyzer to measure the time structure of the signal from the pickup. This instrument has an analog bandwidth of 1 GHz; it samples at 2 Giga-samples/second; and it has a memory depth of 32,000 samples. We could, therefore, capture data for nine turns during a measurement. The data were taken in the following manner. Each measurement was an average over 64 pulses (each pulse containing 84 bunches). We first captured data for turns 1 through 9 and then set the DSA trigger delay to capture turns 9 through 17. The two data sets were normalized such that the  $\mu$  flux for turn 9 was equal in both

data sets. Figure 6 shows the raw data for approximately 10 bunches for turns 3, 4, and 5. In turns 3 and 5, we see the 8 nsec separation between the  $\beta = 1$  particles and the  $\bar{p}$ 's. On the even turns, the  $\bar{p}$  bunches are approximately in time with the  $\beta = 1$  particles and, thus, the rf bunch structure shows only one peak. Therefore, in order to determine the individual particles fluxes, only data from the odd turns are usable. For each of the odd turns between turns 3 and 11, we averaged 60 of the 84 bunches to produce a "bunch averaged" time structure for each of the turns. The data for turns 5, 7, 9, and 11 are shown in Figure 7. These data were fit to two Gaussians plus a constant (the fit curves are also shown in Figure 7). From the fit parameters, (amplitude and  $\sigma$ ) we could then determine, for each turn, the area under the two Gaussians. These numbers are directly proportional to the flux of  $\beta = 1$  particles and  $\bar{p}$ 's. In order to determine the flux of  $\mu$ 's, we then only had to make a correction for the number of  $\pi$ 's remaining at each turn. In order to do this, we used the measured  $\beta = 1$  particle flux from turn 1 and assumed that this entire flux was due to  $\pi$ 's. We then calculated the number of  $\pi$ 's remaining after each turn and subtracted the corresponding number from the measured  $\beta = 1$  flux for a given turn to determine the number of  $\mu$ 's. Our results are shown in Table 2 for turns 3-11.

Table 2: Particle Flux Measurements

Turn	Flux( $\beta = 1$ )	Flux( $\bar{p}$ )	$\frac{(\beta=1)}{\bar{p}}$	$\frac{\mu}{\bar{p}}$
1	33572	—	—	—
3	6251	2126	2.94	0.80
5	2232	1287	1.73	1.12
7	1597	1171	1.36	1.27
9	1306	1132	1.15	1.14
11	934	1122	0.83	0.83

## 4 Conclusions

We have measured the ratio of  $\mu$ 's to  $p$ 's in the Fermilab Debuncher ring. We find a  $\mu/p$  ratio of  $1.0 \pm 0.2$  and the ratio of muons to protons on target is  $\frac{\mu}{p} = 2.0 \pm 0.4 \times 10^{-8}$ . This is in good agreement with the  $\mu/p$  ratio expected from measured values for the number of  $\pi$ 's injected into the Debuncher and simulations of  $\pi \rightarrow \mu$  decay and subsequent  $\mu$  capture.

$$10^{12} p \rightarrow 2 \times 10^9$$

(but not  $10^{10}$ )

## References

- [1] F. Combley, F.J.M. Farley, and E. Picasso, *Physics Reports* **68** (1981) 93.
- [2] AGS 821, *Muon g-2 Design Report*, March, 1989.
- [3] W. Lee and D. Neuffer, in conference proceedings, *New Directions in Neutrino Physics at Fermilab*, September 14-16, 1988, pg. 159-173.
- [4] Gerald Dugan, private communication.
- [5] Tsai, Yung-Su, *Review of Modern Physics*, Vol. **46**, No. 4, 815, (1974).

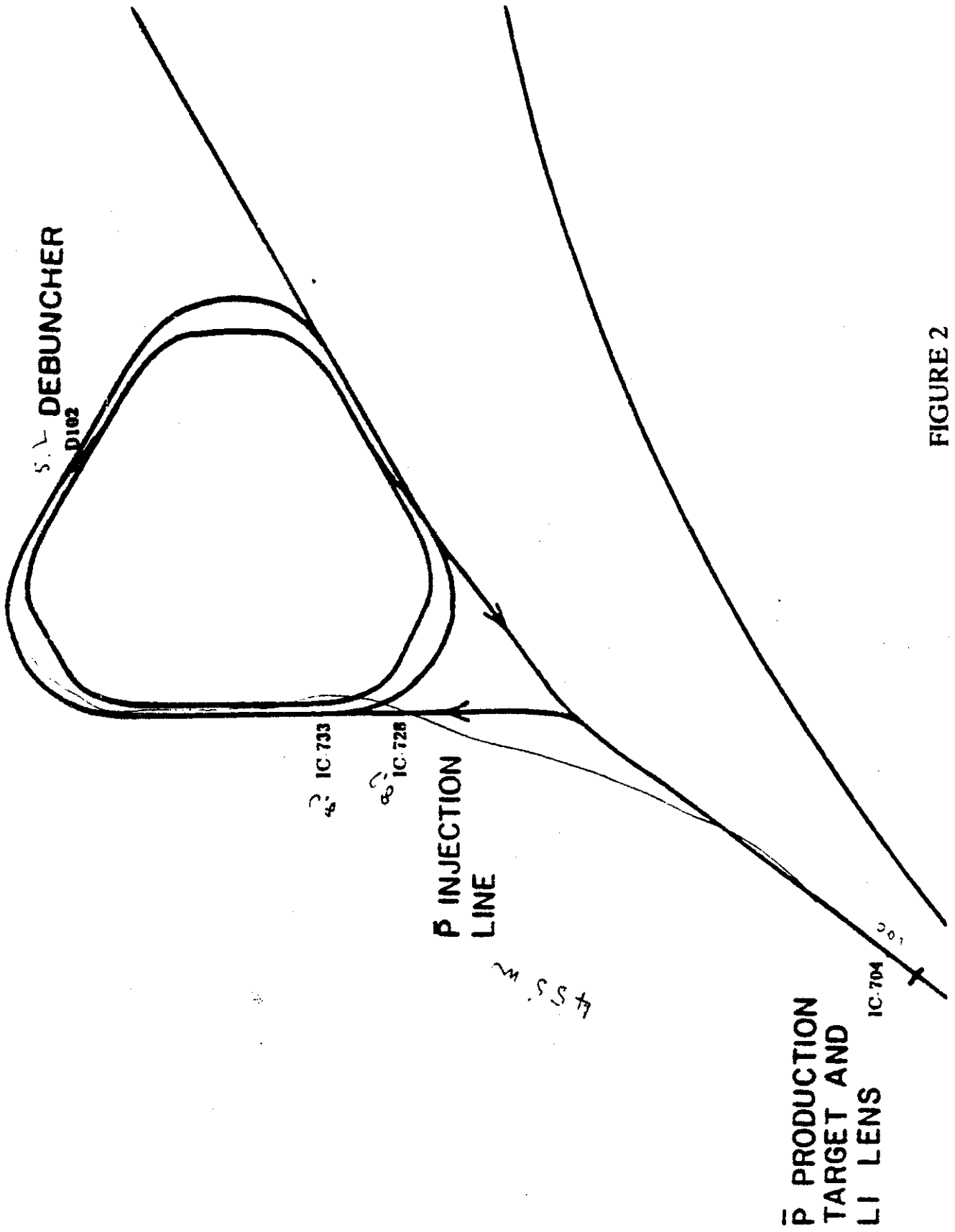


FIGURE 2

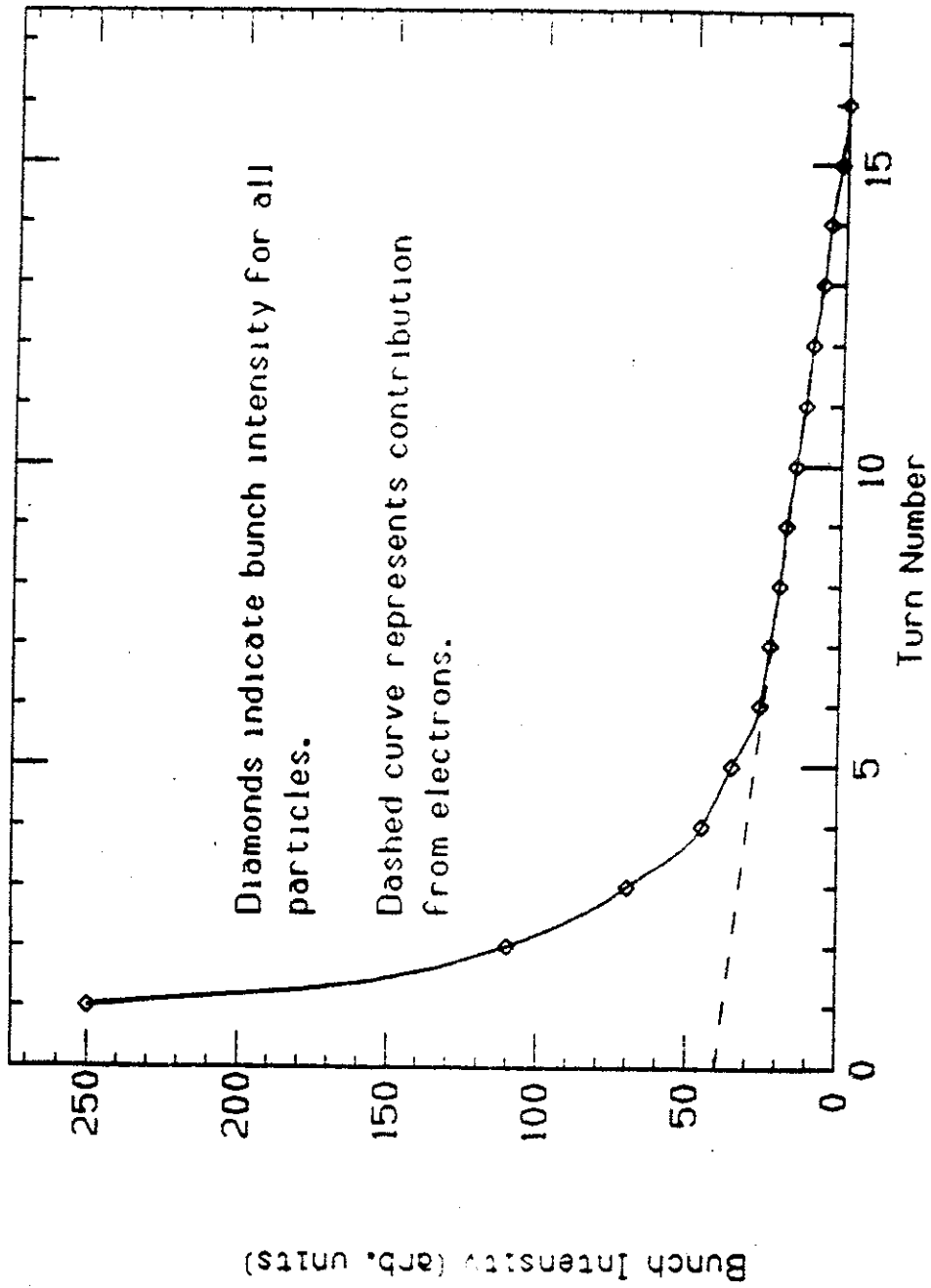


FIGURE 3

0 1 2 4 1 0 0 0

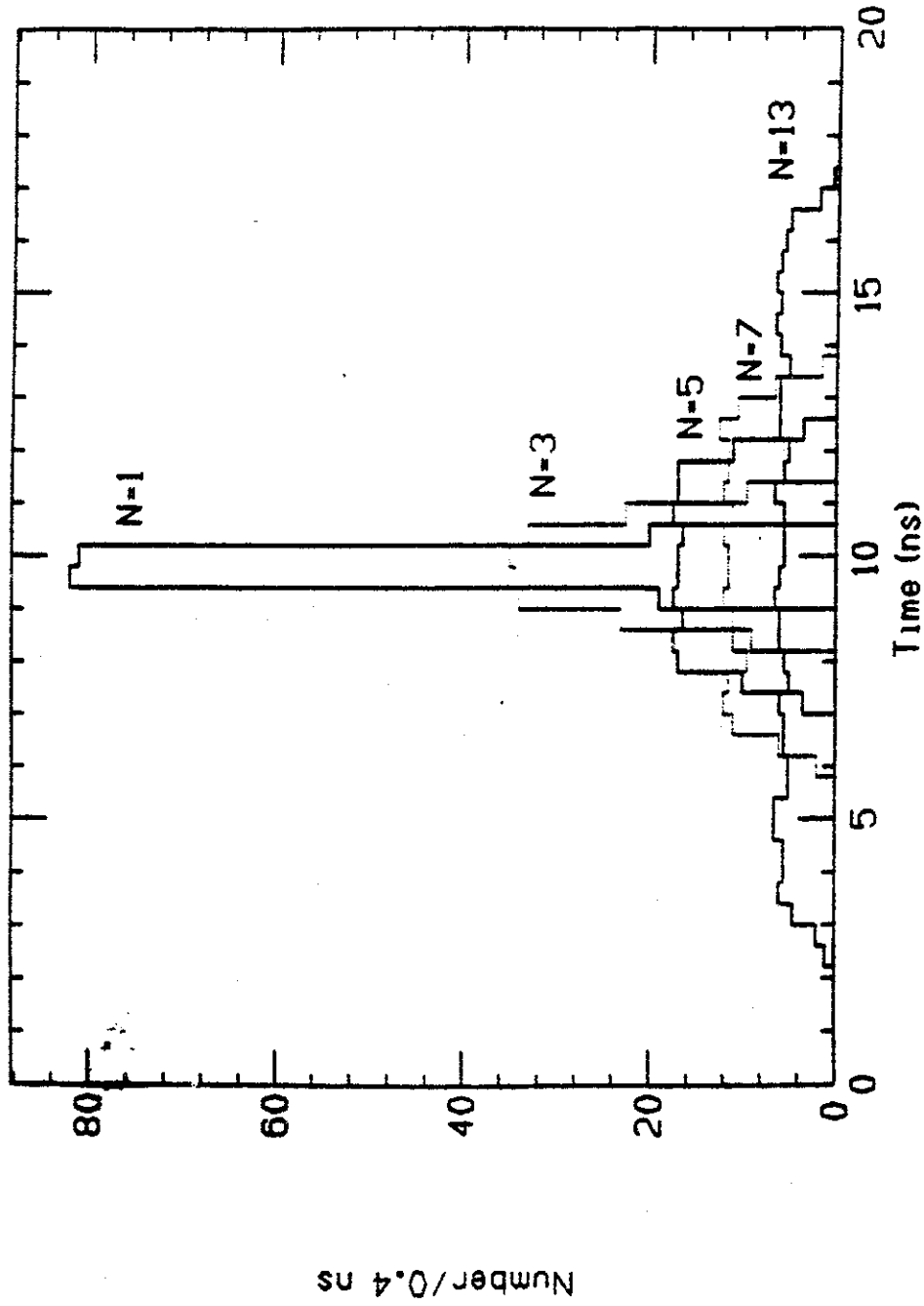


FIGURE 4

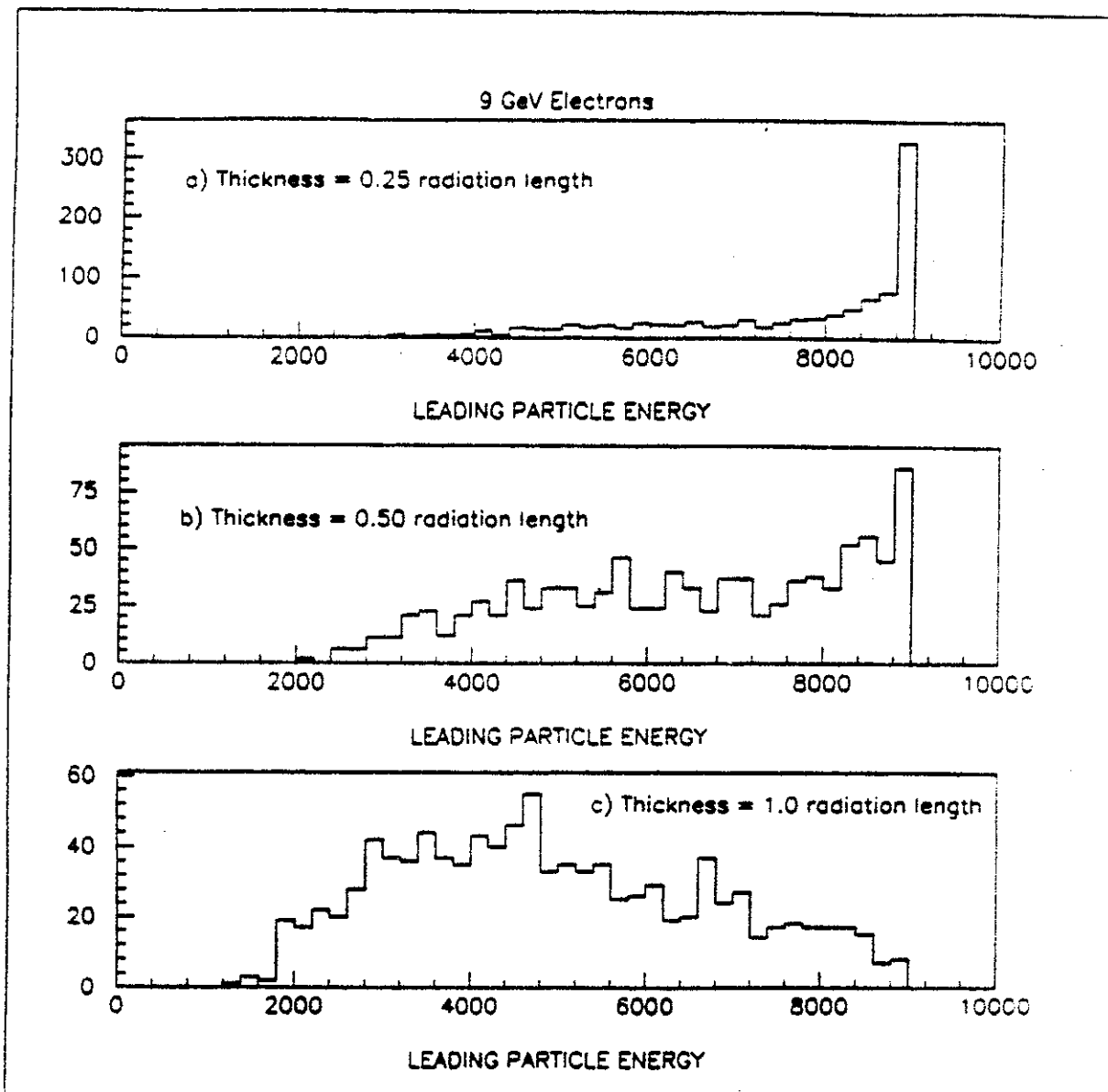


FIGURE 5

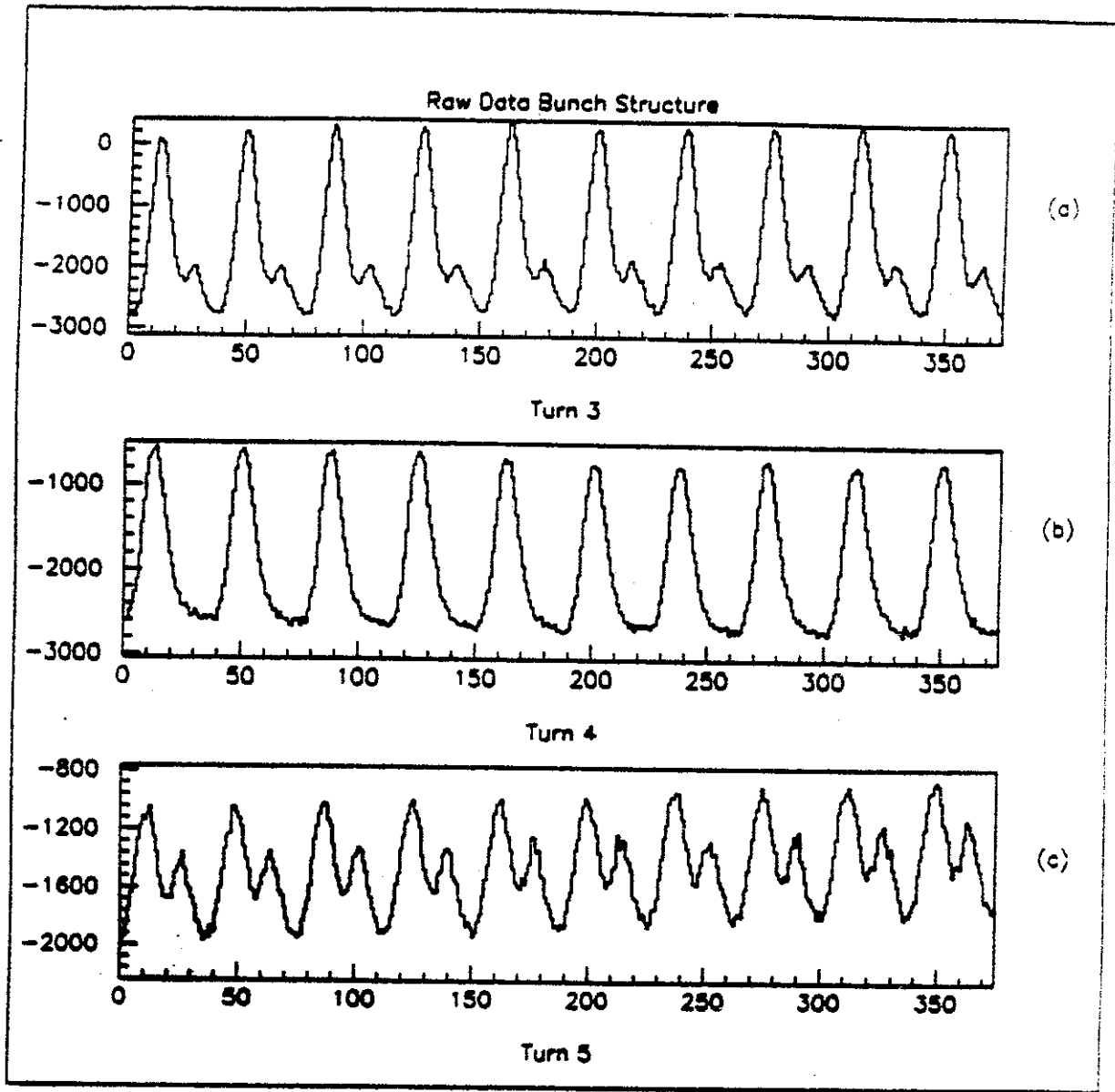


FIGURE 6

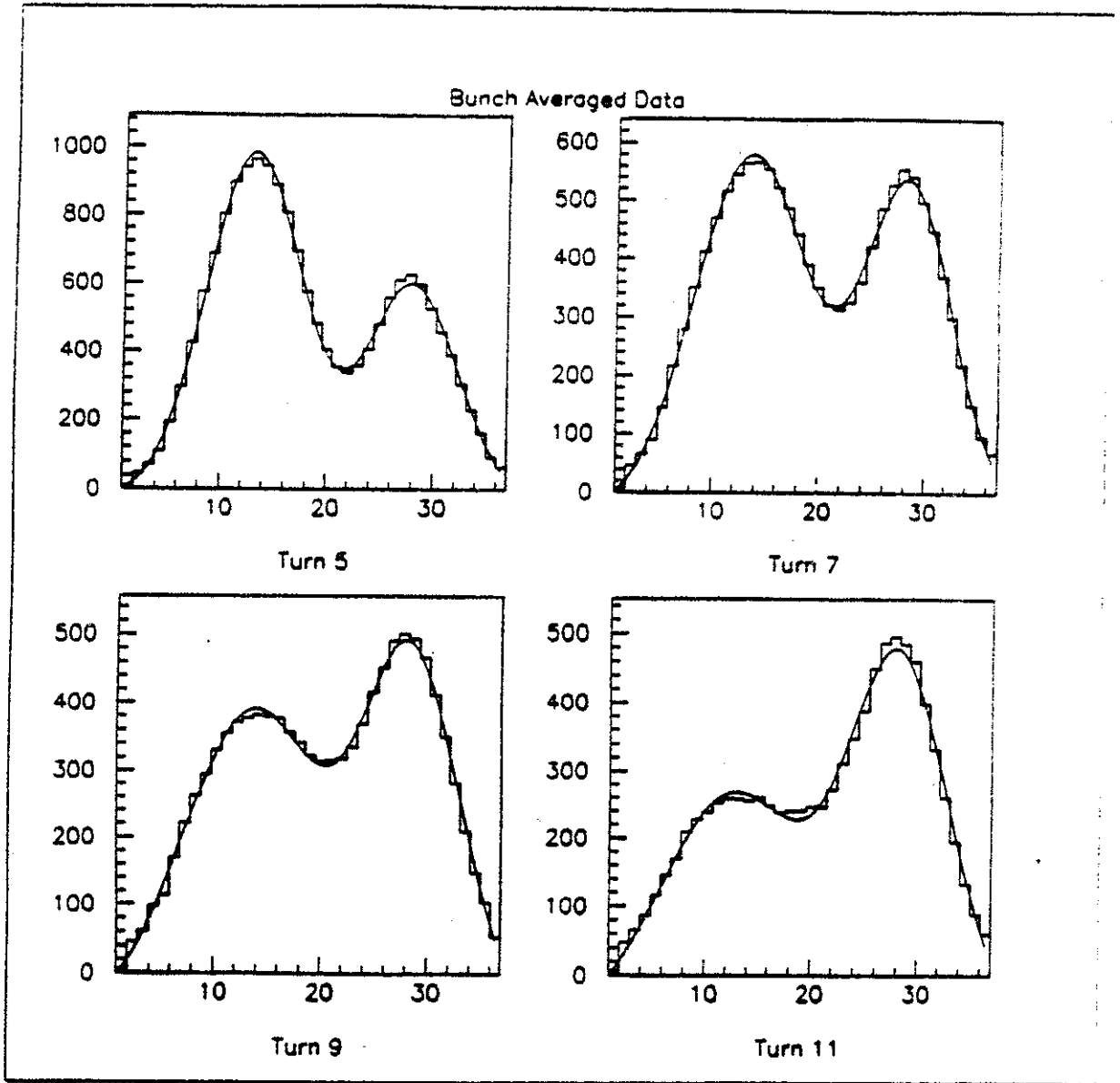


FIGURE 7



0 1 2 4 1 0 0 4

**Comments on 2-GeV Protons**

**Henry A. Thiessen**

**LANL**

~~Thurs~~

Santa Fe Workshop (last week)

$\sim 60$  Hz (could upgrade to  
120 Hz)  
2 GeV

1 MW upgradeable  $\rightarrow$  5 MW

100 ns  $\rightarrow$  1000 ns pulse length

$2 \times 5$  MW  $\Rightarrow 3.1 \times 10^{16}$  protons/sec  
at 2 GeV

PILAC (0.3  $\rightarrow$  1 GeV pion acc.)  
 $\sim$  #5 used by James Langenbrunner  
 200  $\pi$  mm-mrad  
 10% dp/p  
 Demonstrated Acceptance including transit

Can we consider larger  
acceptance at 100 MeV?

**2-GeV Protons as Source of Muons**

**James Langenbrunner**  
**University of Minnesota**

J. Langguth  
Feb. 22, '93

## I. Purpose

A. Ballpark Figures

B. Learn Some Tools

## II. Tool

A. LAHET

S. Frankl

J. D. Zumpf

1. nucleon-pion transport ✓

2.  $\mu$ 's don't scatter

## III. Results

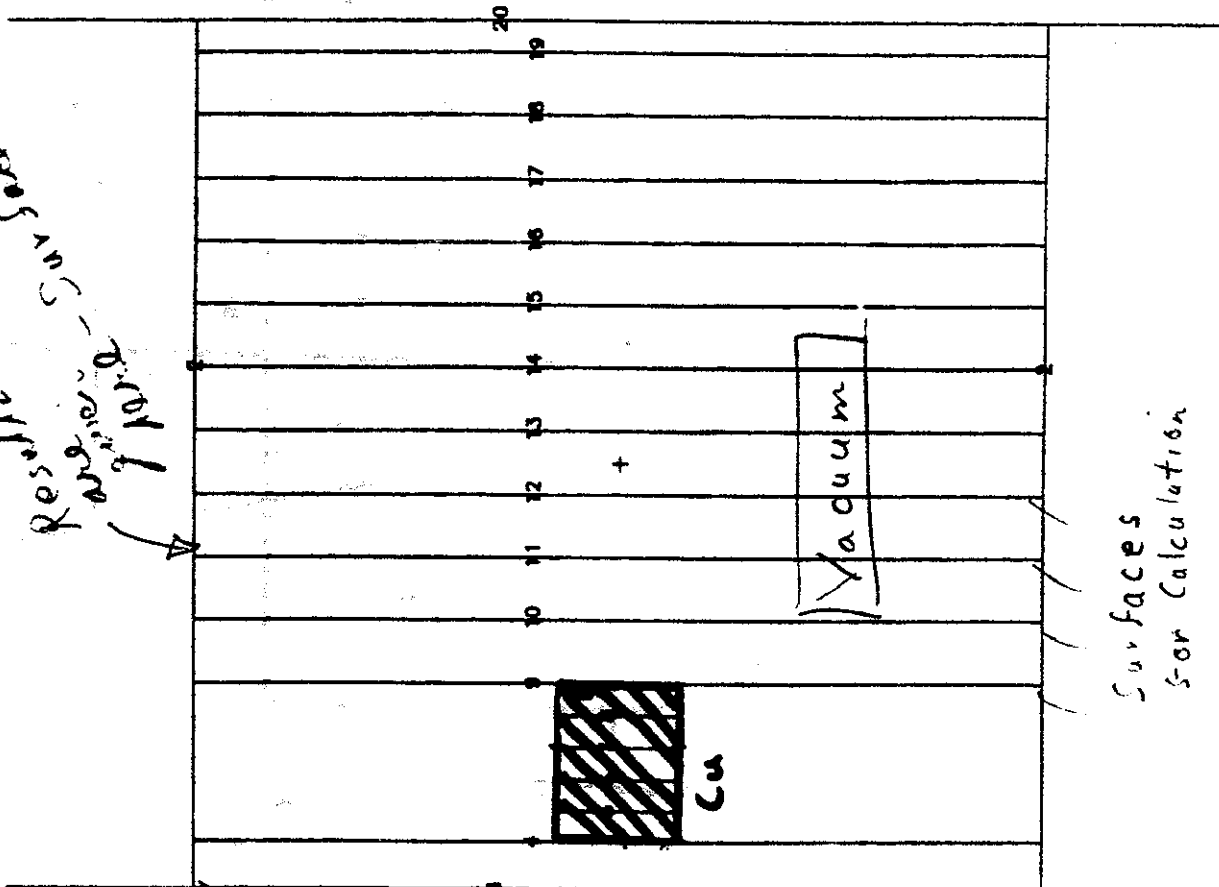
2/ 8/93 08 23 35  
 INPUT FILE FOR COPPER BEAM STOP  
 FOR 2000 MEV PROTONS. THE BEAM  
 PROPID = 2/ 8/93 08 21 10  
 BASIS  
 { .000000, .000000, 1.000000 }  
 { .000000, 1.000000, .000000 }  
 ORIGIN .00, .00, 120.00 )  
 EXTENT = ( 200.00, 200.00 )

LAHET - Los Alamos High Energy  
 Transport

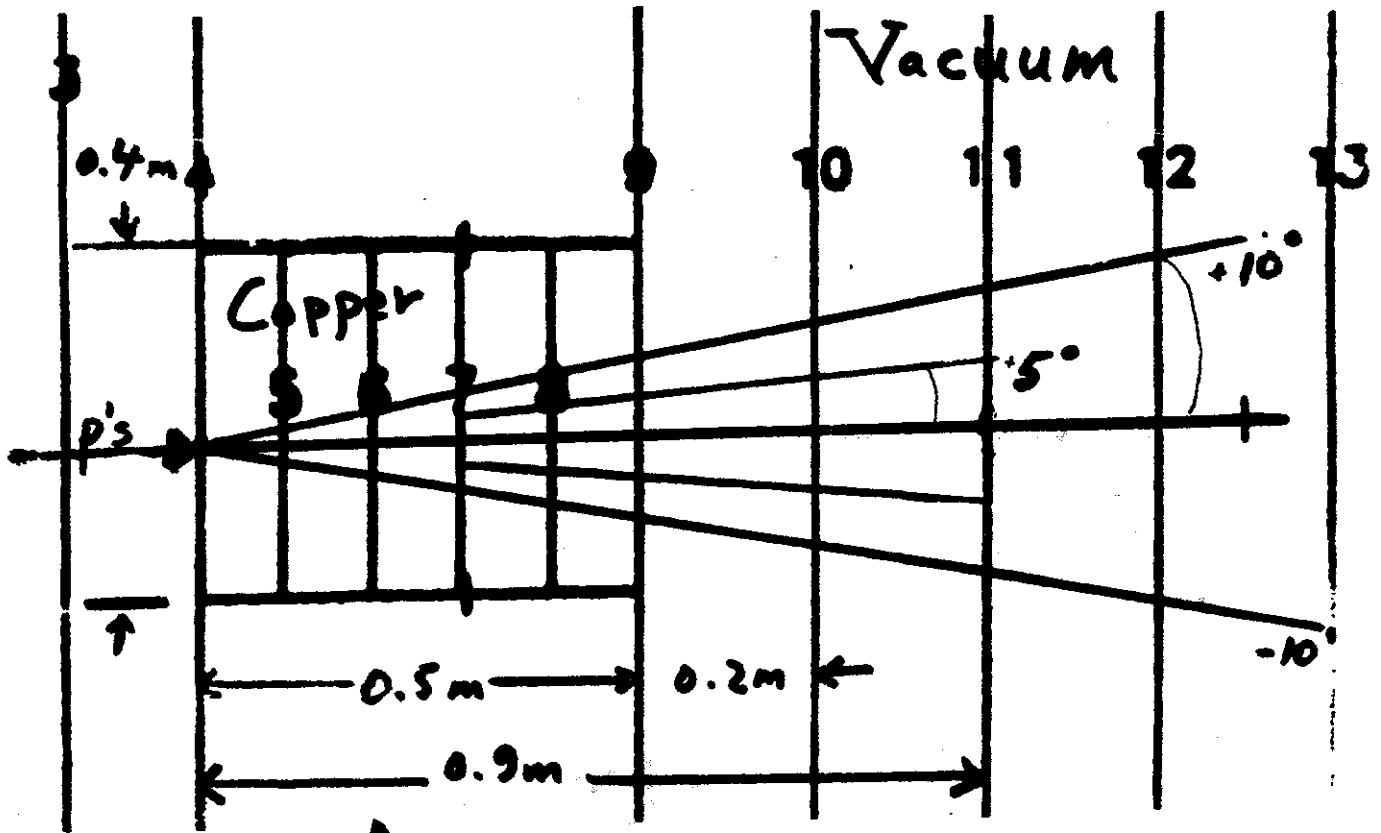
code  
 w/  $4 \times 10^6$  protons  
 @ 2 GeV

2 GeV  
 proton →

Results  
 Review - 5/15/93  
 7/14/93  
 @ 90 cm



\* Angles are given from intersection of beam



0.5m Cu is 3.3 interaction lengths

Results are given at this surface for angles which define concentric annuli.

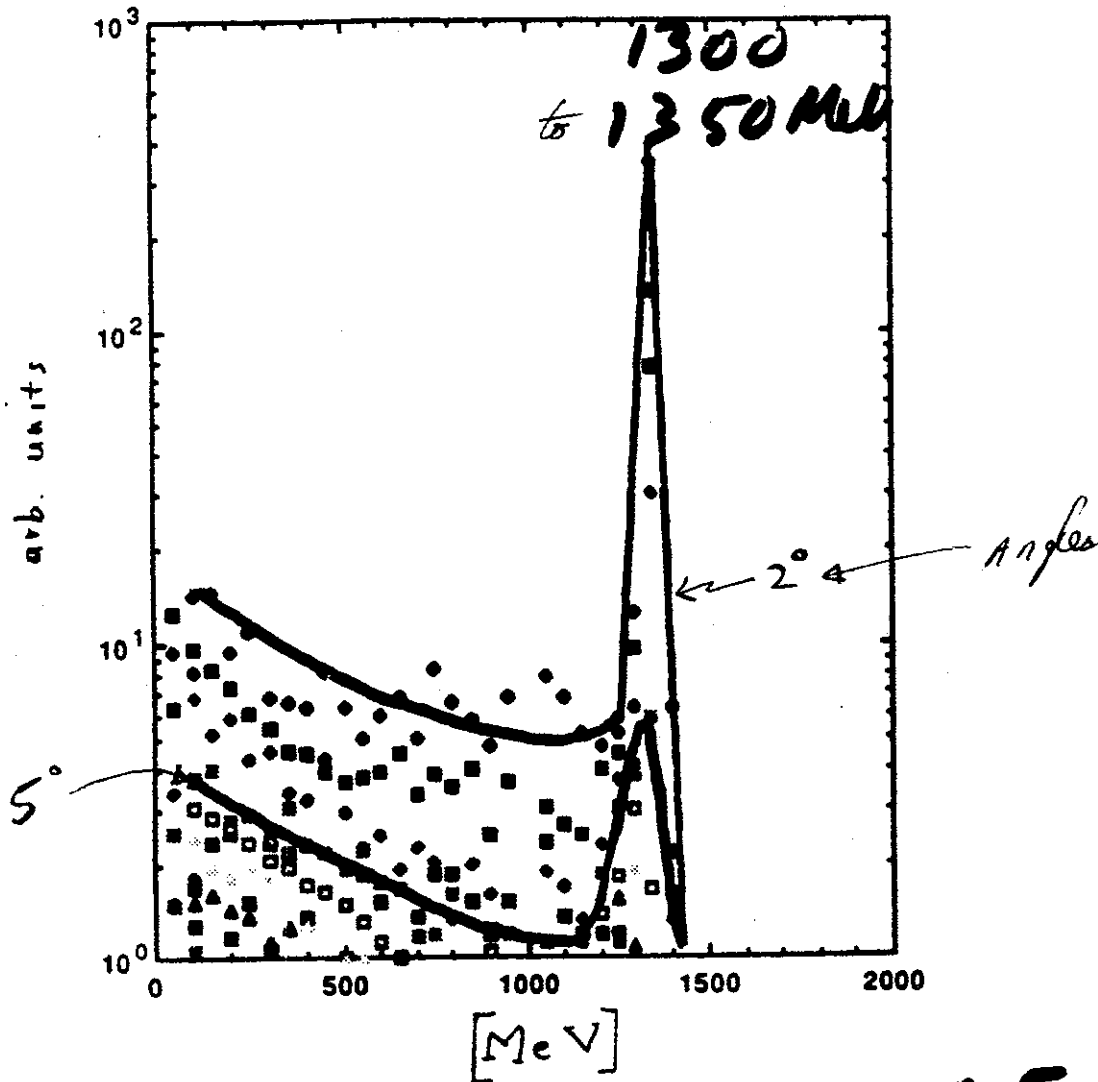
0 2 4 1 0 1 0

# LAHET Results @ 90cm

2 GeV protons incident

Exit of 0.5 m Copper

2 GeV protons incident:  
Figure for exit at 0.5m Cu



0.5m Cu

is 3.3 interac

Q: Do protons cause a s.c. cavity  
to quench?

Test of superconducting radio-frequency cavity bombarded by protons

J.M. O'Donnell, B.J. McCloud, C.L. Morris, J.B. McClelland, B. Rusnak and H.A. Thiessen  
*Los Alamos National Laboratory, Los Alamos, NM 87545, USA*

J.L. Langenbrunner

*Department of Physics and Astronomy, University of Minnesota, Minneapolis, MN 55455, USA*

Received 15 October 1991

A beam of  $2 \times 10^{10}$  protons/s was focused onto a small area on the high-field iris of a superconducting cavity operating at the resonance frequency. The input, reflected, and stored power were monitored. The cavity remained in steady state during this test. We conclude that such superconducting cavities will remain viable in the high-proton-flux environments proposed in the design of a superconducting accelerator for pions (PILAC).

## 1. Introduction

A proposed superconducting accelerator for pions (PILAC) at the Clinton P. Anderson Meson Physics Facility (LAMPF) would accept and accelerate  $10^{10}$  pions/s. In the reference design for PILAC [1,2], injection of optimum-energy pions into the superconducting linear accelerator is achieved by extracting a portion of the pions produced using magnetic focusing and bending elements. Protons (as well as muons, positrons, and electrons) with momenta equal to that of the selected pion momenta will be transported into the superconducting cavities. After injection into PILAC, only the pion particles will be accelerated. Contaminants with velocity different than the pion velocity will not be in phase with the accelerating rf field. It is expected that the transport system of the pion linac has a very broad momentum acceptance and will transport most of these contaminants to the end of the linac with roughly the same momentum as at injection. They will be eliminated in the output beamlines. However, some of the contaminants will bombard the walls of the superconducting cavity, and for this reason we tested a cavity for its response to a focused proton beam incident on a portion of its conducting surface.

## 2. Experiment

The experiment was performed at the low energy pion channel (LEP) at LAMPF. The relevant beam parameters were proton current of  $2 \times 10^{10}$  particles/s,

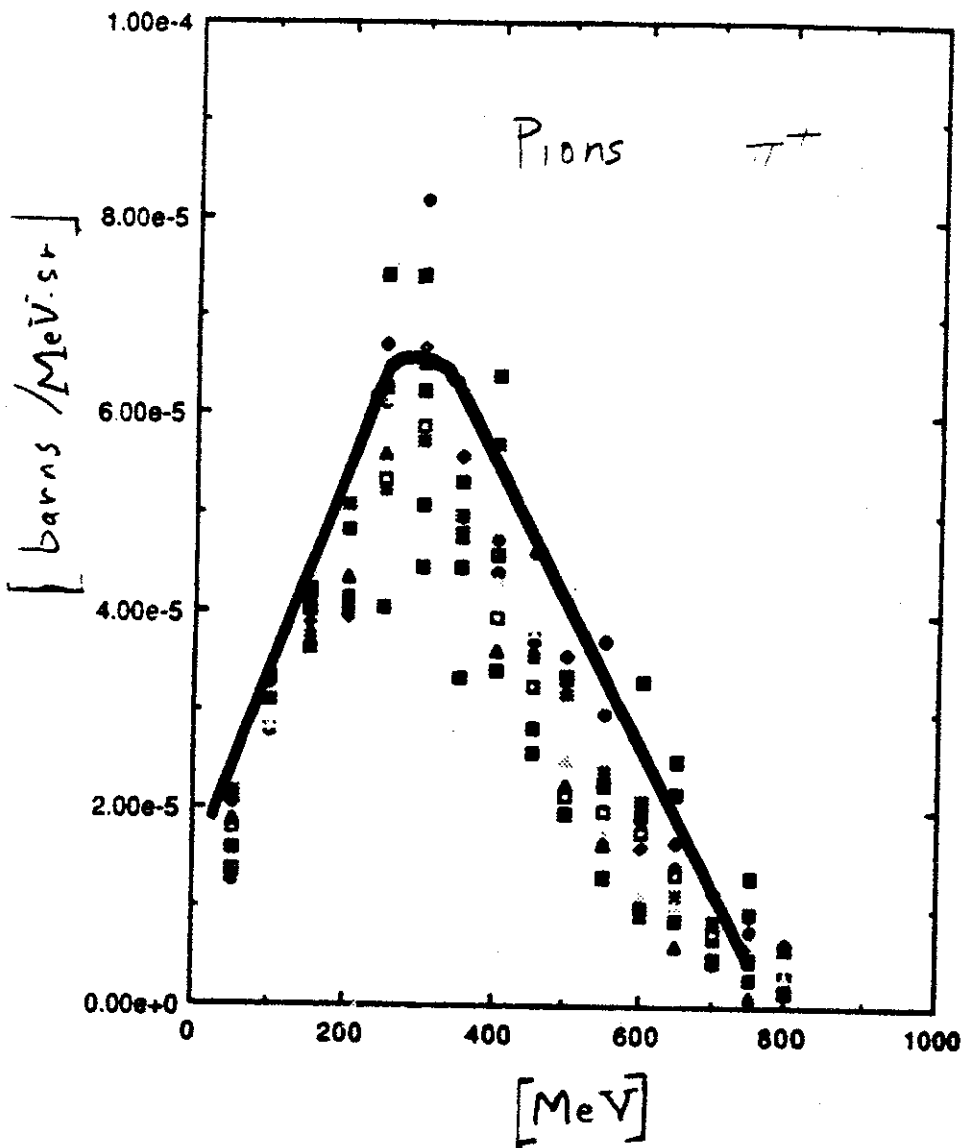
pion current of  $4 \times 10^8$  particles/s, and protons energy equal to 68 MeV. This beam corresponds to the largest proton beam flux available at LEP. The proton-beam spot size at the position where the beam intersected the high-field iris of the cavity was calculated to be 1.5 cm (vertical) and 7 cm (horizontal) by the code TRANSPORT [3]. The code is expected to be a fair approximation of the true spot size in the cavity because it gives qualitative agreement with the spot size at a position 0.78 m away, as determined with photographic film. The total power deposited by the beam was about 220 mW. The power per unit area deposited on the high-field area normal to the beam direction was about  $20 \text{ mW/cm}^2$ .

A schematic of the superconducting cavity is shown in fig. 1. The figure shows the resonant cavity (resonant frequency equal to 402.5 MHz), the adjustable coupler, the rf pickup, and the pieces of vacuum beamline required to couple the cavity to the LEP beamline. The beamline runs at room temperature, while the superconducting niobium section runs at liquid helium temperature. Further details of the cavity are presented in refs. [4,5].

The cavity was positioned at the end of the LEP beamline which enabled us to steer the beam into the high-field iris. The beam was incident on the same position of the cavity for the duration of this test. The 30 W power supply for the cavity was configured such that we could monitor the forward power ( $P_f$ ) fed into the coupler, and also the power reflected back ( $P_r$ ) from the coupler. The coupler was adjusted such that the quality factor of the cavity ( $Q_{cav}$ ) with no beam was

$0.2 \text{ GeV}$  protons<sup>2</sup> incident  
 Labet Results @ 90cm

Data from "pi+ output data"



- angles in degrees
- 1.0
  - ◆ 2.0
  - 3.0
  - ◆ 4.0
  - 5.0
  - 6.0
  - 7.0
  - ▲ 8.0
  - 9.0

energy

0 4 2 4 1 0 1 3  
**Advertisement:**

Nuclear Instruments and Methods in Physics Research A325 (1993) 187-195  
North-Holland

NUCLEAR  
INSTRUMENTS  
& METHODS  
IN PHYSICS  
RESEARCH

## Pion production at small angles

J. Langenbrunner

*Department of Physics, University of Minnesota, Minneapolis, MN 55455, USA*

M.B. Barakat and E.V. Hungerford III

*Department of Physics, University of Houston, Houston, TX 77204-5504, USA*

C.T. Pillai, N. Tanaka<sup>†</sup>, H.A. Thiessen, L.J. Rybarcyk, K.W. Jones, D.B. Barlow,  
J.B. McClelland, D.C. Dressman, S.C. Piltch, D.N. Mihailidis<sup>‡</sup>, J.B. Donahue,  
C.L. Morris and R.D. Werbeck

*Los Alamos National Laboratory, Los Alamos, NM 87545, USA*

Received 31 August 1992

Expt.  
Results  
for 800 MeV  
protons

$\pi^+$  and  $\pi^-$  production cross sections for 800-MeV protons on C and Cu have been measured at laboratory angles of 0°, 3°, 5°, 7°, 10°, 15°, and 20°. Pions were analyzed using the High Resolution Proton Spectrometer (HRS) facility for momenta from 364 to 675 MeV/c. Particle identification was made utilizing a time-of-flight method. We estimate the total systematic and statistical error to be  $\pm 15\%$  for measurements at 0° and 3° and  $\pm 10\%$  at other angles. These data have been used to determine the optimum energy and pion production angle for injection into a proposed superconducting accelerator for pions. Protons are the main source of contamination for a  $\pi^+$  beam. Proton-to-pion ratios are given for laboratory angles of 5° and larger.

### 1. Introduction

Previous measurements of pion production cross sections at small angles have been made by Barlow et al. [1], who measured  $\pi^-$  production cross sections for 800-MeV protons incident on carbon and beryllium at laboratory angles of 0°, 5°, 10°, and 20°. Denes et al. [2] measured  $\pi^+$  production with 800-MeV protons incident on carbon at angles of 7°, 15°, 20°, and 30°. The most extensive measurement of pion production near 800 MeV is that of Cochran et al. [3] for 730-MeV protons incident on a variety of nuclei. Those data span an angular range from 15° to 150° and were used primarily for the design of pion beam lines at the Clinton P. Anderson Meson Physics Facility (LAMPF). We have used the High Resolution Proton Spectrometer (HRS) at LAMPF to measure pion production cross sections for both  $\pi^+$  and  $\pi^-$  at laboratory angles less than 20°. Experimental difficulties are most severe around zero degrees (in the same direction as the bombarding proton beam) where the maximum cross

section for pion-production occurs. These data were obtained to address the question of the optimum energy for injection into a proposed superconducting accelerator for pions (PILAC) [4], which is designed to accept pions produced at zero degrees. These cross sections are also the basis for estimating the yield of pions at the end of such a linac.

### 2. Experiment

The High Resolution Proton Spectrometer was used to select momenta corresponding to pion energies between 250 and 550 MeV at laboratory angles of 0°, 3°, 5°, 7°, 10°, 15°, and 20°. These data were collected with the standard HRS configuration [5]. The energy of the incident proton beam was 800 MeV and its spin orientation was polarized transverse to the scattering plane. The data presented here are the spin-averaged double-differential cross sections.

The trigger used to define an event was the coincidence of three scintillators at the focal plane of the HRS spectrometer. Particle identification was achieved by specifying the time-of-flight of particles through the HRS spectrometer relative to a radio-frequency syn-

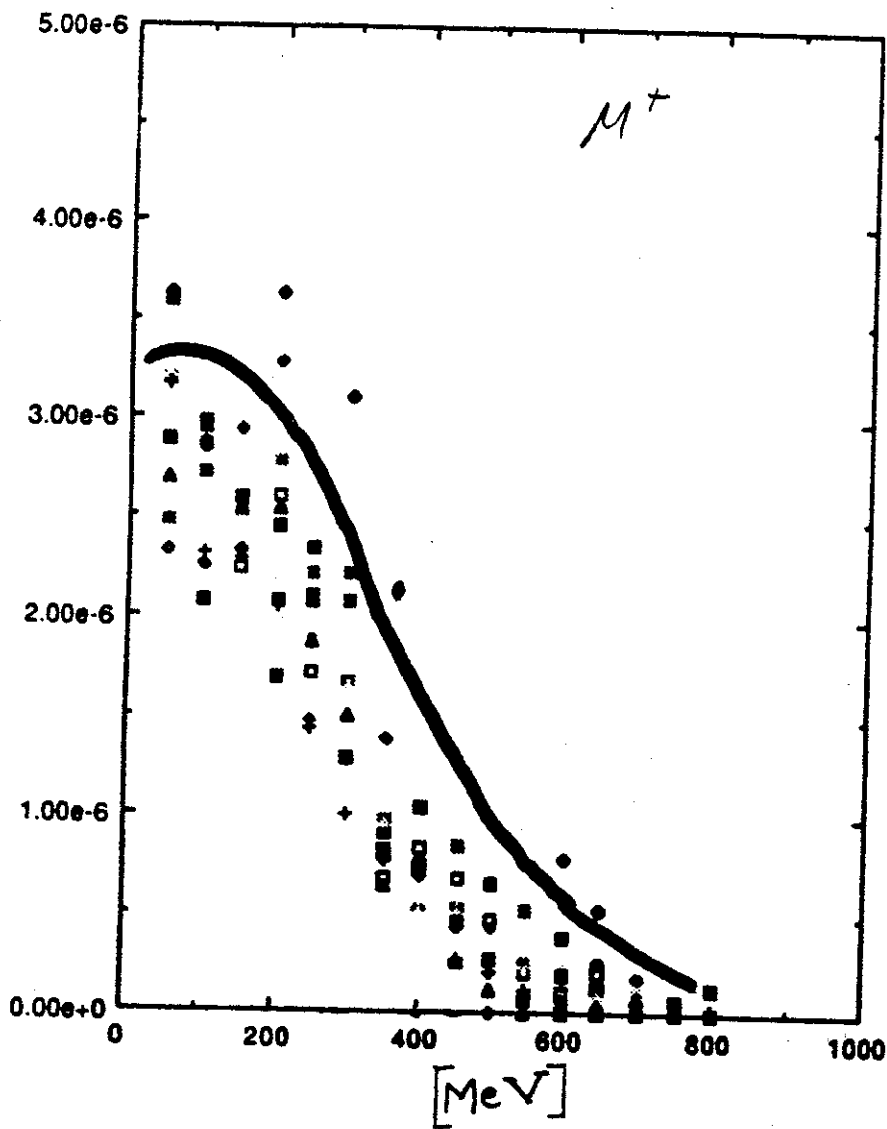
<sup>†</sup> Deceased.

<sup>‡</sup> Department of Physics, University of Minnesota, Minneapolis, MN 55455, USA.

$20 \text{ GeV}$  protons incident

# Lahet Results @ 90 cm

Data from "mu+ output data"



degrees

energy

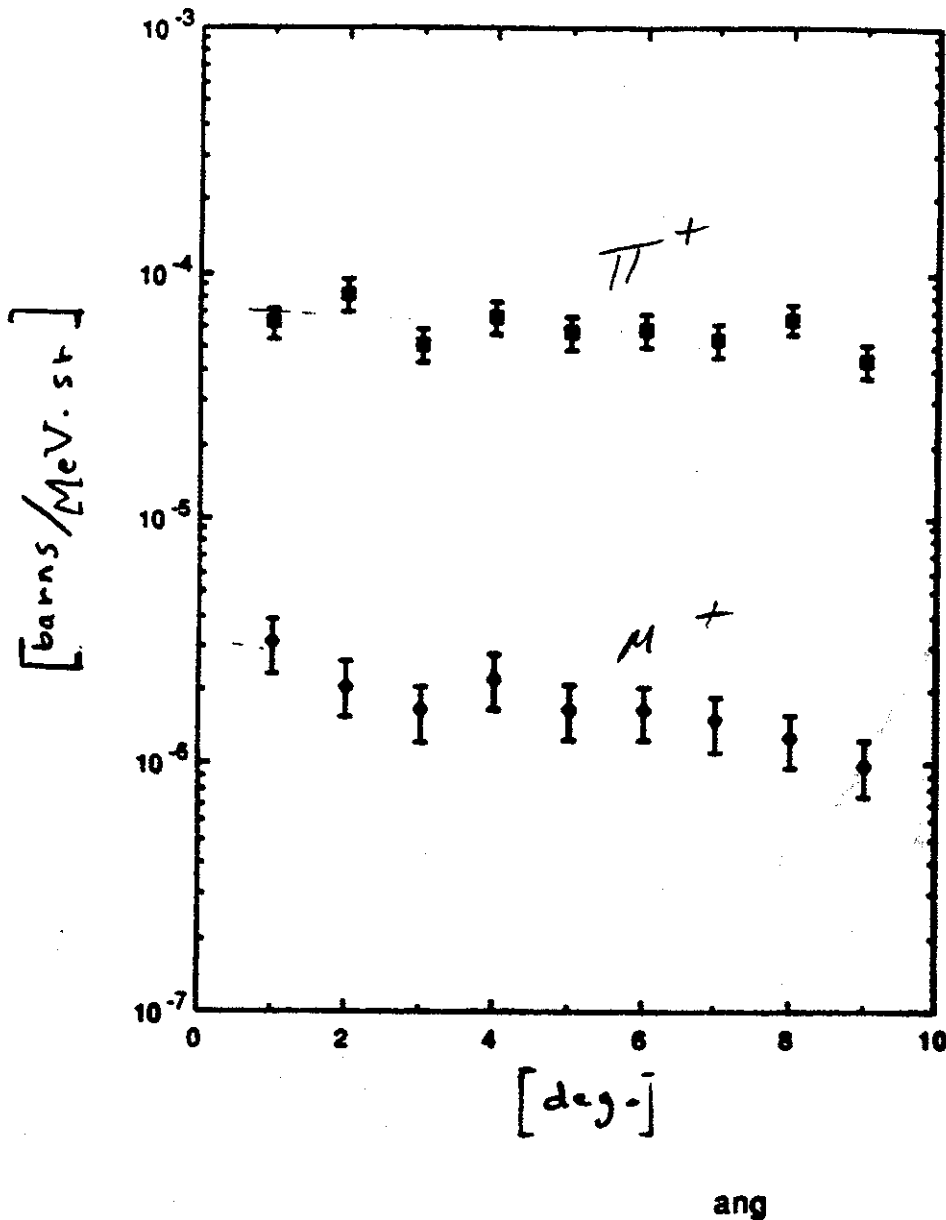
0 4 2 4 1 0 1 5

2 GeV protons incident

# Lahet Results

Data from "pi+ output data"

at 300 MeV  
Angular  
Dist.



### III. Results @ 90 cm.

A.  $\pi^+/\mu^+$  Ratio is  $\approx \underline{\underline{20}}$   
@ small angles

B. The ratio  $R = \frac{\mu^+}{\text{incident protons}}$

cone of  $5.5^\circ$   $R = 10 \times 10^{-6}$   $\pm 7\%$   
from 100 to 200 Me

For  $176 \text{ MeV/c} \pm 10\%$   
 $R = 3.0 \times 10^{-6} \pm 7\%$   
statistical uncertainty

$$10\% = \frac{dF}{F}$$

C. The ratio  $\frac{\mu^+}{\mu^-} = 1.6 \pm 10\%$  statistical uncertainty

# Nuclear Physics Approach to finding appropriate incident beam energy:

Pions are formed predominantly by decay of baryons, esp. (2 GeV) <sup>for protons</sup> by  $\Delta(1232) \rightarrow N\pi$

$$\pi^+ \rightarrow \mu^+ \nu_\mu$$

$$\rightarrow e^+ \nu_e \bar{\nu}_\mu$$

$$\pi @ 2.5 \times 10^5$$

$$\mu @ 2.2 \times 10^5$$

no  $\mu$ 's from  $\pi^0$

$$\eta \rightarrow \pi^+ \pi^- \gamma$$

29%

$$K^+ \rightarrow \begin{matrix} \mu^+ \nu \\ \pi^+ \pi^0 \\ \pi^+ \pi^+ \pi^- \end{matrix}$$

64% } 95%  
21% }  $\mu$   
6% }

0 4 2 4 1 0 1 8  
Summary

I. Could (obviously) do more  
work!

A. iterate story, thickness, density,  
{beam energy, surface placement

B. check w/ analytical  
expressions

C. check  $\mu$ 's w/  $\pi$ -decay,  
kinematics, Bethe-Bloch

D. A quote

Sir Denys Wilkinson  
9.4.92

"Today we know of nothing in  
nuclear structure that demands  
that we include quarks in our  
description of nature, except for  
nuclear beta decay. But it is clear  
that, at some level, we shall have  
to wrestle with particle structure  
just as we struggle with nuclear  
structure." - Just like Higgs Mixing!

0 3 2 4 1 0 1 9

0 4 2 3 1 0 2 0

# **Combined Ionization and Stochastic Cooling**

**Alessandro Ruggiero**

**BNL**

0 4 2 4 1 0 2 1  
 AGR / 2/22/93

①

~~GeV/c~~

~~Time~~

~~(1.15 sec)~~

~~(2.22)~~

~~(1.18)~~

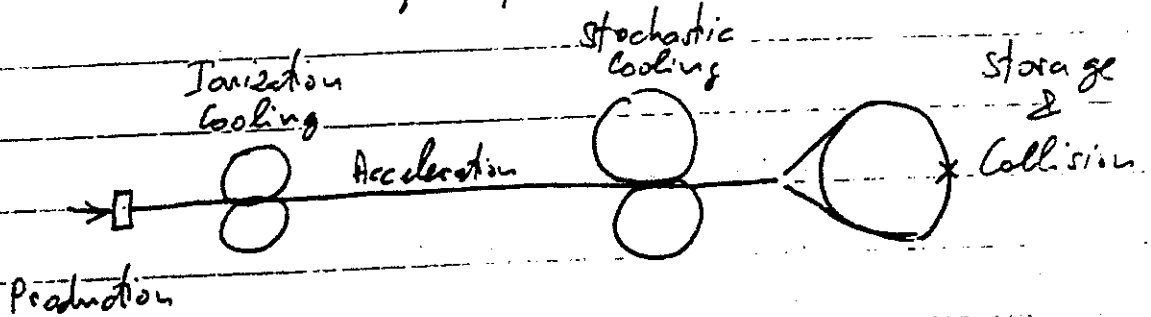
~~(2.65)~~

~~(2.55)~~

~~(7.1 sec)~~

~~(13)~~

Scenario  $\mu^+ - \mu^-$



luminosity  $L = \frac{N_0^2 f_0}{E_n \beta^{\#}} \gamma g$

$$g = g_{ion} g_{acc} g_{sto} g_{col}$$

$$\left\{ \begin{array}{l} g_{ion} = e^{(\alpha_{ion} - \frac{2}{T_{ion}}) T_{ion}} \\ g_{sto} = e^{(\alpha_{sto} - \frac{2}{T_{sto}}) T_{sto}} \end{array} \right. \quad \begin{array}{l} \alpha_{ion} > 2/T_{ion} \\ \alpha_{sto} > 2/T_{sto} \end{array}$$

$$\begin{array}{ll} T_{ion} = 22 \mu s & @ \quad 1 \text{ GeV} \\ T_{sto} = 2.2 \text{ ms} & @ \quad 100 \text{ GeV} \end{array}$$

AGR

0 2 4 1 0 2 2

$$E_0 / c G \tau_0$$

(2)

$$g_{acc} = (E_{init} / E_{final})$$

$$E_0 = 106 \text{ MeV}$$

$$E_{init} = 1 \text{ GeV}$$

$$\tau_0 = 2.2 \text{ } \mu\text{s}$$

$$E_{final} = 100 \text{ GeV}$$

G	10 MeV/m	20 MeV/m	40 MeV/m
$g_{acc}$	0.852	0.926	0.963

$$g_{col} = \frac{\tau_{col}}{\tau_{col}} \frac{1 - e^{-2 \frac{\tau_{col}}{\tau_{col}}}}{2}$$

$$\tau_{col} = \tau_{sto} = 2.2 \text{ ms}$$

$$\tau_{col} = 0$$

$$g_{col} = 1$$

$$\tau_{col} = \tau_{col}$$

$$g_{col} = 0.432$$

$$\tau_{col} \gg \tau_{col}$$

$$g_{col} \approx \tau_{col} / 2 \tau_{col}$$

AGP

0 4 2 4 1 0 2 3

$$L = L_0 g \quad L_0 = \frac{N_0^2 f_0}{\epsilon_n \beta^*} \gamma \quad (5)$$

Modes of Operation :

- (1) No cooling at all
- (2) Ionization cooling only
- (3) Stochastic cooling only
- (4) Both Ionization and stochastic cooling

Proton Source (20 GeV 100  $\mu$ A)  
 yield  $2 \times 10^{-4}$   $\mu$ /p  $I_p = 20$   $\mu$ A

$N_0 f_0 = 1.25 \times 10^{11}$   $\beta^* = 1$  cm  
 $\epsilon_n = 100$   $\pi$  mm.mrad  $\gamma = 1000$

Mode (1) and (2) - (3) and (4)

$f_0$	100 Hz	36 Hz
$N_0$	$1.25 \times 10^9$	40
$L_0$	$5.0 \times 10^{24} \text{ cm}^{-2} \text{ s}^{-1}$	$1.7 \times 10^{17} \text{ cm}^{-2} \text{ s}^{-1}$

Required  $L = 10^{30} \text{ cm}^{-2} \text{ s}^{-1}$

PR

0 1 2 3 1 3 2 4

④

Storage Rings

Ionization

Stochastic

E	1 GeV	100 GeV
$\gamma$	10	1000
B <sub>field</sub>	1 T	6 T
R/p	2	2
$2\pi R$	40 m	700 m
$f_{rev}$	7.2 MHz	0.43 MHz

→ cooling time	< 11 $\mu$ s	< 1.1 ms
# revolutions	1000	17000
T	140 $\mu$ s	38.8 ms
$g_{ion,sto}$	$2 \times 10^5$	$5.9 \times 10^{12}$
→ cooling time	5.6 $\mu$ s	0.6 ms

AGR

0 4 2 4 1 0 2 5

Ionization Cooling

Cooling Rate  $\alpha_{ion} = \frac{f_{rev}}{2} \frac{dU}{dE}$

$$U = \frac{0.307 \text{ MeV}}{\beta^2} \frac{Z}{A} (\rho s) \frac{\text{g/cm}^2}{\text{g/cm}^2} \log \frac{2 Z_0 \beta^2 \gamma^2}{W Z}$$

$Z_0 = 0.5 \text{ MeV}$

$\log \approx 14$

$W = 10 \text{ eV}$

$$\alpha_{ion} = \frac{1}{2} \frac{f_{rev} U}{E \log}$$

$U \sim 0.7 \text{ GeV} \quad \nabla \nabla$

$$E_{cool} = \beta_L \frac{E \langle \theta^2 \rangle}{U}$$

$$\langle \theta^2 \rangle_{rad} = 0.157 B \frac{Z(Z+1)}{A} \frac{(\rho s) \text{g/cm}^2}{(pV)_{MeV}^2} \quad B \sim 10$$

ALR

0 4 2 4 1 0 2 6

⑥

Stochastic Cooling

Cooling Rate:  $\alpha_{sto} = n_{dev} f_{rev} \frac{2g-g^2}{N}$

optimum gain  $g = 1$   $n_{dev} = 4$

$N \approx 1000$  (40)

Gain  $\rightarrow$  140 dB

Thermal Power:  $P_T = 10^{f/10} k_B T_K W A^2$

$f = 3 \text{ dB}$   $W = 3 \text{ GHz}$   $T_K = 1^\circ \text{K}$

$P_T \sim 10 \text{ W}$

$\epsilon_{\infty} = D \tau_{sto}$

$\epsilon_{\infty} = 4 \beta_L N R_K P_L \gamma (e l / d \beta^2 E)^2$

$R_K \sim 100 \text{ ohm}$

$l \sim d$

$\beta_L \sim 10 \text{ m}$

$\epsilon_{\infty} \sim 5 \times 10^{-8} \text{ mm.mrad} \rightarrow \frac{g_{sto}}{g_{sto}} \approx 2 \times 10^9$

$L \sim 0.3 \times 10^{27} \text{ cm}^{-2} \text{ s}^{-1}$

$N = 1000$

$W = 100 \text{ MHz}$

$L \sim 0.8 \times 10^{28} \text{ cm}^{-2} \text{ s}^{-1}$

AGL

# Electron-Muon Collider

(7)



100 GeV/beam

$$L = 10^{31} \text{ cm}^{-2} \text{ s}^{-1}$$

$$L = \frac{N_\mu N_e f_0}{\epsilon_n \beta^2} \gamma g$$

$$g_{ion} = g_{acc} = g_{col} =$$

$$g = g_{sto} = e^{(\nu_{sto} - 1/\tau_{sto})}$$

The two beams match in size  $\epsilon_{0e} = 200 \text{ eom}$

Beam Power Electron	2 MW
average current	20 $\mu\text{A}$
$f_0$	100 MHz
$N_\mu$	1000
$N_e$	$1.25 \times 10^6$
Cooling Time	2.5 $\mu\text{s}$
$\delta_n$ , required	$4 \times 10^{-8}$ $\pi$ mm. <small>needed</small>
$\epsilon$ , electron	$\sim 10^{-5}$ $\pi$ mm. <small>needed</small>

No Disruption on either Beam (?)

ALR

$e^{\pm}$  - Linear Collider <sup>0 4 2 4 1 0 2 8</sup>

(6)

100 GeV/beam

$$L = 10^{32} \text{ cm}^{-2} \text{ s}^{-1}$$

Hi-Frequency Mode to avoid Beam-Beam

$$L = \frac{N_+ N_- f_0}{E_n \beta^2} \gamma g$$

$$g = 1$$

Beam Power / beam	2 MW
average current / beam	20 $\mu$ A
$f_0$	100 MHz
$N_+ = N_-$	$1.25 \times 10^6$
$\gamma$	$2 \times 10^5$
$\beta^2$	1 mm
$E_n$ , required	<u><math>10^{-2}</math></u> $\pi$ mm merid

But

$$D \sim \frac{N}{E}$$

0 4 2 4 1 0 2 9

2/17



0 4 2 4 1 0 3 0

**Proton Storage Ring with Intensity Greater than  
Space Charge Limit**

**Vadim Dudnikov**

**BINP**

PROTON STORAGE RING  
with INTENSITY  
GREATER than SPACE  
CHARGE LIMIT.

Vadim Dudnikov  
Budker Institute of  
Nuclear Physics  
Novosibirsk, Russia.

The proton (ion) beam with  
intensity up to  $10^3$  time greater  
than space charge limit can  
be accumulated in storage  
ring, and can be used for  
secondary particles production  
with high pulsed intensity.

The compensation of space charge is used very effective in transportation of the high intensity ion and electron beams (non circulating).

The space charge compensation of the circulated beams are very attractive

Relativistic stabilized electron beam

BUCKER, 1953.

STARTING POINT- 1960

DEVELOPMENT OF FIRST PROTON-PROTON and proton-antiproton COLLIDER PROJECTS

1960

The Methods for high Brightness beam production  
CHARGE-EXCHANGE INJECTION, ELECTRON COOLING A.E. 22, 1967.  
p. 348.

NEGATIVE ION SOURCES DEVELOPMENT:

DOUBLE ELECTRON CAPTURE METHOD  $H^+ + A \rightarrow H^0 + A^+ \rightarrow H^- + A^+$  up to 0.1 A  
Arc discharge Ion Source, multislit extractor  
PLASMA NI SOURCES (EHLERS-TYPE)

SURFACE-PLASMA NI SOURCES (ADMIXTURE CATALYSIS)  
CESIUM, BARIUM

1971

L. ALVAREZ, REV. SCI. INST., 22, 705, 1951 1 < 1MKA 1960 0.2MKA

HIGH-INTENSITY and HIGH-BRIGHT PROTON BEAM ACCUMULATION  
BY CHARGE-EXCHANGE INJECTION IN STORAGE RING  
1966 G. BUCKER, G. DIMOV and V. DUDNIKOV

1966

ELECTRON-COMPENSATED PROTON BEAM IN STORAGE RING  
WITH INTENSITY 10 TIMES > SPACE CHARGE LIMIT

1976.

DIMOV, CHUPZHYANOV, SHAMOVSKY,  
Bucker, Dudnikov

Rev. Sci. Inst. 63(4) pt. II. p. 2660  
143

0 4 2 4 1 0 3 3

STRONG INSTABILITIES of the BETATRON  
OSCILLATIONS of the CIRCULATED PROTON BEAM

by

VADIM DUDNIKOV

NOVOSIBIRSK, RUSSIA

Budker Institute of Nuclear Physics

AGS Department BNL

Charge Exchange Injection  
development for High  
Brightness proton Beam Production  
G. Budkez, G. Dimov, V. Dudnikov (1960-6)

COMPENSATED PROTON-BEAM PRODUCTION IN  
AN ACCELERATING RING AT A CURRENT ABOVE  
THE SPACE-CHARGE LIMIT

G. Budkez, G. Dimov, V. Dudnikov,  
V. Chupriyanov, V. Shamovsky  
1967 - 1977.

$W = 797 \text{ MeV}$

$2\pi R = 90 \text{ m}$

$\Omega/2\pi = 2.795 \text{ MHz}$

$Q_x Q_y = 3.17, 2.13$

$N \approx 2.3 \cdot 10^{13}$

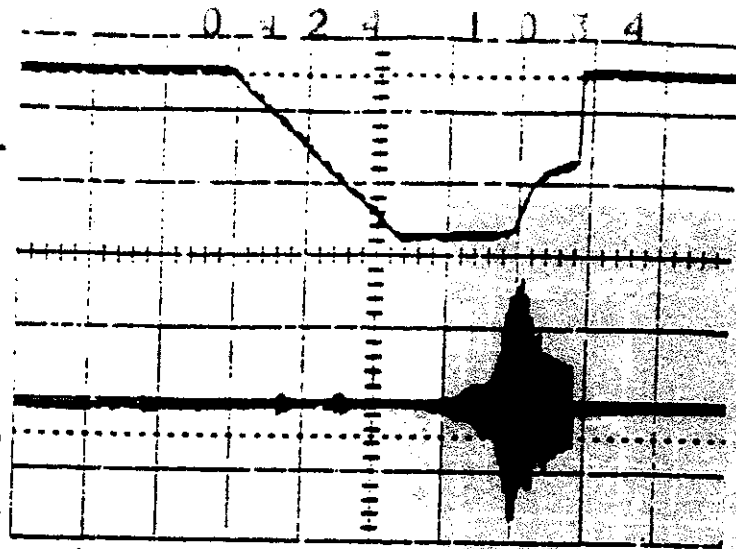
$12 \text{ Hz}$

$5.2 \cdot 10^{13} \text{ design}$

$0.5 \cdot 10^{12} \text{ unbare}$

$1.5 \cdot 10^{12} \text{ bare}$

threshold



Los Alamos PSR 0.5ms  
Beam current (upper trace) and vertical difference signals (lower trace) under unstable conditions.

Small scale storage ring.

$R = 42 \text{ cm}$

$\Delta R = 8 \text{ cm}$

$\Delta Z = 4 \text{ cm}$  RF  
 $5 \text{ MHz}$

weak focusing ring  
 $h = 0.5$

strong focusing ring

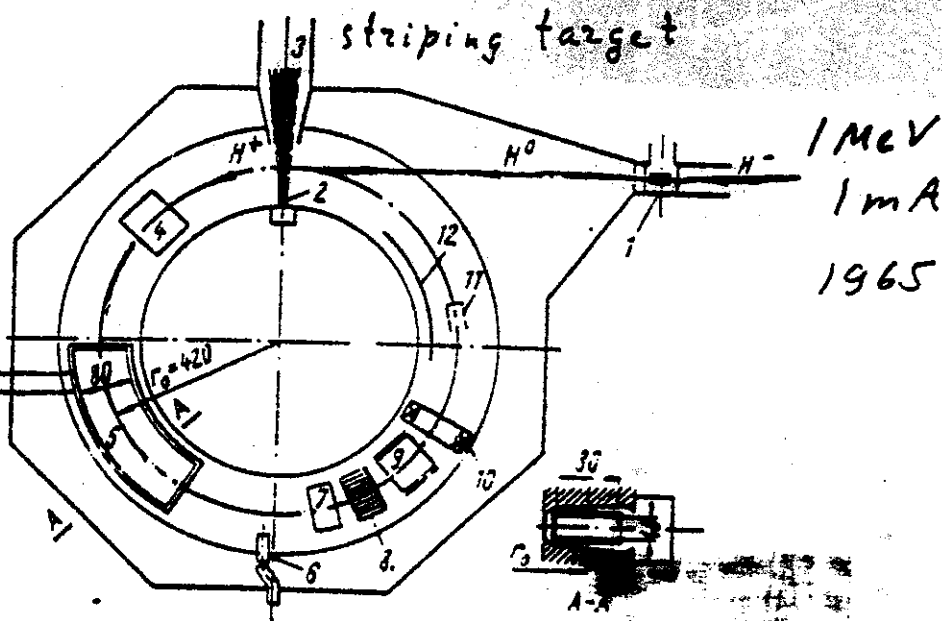
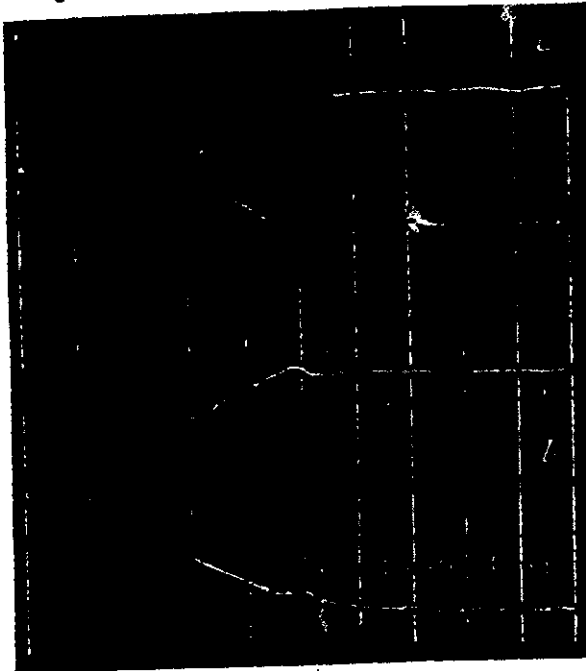


Fig. 2. Schematic diagram of the accumulation chamber. 1) Neutralizing target; 2) Laval nozzle; 3) gas-receiving cone; 4) induction electrode; 5) drift tube; 6) collector; 7) delta electrode; 8) sectioned beam profile delta electrode; 9) induction position electrodes; 10) Rogowski loop; 11) Faraday cylinder; 12) electrode for suppressing coherent oscillations.

# The catalysis of Negative Ion Production in Gas Discharges by doping of small Admixture of Cesium or other substances with low Ionization Potential

Cesium Catalysis of Negative Ion Production in Gas Discharge  
Discovered in 1971 in INP



Осциллограммы тока циркулирующего пучка протонов, накопленного перезарядным методом, иллюстрируют рост накопленного тока с длительностью инжекции, которая в случаях "а" и "б" отличается вдвое.

Oscillogram pictures for the current of a coating proton beam, accumulated by the charge-exchange method, show an increase of a stored current with injection duration, which in cases "a" and "b" is twice as different.

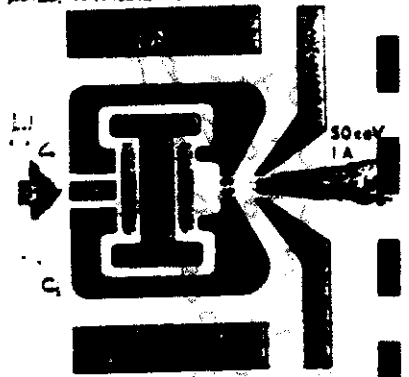
Ионные и атомарные пучки  
Ion and atomic beams

нов, предельные по пространственному заряду, а при использовании специальных мер (обратная связь, компенсация электронами) этот предел удаётся превзойти почти на порядок.

a method enables one to store the maximum proton current and with the use of special means like feedback and compensation with electrons, a proton current exceeding by an order of magnitude the space-charge limit of an uncompensated proton beam can be achieved.

Развитие метода перезарядной инжекции потребовало разработки серии сильноточных источников отрицательных ионов.

The exploitation of the charge-exchange



Поверхностно-плазменный метод получения отрицательных ионов (эмиссионная плотность ионов  $H^-$  до  $2 A/cm^2$ )

The surface-plasma method for obtaining negative ions ( $H^-$  ion emission density, up to  $2.7 A/cm^2$ )

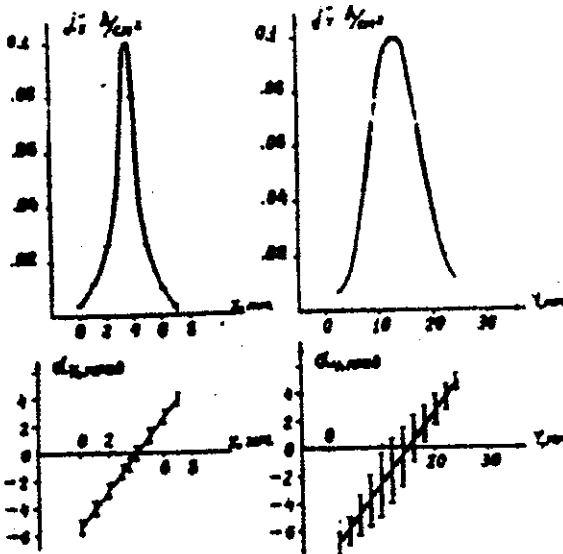
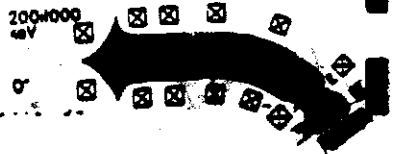


Рис. 12. Основные характеристики пучка в сфокусированном режиме.  
 $0,05 A$ ;  $20 kV$ ;  $E_x \approx 7 \cdot 10^{-7}$  см. рад;  
 $E_y \approx 1,4 \cdot 10^{-5}$  см. рад.

slowly  
large  
The  
In  
a  
for  
ten-  
sur-  
на,  
less  
for  
ivy  
the  
sse  
of  
ve-  
cs.  
in  
vy  
ge  
ch  
a.



Конверсия  $D^+ \rightarrow D^0$  в плазменной ионошени (достигнутая эффективность 82%)

$D^+ \rightarrow D^0$  conversion in plasma ionization (efficiency obtained is 82%)

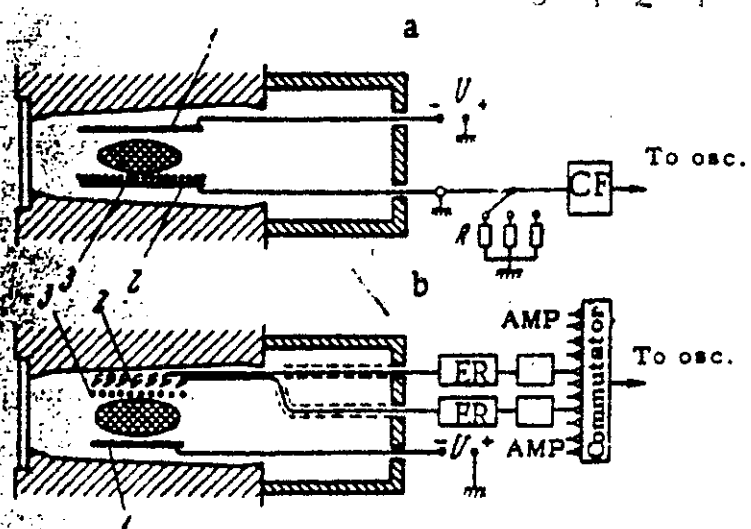


Fig. 1. Arrangements for measuring the proton current in the tract (a) and the radial current distribution (b): 1) reflecting plate; 2) collector; 3) screen grid.

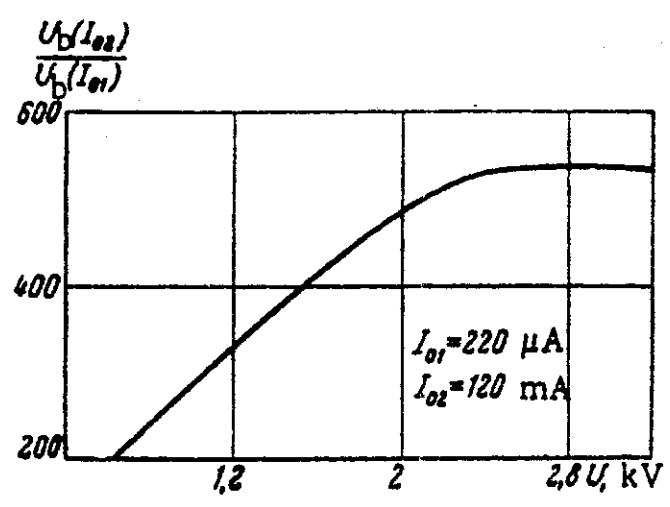


Fig. 2. Ratio of the signals from the collector and Faraday cylinder for the first revolution: a) signal from the Faraday cylinder; b) signal from the proton collector. Pulse length 600 μsec.

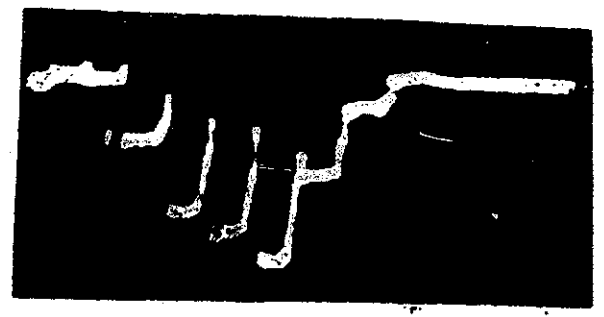


Fig. 4. Oscillogram of the radial proton distribution. Step 9 mm.

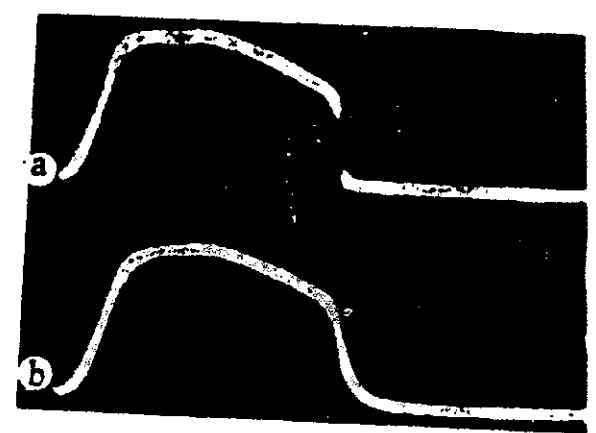


Fig. 3. Oscillograms of proton current in the tract: a) signal from the Faraday cylinder; b) signal from the proton collector. Pulse length 600 μsec.

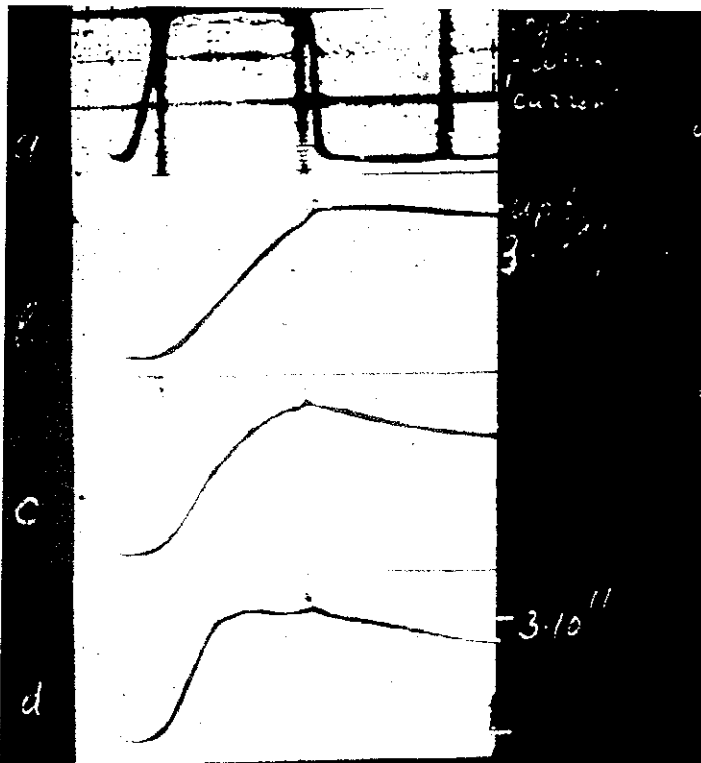


Fig. 3.  
Charge-Exchange injection

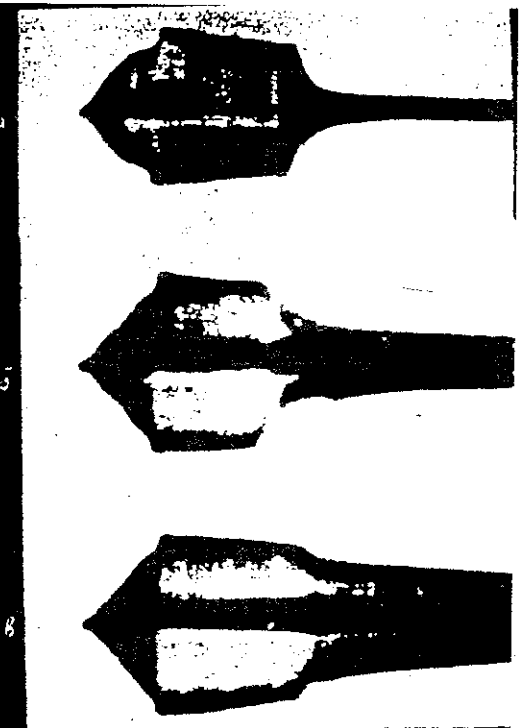
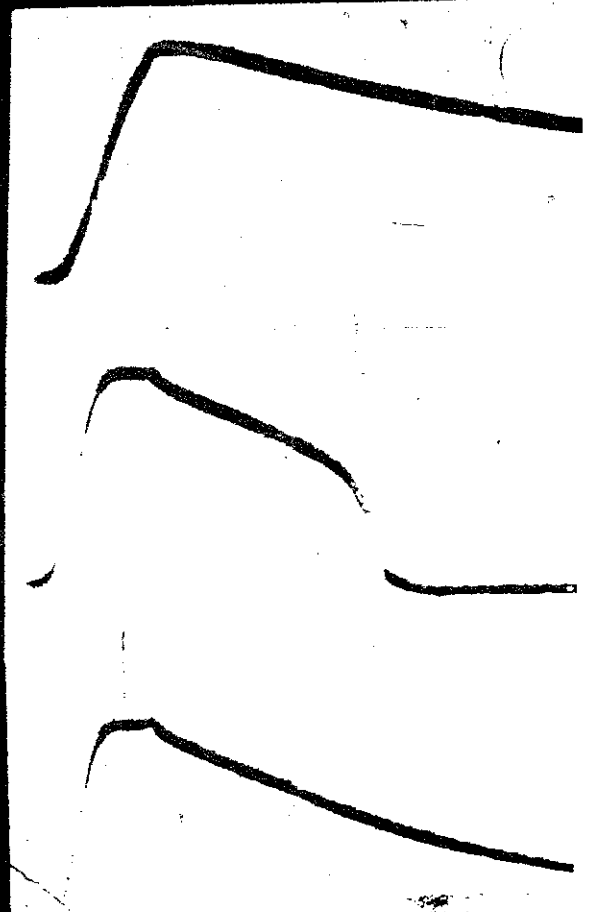
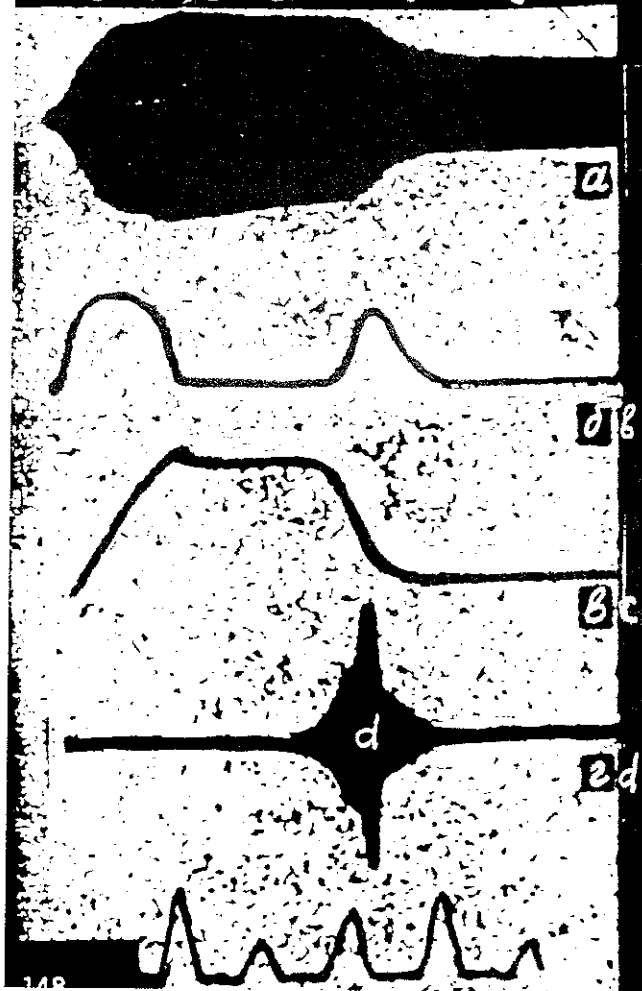
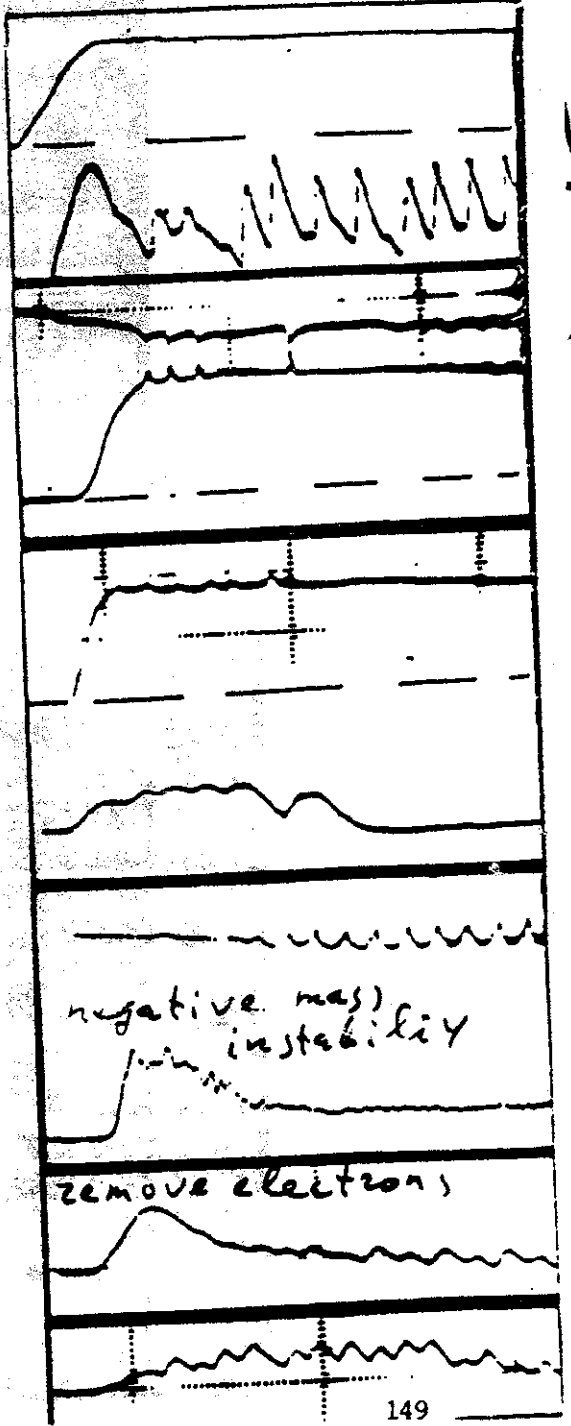
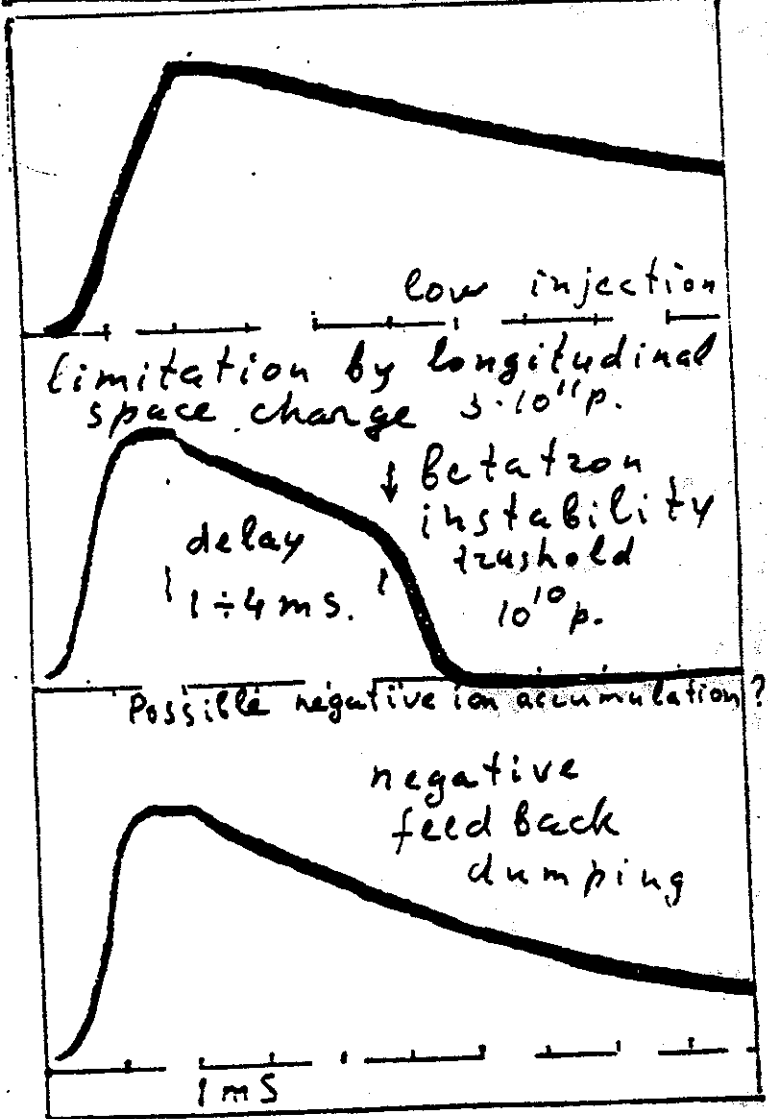
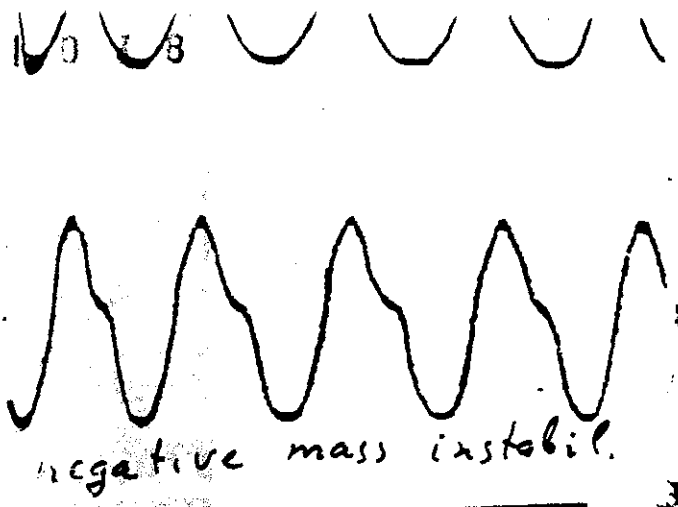
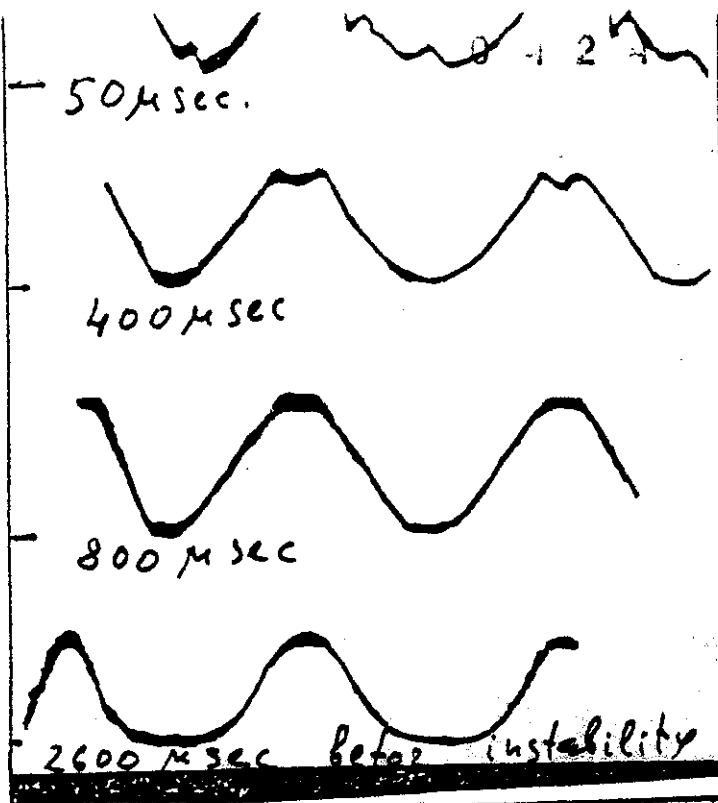


рис. 14 индукционный сигнал при наличии когерентных бетатронных колебаний  
 а -  $V_{\beta} = 1,4$  кв; б -  $V_{\beta} = 2,8$  кв; в -  $V_{\beta} = 4,2$  кв.  
 Transverse coherent instability of betatron





# TRANSVERSE COLLECTIVE INSTABILITY

proton  
beam  
(bunched)  
Novosibirsk  
INP  
1966

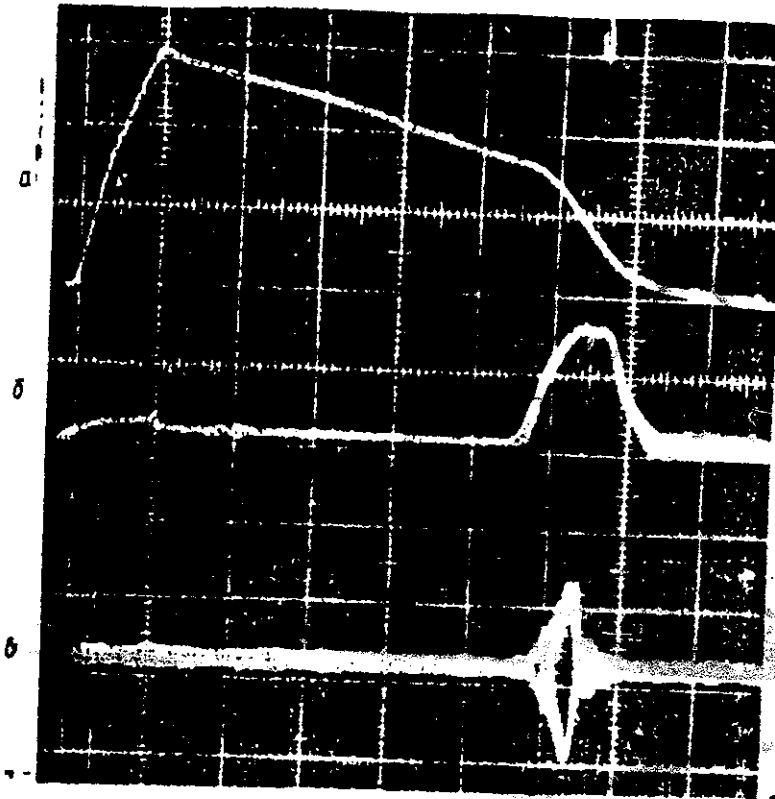
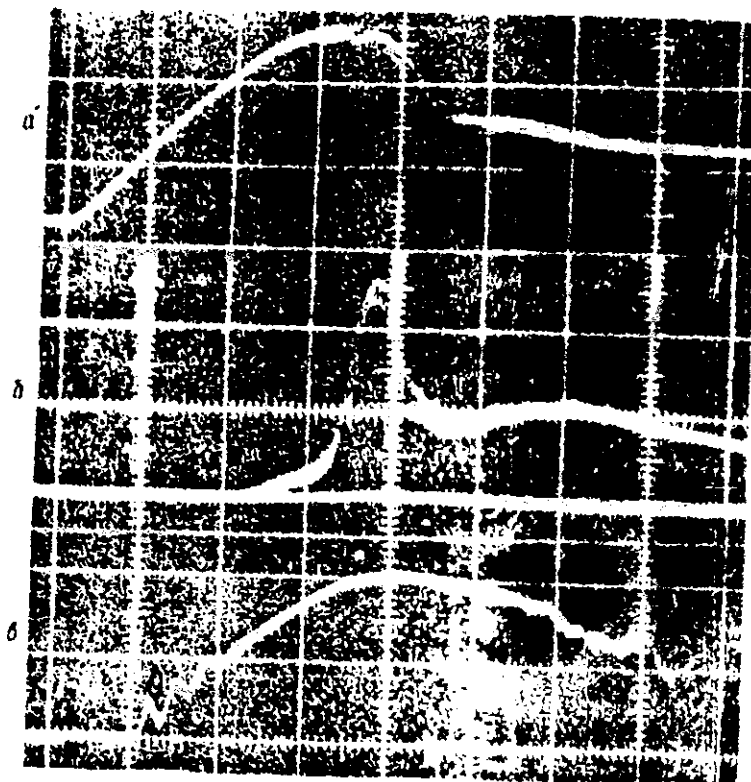


Рис. 1. Осциллограммы тока на дорожке (а) тока на внутренней стенке (б) и в.ч. сигнала с индукционного электрода радиального положения (в). По горизонтали 500 мксек на деление



proton  
beam  
(unbunched)

Рис. 2. Осциллограммы тока в (а) ток на дорожке (б) и детектирование (в) под пучком

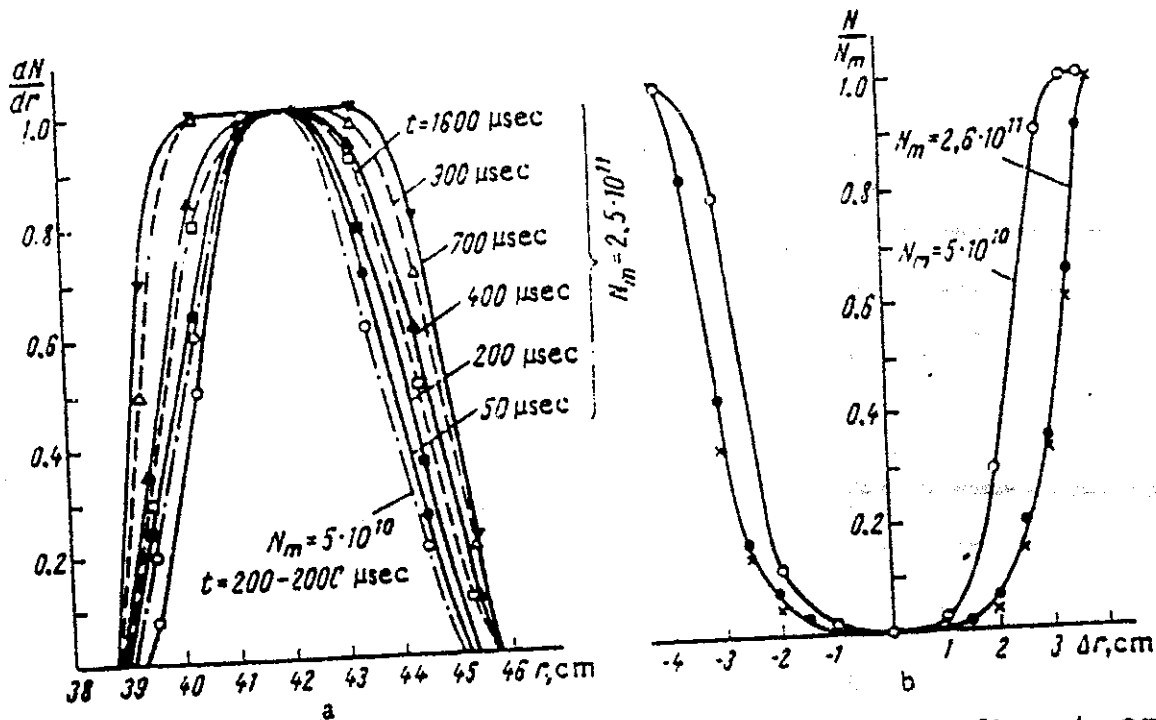


Fig. 9. Distribution of the proton current along the radius at various instants of time (a) and its dependence on the radial aperture  $\Delta r$  (b).  $\uparrow$  measured by gas ionization beam profile monitor.

In the weak focused accelerators the intensity of accumulated proton beam is limited by longitudinal space charge electric field of bunches, often magnified by "NEGATIVE MASS" instability.

In strong focused accelerators it is possible to accumulate proton (ion) beam up to transverse space charge limit in bunched beam.

1967 4 24 1041

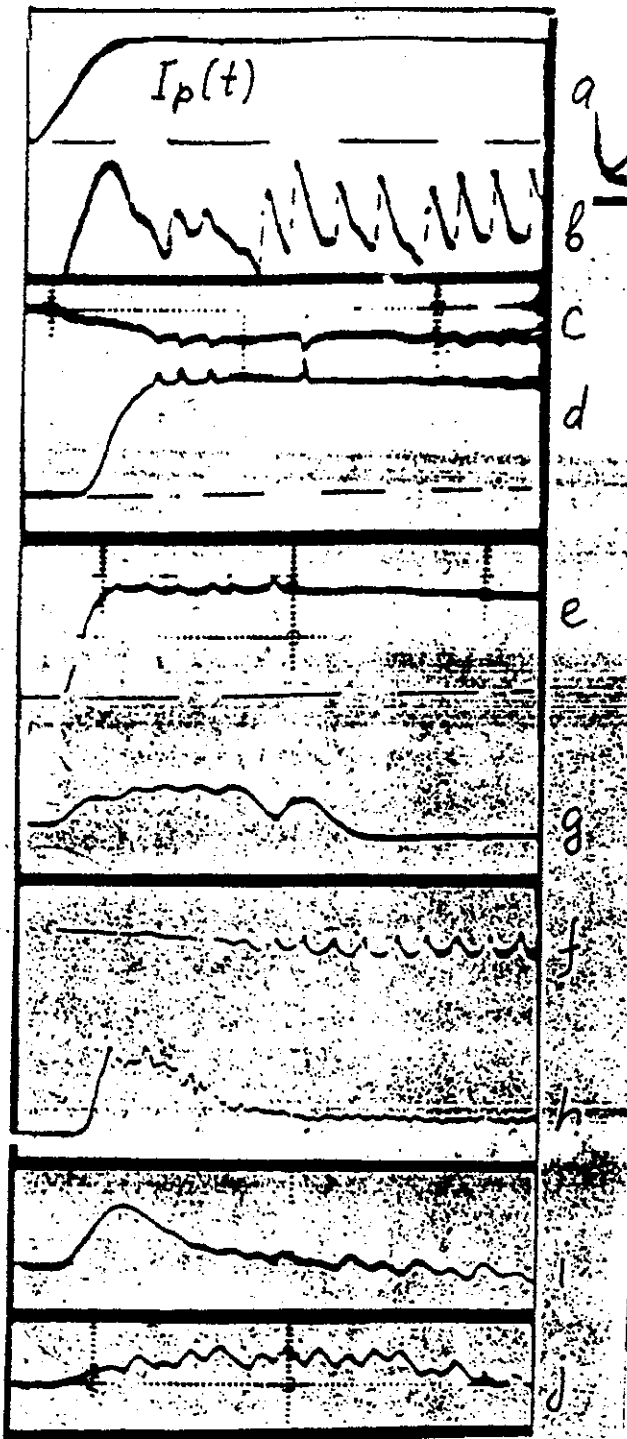


Fig. 1. Oscillograms of the relaxation oscillations of the density of the compensating electrons (along the horizontal, 20  $\mu$ sec/division): a) current on the track; b) induction signal from the ring electrode (pass band 5 MHz); c) current to the electron collector at a repelling potential of 20 to 30 V; d, e, g) coupling induction signals from the electrodes; f) current to the ion collector having a blocking voltage of 15 V; h) detection signal which registers the longitudinal bunching of the beam; i) current to the ion collector having a blocking voltage of 30 V; j) the same, with an energy spread in the injected beam.

relaxation of compensation

u-p instability

Chirikov B.V.

The Stability of partly  
Compensated Electron  
Beam, Sov. Atomic

Energy" v. 19

p.p. 239-44, 1965.

Small RF modulation of  
proton density is remove  
the electrons and dump  
transverse instability.

accumulation of protons  
in betatron regime

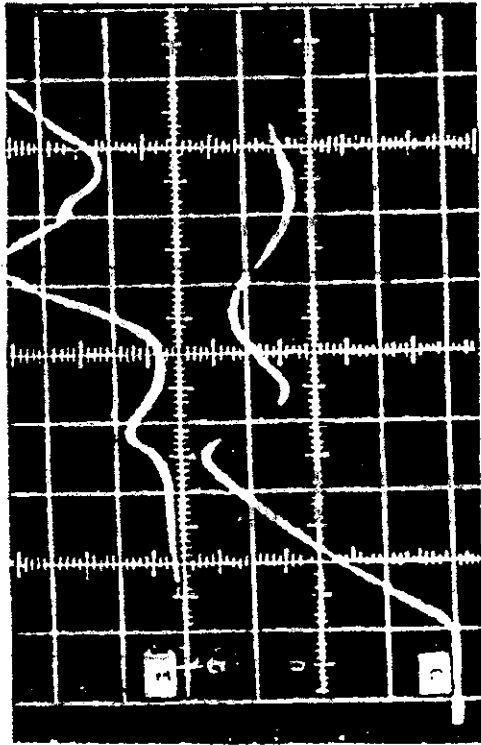


Fig. 4

Fig. 4. Current on the track (a) and current to the sampler above the beam (b) (along the horizontal, 20  $\mu$ sec/division).

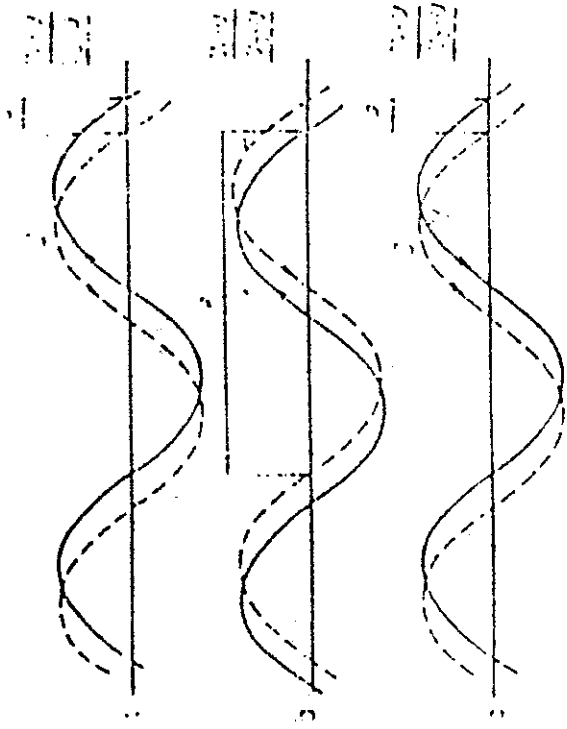


Fig. 5

Fig. 5. The effect of attraction between two pinches on the development of a transverse wave: 1) pinch of positively charged particles; 2) pinch of negatively charged particles;  $v$  is the phase velocity of the wave;  $v_1$  and  $v_2$  are the longitudinal velocities of the pinches: a) mutual build-up,  $v_2 < v < v_1$ ,  $\varphi = 0 - \pi$ ; b) mutual damping,  $v_2 < v < v_1$ ,  $\varphi = \pi - 2\pi$ ; c) first pinch is damped, while the second builds up,  $v_2 < v > v_1$ ,  $\varphi = 0 - \pi$ .

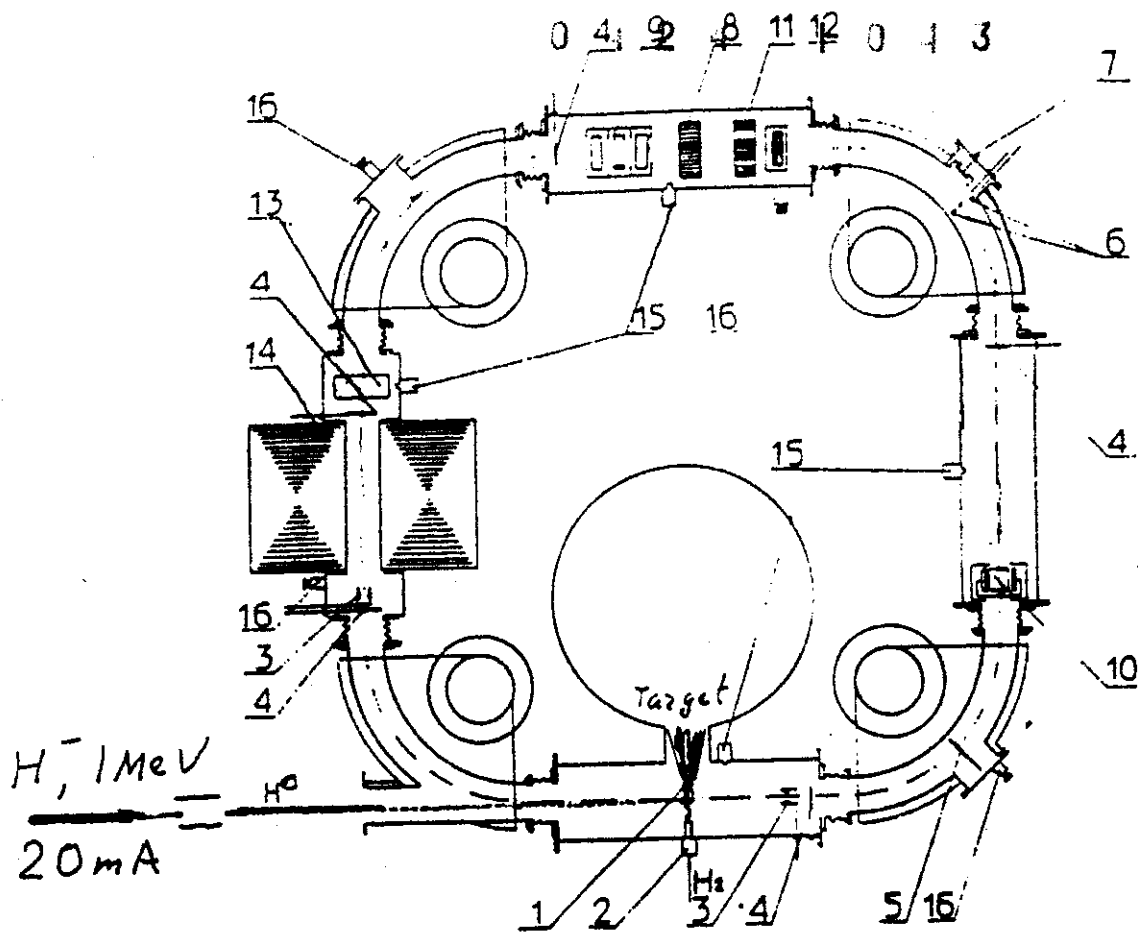


FIGURE 1 Layout of the proton storage ring. 1—secondary stripping gas target. 2—pulsed gas valve. 3—Faraday cups. 4—quartz screens. 5, 6—mobile targets. 7—ion collector. 8—Rogovsky coil. 9—“pick-up” station. 10—electrostatic transducer of quadrupole beam oscillations. 11—magneto-inductance transducer. 12—transducer of vertical beam losses with high time resolution. 13—device for measuring the secondary charged-particle concentration in the beam region. 14—betatron core. 15—electromagnetic gas valves of the system of pulsed gas leak-in. 16—microleaks of the system of stationary gas leak-in.

TABLE I  
Storage-Ring Parameters

1. Proton energy	1 MeV
2. Field intensity in bending magnets	3500 G
3. Index of field decrease	0.2 to 0.7
4. Radius of rotation in magnets	42 cm
5. Length of the straight sections of an orbit	106 cm
6. Aperture of vacuum chambers in bending magnets	6 x 4 cm
7. Revolution frequency of protons in the storage ring	1.86 MHz
8. Duration of injection pulse	up to 300 μsec
9. Repetition frequency of injection pulse	0.2; 0.1 Hz
10. Injection current	up to 8 mA

$$\Delta V_z \rightarrow 0.85 \rightarrow 0.5 \quad N = 1.9 \cdot 10^{11} p.$$

$$\Delta V_z \quad 0.85 \rightarrow C \quad \Lambda = 2.9 \cdot 10^{11} p.$$

$$F = \frac{P \frac{m_0}{m}}{(K-f)^2 - v^2} + \frac{P \frac{M}{m}}{f^2 - p \frac{M m_0}{m^2}} = 1.$$

$$K < v + \sqrt{\frac{M m_0}{m^2}}$$

STABILITY OF A CLOSED PROTON BEAM

1663

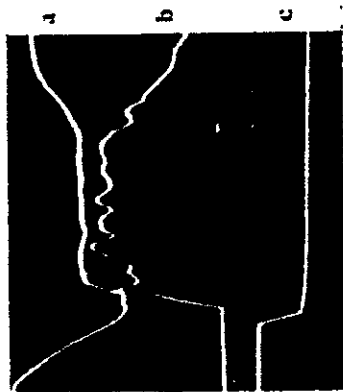


Fig. 2. a) Proton current on track; b) detected signal from induction electrodes for vertical position of beam; c) voltage on extraction plates. Horizontal scale: 100 psec/div.

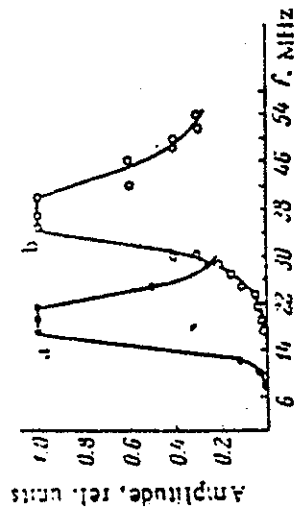


Fig. 3. Spectrum from induction electrodes for vertical position of beam. a)  $N = 1.7 \cdot 10^{10}$ ; b)  $1.5 \cdot 10^{11}$  particles.

$$P = 4 \cdot 10^{-4} \text{ torr} \quad n: 3 \cdot 10^8 \quad K \sim 60$$

the beam on resonance (11-95 oscillation modes) for

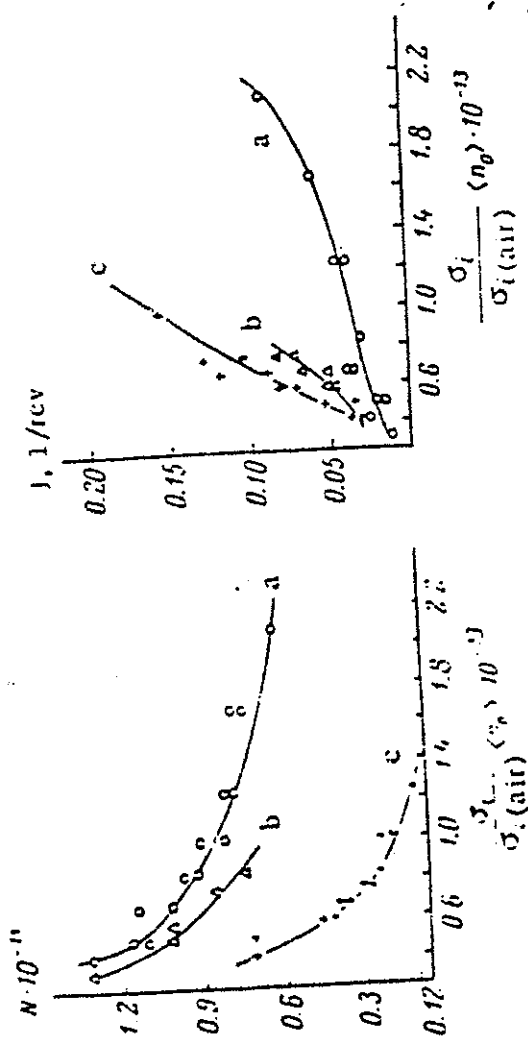


Fig. 4. Growth rate ( $N$ ) and threshold ( $I$ ) of the instability as functions of mean density and kind of residual gas. a) Hydrogen; b) helium; c) air.

# Proton accumulation with removing of secondary particles



Fig. 5. a) Proton current on track. b) detected signal from induction electrodes for vertical position of beam; c) voltage on extraction plates. Horizontal scale 50  $\mu\text{sec} / \text{div}$ .

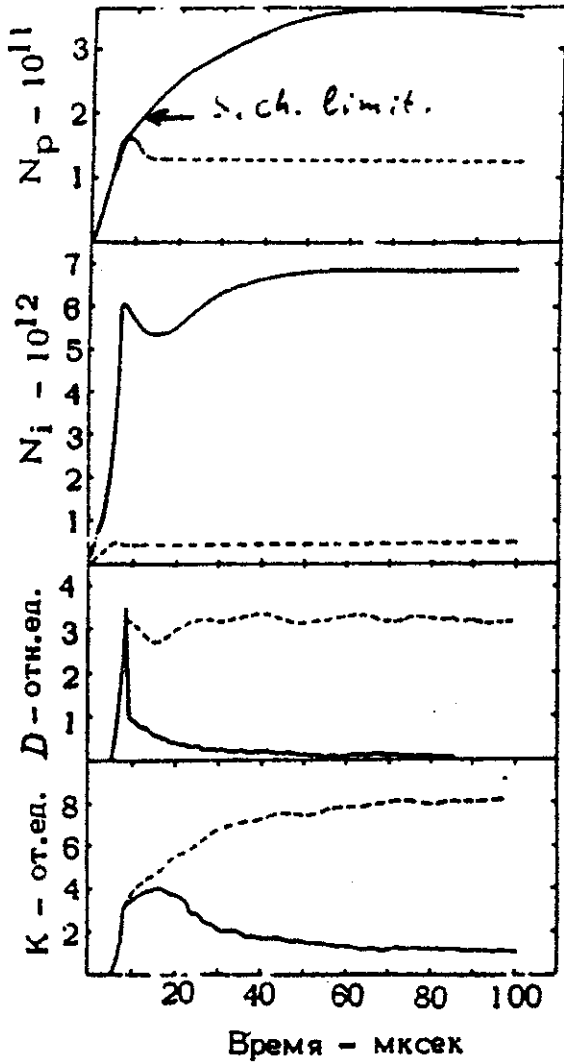


Рис. 1. Процесс накопления протонов в компенсированном пучке перезарядным методом при давлении водорода  $1,4 \cdot 10^{-3}$  тор (пунктирные кривые) и  $3,6 \cdot 10^{-3}$  (сплошные кривые). Ток инжекции протонов  $5,5$  (в конце 1-го оборота).

$N_p$  - число протонов в пучке;  
 $N_i$  - число вторичных ионов в пучке;  
 $D$  - амплитуда высокочастотного сигнала с электродов вертикального положения на единицу орбитальной скорости;  
 $K$  - то же с квадрупольных электродов.

*dipol oscillat.*

*quadrupol oscillation*

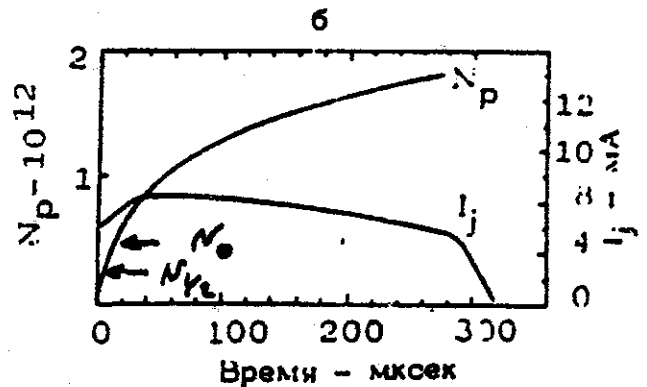
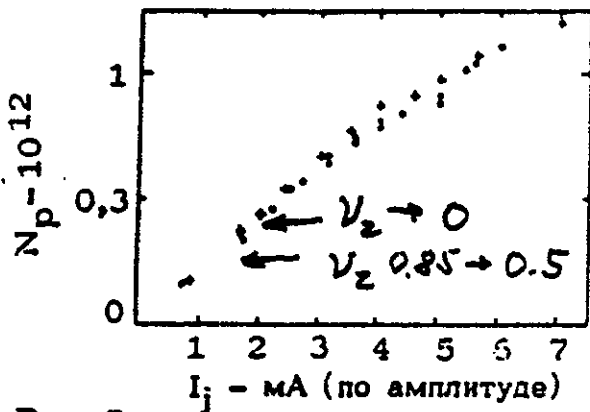
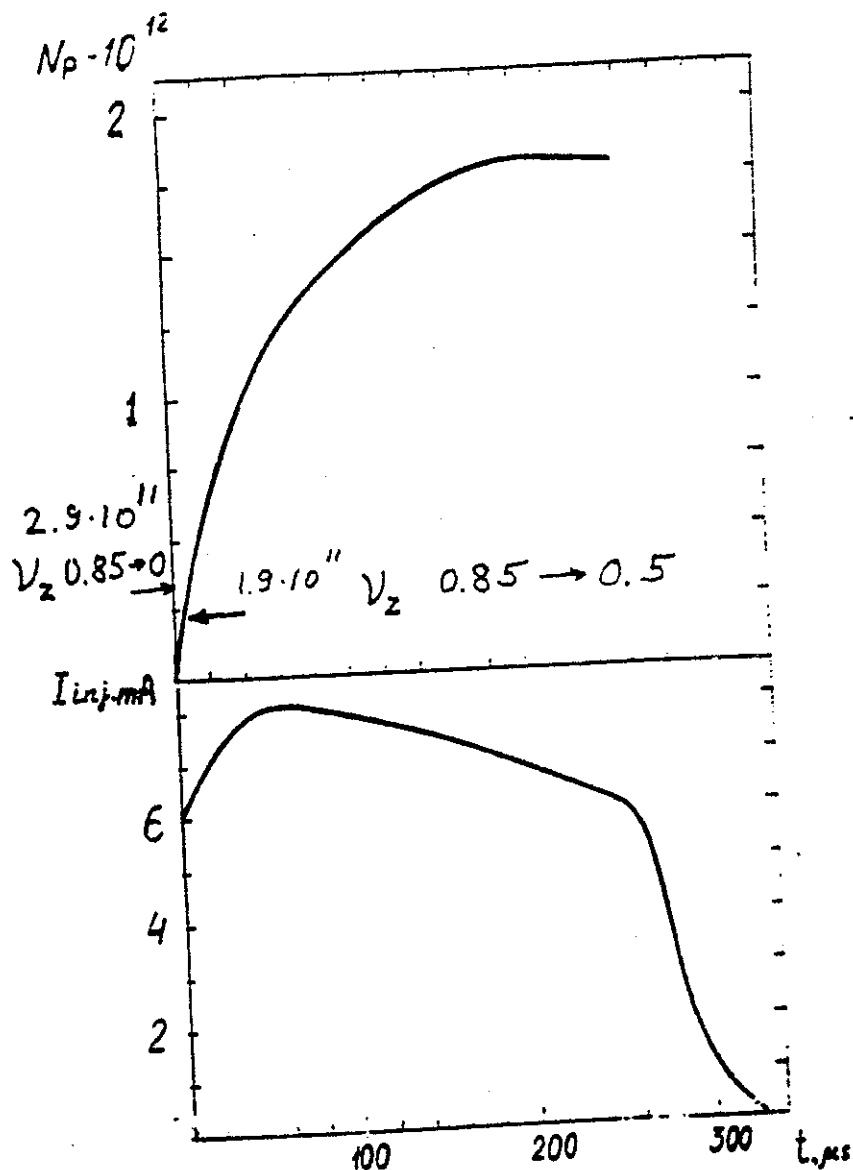


Рис. 5.

а - зависимость от тока инжекции максимального числа протонов, накопившихся в квазибетатронном режиме, при оптимальных давлениях водорода (+) и дейтерия (o);  
 б - копии осциллограмм орбитального тока ( $N_p$ ) и тока инжекции протонов (при накоплении протонов в бетатронном режиме при импульсном напуске водорода и темизированных геометрических параметрах инжекции. Максимальный захватываемый протонов  $5$  мА.



ograms of stored protons in betatron mode (a) and the injection current  
g pulsed pumping of hydrogen.

It is possible to reach  
stable existing in storage  
zing of ion beam, compensated  
by electrons, with intensity  
more higher, than space charge  
limit.

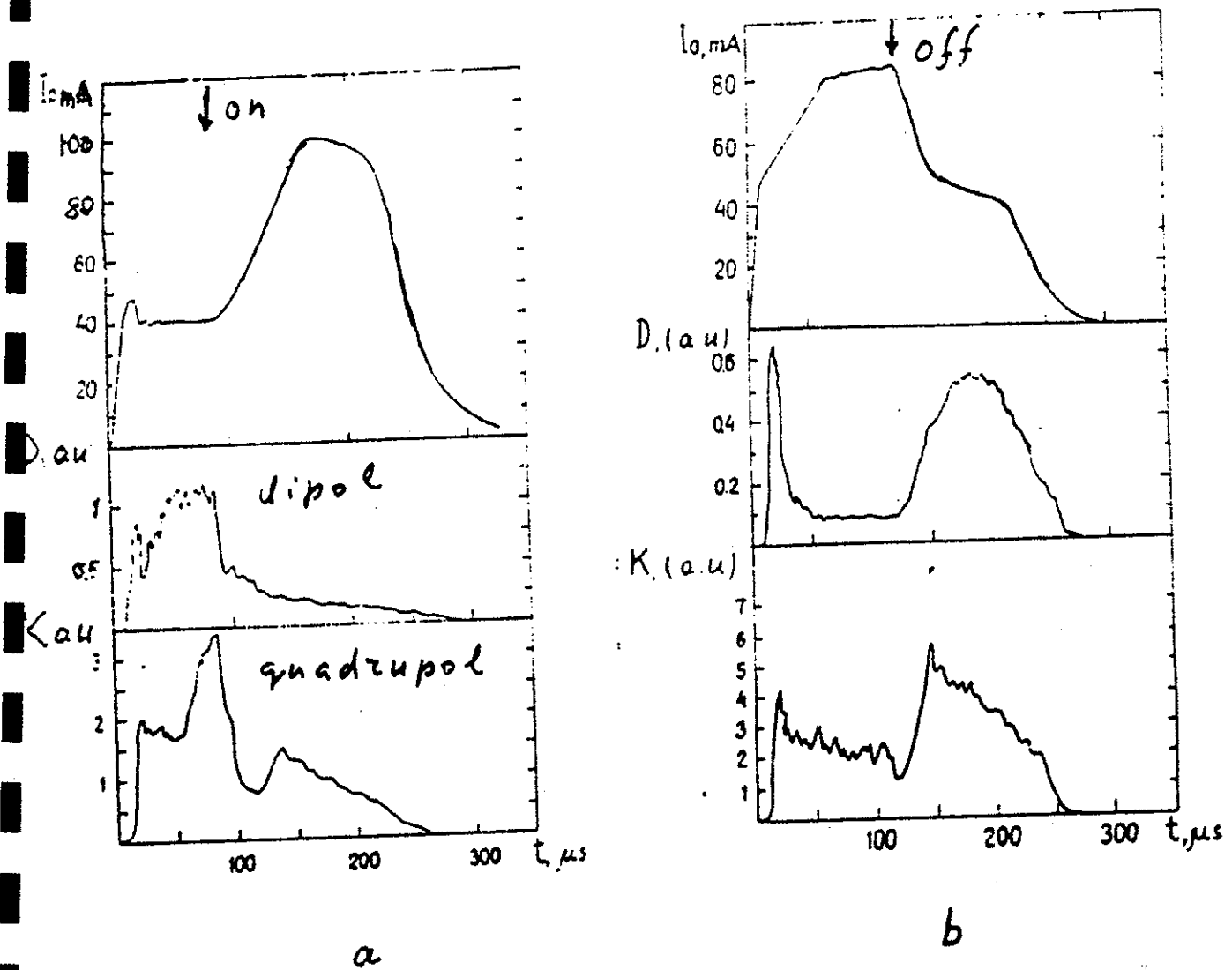


FIGURE 15. Proton current  $I_0$  and the envelopes of rf signals from the electrostatic vertical-position electrodes ( $D$ ) and from the quadrupole oscillations transducer ( $K$ ) of a proton beam. (Copies of oscillograms). The emission current in the ionizers is 25 A. The arrows indicate the times of switching on (a) and switching off (b) the extracting voltage.

Protons accumulation with additional ionization by electrons.

It is very acceptable to use microwaves for additional gas ionization.

$$\frac{\omega_e^2 + \omega_i^2}{\omega_p^2} \approx \frac{\omega_e^2}{\omega_p^2} = \frac{n_e m_p}{n_p m_e} \gg 1; \quad G = \frac{\omega_e}{\omega_z} \frac{n_p m_e}{n_e m_p} \ll 1;$$

$$k v_p = \omega_z + \omega_e (1 \pm G^{1/2});$$

$$\lambda = \frac{2\pi}{k} \lesssim a_z \rightarrow n_e \gtrsim \frac{m_e v_p^2}{2\pi e^2 a_z} = \frac{\beta_p^2}{2\pi z_e a_z^2}$$

The equations for the coupled vertical motions of the protons and electrons within the beams are:

$$\ddot{y}_p + (Q_y^2 + Q_p^2)\Omega^2 y_p = Q_p^2 \Omega^2 \bar{y}_e,$$

and

$$\ddot{y}_e + Q_e^2 \Omega^2 y_e = Q_e^2 \Omega^2 \bar{y}_p,$$

$$\text{where } Q_e \Omega \cong \sqrt{\frac{2N r_e c^2 (1-n_e)}{\pi b(a+b)R}}, \text{ and } Q_p \Omega = \sqrt{\frac{2\eta_e N r_p c^2}{\pi b(a+b)\gamma R}}.$$

The motions are coupled through the center of mass  $\bar{y}_e$ ,  $\bar{y}_p$  oscillations. Assuming harmonic motion obtains the dispersion relation.

$$(Q_e^2 - x^2)(Q_y^2 + Q_p^2 - (n - x)^2) = Q_e^2 Q_p^2,$$

where  $x = \omega/\Omega$  is the oscillation frequency in terms of the revolution frequency. For PSR parameters,  $Q_e \cong 40$  ( $\sim 100$  MHz). The dispersion relation has complex solutions (instability) near  $x \approx Q_e \approx n - Q_y$ , provided  $Q_p$  is large enough. For the PSR, this means  $Q_p > 0.1$ , which implies that a neutralization of  $\eta_e > 0.01$  (1%) can lead to instability at a relatively low electron density. Some stabilization by Landau damping (frequency spread) is possible; the stabilization effects seen in the PSR are qualitatively in agreement with the e-p model.

$$p, e, i \quad \ddot{y}_p + \omega_y^2 y_p = \frac{2\pi e^2}{m_p} [n_e y_e - n_i y_i - (n_e - n_i) y_p]$$

$$\omega_e^2 = \frac{2\pi e^2 n_e}{m_e} \quad \ddot{y}_i = \frac{2\pi e^2}{m_i} [n_e y_e - n_p y_p - (n_e - n_p) y_i]$$

$$\ddot{y}_e = \frac{2\pi e^2}{m_e} [n_p y_p + n_i y_i - (n_i + n_p) y_e].$$

$$F(\omega) = \frac{\omega_p^2}{(k v_p - \omega)^2 - \omega_y^2} + \frac{\omega_e^2 + \omega_i^2}{\omega^2} = 1.$$

$$\frac{e\omega_e^2 + \omega_i^2}{\omega_p^2} \approx \frac{\omega_e^2}{\omega_p^2} \approx \frac{n_e m_p}{n_p m_e} \gg 1; \quad G = \frac{\omega_e}{\omega_y} \frac{n_p m_e}{n_e m_p} \ll 1$$

instability for  $kV_p = \omega_y + \omega_2 (1 \pm G^{1/2})$

stability, if  $\lambda = \frac{2\pi}{k} \lesssim a_y \rightarrow$

$$n_e \gg \frac{m_e V_p^2}{2\pi e^2 a_y^2} = \frac{\beta_p^2}{2\pi r_e a_y} \quad \text{for } n_p = n_e$$

$$I_p = en_p S V_p = \frac{e \beta_p^2}{2\pi r_e a_y} \pi a_y^2 c \beta_p = \frac{e c}{2 r_e} \beta_p^3 = I_0 \beta_p^3$$

$$I_0 = \frac{e c}{2 r_e} = e \cdot \frac{3 \cdot 10^{10}}{2 \cdot 2.8 \cdot 10^{13}} = e \cdot 5 \cdot 10^{22}$$

$$I_0 = 8 \cdot 10^4 \text{ A}$$

$$\text{for } W_p = 10 \text{ MeV} \quad I_p = I_0 \beta_p^3 = 240 \text{ A}$$

for inertial fusion drives.

$$\text{for } W_p = 1 \text{ GeV} \quad I_p \approx 5 \cdot 10^4 \text{ A}$$

secondary particles production

It is interesting to repeat the small scale experiment with accumulation of proton beam with super space charge intensity.

$$W_p \sim 10 \text{ MeV}, \quad R \sim 1 \text{ m}, \quad I_n \sim 0.1 \div 0.2 \text{ A}$$

$$j_n \sim 1 \text{ A/cm}^{162} \sim 10 \frac{\text{A}}{\text{cm}}$$

## SUMMARY

1. The circulated proton (ion) beam with intensity more high, than space charge limit can be accumulated in storage ring by using of charge exchange injection and space charge compensation by plasma electrons.
2. The using of high current density beam injector is important.
3. The using of microwave ionizer of low density gas can be useful.
4. Superintense proton beam can be used for neutron, muons, puls production.

0 1 2 4 1 0 5 2

**Muon Collider Work at Novosibirsk**

**Gregory Silvestrov**

**BINP**

1. Pions and Muons Acceleration at Super-Linacs of the VLEPP Facility.  
(Conceptual Project)
2. Liquid Metal Jet Target Technology for High Intensity Beams Operation
3. Liquid Lithium Cylindrical Lenses for Multi-Hertz Operation
4. Wide Angle Parabolic Lenses (Magnetic Horns) with Intense Cooling for Multi-Hertz Operation

See p. 201

1 G.I. Silvestrov, A.N. Skrinsky and T.A. Vsevolozhskaya  
 PIONS AND MUONS ACCELERATION AT THE UNK-VLE  
 FACILITY Preprint INP 91-36. Novosibirsk 1991

Not Available

2 B.I. Grishanov and G.I. Silvestrov. East Bunch to  
 Bunch Extraction of Proton from UNK Storage Ring  
 at an Energy 3 Tev  
 Report for All Union Acc. conf. - Moscow. 1990

See p. 214

3 T.A. Vsevolozhskaya. The Optimisation and Efficiency  
 of Antiproton Production within Fixed Acceptance  
 NIM 190 (1981) 479-480

See p. 222

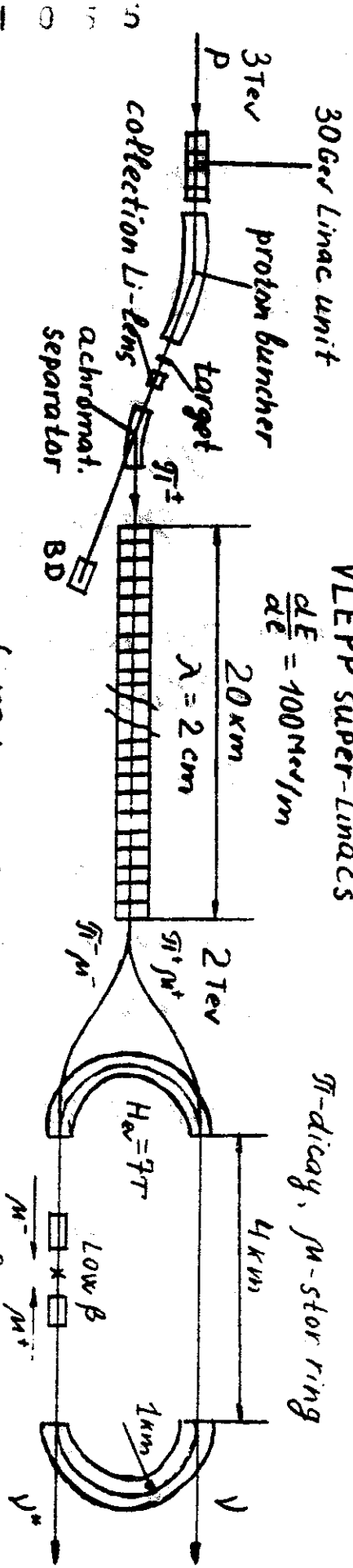
4 G.I. Silvestrov and V.A. Tayursky. A Wide-Angle Mag-  
 netic Lens for Collecting Low-Energy  $\pi$ -Mesons in a  
 Solid Angle of 40 sr. NIM 152 (1978) 371-377

See p. 229

5 B.F. Bayanov, G.I. Silvestrov et al.  
 Large Cylindrical Lenses with Solid and Liquid Lithium.  
 1st EPAC Conf. ROMA. 1989

See p. 232

6 G.I. Silvestrov. PROBLEMS OF INTENSE SECONDARY  
 PARTICLE BEAMS PRODUCTION.  
 Report for the III Int. Conf. on High Energy Acc  
 Novosibirsk 1986



VLEPP super-linacs

$\frac{dE}{dE} = 100 \text{ MeV/m}$

20 km

$\lambda = 2 \text{ cm}$

$\pi$ -dicay,  $\mu$ -stor ring

2 TeV

4 km

$H_{av} = 7T$

Low  $\beta$

1 km

$f = 100 \text{ Hz}$   $E_{\mu} = 2 \text{ TeV}$   $\tau_{\mu} = 44 \mu\text{sec}$   $n \approx 10^3 \text{ turn}$   
 $N_p = 3 \cdot 10^{14}$   $N_{\mu} \sim 5 \cdot 10^{10}$   $\mu$  per second  $\mathcal{L}_{\mu\mu} \approx 10^{28} \text{ cm}^{-2} \text{ sec}^{-1}$

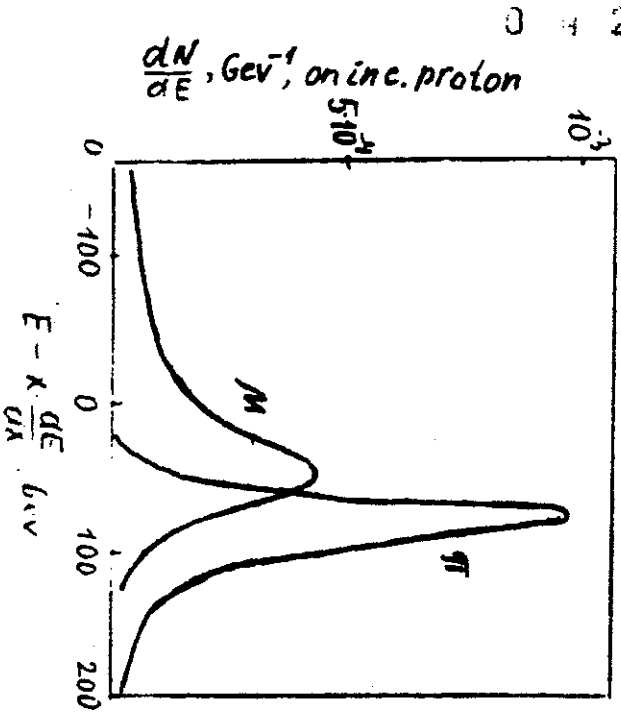
$\bar{E}$  - mean collection energy  $E_0 \approx 80 \text{ GeV}$

Accepted  $\mathcal{E}_{\pi} \sim 1.5 \cdot 10^{-3} \text{ mm rad}$ ,  $(\frac{\Delta E}{E})_{\text{accept}} \sim 0.5$

Full number accel. up to 2 TeV pions:  $N_{\pi} \approx 5 \cdot 10^{22}$  per incident prot

$\mathcal{E}_{\pi, 2\text{TeV}} = 6 \cdot 10^{-5} \text{ mm rad}$   $(\frac{\Delta E}{E})_{2\text{TeV}} \approx 2\%$

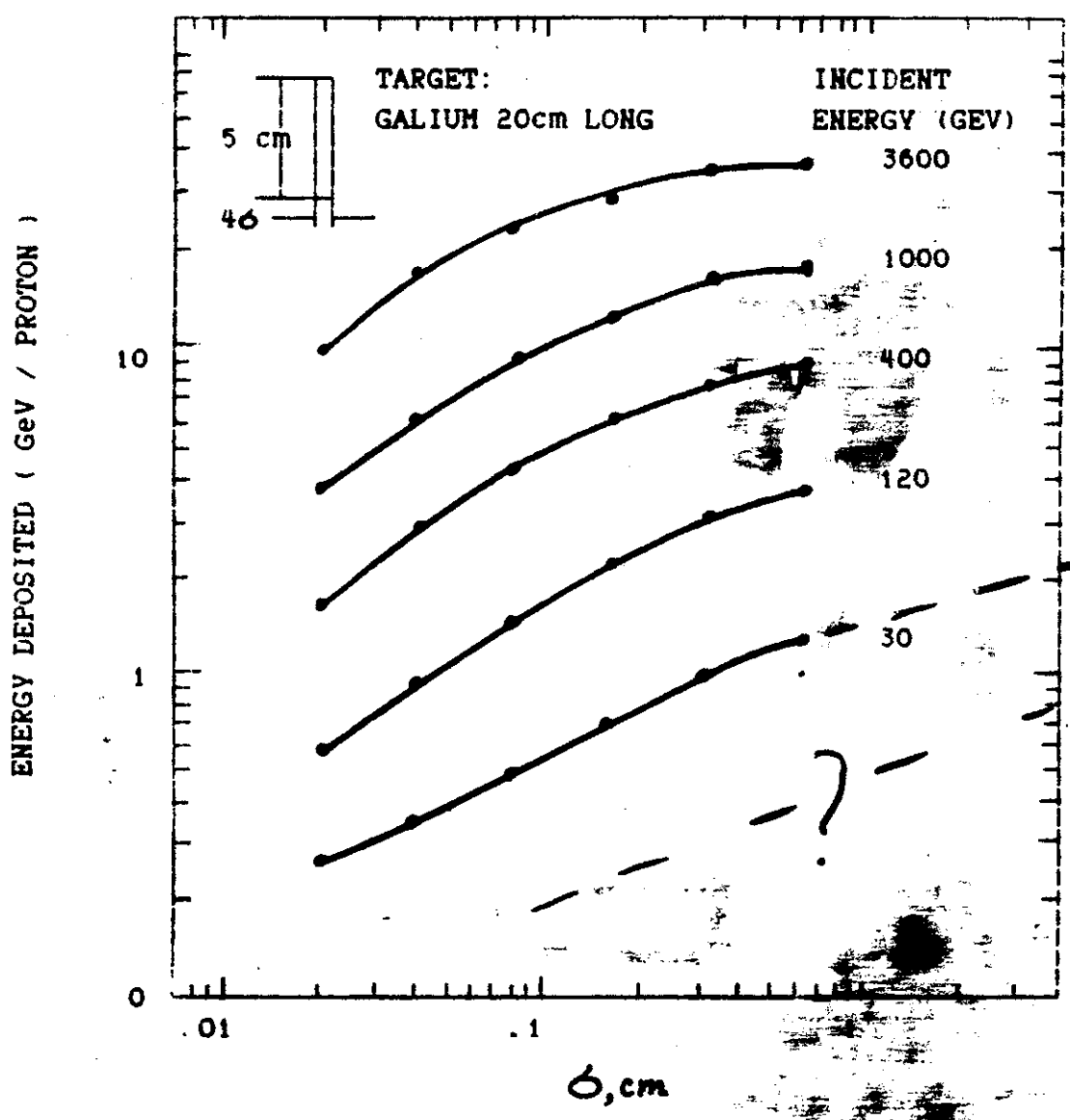
$N_p = 3 \cdot 10^{14}$   $f = 100 \text{ Hz}$   $N_{\pi} \approx 10^4$   $\pi$  per sec



0 4 2 4 1 0 5 5

## Main Reasons to develop Liquid Metal Jet Target Technology:

1. Reduction of beam energy deposition in target due to side exit of secondary
2. Decision of heat removal problem
3. Decision of target destruction problem



Full energy disposition in thin slot target  
at target thickness  $\Delta = 4.6$  vs. beam  $\sigma$

## KAON FACTORY BEAMS PARAMETERS:

$$E_p = 30 \text{ GeV} \quad I = 100 \mu\text{A} \quad N = 6 \cdot 10^{14} \text{ p.p.}$$

$$f = 10 \text{ Hz} \quad N_0 = 6 \cdot 10^{13} \text{ p.p.}$$

## EXPERIMENT WITH BEAM IN IHEP:

$$E_p = 70 \text{ GeV} \quad f = 1 \text{ pulse per } 7 \text{ sec.}$$

$$N_0 = 8 \cdot 10^{12} \text{ p.p.} \quad E_s \approx \pi 3 \text{ mm-mrad}$$

Lithium Lens focused ~~the~~ Beam to size:

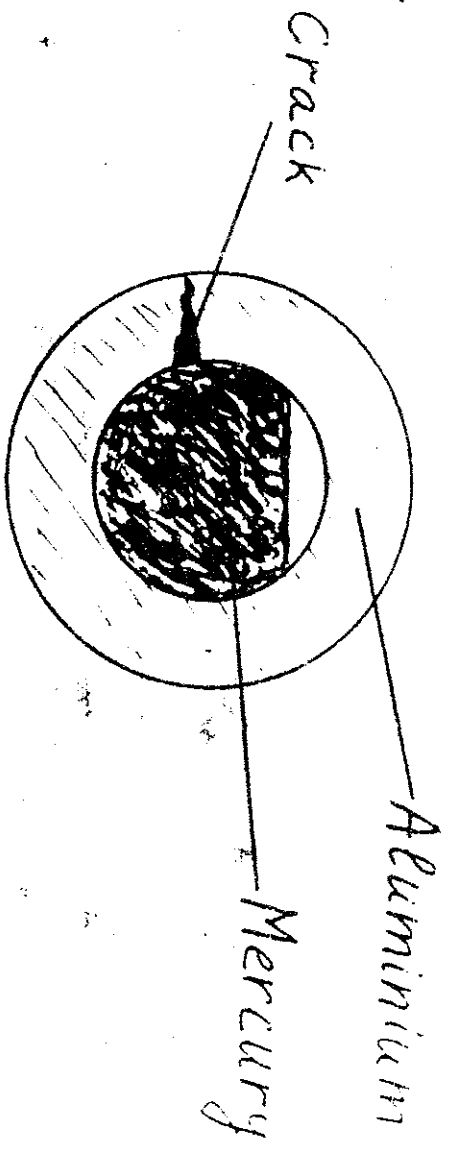
$$\sigma = 1.5 \div 0.5 \text{ mm.}$$

More interesting results of these experiments:

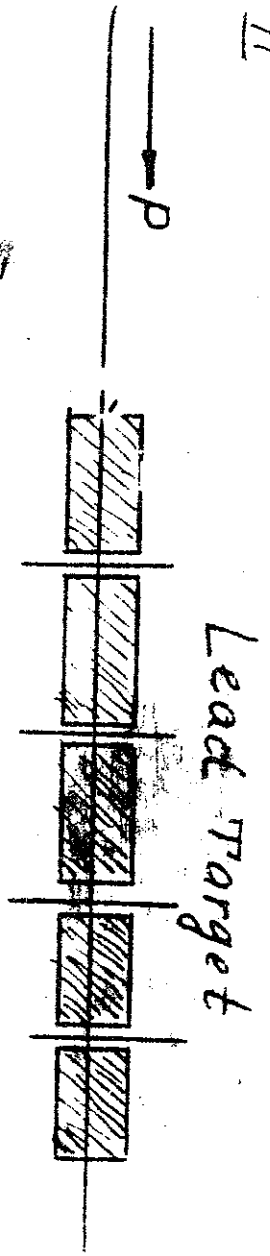
Li - Lens



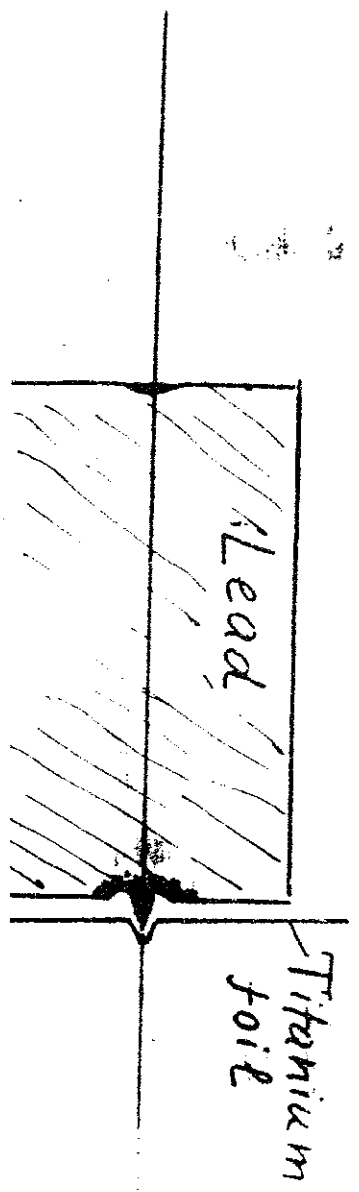
I



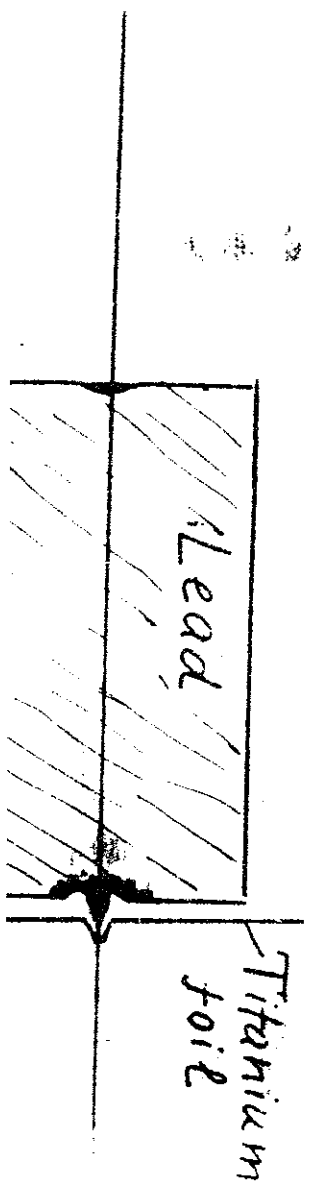
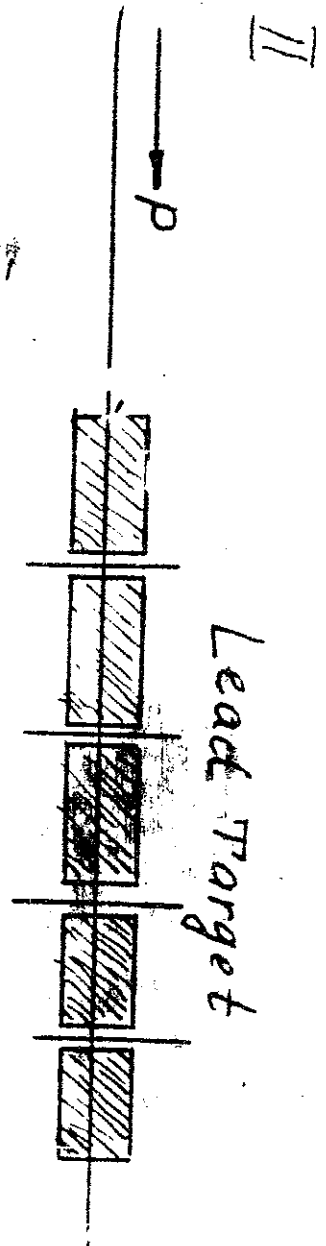
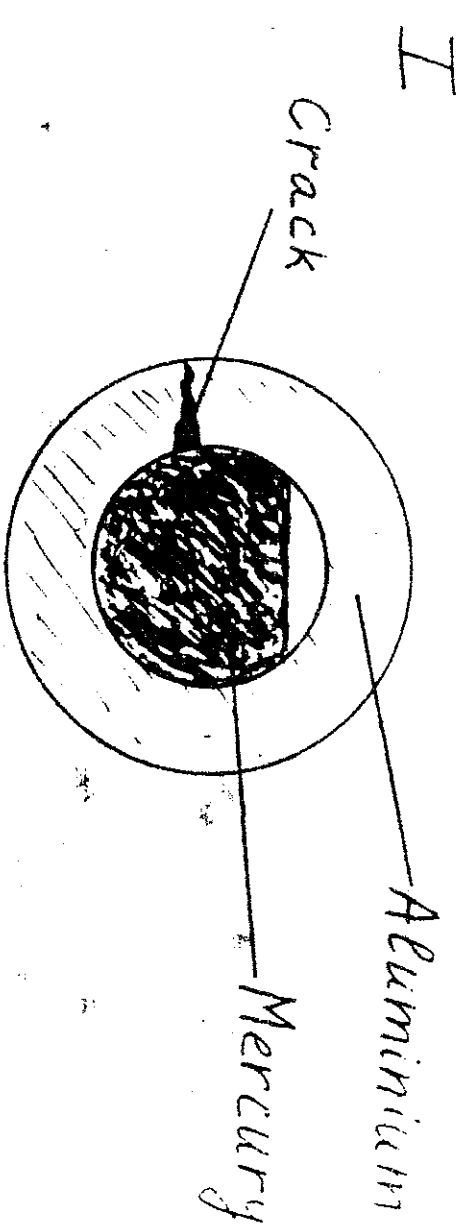
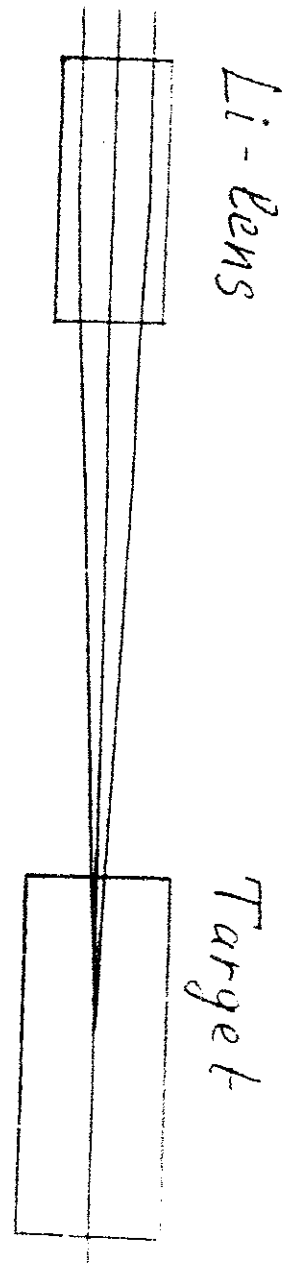
II

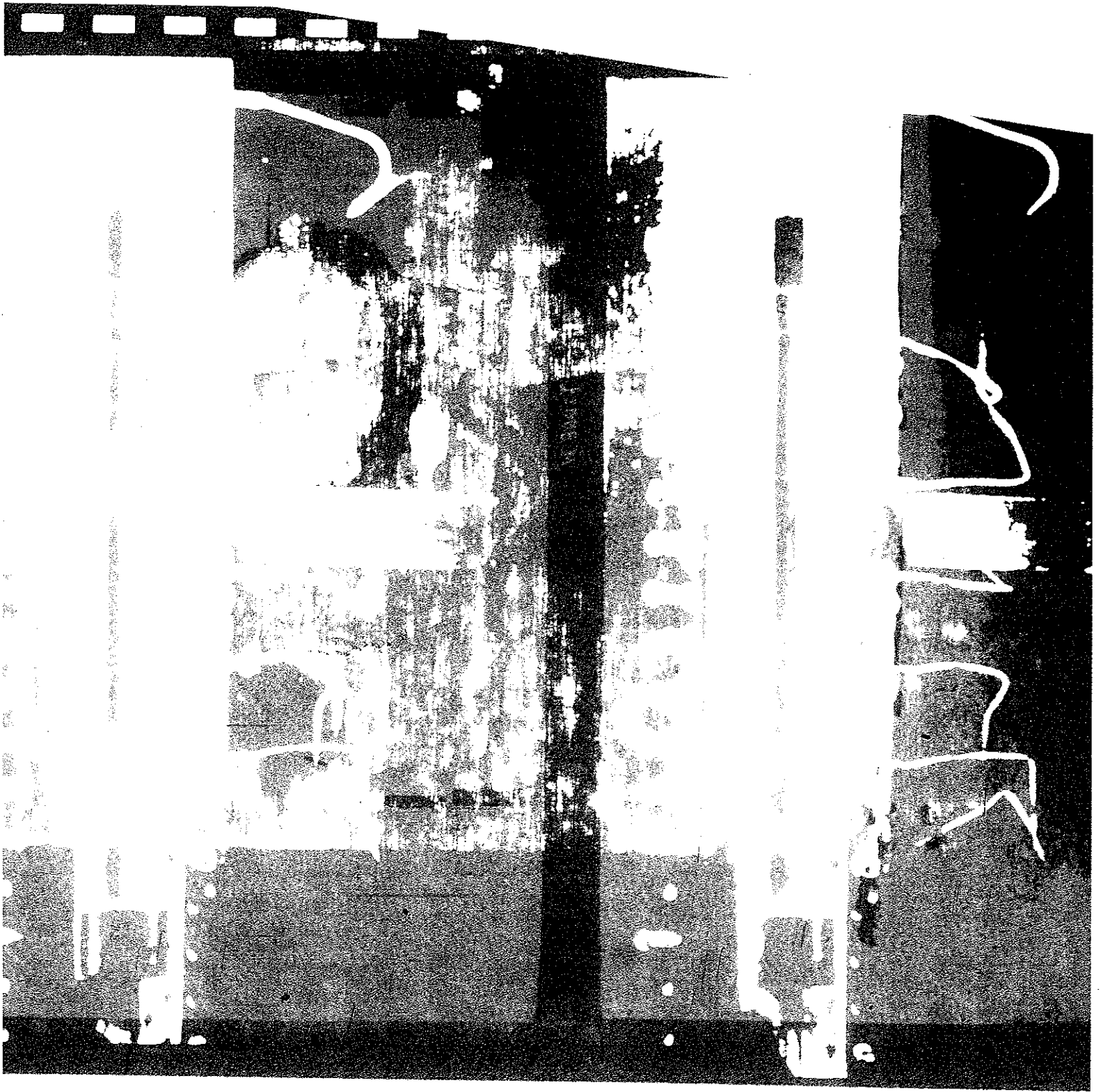


3



$E_p - TV_{GeV}$   $V = 8.70$  pp.







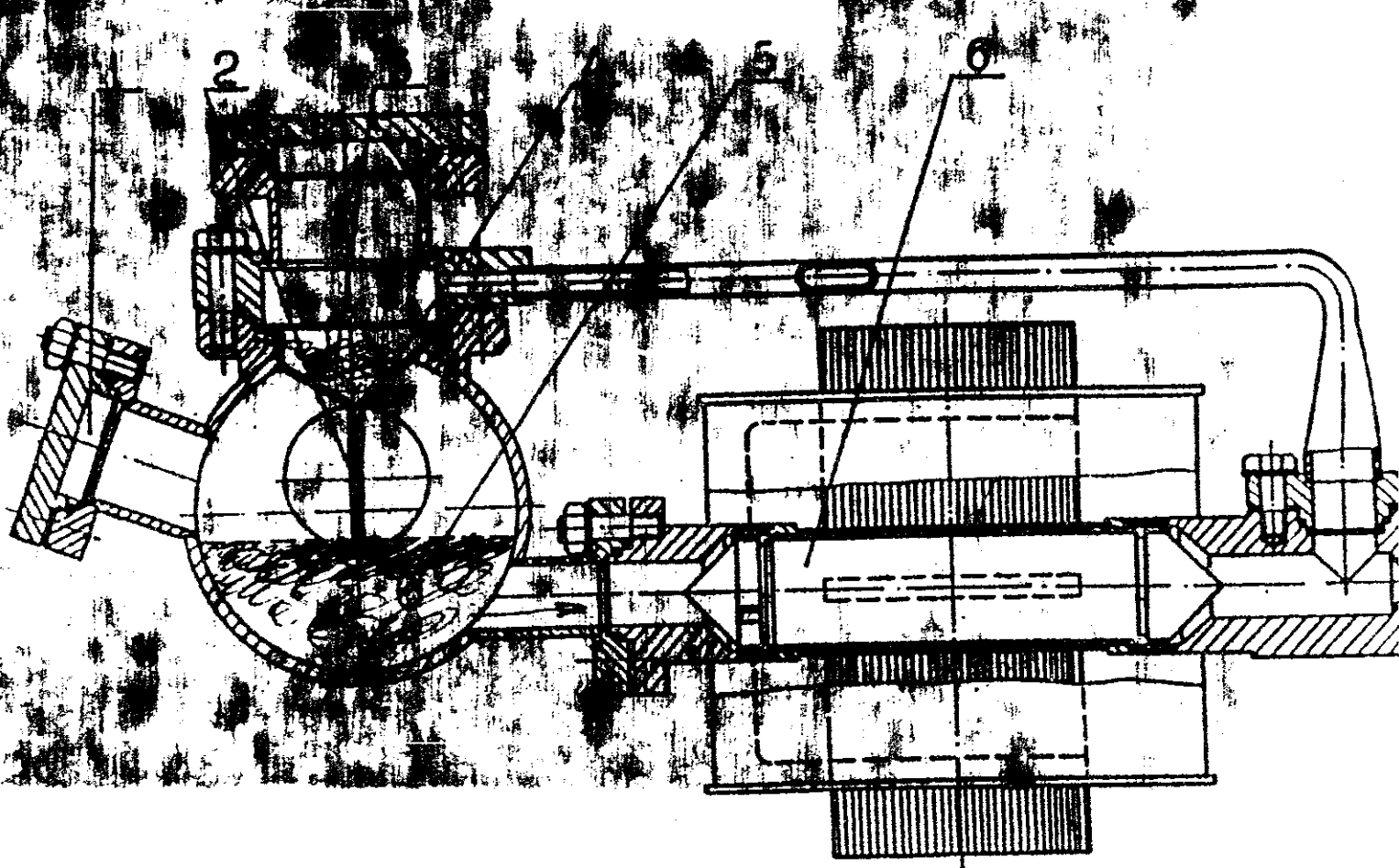
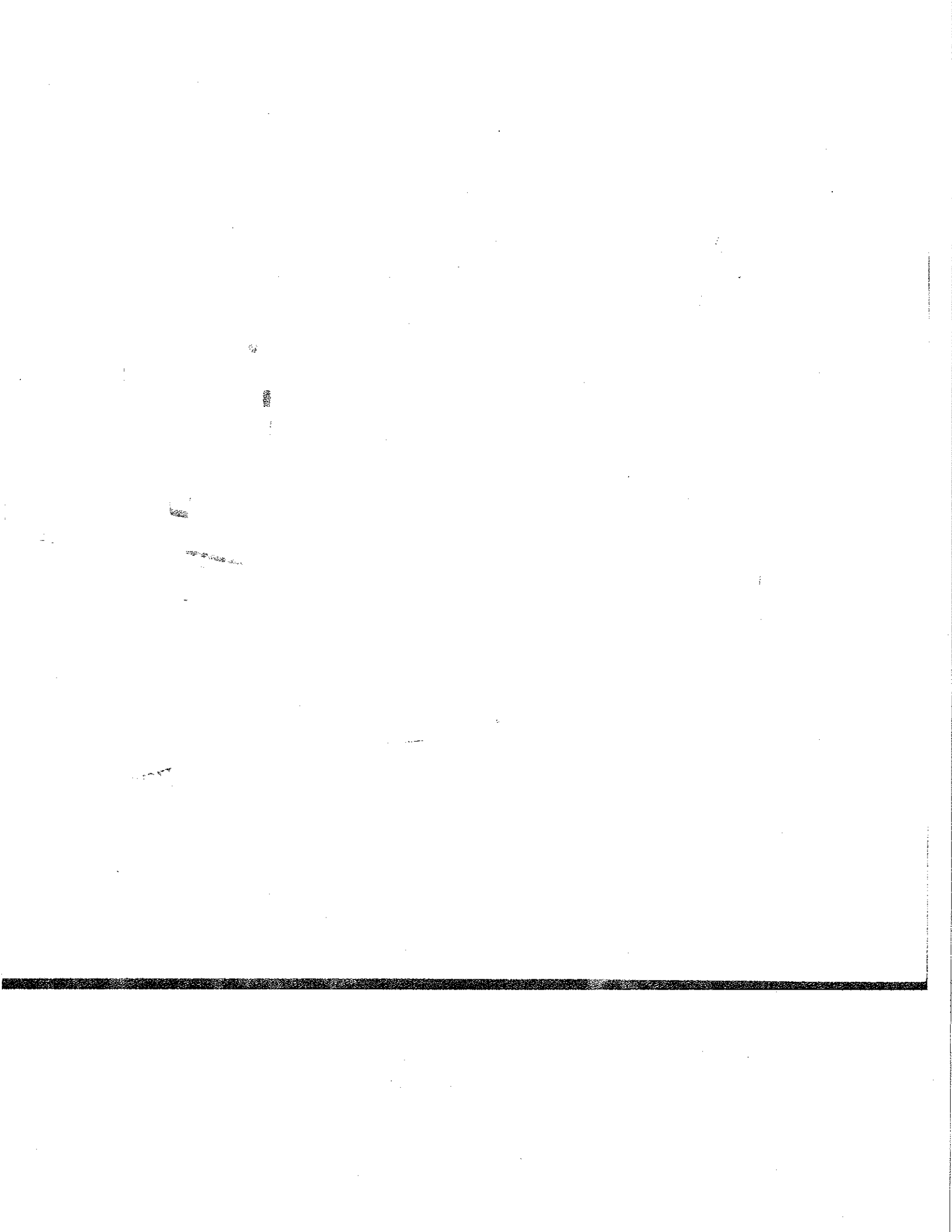
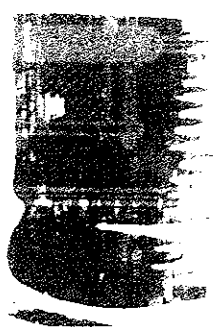


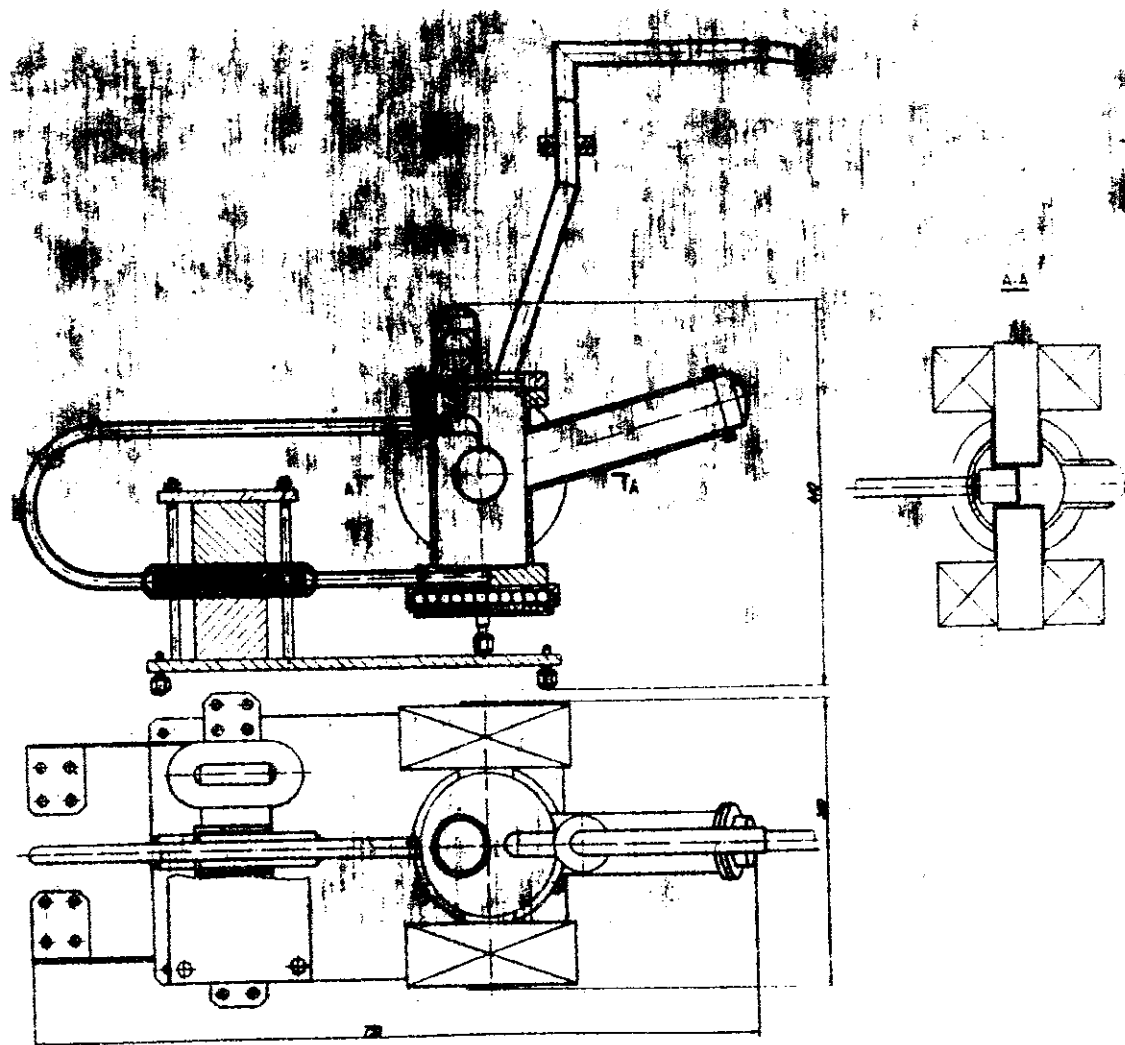
Fig. 4. A stationary jet target:

1—observation hole; 2—beam axis; 4—nozzle of the drain chamber; 5—liquid metal; 6—pump

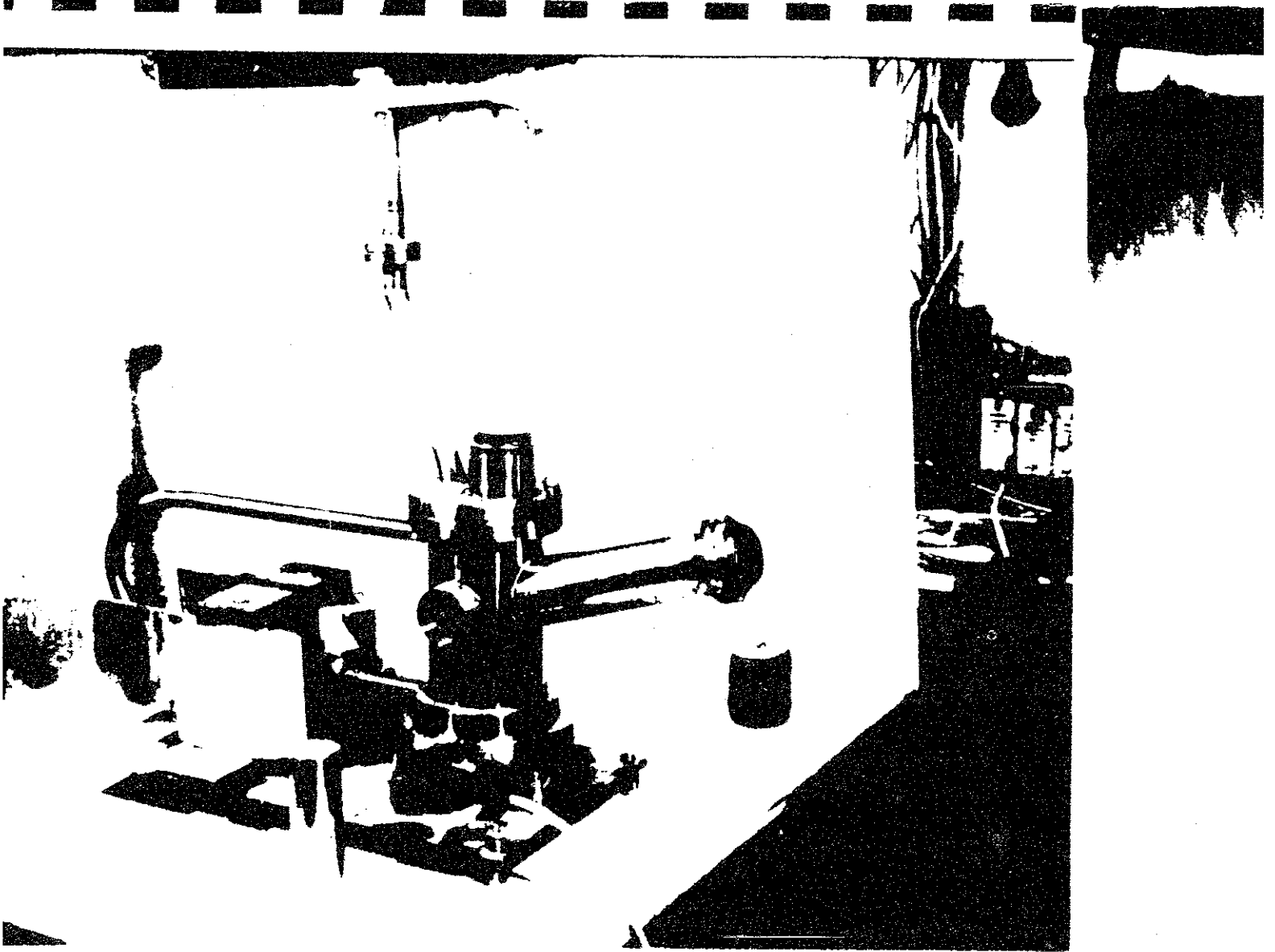




*Gallium jet*



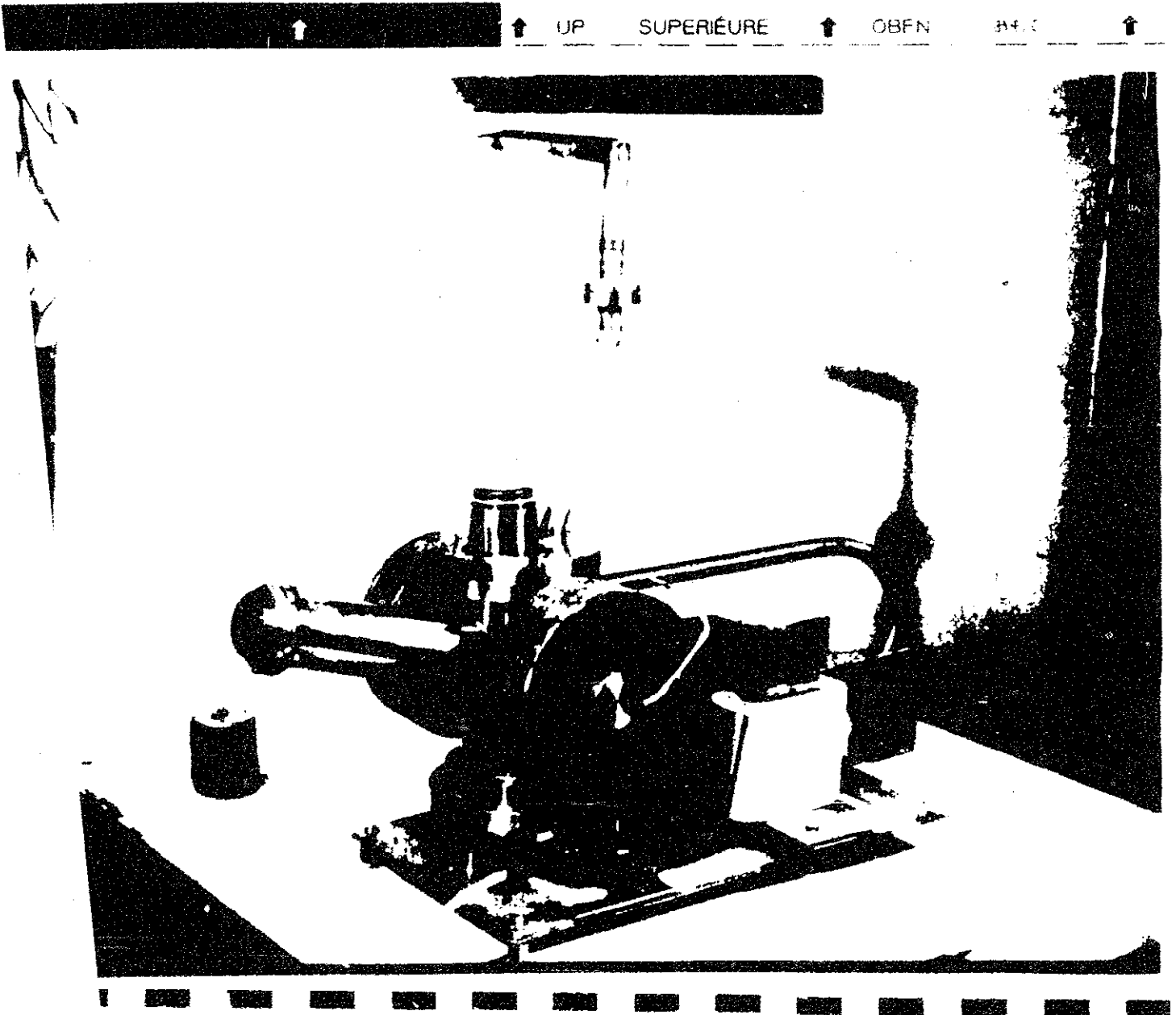
Liquid jet target device - positron production target

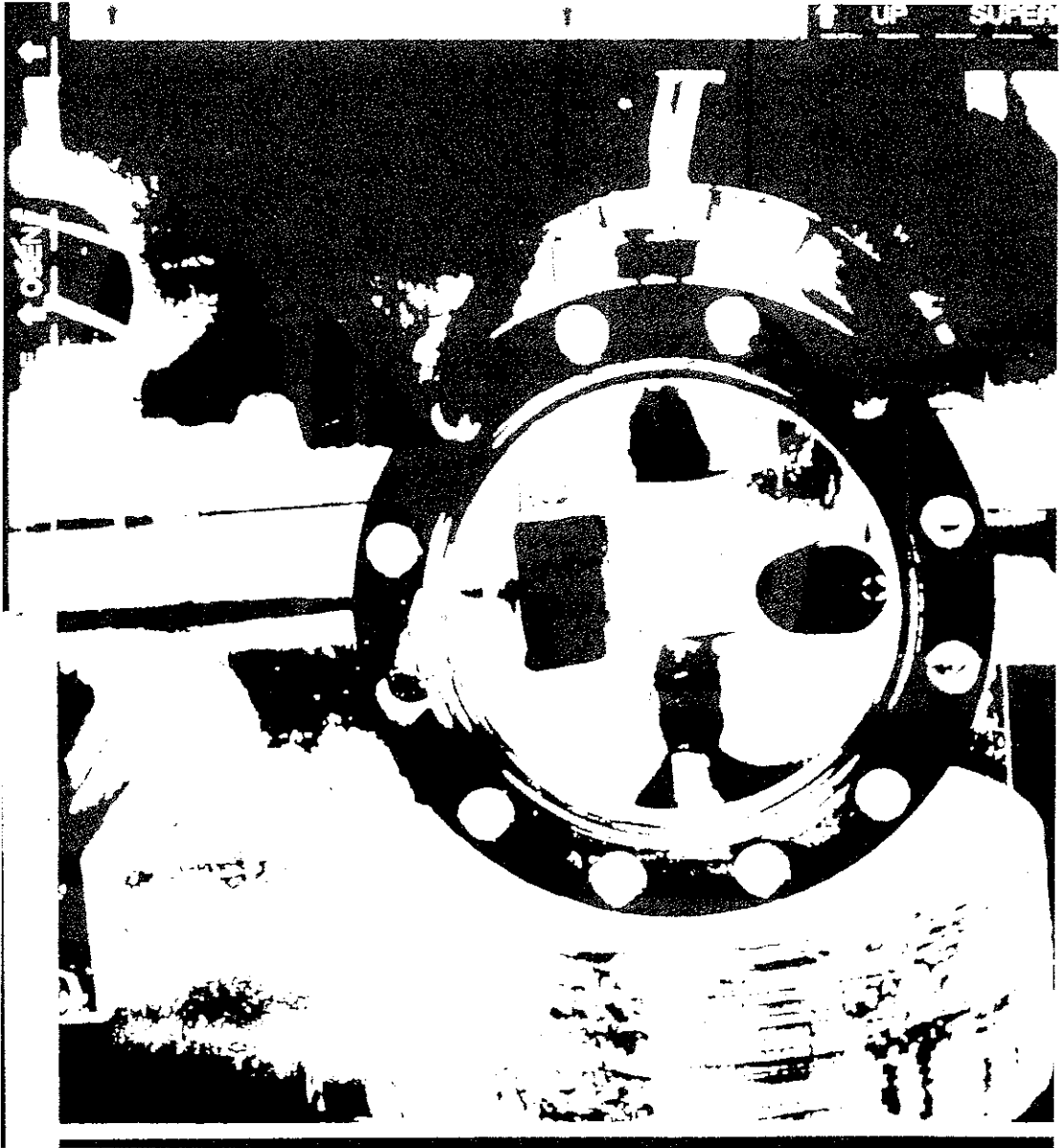


↓ 95 SUPERIEURE ↓ 0851 945 ↓

Liquid lead jet target device - neutron production target

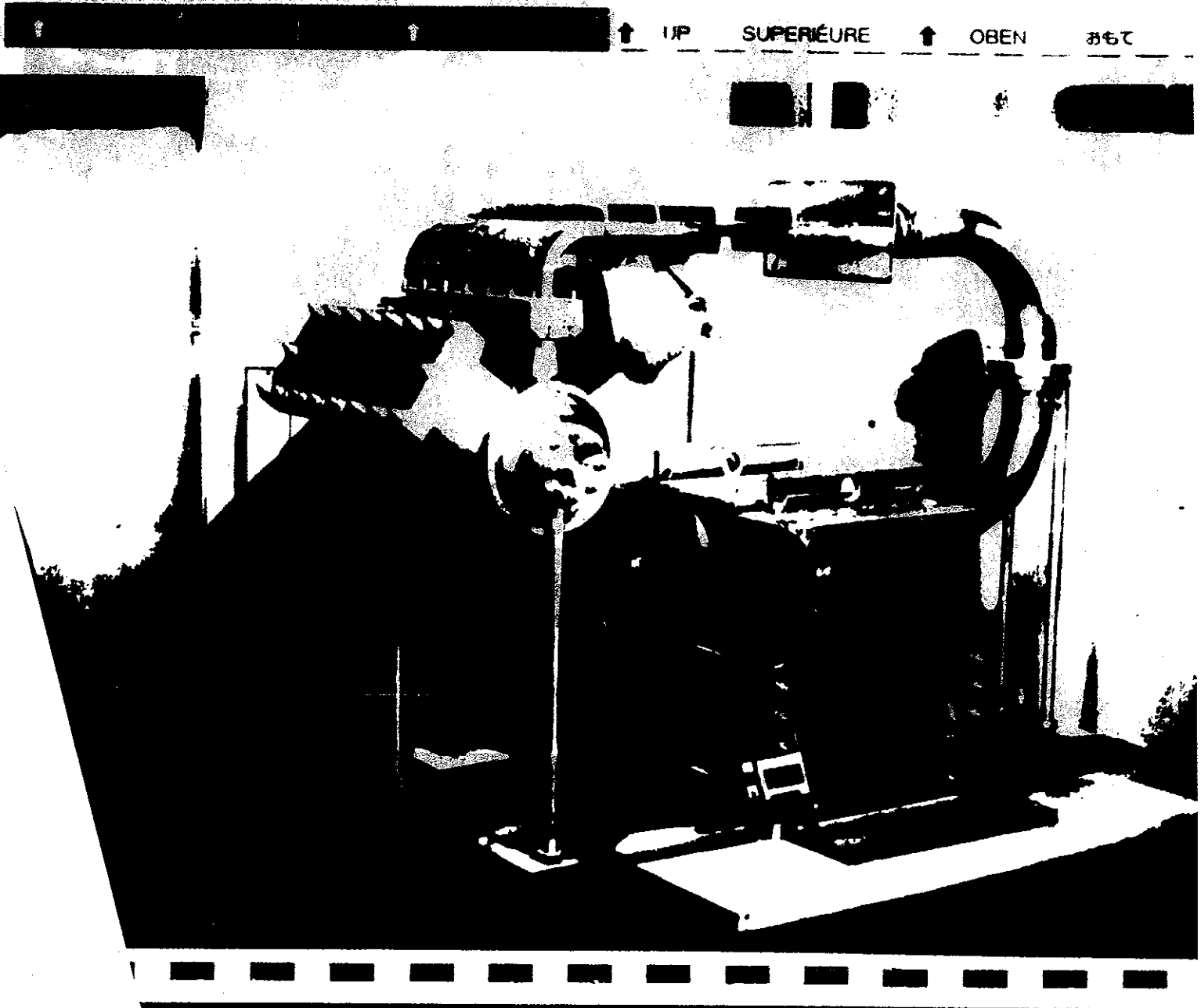
led jet target device with long-focal microscope

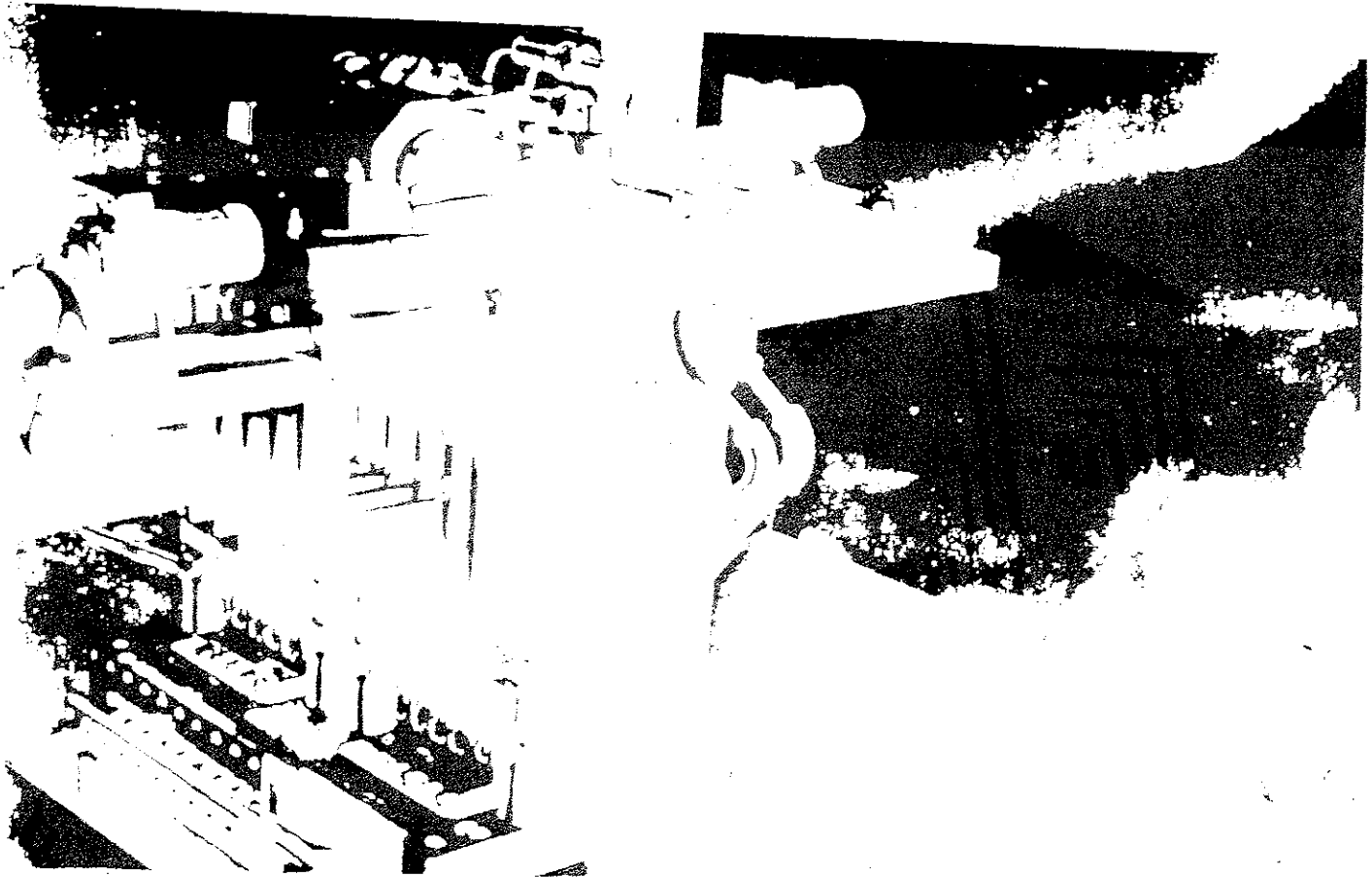




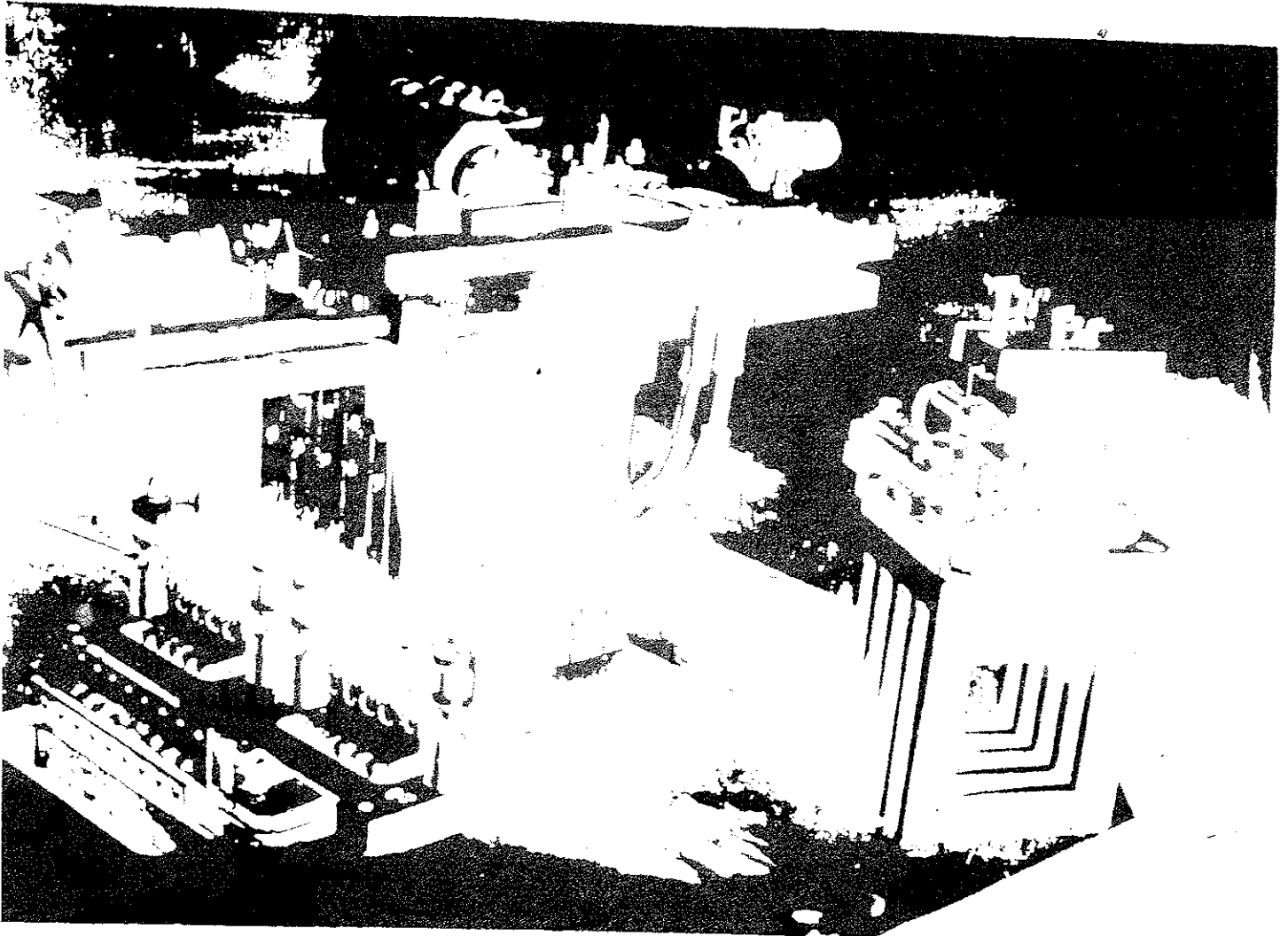
Big liquid lead jet target device

$l_{jet} = 25\text{ cm}$   $\Delta_{jet} = 2\text{ mm}$   $V = 10\text{ liters liquid lead}$



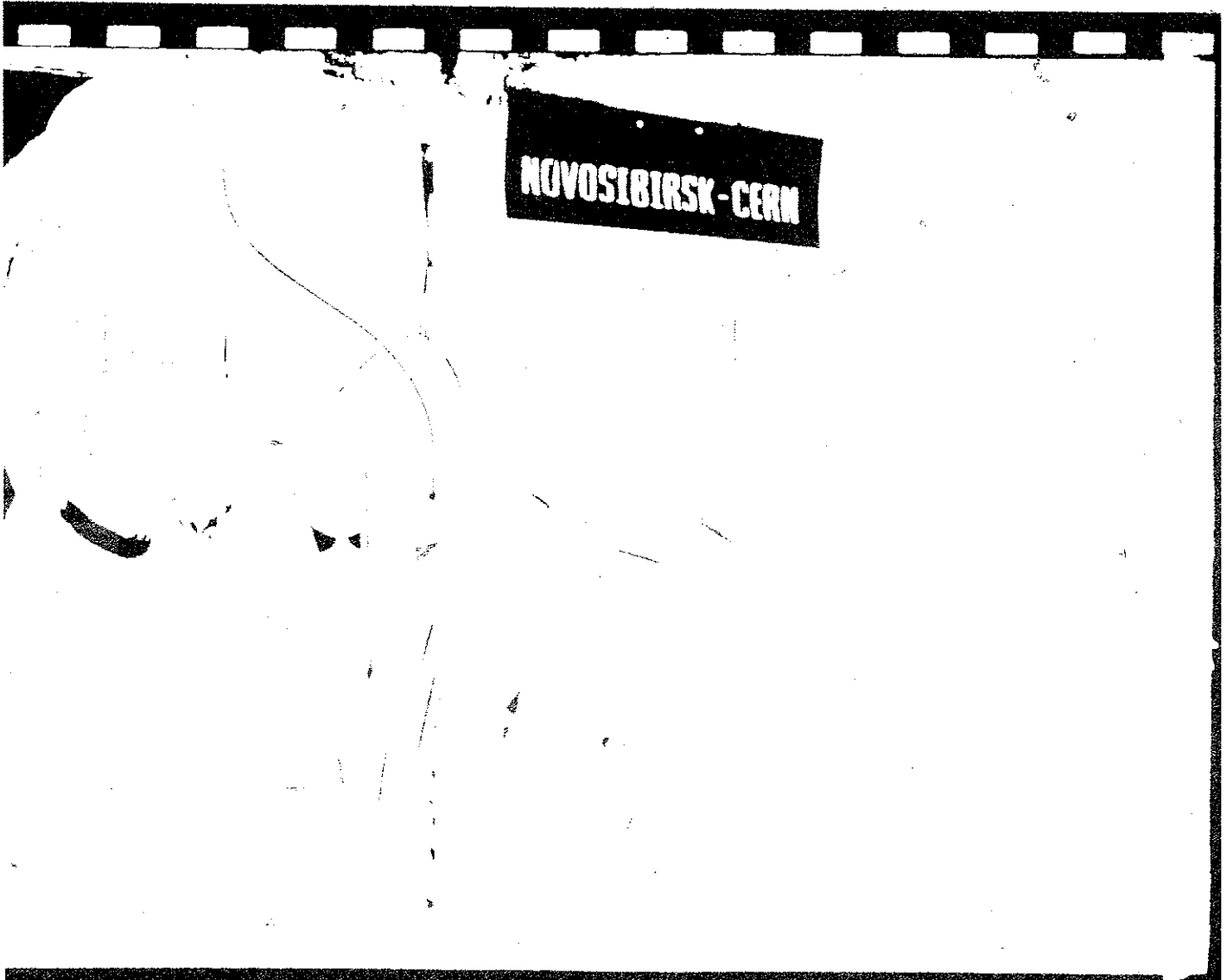


double cylindrical lithium lenses being build in BINP for  
electron beam focusing at FNAL antiproton target station  
 $b = 0.5 \text{ cm}$ ,  $l = 12 \text{ cm}$ ,  $H_{\text{max}} = 10 \text{ T}$ ,  $f = 10 \text{ Hz}$  (1981)

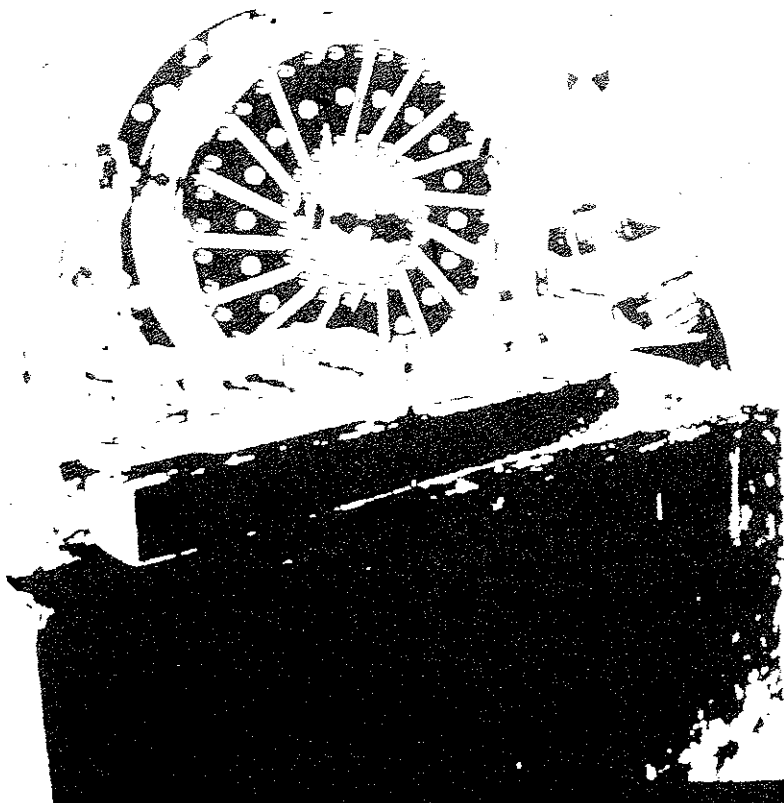


the lens is disassembled and removed from mounting  
transfer

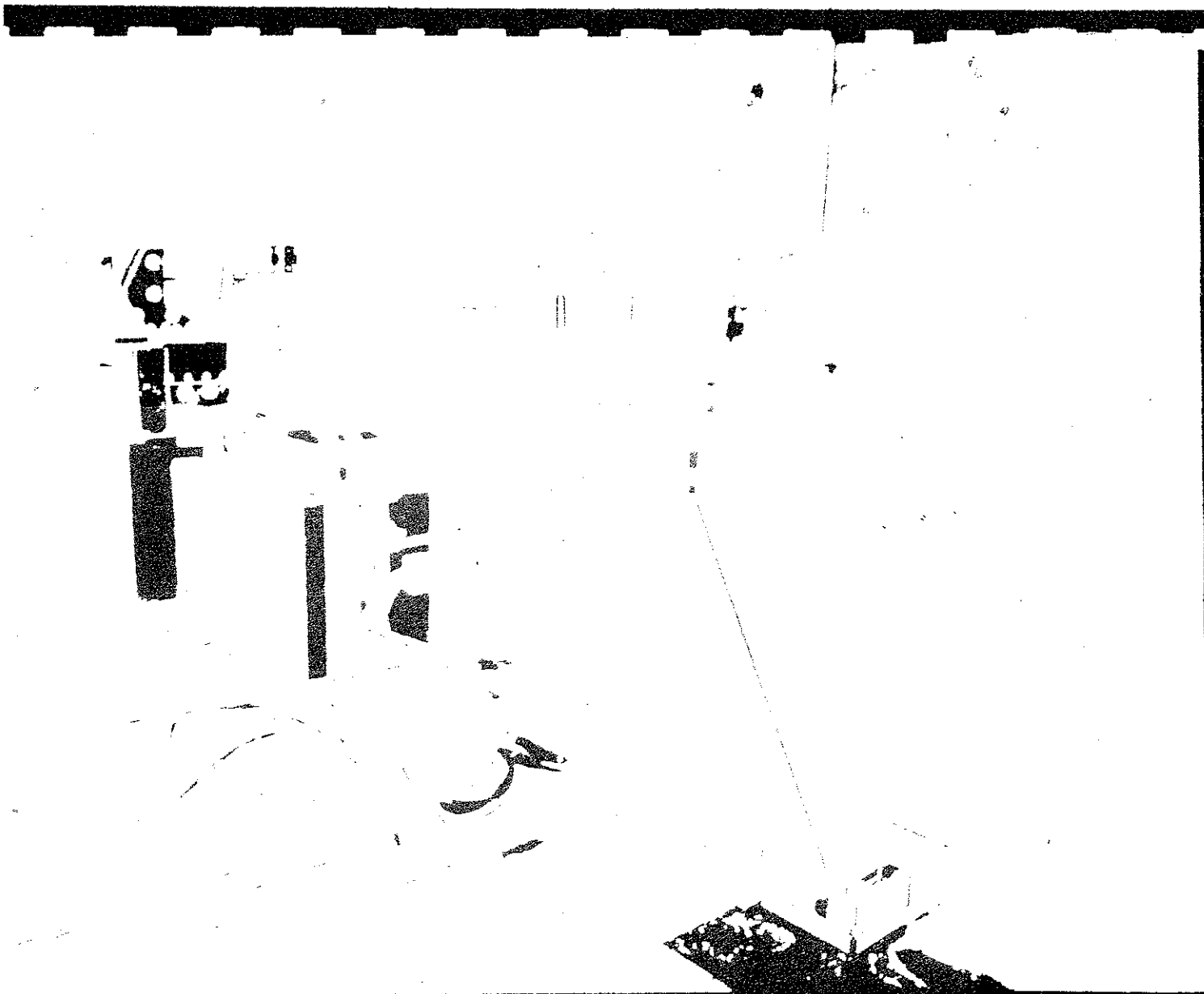




Novosibirsk-CERN team during test for EERN  
in lens in BTNP

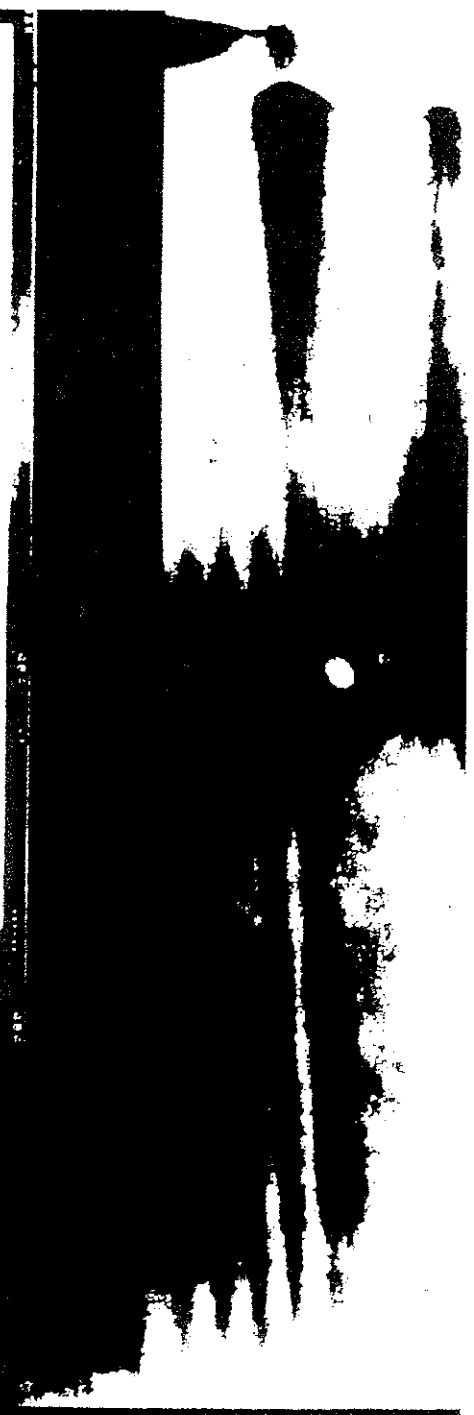


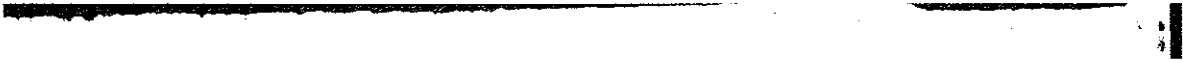
5 MA toroidal matching transformer for big Lithium  
( $\Phi=3.8\text{cm}$ ) supply beam feed in BINP-after de

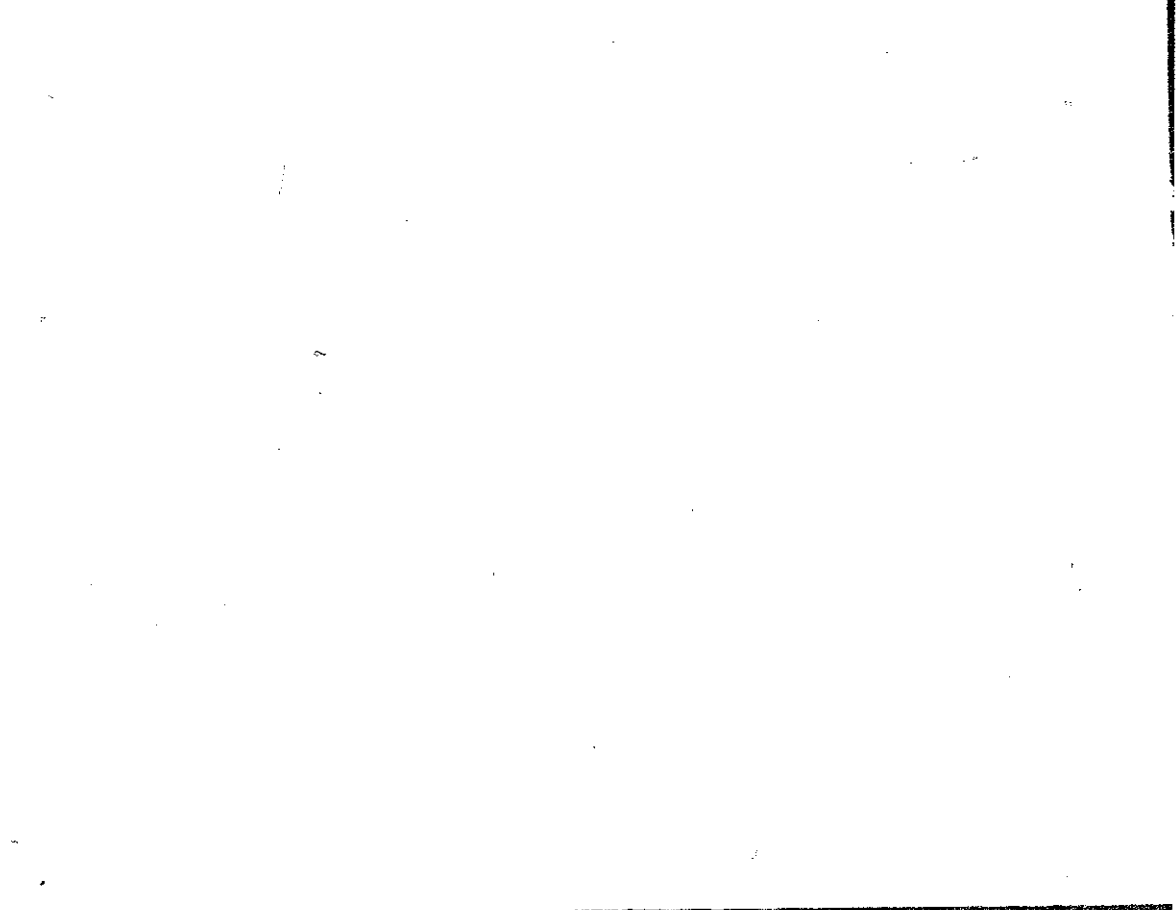
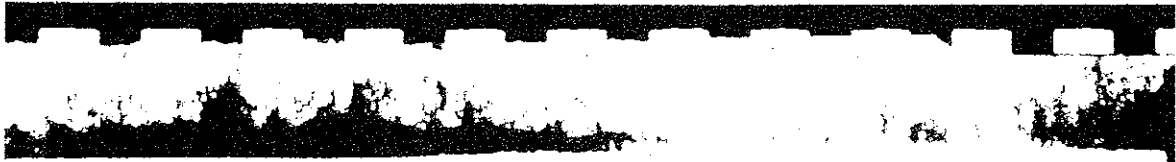


ous-transformer assembly in GERN outpro for  
erget station

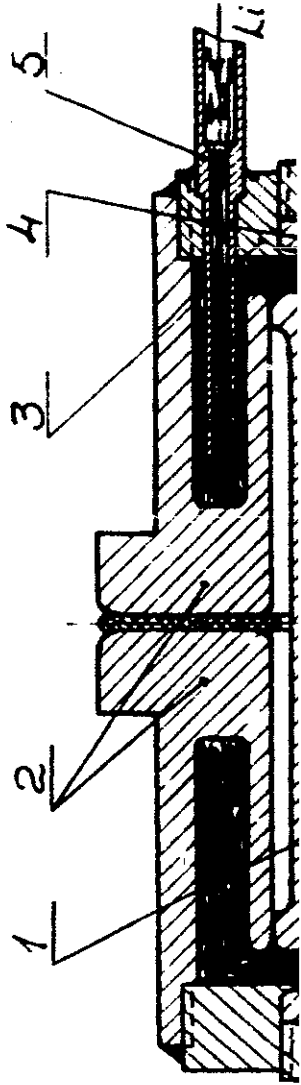
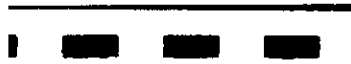
ms collection liquid channel lens assembly with pumping  
lithium. (front view)  
 $C = 1.5 \text{ cm}$   $H_{\text{max}} = 0.7 \pi$   $f = 100 \text{ Hz}$







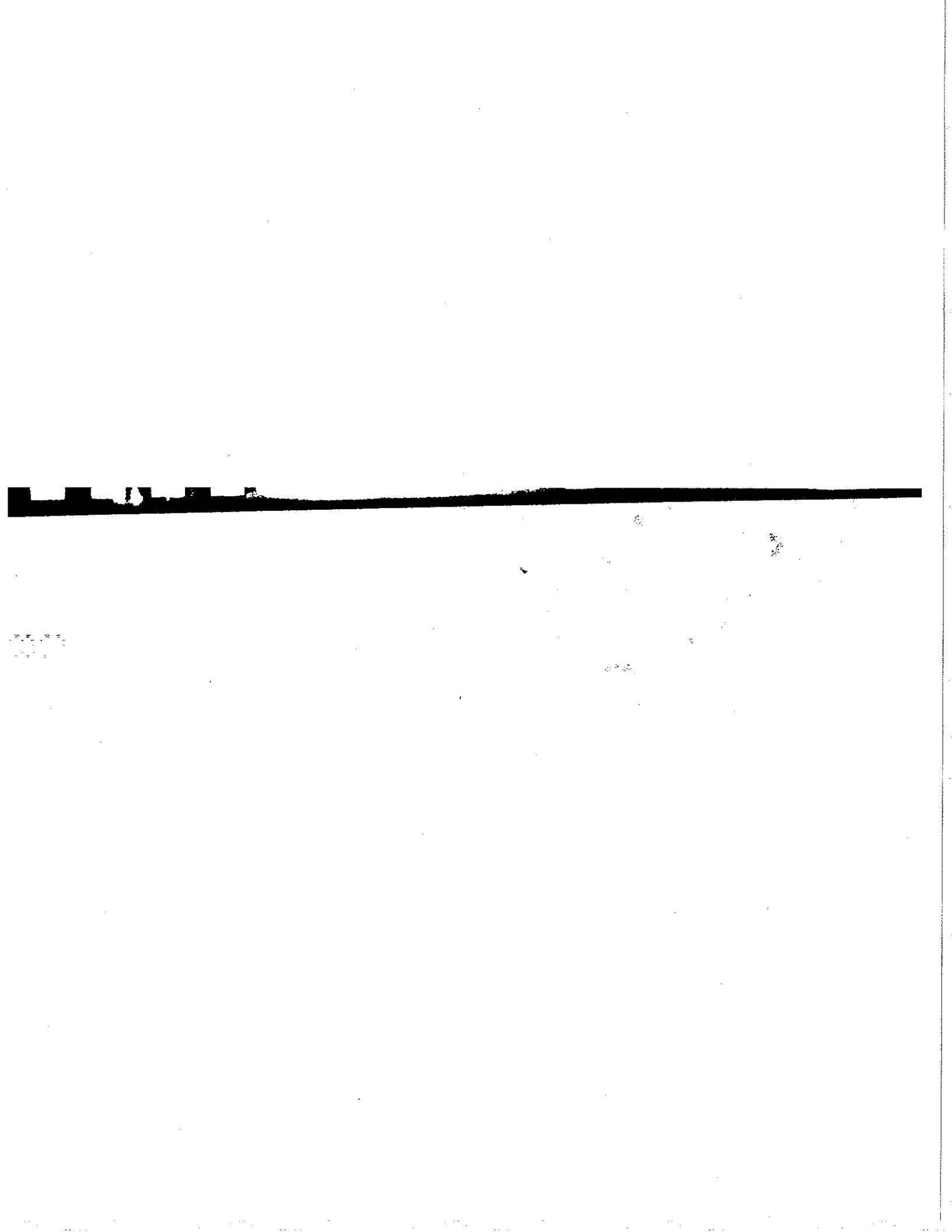
ous with flat current input  
1 tube of liquid lithium input for per



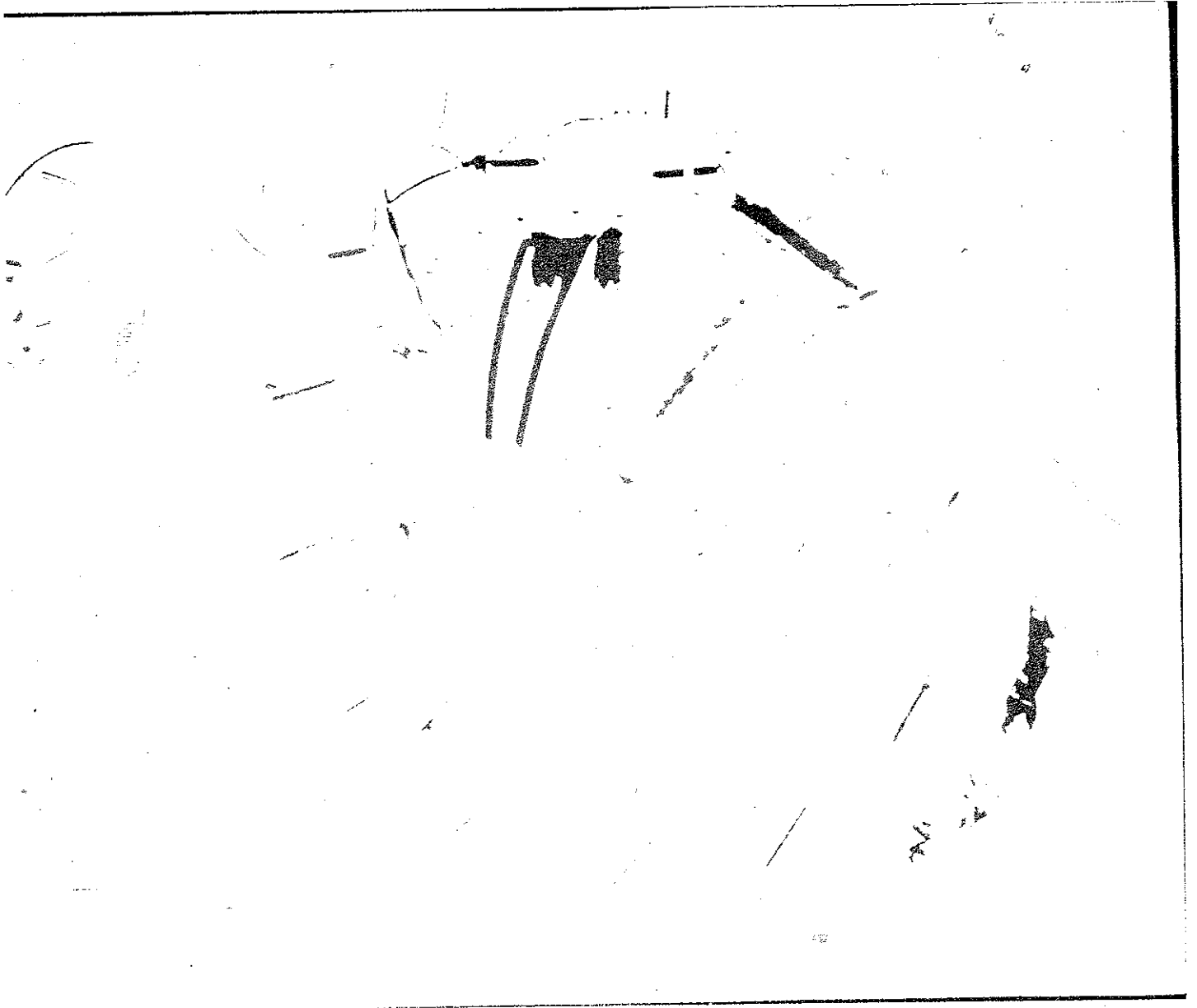
bus supply toroidal matching transformer  $\eta = 1.2$





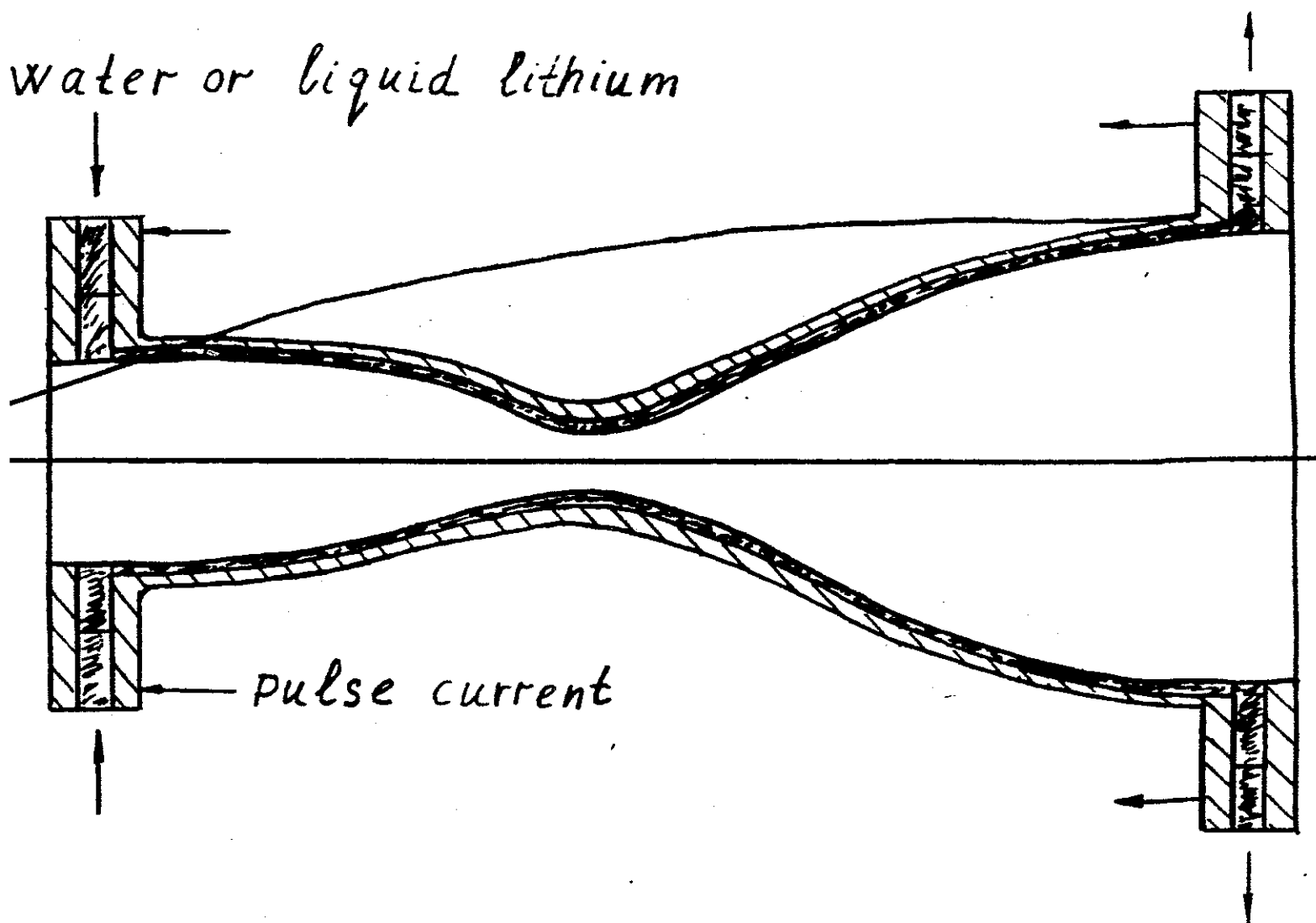


and Lithium Pumping System - disassembled



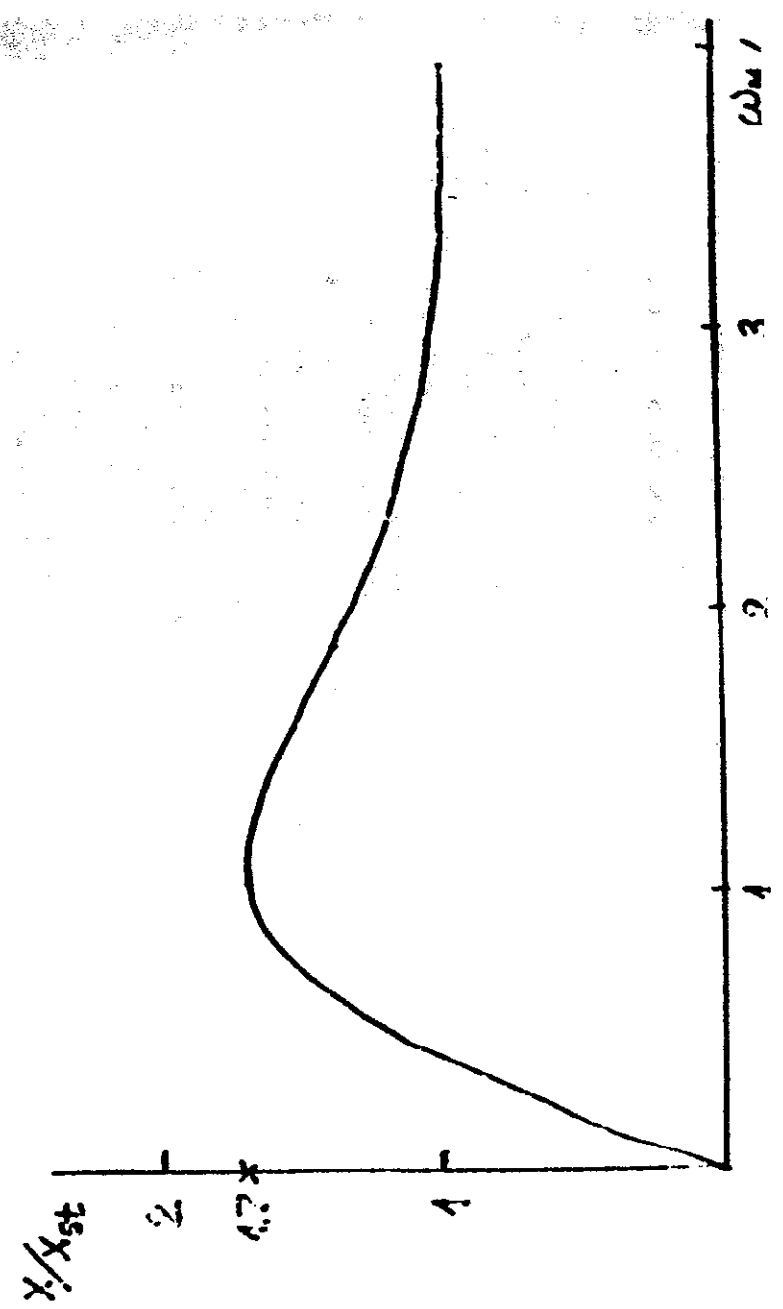
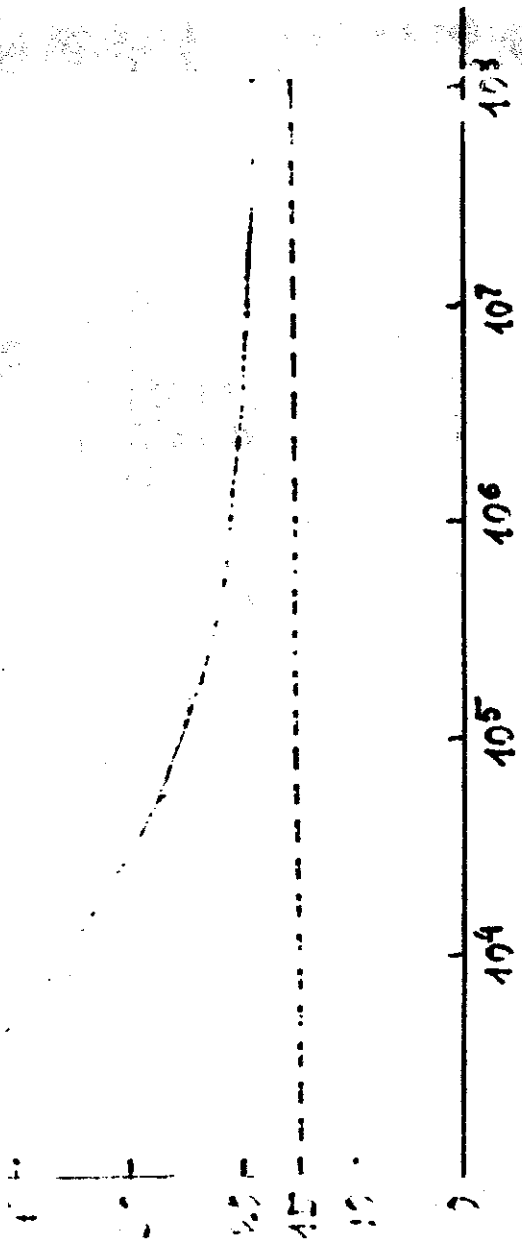
[Redacted]

[Redacted]



Magnetic Horn with two-walls current Envelope





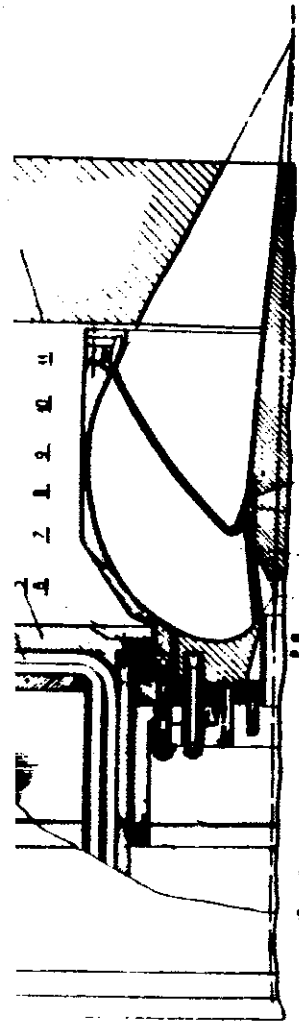


Fig. 3. The complete view of the focusing device. 1 - transformer; 2 - toroidal iron; 3 - secondary coil winding of the transformer; 4 - primary coil windings; 5 - cover; 6, 12 - pressing rings of the grip contacts; 7 - profiled coaxial tyre; 8 - body of the lens; 9 - pressing contact ring; 10, 17 - entrance and exit of the colling system; 11 - lead shield; 13 - coaxial current contacts; 14 - load-bearing bolts, supporting the tyre; 15 - contact grips; 16 - stop flange for supporting the pressing and pressing out bolts; 18 - converter target; 19 - tungsten stopper; 20 - stop passage detail; 21 - corpus of the water cooling

orating of the lens is a construction of electrical contacts for currents up to 1.4 MA. For rigidly done up ends of the lens and for necessary contact efforts the electrical contacts must not give additional static strains in cross-sections of the lens. Another important problem is a creation of an intensive cooling of the thin-walled current surfaces, operating at several Hertz rate. Fig. 3 gives the lens with contact buses and a transformer. The lens is inserted in the profiled along the external trajectory coaxial tyre (7); the pressing ring (9) reinforces the lens at its end. The second end of the lens is not rigidly reinforced in the longitudinal direction and it's connected with the electrical contact (13) with the help of 18 grip dummies (15), uniformly distributed along the perimeter of the end. After dighting the contacts, the free end of the lens is firmly fixed relative to the detail (16) with the help of a system of the alternating pressing and pressing out bolts. The cone-like tungsten stopper (19), serving for absorption of particles after the target, is a load-bearing element of the construction in the same time. Through the passage detail (20), the stopper is pressed to the body of the lens at the place, where the entrance and exit surfaces join together. This place is the third point of support of the lens.

There are two variants of a water cooling of the lens. At cycles rate  $\sim 0.2$  Hz and less, the power, emitted in the lens, can be dissipated by a pulverization of water at its internal surface<sup>(2)</sup>. In fig. 3 the more intensive cooling system is represented.

In this case we lose a little in transparency, but such cooling system can provide a better dissipation of heat. This cooling system can dissipate about  $100 \text{ W/cm}^2$  from the cone part of the lens and operate at several hertz current pulses repetition frequency. For this purpose the body of the lens is done out of two layers. This permits to create better conditions for the dissipation of heat with the help of a continuous stream of water between the layers. The internal non-current surface of the lens is done out of two parts. The parts are hermitized at the ends at the place of contact with the stopper, as it is shown in fig. 3.

The lens is supplied by the unipolar puls of sinusoidal current formed by the discharge of a capacity battery on the lens, that represents an inductive load. The capacity battery is switched on with the help of a thyristor valves system and discharges on the lens through the matching transformer having a small dissipation. The technique of creation of such generators is well developed at present<sup>(4)</sup>. The lens has an inductance of  $50 \text{ nH}$  and at a current of  $1.4 \text{ MA}$  the magnetic field energy in the operating volume is about  $50 \text{ kJ}$ . For a pulse duration of  $100 \mu\text{s}$  the voltage on the lens is equal to  $2.5 \text{ kV}$  and for a transformation ratio of 10, it is necessary to commutate in the primary coil a current of  $140 \text{ kA}$  at a voltage of  $V_1 = \pm 15 \text{ kV}$ . This voltage is calculated taking account of parasitic parameters of the transformer. The transformer has the grounded center point. A reactive power of the transformer is equal to



ИНСТИТУТ ЯДЕРНОЙ ФИЗИКИ СО АН СС

G.I. Silvestrov, A.N. Skrinsky  
and T.A. Vsevolozhskaya

PIONS AND MUONS ACCELERATION  
AT THE UNK-VLEPP FACILITY

PREPRINT 91



НОВОСИБИРСК

---

**Budker Institute of Nuclear Physics**

**G.I. Silvestrov, A.N. Skrinsky  
and T.A. Vsevolozhskaya**

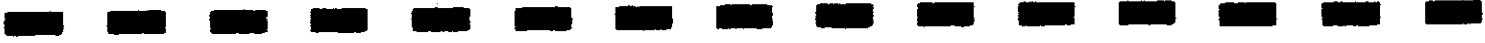
**PIONS AND MUONS ACCELERATION  
AT THE UNK - VLEPP FACILITY**

**PREPRINT 92-36**

**NOVOSIBIRSK**

**1992**

---



**Pions and Muons Acceleration  
at the UNK - VLEPP Facility**

**G.I. Silvestrov, A.N. Skrinsky  
and T.A. Vsevolozhskaya**

**Budker Institute of Nuclear Physics,  
630090, Novosibirsk, Russia**

**ABSTRACT**

It is a scheme of acceleration in the VLEPP linacs generated by 3 TeV proton beam extracted from the UNK. To match the time structure of extracted beam with that of the linacs, the beam ejection is carried out one by one of  $10^4$  bunches with 100 Hz repetition rate by means of a special ejection system. In ejected bunch the longitudinal spread of energy is produced with use of a regular regular linac structure. That permits by using a special ejection tract to group the protons into very short sub-bunches corresponding to linac time structure. The pions are produced from target in tens GeV energy range in a wide energy interval  $\Delta E/E \approx 1$ . The lithium lens of 0.5 m focal length is used to match the pion beam emittance with linac structure. Linac with its attendant focusing serves as well as a decay tract providing the produced muons with an acceleration up to the final energy.

© Budker Institute of Nuclear Physics

The VLEPP linear accelerators [1] with their accelerating gradient  $\sim 100$  MV/m being built in the same center, where the 3 TeV proton storage ring UNK [2] is under construction, will open the unique possibility to accelerate beams of pions and muons in TeV's energy range. High accelerating rate here is of the principal importance to prevent a significant part of pions from decay during acceleration. High energy of extracted from the UNK proton beam will provide with a high efficiency for muon production.

To match the time structure of extracted proton beam with the VLEPP linacs time structure the beam ejection can be carried out one by one of  $\sim 10^4$  stored bunches by means of a special ejection system [3], operating at 100 Hz repetition frequency, that of the VLEPP operation. The bunch length is of  $\sim 10$  cm r.m.s. length. To be matched with the wave length of the linacs it is to pass through a buncher consisting of a 30 GeV regular linac up to the final energy.

ending channel. Correlation of energy gain in linac longitudinal coordinate of particle results in a group of protons in the channel into short subbunches, by 2 cm. Such grouped the proton beam is used for acceleration.

Number of pions, produced by high energy proton, in each part of collision is described in accordance with a hydrodynamic model by the gaussian distribution in rapidity  $y$  about the CMS rapidity  $y_0$  with a spread defined through the CMS Lorentz-factor logarithm [5, 6c, 6d]:

$$\frac{dN_{\pi}}{dy} = \frac{\langle n_{\pi}^{\pm} \rangle}{\sqrt{2\pi L}} e^{-(y-y_0)^2/(2L)} \quad (1)$$

$\langle n_{\pi}^{\pm} \rangle$  denotes the mean pion multiplicity per collision, which is practically equal to a relative energy bite. The transverse momentum spread of pions is defined by the exponential distribution of their energy  $E^*$ :  $\omega(E^*) \propto e^{-E^*/T}$  inside a hydrodynamically moving volume element of length  $L$  and temperature  $T$  being of the order of pion mass  $m_{\pi}$  [5]. The full expression for momentum distribution looks like

$$E \frac{d^3 N_{\pi}}{d^3 p} \approx \text{const} \int E^* \omega(E^*) e^{-(y-y_0)^2/(2L)} dy, \quad (2)$$

instant providing with the proper value of  $\langle n_{\pi}^{\pm} \rangle$ . The rapidity distribution from (2) is in a good agreement

with (1) by  $L \gg 1$  and  $y < L$ , the transverse momentum distribution:

$$\rho(p_{\perp}) d^2 p_{\perp} \approx \text{Const} m_{\perp} \sum_{k=1}^{\infty} K_1 \left( \frac{km_{\perp}}{T} \right) d^2 p_{\perp},$$

where  $K_1$  is the modified Bessel function and  $m_{\perp} = \sqrt{m_{\pi}^2 + p_{\perp}^2}$  agrees well enough with a form:  $\rho(p_{\perp}) \propto \exp(-bp_{\perp})$ , experimentally with  $b \approx 6 \text{ GeV}^{-1}$  (the masses and above are measured in energy terms).

In proton-nucleus collision the incoming proton interacts with a so called nuclear tube of length proportional to  $A^{1/3}$  [6]. Due to that the pion spectrum occurs shifted by  $\Delta y = -1/6 \ln A$  as compared to the pCu collision with equal to 3 TeV proton energy place near the pion momentum  $p \approx 2.8 \text{ GeV}$ .

An account of energy dependent probability decay during the acceleration results in effect of spectrum maximum to the high energy region. The pions of initial energy  $E$  and longitudinal momentum  $p_{\parallel}$  reduced during the acceleration up to an energy  $E_{\text{fin}}$  factor:  $\left( \frac{E + p_{\parallel}}{2E_{\text{fin}}} \right)^{\mu} = \left( \frac{m_{\perp}}{2E_{\text{fin}}} \right)^{\mu}$  where  $\mu = \frac{m_{\pi}}{c\tau_0 dE/dx}$  standing for the accelerating rate and  $\tau_0$  - formation time. By insertion of this factor into (1) the spectrum is found to be:

$$n_{\pi^{\pm}} = \frac{\langle n_{\pi^{\pm}} \rangle}{\sqrt{2\pi L}} \left( m_{\pi} \frac{\gamma^{1+\mu/2}}{E_{\text{lin}}} \right)^{\mu} e^{-\frac{[y-(y_0+\mu L)]^2}{2L}} \quad (4)$$

is shifted by  $\Delta y = \mu L$  that is up to  $p = 5.4$  GeV/c collision with  $E_p = 3$  TeV by  $dE/dx = 100$  MeV/m that The whole number of pions is reduced by a factoring the 2 TeV acceleration.

inverse emittance of pion beam is found as  $\epsilon \sim$  in dependence on nuclear absorption length  $\lambda$ , momentum  $p$  and mean square of its transverse displacement which is equal to  $\sim 0.15$  (GeV/c)<sup>2</sup> for distribution  $T = m_{\pi}$ . At  $p = 5.4$  GeV/c the emittance value, 1 mm.rad., exceeds by several orders the VLEPP value. That means the pion momenta available to get into the linac are situated far away the spectrum maximum. Fortunately the loss in capture efficiency is not very large because of a slow fall of pion yield from the maximum with energy growth. That is a faint dependence of capture efficiency on energy (fig. 1).

Energy bite of particle capture into the linac is determined by a width of stability region for transverse motion. Linac lattice is composed of FODO type elements, occupied with the accelerating units, and is as short as possible to keep high the average capture rate. The minimum drift length is equal to 1 m

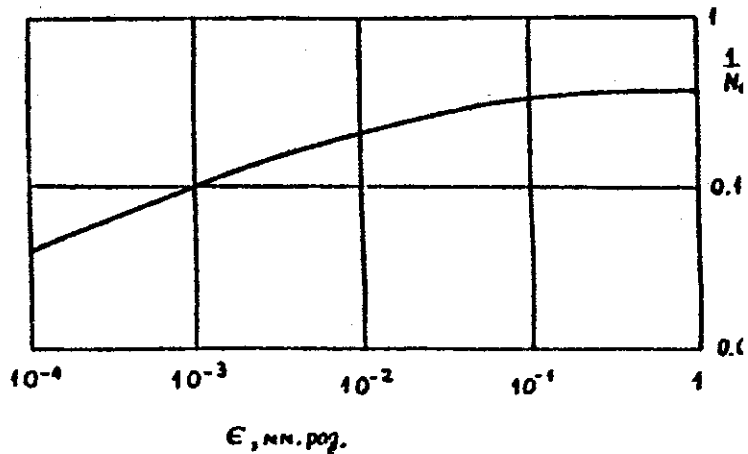
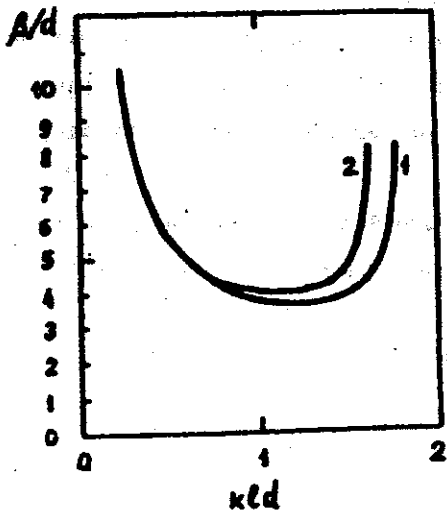


Fig. 1. Pion yield versus an emittance per relative interval per incident proton of 3 TeV energy; decay probability during the 2 TeV acceleration  $dE/dx = 100$  MeV/m included.

the length of one accelerating unit. Magnetic field gradient in quadrupoles is equal to 5 kOe/mm being confined by induction onto the pole tip and 3mm half-aperture. In 2 the maximum beta function in periodicity element is versus a quadrupole strength in terms of product  $kld$  standing for quadrupole length,  $d$  - for that of the drift



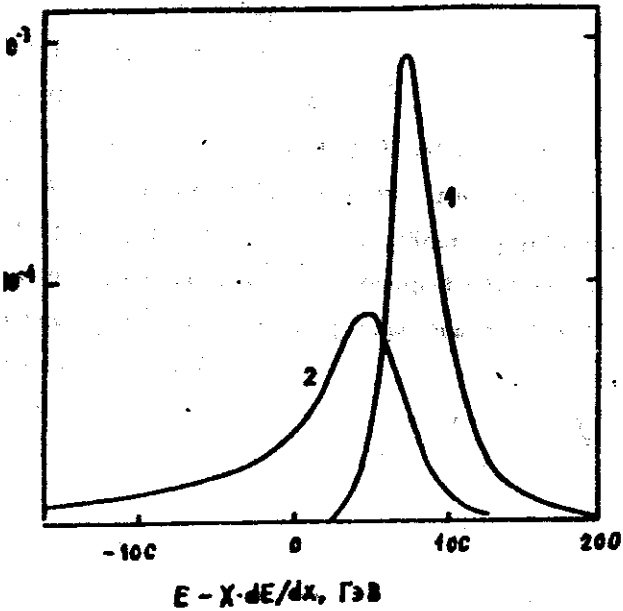
beta-function maximum in linac for l/d ratio equal 0.1 (1) and to 0.2 (2) versus focusing strength kld units.

c. Ratios  $\beta/d$  for different l/d practically coincides means the widening of captured energy bite and its shift into high energy region in proportionality with lengthening. The minimum captured energy is  $E_{min}$  and d in meters like  $E_{min}, GeV = 100 ld$ . By an increase with l and d kept constant the beam is moving along the curves fig. 2 so that the beta-function grows

up almost in proportionality with energy grow and the size is conserved constant despite the emittance decrease. The oscillation phase increment through the period element kept constant, i.e. the l and d are altered the linac length in proportionality with  $E^{1/2}$ , the function grows also as  $E^{1/2}$  and the beam size is decreasing in proportionality with  $E^{-1/4}$ . That allows to maintain aperture of linac reducing along with a rate up to described as  $a \propto E^{-1/3}$ .

To match the pion beam emittance, having on target effective beta-function of the order of  $\lambda/2$ , with the acceptance we use the lithium lens of 0.5 m focal distance. The lens being practically thin does not provide wide ideal matching in a wide energy bite accepted in linac, but a big length of hadron target by short lens distance together with a wide angular spread of production compensate to a significant extent the chromatic aberration of lens focusing.

Shown in figure 3 are the spectra of pions and after the 2 TeV acceleration in both VLEPP linacs with 0.25 l/d ratio. Mean collection energy is equal to 8 - the optimum value for such a ratio. Relative energy spread in accepted beam is equal to  $\sim 0.5$ , the transverse emittance - to  $\sim 1.5 \cdot 10^{-3}$  mm.rad. Full number of accelerated pions  $N_{\pi} = 5 \cdot 10^{-2}$  per incident proton that with  $3 \cdot 10^{14}$  p in UNK means  $\sim 1 \cdot 10^{11}$  pions per second inside  $\sim 2\%$  energy



Spectra of pions (1) and muons (2) after the 2 TeV acceleration. Quadrupole length  $l$  is equal to 0.25m, field gradient - to 5 kOe/mm, half-aperture  $a$  - to 3 mm. Drift length  $d$  is 1 m, and accelerating field-100 MV/m.

$10^{-5}$  mm·rad. transverse emittance. An efficiency for ception into the acceleration is close to unit. Muon density in the maximum achieves almost a half of stream density.

dependence of accelerated pions number on collection is shown in fig. 4 for different values of  $l/d$  ratio.

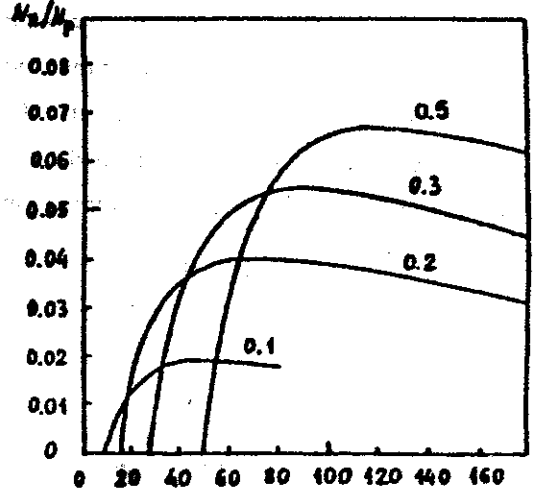


Fig. 4. Accelerated pion yield in dependence on  $t$  of particle collection from target for  $d$  values (shown on curves in meters);  $d=1$  m.

An increase in maximum  $N_x$  is seen in a wide quadrupole length grow. To utilize that w significant loss in average acceleration rate the is to be made altered along the linac length - corr large at the beginning and being reduced with an in beam energy by means of drift lengthening. The l

by the decrease of the acceleration unit length. To  
 up to an energy higher than the energy is  
 diminishing in lattice function. That is  
 by the decrease of the acceleration unit length  
 and so a loss in particle number occurs to be  
 Thus, if with the equal to 0.5 m length of  
 the drift length is taken equal to 1 m at the  
 start and to 2 m after a gain of first ~ 100  
 number of accelerated pions will be ~ 1.5 per  
 ion, that is ~ 1.5 times more than by  $l/d = 0.25$   
 whole linac length. An increase in the former by  
 near 200 m that is not more than 1% of the  
 of two VLEPP linacs. Further lengthening of the  
 conserved quadrupole length will result in a  
 each of linac length to its minimum - the sum of  
 accelerating units.

ence of  $N_p$  on linac half-aperture  $a$  by kept equal  
 e maximum field  $H_{max}$  in quadrupoles, and of  $H_{max}$   
 equal to 3 mm are shown in figure 5 together with  
 nce on  $a$  by kept constant the field gradient,  
 $x$  varied in proportionality with  $a$ . It could be  
 that at  $a = 3$  mm and  $H_{max} = 15$  kOe the yield of  
 d pions though rather high occurs to be a small  
 produced in target.  
 oid the significant increase in energy spread

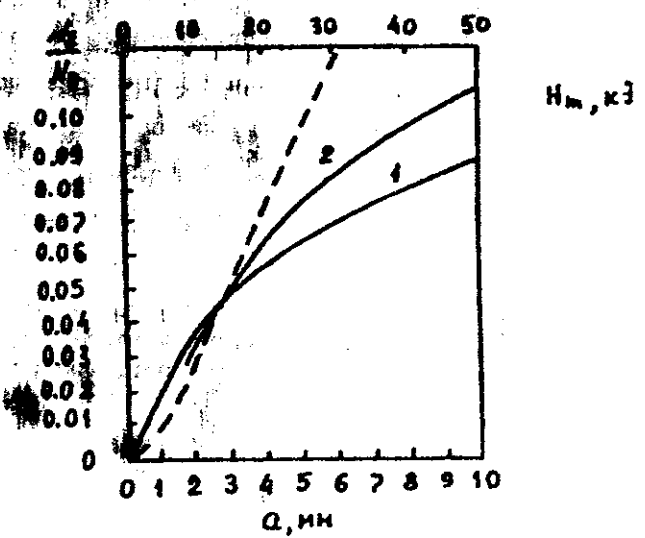


Fig. 5. Accelerated pion yield in dependence: 1 - c  
 $H_{max} = 15$  kOe, 2 - on  $H_{max}$  by  $a = 3$  mm, dashe  
 on  $a$  by grad  $H = 5$  kOe/mm;  $l = 0.25$  m,  $d =$

during the acceleration the bunch length in pion beam  
 to that in proton beam at the target, is to be  
 sufficiently short. The degree of proton bunching  
 buncher is characterized (see Supplement) by a collec  
 ~ 70% particles into the bunches of  $0.3\lambda_0$  length or  
 of  $0.1\lambda_0$  length. The length  $\sim 0.1\lambda_0$  seems to be adeq  
 the angular and energy spreads captured into the linac  
 homogeneous particle distribution inside them and  
 bunch length, the r.m.s. energy spread at linac exit  
 equal to  $\sim \pm 20$  GeV by a negligible bunch lengthening.

Technical problems in pion producing system are  
with high energy deposition in target and  
in lithium lens. Passage through the target of  
the UNK protons for a time of  $\sim 100$  s will  
used power of the order of 1 MW. The only  
remove such a power from a confined target  
is in a use of liquid metal target - the melted  
is leaking with a high velocity through the  
ion region - as a free jet from a long narrow  
open trough a heat exchanger [7].

Operational conditions in lithium lens are defined both  
by position of primary and secondary beams and by  
beam current. The focal distance of 0.5 m for  
400 GeV and collection angle  $\sim 5 \cdot 10^{-3}$  rad is  
for 10 cm lens length and 125 kA current amplitude.  
At repetition rate the Joule power will be of the  
order of 1 MW inside a  $\sim 12$  cm<sup>3</sup> operational lens volume.  
Cooling will be fulfilled by means of liquid  
metal flowing through the lens volume that will simulta-  
neously provide with an intensive cooling of structural  
elements of lens heated by beams.

The necessary conditions for pion acceleration  
in linacs consists in their protection from the  
beam hit that would result in unacceptable  
radiation load in accelerating structures.  
Such conditions for primary and secondary beams could be achieved

by means of the achromatic bend by a small angle with  
magnets disposed in a 100 m distance with a quadrupole  
doublet, placed in the middle to provide the pions of  
energy with a half-wave focusing between the central  
magnets. With a bending angle of each magnet equal to  
10 mrad, that by the order exceeds the pion angular spread  
quadrupole doublet half-aperture is to be  $\sim 6$  cm  
and energy bite  $\sim 0.5$ . With  $\sim 100$  GeV particle energy the  
magnetic poles in doublet could be of  $\sim 2$  kOe/cm gradient and  
10 cm length.

Use for pion production of protons of lower energy  
in the UNK "warm" ring 400 GeV energy, for instance, results  
in a less production efficiency but looks rather more attractive  
due to the problem of pion acceleration in the VLEPP  
because of the lower optimum collection energy, less  
L/d ratio, significantly more simple the primary proton  
manipulation. Number of accelerated pions with  $E_p=400$   
 $\sim 50$  GeV collection energy is equal to  $\sim 8 \cdot 10^{-3}$  per  
proton.

An efficient way for optimization of VLEPP is  
to gain the accelerated pions and muons yield consistent  
with increase of aperture by conserved focusing rigidity  
if half-aperture changed from 3 mm to 10 mm by kept  
5 kOe/mm field gradient and  $L/d = 0.25$  the acceleration  
number is growing up to  $N_{\pi} = 2.4 \cdot 10^{-1}$  per incident proton  
is by factor  $\sim 5$ . Such a modification of linac will,

$\lambda$  is equal to  $0.09 \lambda_0$  with got inside  $\sim 50\%$  of  $n$  particles.

term being added to longitudinal dispersion the tract with the optimum values for  $\chi_1$  and  $\chi_2$  in a shortening of bunch length but the effect small. For all particles the  $\sqrt{\langle S^2 \rangle}_{min}$  is reduced  $\lambda_0$ , for  $2/3$  of them - down to  $0.038 \lambda_0$ .

To evaluate the bending tract parameters let us consider a tract consisting of a bending magnet with radius  $R$  and tune  $\nu$ . In the magnet length an integer number of oscillation waves is to go to provide with zero in the transverse dispersion function  $\psi$  and its derivative  $\psi'$ . The longitudinal dispersion coefficient  $\chi_1$  is defined by integration over the bending angle  $\chi_1 = \int \psi \, d\phi$  and  $\frac{2\pi j R}{\nu^3}$ . The  $\chi_1 \epsilon_0$  product is defined by the bunch length  $\sigma_z$ ; the  $\epsilon_0$  - to minimize the linac section the tract aperture, is to be chosen small much more than an energy spread in a beam. That choice of  $\epsilon_0 \sim 1\%$  and  $\chi_1 \approx 0.6$  m. By that the tune is determined by magnet radius and oscillation waves or  $j=1$  with  $\sim 7T$  magnetic field and 3 TeV beam tune is 25, tract length - 400m, bending angle - magnet aperture - 5 cm. An increase of  $j$  by conserving the aperture decrease in proportionality with length by that increases in proportionality with  $j^{1/3}$ .

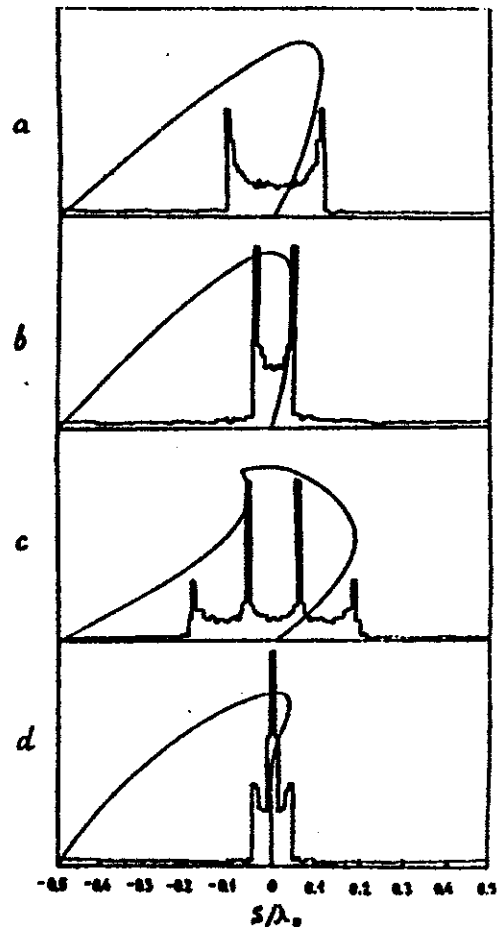


Fig. 6. Bunching efficiency: proton density distribution through a length  $\lambda_0$ , and phase half-profile after the buncher for a beam with null initial energy spread; a -  $\chi_1$  for all particles,  $\chi_2 = 0$ ; b - the same for  $2/3$  of particles; c -  $\chi_1$  and  $\chi_2$  are optimum for a; d - the same for  $2/3$  of particles.

example of real tract lattice, that consisting  
 lls could be considered with B standing for  
 s and F and D - for quadrupoles, focusing and  
 the radial plane. If magnet radius and length  
 1500 and 15 m, accordingly, the quadrupole  
 m by 10 kOe/cm magnetic field gradient, then  
 lls will compose the one wave tract with the  
 dispersion coefficient  $\chi = 61$  and the maximum  
 dispersion function in the tract  $\Delta x_{max} =$   
 ll length - 432 m. If the length of magnets is  
 quadrupoles - 1.1 m by 20 kOe/cm field gra-  
 is reduced down to 2.8 m, but the number of  
 same  $\chi_1$  increases up to 48 (three oscillation  
 tract length- up to 935 m.

possibility for bunch-wise operation on proton  
 ring could be used as a bending tract for the  
 linac section in this case is located by-pass  
 ift and ejected bunch passed through the section  
 ain into the ring by means of a section similar  
 ejection. Longitudinal dispersion coefficient in  
 of the order of 15 m per revolution, that is 25  
 an in above considered tracts, and thus requires  
 lower linac section energy, namely, ~ 1.2 GeV  
 ) GeV. With energy spread in a beam  $\delta E$  of  
 by  $10^{-5}$  and bunch length  $\delta l$  of  $\sim 0.1\lambda_0$  that  
 the energy spread smallness condition:  $\delta E/\Delta E_0 \sim$

If the wave length of linac section could be ma-  
 the order of or more than the UNK proton bunch length  
 former scheme provides with a proton bunch compression  
 equal lengths of a wave and a bunch the compr-  
 efficiency is the same as for continuous beam bunching  
 it is significantly higher when the wave is longer  
 bunch. So, with  $\lambda_0 = 30$  cm and r.m.s. bunch length l  
 about 80% of protons could be collected inside a length  
 cm. By that the compression could be fulfilled for s  
 bunch revolutions in the ring that allows to redu-  
 proportionality the linac section energy from 10-12 GeV  
 to ~1 GeV - the minimum determined by the energy spread  
 beam.

Pass of such formed proton bunch through the  
 described external buncher will result in its f  
 compression till a collection inside the 2 mm length of  
 of primary beam protons when  $\lambda_0 = 2$  cm and of ~ 70% .  
 $\lambda_0 = 4$  cm.

## REFERENCES

- Leev et. al. The IIEP Accelerating and Storage  
Status and Development. EPAC. Rome, 1988, p.233.
- Skrinsky. Linear Colliders. Proc. of XII Int. Conf.  
Energy Acc., Batavia, 1983, p 104.
- Trishanov, G.I. Silvestrov et. al. Fast Bunch-Wise  
ion of Protons from the UNK Storage Ring at an  
3 TeV. Report for AllUnion Conf. on Accelerators.  
, 1990.
- Landau. Izvestiya Acad. Nauk USSR, Phys. Section,  
(1953).
- Belen'ky and L.D. Landau. Uspekhi Phys. Nauk, 52,  
54).
- Rosental and D.S. Chernavsky. Uspekhi Phys. Nauk,  
2, 185(1954);
- Docoon. Phys. Rev., v.93, 1107(1954);
- Shuryak. Yadernaya Physika, v.24, 630(1976)
- Shuryak, O.V. Zhurov. Simple Model of Collective  
moments in High Energy Hadron-Nucleus Collisions.  
print INP 77 - 20, Novosibirsk, 1977.
- Silvestrov. Problems of Intense Secondary Particle  
Production. Proc. of the XIII Int. Conf. on High  
y Accelerators. Novosibirsk 1986, v.2, p.258. Pre-  
86-163. INP, Novosibirsk.

G.I. Silvestrov, A.N. Skrinsky  
and T.A. Vsevolozhskaya

Pions and Muons Acceleration  
at the UNK-VLEPP Facility

Г.И. Сильвестров, А.Н. Скринский,  
Т.А. Всеволожская

Ускорение пионов и мюонов в комплексе  
установок УНК-ВЛЭПП

Ответственный за выпуск С.Г. Попов

Работа поступила 10 апреля 1991 г.

Подписано в печать 20.1 1992 г.

Формат бумаги 60x90 1/16 Объем 1,5 печ.л., 1,2 уч.-л.

Тираж 150 экз. Бесплатно. Заказ N 6

Ротапринт ИЯФ им. Г.И. Будкера СО РАН,  
Новосибирск, 630090, пр. академика Лаврентьева,

# THE OPTIMISATION AND EFFICIENCY OF ANTI-PROTON PRODUCTION WITHIN A FIXED ACCEPTANCE

T. A. VSEVOLOZSKAYA

USSR Academy of Sciences, Siberian Division, Institute of Nuclear Physics, Novosibirsk 90, USSR

Received 1 April 1981

A study of the optimum conditions for antiproton production within a fixed phase volume — the acceptance of the antiproton accumulator or other device, has been made in order to determine the requirements for optical systems used for proton focusing onto the target and antiproton collection. An analytical evaluation of particle capture efficiency is reported and compared to computer simulation results. The possibility of increasing the capture efficiency by means of antiproton focusing within the target is considered for the examples of a target with current providing the distributed focusing through the target length and a target with concentrated focusing carried out with lenses placed between target sections.

## 1. Antiproton emittance and optimum target conditions

The optimisation of antiproton production inside a fixed phase volume — the acceptance of a storage ring or other device — consists of matching the acceptance form to a particle distribution in phase space by optimum choice of the target and incident proton beam parameters to provide a high particle density inside the acceptance.

To find the antiproton distribution function in a first approximation one can neglect the elastic nucleus and multiple scattering of protons and antiprotons, angular spread in the proton beam, and ionization losses of energy in comparison to the production angle and momentum spread of the antiprotons.

The equations determining the distribution function (the kinetic equations) of the antiprotons produced by incident protons interacting in a target, are in this approximation

$$\frac{\partial P}{\partial z} + \theta \frac{\partial P}{\partial r} = P(r, z) n_0 \frac{d^2 \sigma}{d\Omega dp} - \bar{\sigma}_{in} n_0 P, \quad (1)$$

$$\frac{\partial P}{\partial z} = -\sigma_{in} n_0 P,$$

where  $P(r, z) = P_0(r) e^{-z/\lambda}$ , where  $P_0(r)$  is the proton distribution across the incident proton beam,  $\lambda = 1/\sigma_{in} n_0$  — the proton-absorption length, and so the equation for  $P$  is

$$\frac{\partial P}{\partial z} + \theta \frac{\partial P}{\partial r} = P_0(r) e^{-z/\lambda} n_0 \frac{d^2 \sigma}{d\Omega dp} - \bar{\sigma}_{in} n_0 P. \quad (2)$$

After the integration of (2) over transverse phase space with the condition that  $P \rightarrow 0$  at  $r, \theta \rightarrow \infty$ , we have the equation, determining the antiproton yield dependence on the position  $z$  along the target ( $0 < z < L$ ):

$$\frac{d}{dz} \left( \frac{dN}{dz} \right) = N_0 e^{-z/\lambda} n_0 \frac{d^2 \sigma}{d\Omega dp} - \bar{\sigma}_{in} n_0 \frac{dN}{dz},$$

which gives:

$$\frac{dN}{dz} = N_0 \frac{d\sigma}{dp} \frac{e^{-\sigma_{in} n_0 z} - e^{-\bar{\sigma}_{in} n_0 z}}{\bar{\sigma}_{in} - \sigma_{in}} = \frac{N_0}{\bar{\sigma}_{in} - \sigma_{in}} \frac{d\sigma}{dp} z \frac{e^{-\sigma_{in} n_0 z} - e^{-\bar{\sigma}_{in} n_0 z}}{z} \quad (3)$$

where  $N_0$  is the number of incident protons. The maximum value of  $dN/dp$  occurs at  $z = z_m = \ln(\bar{\sigma}_{in}/\sigma_{in}) / n_0(\bar{\sigma}_{in} - \sigma_{in})$ . Because  $\bar{\sigma}_{in} \approx \sigma_{in}$ , one has

$$\frac{d}{dz} \langle r^2 \rangle \frac{d\bar{V}}{dp} - z \langle r \theta \rangle \frac{d\bar{V}}{dp}$$

$$= N_0 n_0 \frac{d\sigma}{dp} e^{-z/\lambda} \langle r_0^2 \rangle - \bar{\sigma}_{in} n_0 \langle r^2 \rangle \frac{d\bar{V}}{dp},$$

$$\frac{d}{dz} \langle r \theta \rangle \frac{d\bar{V}}{dp} - \langle \theta^2 \rangle \frac{d\bar{V}}{dp} = -\bar{\sigma}_{in} n_0 \langle r \theta \rangle \frac{d\bar{V}}{dp}, \quad (4)$$

$$\frac{d}{dz} \langle \theta^2 \rangle \frac{d\bar{V}}{dp} = N_0 n_0 \frac{d\sigma}{dp} e^{-z/\lambda} \langle \theta_0^2 \rangle - \bar{\sigma}_{in} n_0 \langle \theta^2 \rangle \frac{d\bar{V}}{dp},$$

where  $\theta_0$  and  $r_0$  denote the angle and coordinate of antiproton production. Using (3) the system of equations is easily solved. For small difference between  $\bar{\sigma}_{in}$  and  $\sigma_{in}$  we have

$$\langle r^2 \rangle \cong \langle r_0^2 \rangle + z^2 \langle \theta_0^2 \rangle / 3,$$

$$\langle r \theta \rangle \cong z \langle \theta_0^2 \rangle / 2, \quad \langle \theta^2 \rangle = \langle \theta_0^2 \rangle.$$

Values of  $\langle r^2 \rangle$ ,  $\langle r \theta \rangle$  and  $\langle \theta^2 \rangle$  determine the effective emittance of the antiproton beam  $\epsilon_{\bar{p}}$  as

$$\epsilon_{\bar{p}} = \sqrt{\langle r^2 \rangle \langle \theta^2 \rangle} - \langle r \theta \rangle^2,$$

its envelope function  $\beta_{\bar{p}}$  as

$$\beta_{\bar{p}} = \langle r^2 \rangle / \epsilon_{\bar{p}},$$

the distance to the beam waist from the target exit as

$$\Delta z = -\langle r \theta \rangle / \langle \theta^2 \rangle,$$

and the value of  $\beta_{\bar{p}}$  in it as  $\beta_{\bar{p}} = \epsilon_{\bar{p}} / \langle \theta^2 \rangle$ . For an extremely thin proton beam ( $\langle r_0^2 \rangle \ll z^2 \langle \theta_0^2 \rangle / 12$ ) and  $\bar{\sigma}_{in} \cong \sigma_{in}$  these are

$$\epsilon_{\bar{p}} = z \langle \theta_0^2 \rangle / 2\sqrt{3},$$

$$\Delta z \cong -z/2,$$

$$\beta_{\bar{p}} = z/2\sqrt{3} \quad (5)$$

The emittance value at a target length corresponding to the maximum antiproton yield, i.e.  $z \cong \lambda$ , can be taken as the characteristic emittance,  $\epsilon_0$ , of antiproton production for chosen antiproton momentum and target material.  $\epsilon_{\bar{p}}$  has a linear dependence on target length whereas the time of antiproton yield is proportional to  $z e^{-z/\lambda}$ , this shows that the optimum

$$\omega(p) dp^2 \propto \sqrt{m_1} \exp(-m_1/T)$$

which agrees well enough with experimental data at small value of  $p_1$  ( $p_1^2 \ll m^2$ ) when the temperature  $T$  is taken to be of the order of the  $\pi$ -meson's mass  $m_\pi$ . The  $m_1$  in (6) is transverse mass  $m_1 = \sqrt{m^2 + p^2}$ . The angular distribution which follows from (6) is nearly Gaussian with mean square of angle  $\langle \theta^2 \rangle \cong 2mT/p^2 \cong 2mm_\pi/p^2$ , where  $m$  and  $p$  are the antiproton mass and momentum. So the production of antiprotons for the antiprotons with momentum  $p$  is  $\propto mm_\pi \lambda / \sqrt{3} p^2$ .

The equation which determines the number of antiprotons  $N_e$ , captured into an acceptance  $\epsilon$ , is obtained after integration of (2) over angles and transverse coordinates inside the acceptance. Then one easily sees that on the left side there remains only the term  $\partial/\partial z \int^{\epsilon} \int^{\epsilon} d^2r dO \sim dN_e/dz$  in accordance with conservation of phase volume by free particle motion. So we have

$$\frac{dN_e}{dz} = n_0 e^{-z/\lambda} \Delta p \int P_0(r) \frac{d^2\sigma}{dp dO} d^2r dO$$

where  $\Delta p$  is the momentum bite captured.

To determine the sphere of integration for the right side of (7) we must use the dependence of acceptance  $\beta$  and  $\alpha$  or  $\gamma$  and  $\alpha$  functions on longitudinal target coordinate  $z$ . The second pair is preferable because  $\gamma$  has a constant value in a drift section determined by the value of  $\beta$  at a waist,  $\beta_{\min}$ :  $\gamma = 1/\beta_{\min}$ . The  $\alpha$  of acceptance has, evidently, to be zero at the antiproton beam waist, i.e. in the target centre  $\bar{\sigma}_{in} \cong \sigma_{in}$ . Thus  $\alpha$  is related to the  $\gamma$  and  $\beta_{\min}$  as  $-\gamma(z - L/2) = -[1/\beta_{\min}](z - L/2)$ , where  $L$  is the target length.

Let the proton beam have a radius  $r_0$  less than the minimum coordinate size of acceptance  $\gamma < \sqrt{\epsilon(\gamma)} = \sqrt{\epsilon\beta_{\min}}$ . Then for a Gaussian distribution of antiproton production angles, and  $\bar{\sigma}_{in} \cong \sigma_{in}$  we have

$$N_e = n_0 \frac{d\sigma}{dp} \Delta p e^{-L/\lambda} \int_0^L \int_0^{2\pi} \int_0^{\beta} \text{erf} \frac{\beta}{\sqrt{\langle \theta_0^2 \rangle}}$$

$$\times \text{erf} \frac{\beta}{\sqrt{\langle \theta_0^2 \rangle}} P_0(r) r dr d\varphi dz,$$

case: For an infinitely thin proton beam,  $P_0(r) = \delta(r) \delta(\nu)$ , expression (8) is simplified to

$$N_e = N_0 n_0 \frac{d\sigma}{dp} \int_0^L \left[ \operatorname{erf} \sqrt{\frac{\epsilon \gamma}{(\theta_0^2)(1+z^2\gamma^2/4)}} \right]^2 dz. \quad (9)$$

In the case where the range of angles captured is small compared to the range produced,  $\epsilon \gamma \ll (\theta_0^2)$ , the expression under the integral can be expanded in a series, and taking into account only the first term we have

$$N_e \approx N_0 \frac{\Delta p}{\sigma_{in}} \frac{d\sigma}{dp} \frac{8\epsilon e^{-L/\Lambda}}{\pi \lambda (\theta_0^2)} \operatorname{arctg} L\gamma/2. \quad (10)$$

If we set  $\gamma$  of the acceptance equal to that of the antiproton beam,  $\gamma \bar{p} = 2\sqrt{3}/L$ , which is close to optimum for the acceptance, not too small compared to  $\epsilon_0$ , we see the exponential decrease of  $N_e$  with target length when  $L = 2\sqrt{3}/\gamma \gg 2\sqrt{3}\epsilon/(\theta_0^2)$ .

To find the optimal target length  $L_{opt}$  for the accepted dependence of  $\gamma$  on  $L$ , we have to solve the equation  $dN_e/dL = 0$ . Taking into account two terms of the series in the right side of (9) we have

$$L_{opt} \approx 1.28\lambda \sqrt{\frac{\epsilon}{\lambda(\theta_0^2)}} \left( 1 + 0.64 \sqrt{\frac{\epsilon}{\lambda(\theta_0^2)}} + \dots \right) \quad (11)$$

$$N_e(L_{opt}) \approx N_0 \frac{\Delta p}{\sigma_{in}} \frac{d\sigma}{dp} \frac{8}{3} \frac{\epsilon \exp(-L_{opt}/\Lambda)}{(\theta_0^2)(\lambda + L_{opt})}.$$

For a proton beam of finite radius and uniform particle distribution in it the ratio  $\epsilon/(\lambda\theta_0^2)$  in the expression for  $L_{opt}$  is to go with  $\frac{1}{2}r_0^2/\epsilon\lambda$ , so using the designation

$$R = 1.65 \left( \frac{\epsilon}{\lambda(\theta_0^2)} + \frac{3}{8} \frac{r_0^2}{\epsilon\lambda} \right), \quad (12)$$

we have

$$L_{opt} \approx \sqrt{R(1 + \frac{1}{2}\sqrt{R} + \dots)}.$$

For very small values of acceptance the  $\gamma = 2\sqrt{3}/L$

$$\frac{1}{\gamma_{opt}} = \beta_{min,opt} \approx \frac{\lambda}{\pi} \frac{R^{2/3}}{1 - (4/3\pi)R^{1/3}}$$

$$L_{opt} \approx \frac{2\lambda}{\pi} \frac{R^{1/3}}{1 - (4/3\pi)R^{1/3}}$$

$$N_{e,max} \approx N_0 \frac{\Delta p}{\sigma_{in}} \frac{d\sigma}{dp} \times \frac{4\epsilon e^{-L_{opt}/\Lambda}}{(\theta_0^2)\lambda} (1 - (4/3\pi)R^{1/3})^3. \quad (13)$$

At the limit  $R \rightarrow 0$  the value of  $N_{e,max}$  (eq. 13) differs from  $N_e$  (eq. 11) by a factor of 1.5, but already at  $R \sim 10^{-2}$  the difference is less than 10%.

The thin proton beam condition  $r_0^2 \ll \frac{1}{2}\epsilon^2/(\theta_0^2)$ , following from (12) and (13), is more strict than that obtained from the antiproton beam emittance definition (see (5)). This difference is due to the strong inhomogeneity of the antiproton distribution at small angles and coordinates, which does not influence sufficiently the integral characteristics of the whole distribution.

Analytical estimates of the optimum values of capture efficiency, collection angle, target length and of the efficiency dependence on proton beam size are consistent with results of Monte-Carlo simulation (see figs. 1-4), in which the multiple and elastic nuclear scattering of protons and antiprotons, the difference in their absorption lengths, the angular spread and real coordinate distribution in proton beam were taken into account. The capture efficiency is characterized by a function  $F$  equal to the ratio of the number of antiprotons captured to the number that would be produced in the whole transverse phase space by interaction of all primary protons without antiproton absorption. The  $F = 1$  in the case of an infinitely large acceptance, long and thin target and thin proton beam. The number of antiprotons captured is determined with  $F$  from

$$N_e = N_0 \frac{\Delta p}{\sigma_{in}} \frac{d\sigma}{dp} \cdot F = N_0 \frac{d^2\sigma}{dp dO} \cdot \frac{\Delta p}{dp dO} \pi(\theta_0^2) F. \quad (14)$$

In fig. 1 is shown the dependence of  $F$  on the acceptance value at optimum values of the  $\gamma$ -function, in fig. 2 the dependence of  $F$  on the mean

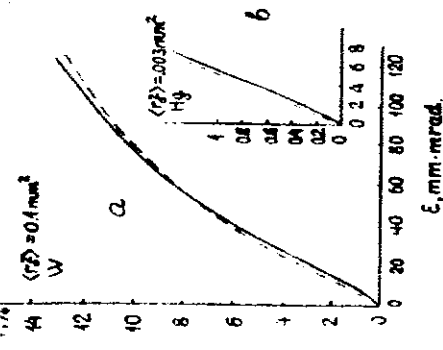


Fig. 1. Capture efficiency dependence on an acceptance value from computer simulation (solid lines) and eqs. (1.1) marked a and (1.3) marked b (dashed lines). Antiproton and proton momenta are 5.5 and 70 GeV/c; mean square proton beam radius and target material are indicated.

In the computer simulation the proton distribution across the beam is taken to be Gaussian. The differences in the curves in fig. 2 at very small  $\langle r_0^2 \rangle$  is due to the influence of the angular spread in the proton beam, when this spread, increasing with beam size decrease for a finite value of beam emittance, becomes of the order of, or more than, the range of angles captured. The  $F$  dependence on target length (fig. 3) is shown for a target with a very large cross section and for a thin one with a cross section of the

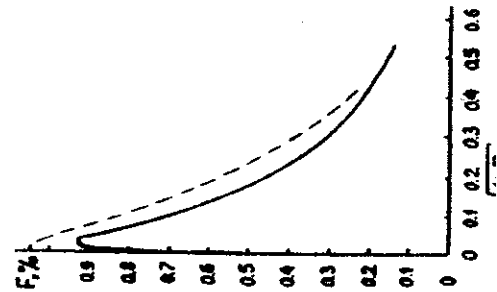


Fig. 3. Capture efficiency dependence on target length  $L$ : 1 - target with infinitely large cross-section; 2 - thin target;  $\langle r_0^2 \rangle = 0.003 \text{ mm}^2$ ,  $\epsilon$  and  $p$  the same as in fig. 2.

order of the proton beam cross section. At large  $L$  the thin target gives a marked gain due to the smaller absorption of antiprotons, but the difference in  $F$  at optimum target lengths does not exceed 15%.

The optimisation of antiproton capture into an accumulator includes the optimum choice of injec-

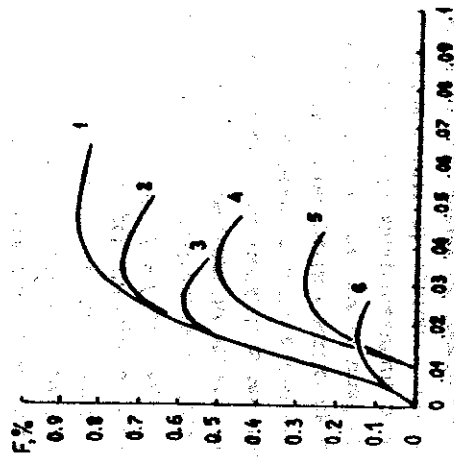


Fig. 4. Capture efficiency ( $v = 5 \times 10^8 \text{ m}^{-1} \text{ rad}$ ,  $p_0 = 2.4 \text{ GeV}$ ) versus an angular size of acceptance at the target for the antiproton collection with: 1 - ideal lens; 2 - lithium lens with 10 cm focal distance,  $f = 7.5 \text{ cm}$  length,  $l = 10 \text{ mm}$  aperture,  $\phi = 2.5 \text{ mm}$  beryllium end flanges thickness; 3 - lithium lens with  $f = 20 \text{ cm}$ ,  $l = 7.5 \text{ cm}$ ,  $\phi = 20 \text{ mm}$ ,  $\phi_0 =$

proton deceleration before cooling, as in the INP-HEP project [1], the maximum accumulation rate is achieved by the injection at the maximum of  $r \cdot J^3 \sigma dp^3$  the cross section of antiproton production within a phase volume element  $d^3p/p$ , which is conserved at the adiabatic particle deceleration. This element contains in a product  $p^2 \epsilon \Delta p/p$  in eq. (11) [or (13)], when as a result of the relation

$$\frac{d\sigma}{dp} = p \frac{d^3\sigma}{dp^3} \Big|_{\theta=0^\circ} \cdot p\pi(\theta_0^2)$$

use it turns into

$$V_c = N_0 \frac{1}{\sigma_{in}} \cdot p \frac{d^3\sigma}{dp^3} \Big|_{\theta=0^\circ} \cdot \frac{8\pi e^{-L_{opt}/\Lambda}}{3(\lambda + L_{opt})} \cdot p^2 \epsilon \frac{\Delta p}{p} \quad (15)$$

In the case of the stochastic cooling of the antiproton momentum spread before the deceleration, as in the FNAL project [2], the cross-section  $d^2\sigma/dp d\theta$  has to be maximized.

### 2. Antiproton collection

Antiproton collection from the target requires an optic system with a large angular acceptance and a short focal distance. The optimum collection angle  $\vartheta_c$  is determined by values of the acceptance and its  $\gamma$ -function at the target through  $\vartheta_c = \sqrt{\epsilon\gamma}$ . For  $\gamma = \gamma\bar{p}$ ,  $r_0 \approx 0$  and  $L = L_{opt}$  (eq. 11),  $\vartheta_c = 1.65(\epsilon\theta_0^2/\lambda)^{1/4}$ . The restriction of focal distance does not directly follow from the above consideration of optimum target conditions. It arises from taking into account the beam emittance distortion in the lens due to aberration, particle scattering and so on. And it is most strict in the case of small acceptance, because, thanks to the sharp maximum of antiproton density at the center of emittance, the aberration increase of particle angles or coordinates does not lead to a marked reduction of capture efficiency when this increase is small compared to the corresponding dimension of acceptance only. Restriction of the aberration (or scattering) angle  $\alpha_{ab}$  is also a restriction of the lens focal distance  $f$ , i.e.:

$$(\alpha_{ab}^2) < \epsilon/\beta \approx \epsilon\theta_0^2/f \quad (16)$$

lithium lenses [3] with focal distances  $f = 10$  cm and 20 cm, parabolic lenses (magnetic horns) [4] with  $f = 25$  cm, made of beryllium and aluminium, and quadrupole triplet — compared with the ideal focusing for the FNAL project parameters ( $\epsilon = 5 \times 10^{-6}$  m rad,  $p_c = 5.4$  GeV,  $\Delta p/p = \pm 2\%$ ). In the case of the lithium and the parabolic lenses the capture efficiency reduction is mainly due to the nuclear absorption and multiple scattering, in the case of the triplet to chromatic aberration [5]. The lithium lenses considered [3] have: length  $l = 7.5$  cm; beryllium end flanges of thickness 0.25 cm (for  $f = 10$  cm) and 0.5 cm (for  $f = 20$  cm); aperture diameters of 1 cm and 2 cm; 140 kOe maximum field. Under a focusing, characterized by a particle oscillation frequency  $\omega$ , the multiple scattering in lithium results in the mean square angle  $\langle\theta^2\rangle_{Li}$  smaller by a factor of  $\frac{1}{2}(1 + \sin 2\omega/2\omega)$  than  $\langle\theta^2\rangle_{Li}$  without focusing. At  $f = 10$  cm, the angle of scattering in lithium and beryllium flanges,  $\sqrt{\langle\theta^2\rangle} = 7 \times 10^{-4}$  rad, meets the condition (16) and losses in capture efficiency scarcely exceed the nuclear one. At  $f = 20$  cm the multiple scattering leads to a marked loss in capture efficiency.

### 3. Antiproton focusing within the target

As is seen from the first item, the effective transverse antiproton beam emittance on the condition of infinitely thin proton beam arises from the target length — the spread of longitudinal production coordinate,  $z$ , turns into transverse coordinate,  $r$ , spread in a beam cross section in accordance with the linear dependence of  $r$  on  $z$ . Full four-dimensional transverse beam phase volume remains zero because of the zero value of the particle  $\psi$ -velocities. Changing the dependence of  $r$  on  $z$  one can decrease the transverse antiproton beam emittance and, hence, increase the particle density inside the acceptance.

Antiproton focusing by the magnetic field of a current passing through the target along the beam axis [6], at high enough current value, eliminates the emittance dependence on target length. It allows the target length to be extended up to the value corresponding to the maximum antiproton yield. The antiproton beam emittance in this case is determined by

target efficiency, i.e.  $F \cong 1/e$  when  $\sigma_{im} \cong \sigma_{in}$ , if proton defocusing in the target can be neglected. To take the antiproton focusing into account in kinetic equations, we have to add the term  $-\omega^2 r \partial \bar{p} / \partial \theta$  to the left hand side of the first equation of system (1). On the left hand sides of the second and third equations of system (4) there appear the terms  $\omega^2 \langle r^2 \rangle d\bar{N}/dp$  and  $2\omega^2 \langle r\theta \rangle d\bar{N}/dp$ , respectively. With  $\bar{\sigma}_{im} \cong \sigma_{in}$ , taking into account (3), one obtains

$$\begin{aligned} \langle \theta^2 \rangle &= \frac{\langle \theta_0^2 \rangle}{2} \left( 1 + \frac{\sin 2\omega z}{2\omega z} \right) + \frac{\omega^2 \langle r_0^2 \rangle}{2} \left( 1 - \frac{\sin 2\omega z}{2\omega z} \right) \\ \langle r^2 \rangle &= \frac{\langle \theta_0^2 \rangle}{2\omega^2} \left( 1 - \frac{\sin 2\omega z}{2\omega z} \right) + \frac{\langle r_0^2 \rangle}{2} \left( 1 + \frac{\sin 2\omega z}{2\omega z} \right) \\ \langle r\theta \rangle &= \frac{\langle \theta_0^2 \rangle - \omega^2 \langle r_0^2 \rangle}{4\omega^2 z} (1 - \cos 2\omega z), \end{aligned} \quad (17)$$

where  $\omega = \sqrt{qG/pc}$  is the frequency of the antiproton oscillation in a field inside the target,  $G$  — the field gradient,  $p$  and  $q$  — the antiproton momentum and charge. The effective emittance of antiproton beam with  $\omega^2 \langle r_0^2 \rangle \ll \langle \theta_0^2 \rangle$  is

$$\epsilon_{\bar{p}} = \frac{\langle \theta_0^2 \rangle}{2\omega} \sqrt{1 - \frac{\sin^2 \omega z}{\omega^2 z^2}}.$$

The emittance dependence on target length nearly vanishes already at  $\omega z = \pi/2$ , but the value of  $\epsilon_{\bar{p}}$  for that slightly differs from the emittance for a target of the same length without field. It means that to obtain a marked gain in capture efficiency, the field gradient has to be large enough to ensure the above equality at a  $z$  less than the optimum target length without field  $L_{opt}$ , determined by eq. (11) (or eq. (13) for a very small  $\epsilon$  compared to  $\lambda(\theta^2)$ ). So we have  $\omega > \pi/2L_{opt} \cong \sqrt{\langle \theta_0^2 \rangle / \epsilon \lambda}$  and  $G > 2mm \cdot c^3 / qpe\lambda$ . For the INP-IHEP antiproton source project [1] ( $\epsilon = 6 \times 10^{-5}$  m rad,  $pc = 5.5$  GeV) it means that  $G > 0.27$  MOe/mm. The estimate for the FNAL project with  $L_{opt}$  determined in eq. (13) with  $\langle r_0^2 \rangle = 0.003$  mm<sup>2</sup> gives  $G > 1.1$  MOe/mm.

For  $\omega L \gg \pi/2$ , an infinitely thin proton beam, and  $\bar{\sigma}_{im} \cong \sigma_{in}$  the capture efficiency into acceptance  $\epsilon$  is found to be

$$F = \frac{1}{\epsilon} \left[ \text{erfc} \sqrt{\epsilon \omega / \langle \theta_0^2 \rangle} \right]^2.$$

capture efficiency for the FNAL and IHEP beam parameters is clearly seen (figs. 5 and 6) from the comparison of the  $F$  dependence on the field gradient  $G$  at different values of the proton energy  $E_0$  and the beam emittance  $\epsilon_p$  ( $\epsilon_p \propto 1/E_0$ ) and the  $\beta$ -function in the target  $\beta_p$  ( $\beta_p \propto E_0$ ). Fig. 5b shows the dependence of optimum target length  $L_{opt}$  on  $G$  for the same case as in fig. 5a. The decrease of  $L_{opt}$  with an increase of  $G$  above some value also shows the onset of proton defocusing.

Antiproton focusing inside the target leads to some decrease of angular spread at the target exit [see eq. (17)]. For a fixed value of the emittance  $\epsilon_p$ , this means an increase of the beam  $\beta$ -function in the waist,  $\beta_{min} = \epsilon_p / (\theta^2)$ , as compared to its value in the case of a target, without field, with the same value of  $\epsilon_p$ . This increase has a maximum at  $\omega L \cong 0.7 \pi$  and is characterized by a factor of about 2.5. Hence the increase of the beta-function for acceptance  $\beta$  with

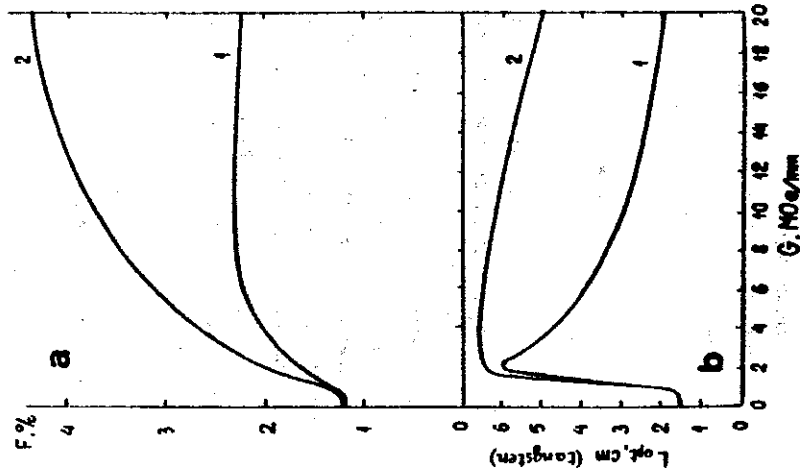


Fig. 5. Capture efficiency (a), and optimum target length dependence on a magnetic field gradient inside the target (b).

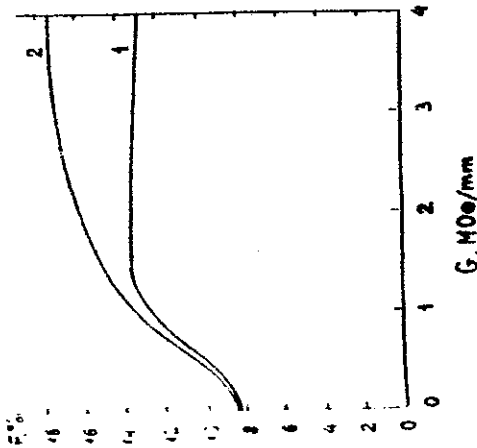


Fig. 6. The same as in fig. 5 for  $\epsilon = 6 \times 10^{-3}$  m · rad;  $p = 5.5$  GeV/c;  $E_0 = 70$  GeV (1) and 350 GeV (2);  $(r_0^2) = 0.1$  mm<sup>2</sup>.

out losses in phase particle density does not significantly exceed the factor 2 or 3. In the case of fig. 5 the optimum  $\beta$  for acceptance is a maximum and equals  $\sim 1.3$  cm at  $G \sim 1.5$  MOe/mm. At  $\omega L \gg \pi/2$ ,  $\beta \sim \omega^{-1}$ .

The magnetic field with a gradient of several mega-coersted per millimeter requires a very high current density in the target ( $[A/mm^2] = (1/2\pi) G[Oe/mm]$ ), which will be accompanied by very high density of resistive energy deposition. This leads to thermal distortion of the target within a very short time that can be less than the proton spill duration. Taking into account the alteration of the target electro-conductivity  $\sigma$ , by  $\sigma = \sigma_0/(1 + \beta Q)$  [7], the time taken for the target to heat up to the melting temperature  $T_{\text{melt}}$  is determined as follows:

$$t = \frac{\sigma_0}{\beta^2/2} \cdot \ln(1 + \bar{\alpha} \cdot T_{\text{melt}}), \quad (18)$$

where  $\sigma_0$  is the initial value of  $\sigma$ ,  $\beta$  — its thermal coefficient, nearly constant in the temperature interval from 20°C to  $T_{\text{melt}}$ ,  $\bar{\alpha}$  — the mean value of the temperature coefficient,  $Q$  — the density of deposited energy,  $\bar{\beta}$  — the mean square current density. For a

The deposited energy that goes into the latent heat of fusion increases this time by not more than 15%, and so the target distortion at a field gradient of several MOe/mm begins within a microsecond. This agrees very well with the results of an experimental study of target behaviour at such fields, carried out in the INP [6,8] in 1968.

Another way of increasing the phase density of antiprotons inside the acceptance [9] consists of replacing the target by several short ones with strong lenses placed in between to focus the antiprotons from one target to another. In this case the trajectories of the antiprotons produced in different targets coincide and the whole beam emittance does not exceed the emittance from one short target. The optimum value of the total target length  $L_{\text{opt}}^{(n)}$  depends on the number of targets  $n$  as

$$L_{\text{opt}}^{(n)} = n \cdot \frac{e}{\beta^2} \cdot \frac{\exp(-L_{\text{opt}}^{(n)}/\lambda)}{L_{\text{opt}}^{(n)} + \lambda}$$

$$i = 1, 2, 3, \dots, n,$$

where  $R$  has the same value as in eq. (12). The value of the beam  $\gamma$ -function is determined by the length of one target  $l^{(n)}$ ,  $\gamma_p = 2\sqrt{3}l^{(n)} \sim 2\sqrt{3}R/\sqrt{n}$ . Thus the  $\gamma$  of acceptance equal to  $\gamma_p$ , and the solid collection angle  $\pi\theta^2 = \pi\gamma$  increase with  $n$  as  $\sqrt{n}$  together with the same increase of the total target length, and so the capture efficiency increases approximately as  $n$ :

$$F \approx \frac{1}{2} n \cdot \frac{e}{\beta^2} \cdot \frac{\exp(-L_{\text{opt}}^{(n)}/\lambda)}{L_{\text{opt}}^{(n)} + \lambda} \quad (20)$$

The transformation of expressions (13) to the case of  $n$  targets also consists of replacing  $R$  by product  $nR$  and multiplying the expressions for  $\gamma_{\text{opt}}$  and  $F$  by  $n$ .

The lenses between the targets must have the shortest focal lengths to minimize the aberration effect and the length of the whole system, which determines the value of the proton beam  $\beta$ -function at the targets. For lithium lens, occupying the whole distance between targets  $d$ , the value of  $d$  is related to the maximum field in a lens by  $H_{\text{max}} \cdot d = \pi\sqrt{\epsilon\gamma}$  pc/q. For  $H_{\text{max}} \sim 300$  kOe using the dependence of

The author is thankful to G. Silvestrov and members of his group whose enthusiasm for and progress in the development of effective targetry methods supported this investigation.

#### References

- [1] T.A. Vsevolozhskaya, Ya.S. Derbenev, N.S. Dikansky, I.N. Meshkov, V.V. Parhomchuc, D.V. Pestrucov, G.I. Silvestrov and A.N. Skrinsky, Antiproton Source for UNC IHEP. INP report 80-182 (Novosibirsk 1980) in Russian.
- [2] Design report. The Fermilab high-intensity antiproton source (FNAL October 1979).
- [3] B.F. Bayanov, A.D. Chernyakin, V.N. Karasyuc, G.I. Silvestrov, T.A. Vsevolozhskaya, V.G. Volohov and G.S. Willewald, Proc. of 11th Int. Conf. on High energy accelerators, CERN 1980 (Geneva, 1980) p. 362.

- [5] T.A. Vsevolozhskaya, The chromatic aberration of lenses with large angular acceptances, INP report 80-221 (Novosibirsk 1980) in Russian.
- [6] G.I. Budker, T.A. Vsevolozhskaya, G.I. Silvestrov and A.N. Skrinsky, Proc. of 2nd All Union Conf. on Particle Accelerators, Moscow 1970 (1972), vol. 2, p. 196 in Russian.
- [7] H. Knoepfel, Pulsed high magnetic fields (North-Holland Amsterdam, 1970).
- [8] V.M. Highdarov, Facility for study of the possibility of 1-2 MG magnetic field production at tungsten rod surface and the rod behaviour study, Graduation Work, INP (Novosibirsk 1968) in Russian.
- [9] B.F. Bayanov, G.I. Budker, G.S. Willewald, T.A. Vsevolozhskaya, V.N. Karasyuc, G.I. Silvestrov and A.N. Skrinsky, Proc. of 5th All Union Conf. on Particle Acceleration, Dubna 1976, (Moscow, 1977) vol. 2, p. 299 in Russian.

# A WIDE-ANGLE MAGNETIC LENS FOR COLLECTING LOW-ENERGY $\pi$ -MESONS IN A SOLID ANGLE OF 10 sr

G. I. SIL'VESTROV and V. A. TAYURSKY

*Institute of Nuclear Physics, Novosibirsk 90, USSR*

Received 14 September 1977

Optical characteristics and construction of a focusing device for collecting low-energy  $\pi$ -mesons in a solid angle of about 4 sr are considered. The focusing device is an axially-symmetric magnetic lens with magnetic field of  $\approx 100$  kOe and pulsating current of  $\approx 1.4$  MA. Parameters of a supply system operating at several hertz rate are given.

At area of  $100 \text{ cm}^2$  in the focus plane of the system the  $30 \text{ MeV } \pi^-$ -meson flux, produced by 1 GeV electron beam, is  $\approx 10^{-5}$ /electron with a maximum density of  $3 \times 10^{-7} \pi^-/\text{cm}^2$ .

## 1. Introduction

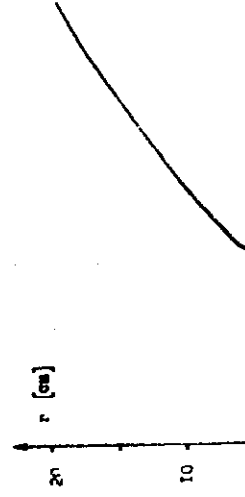
A production of intensive low-energy pion and muon beams is an actual problem for nuclear physics researches (see, for example, ref. 1), a mesochemistry<sup>2)</sup> and a  $\pi$ -meson radiotherapy<sup>3-5)</sup>. For the pion production 600–800 MeV proton accelerators, having large currents (up to  $6 \times 10^{15}$  protons  $\text{s}^{-1}$ ), are presently used. However, practically isotropically produced low-energy pions are being collected in a small solid angle. Therefore the question about an increase of pion-beams intensities, except an obvious way, an increase of proton currents, reduces to designing of focusing devices with maximum acceptance angles. There are several types of wide-angle focusing devices that, unlike traditional optical systems with quadrupoles for paraxial beams, enlarge an acceptance angle up to approximately one steradian. Such systems are divided into two classes: the solenoidal lenses with a uniform and a non-uniform magnetic field (the axis<sup>6)</sup> and the iron<sup>7)</sup> and non-iron<sup>8)</sup> toroidal lenses. Magnetic fields in such lenses are being excited by direct currents and this fields are less than 20 kOe. Further increase of an acceptance angle is limited by two reasons. The first one is the spherical aberrations for the solenoidal lenses for the fringe effects because of scattered fields between current windings for the toroidal lenses. The second reason is an abrupt increase of lenses sizes and, consequently, a power consumption.

spherical aberrations for any acceptance angle<sup>11)</sup>. Moreover, the field amplitude in a pulsating regime can be enlarged to quantities more than 100 kOe<sup>12)</sup>, that decreases the dimensions of the system and the power consumption.

The subject of the paper is a design of this type lens with an acceptance angle of about 10 sr. The efficiency of application of such systems for an intensive pion beams production by  $\approx 1$  GeV electron or proton beams is considered.

## 2. Focusing device

A possibility of the wide-angle focusing is obvious from the following consideration. Consider a point source with an isotropic angular distribution of particles on the axis of a thin-walled cylinder, through the walls of which leaks an electric current. This cylinder is an entrance surface. All particles with angles  $0^\circ < \alpha < 180^\circ$  will cross the walls and move in an axially-symmetric magnetic field ( $B \propto 1/r$ ). If we give for an exit surface, limiting the field, the shape, that all trajectories crossing it



have the zero angle with the axis, we shall receive the focusing device, collecting practically all particles in a parallel beam. Changing the shape of the exit surface, one can receive the beam, that converges in a given point on the axis of the system. Fig. 1 gives the profile of the lens for which the focusing properties were studied. For decreasing of mechanical stresses in the place, where the cylindrical surface goes into the exit surface, the entrance surface was chosen to have the conic form. Its profile in  $r, z$  coordinates is given by the equation:

$$r = 0.1z + 4.2. \quad (1)$$

The exit surface was determined from the condition of hit of particles with momentum  $P = 100$  MeV/c in the point  $z = 50$  cm. The source was placed in the point  $z = -15$  cm. The exit surface was calculated by means of numerical integration of equations of motion of particles in an axially-symmetric magnetic field:

$$B = B_0 \frac{r_0}{r}, \quad (2)$$

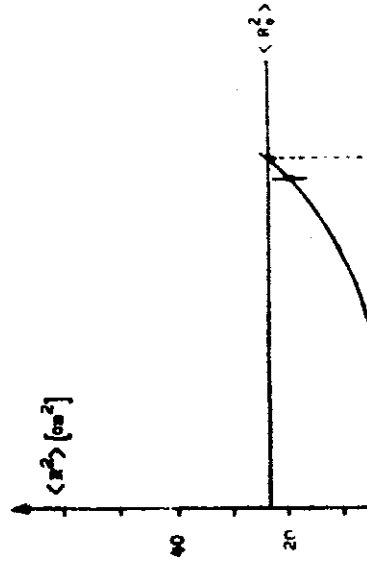
where  $B_0$  is the field strength at the surface of radius  $r_0$ . The lens collects the particles with angles  $30^\circ < \alpha < 150^\circ$ . The convergence angle in the focus of the system is  $\alpha_{\text{conv}} \approx 25^\circ$ . The maximum trajectory radius for  $\alpha = 150^\circ$  is  $r_{\text{max}} = 22$  cm. For a pulsating current amplitude of 1.4 MA, a maximum field at the entrance surface at  $r = 2.5$  cm is  $B_{\text{max}} = 112$  kOe. In this focusing device the spherical aberrations are absent, but appears an additional size of the beam in the focal plane because of scattering in the walls. The last can be neglected, if it is small compared with the size, that is due to a non-point likeness of the source. In calculations of the scattering effects in the lens the entrance surface was taken of 0.5 cm thickness and the exit surface of 0.2 cm thickness. The walls were assumed to be made out of aluminium, that bears the maximum strains of 2000 kg/cm<sup>2</sup>. The scattering was calculated according to the Molière theory. With the mentioned parameters and the point-like source (placed in the point  $z = -15$  cm)

scattering of particles in the walls. It was assumed that particles are uniformly produced along the target axis. This quantity is being compared with  $\langle R_0^2 \rangle$ . One can see, that for the target of more than  $L_0 \approx 2.1$  cm length,  $\langle R_0^2 \rangle > \langle R_1^2 \rangle$ . Thus the scattering can be neglected for the target of  $L < 2.1$  cm length.

The lens does not collect the particles going to ward in a solid angle of about 1 sr. There is placed a tungsten cone stopper. This stopper restricts the drift space outside the exit surface (fig. 3). For trajectories with a big radius, the drift space is limited by the walls of a cone hole in the shield. Thus, the space between this cone surfaces serves as a diaphragm for a pion beam and restricts a momentum spectrum of particles passing across the lens (fig. 5). To separate a beam better one can place inside the lens several additional cone diaphragms along the trajectories of equilibrium particles.

### 3. Construction of the lens and a supply system

The experience of designing and investigation of the thin-walled covers with a big pulsating current<sup>9,10,12</sup> shows, that the covers conserve the mechanical firmness at more than 100 kOe magnetic field. A specific form of the current surfaces profiles of the described lens needs a special investigation of its mechanical properties in the regime of the dynamical loading, but this question is not discussed in the paper. The major problem in elab



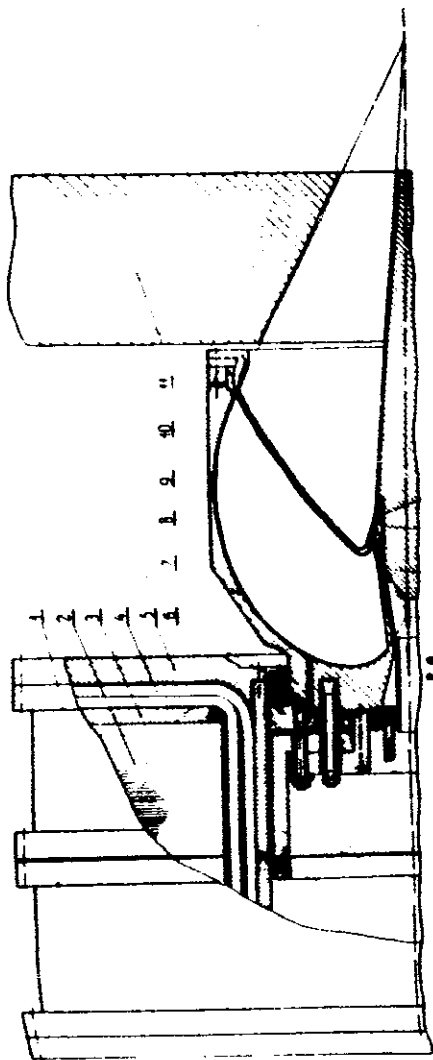


Fig. 3. The complete view of the focusing device. 1 - transformer; 2 - toroidal iron; 3 - secondary coil winding of the transformer; 4 - primary coil windings; 5 - cover; 6, 7 - pressing rings of the grip contacts; 8 - hold; 9 - pressing contact ring; 10, 17 - entrance and exit of the colling system; 11 - lead shield; 13 - coaxial current contacts; 14 - load-bearing bolts, supporting the tyre; 15 - contact grips; 16 - stop flange for supporting the pressing and pressing out bolts; 18 - converter target; 19 - tungsten stopper; 20 - stop passage detail; 21 - stop passage detail.

operating of the lens is a construction of electrical contacts for currents up to 1.4 MA. For rigidly done up ends of the lens and for necessary contact efforts the electrical contacts must not give additional static strains in cross-sections of the lens. Another important problem is a creation of an intensive cooling of the thin-walled current surfaces, operating at several Hertz rate. Fig. 3 gives the lens with contact buses and a transformer. The lens is inserted in the profiled along the external trajectory coaxial tyre (7); the pressing ring (9) reinforces the lens at its end. The second end of the lens is not rigidly reinforced in the longitudinal direction and it's connected with the electrical contact (13) with the help of 18 grip dums (15), uniformly distributed along the perimeter of the end. After dighting the contacts, the free end of the lens is firmly fixed relative to the detail (16) with the help of a system of the alternating pressing and pressing out bolts. The cone-like tungsten stopper (19), serving for absorption of particles after the target, is a load-bearing element of the construction in the same time. Through the passage detail (20), the stopper is pressed to the body of the lens at the place, where the entrance and exit surfaces join together. This place is the third

In this case we lose a little in transparency, but such cooling system can provide a better dissipation of heat. This cooling system can dissipate about  $100 \text{ W/cm}^2$  from the cone part of the lens and operate at several hertz current pulses repetition frequency. For this purpose the body of the lens is done out of two layers. This permits to create better conditions for the dissipation of heat with the help of a continuous stream of water between the layers. The internal non-current surface of the lens is done out of two parts. The parts are hermitized at the ends at the place of contact with the stopper, as it is shown in fig. 3.

The lens is supplied by the unipolar puls of sinusoidal current formed by the discharge of a capacity battery on the lens, that represents an inductive load. The capacity battery is switched on with the help of a thyristor valves system and discharges on the lens through the matching transformer having a small dissipation. The technique of creation of such generators is well developed at present<sup>(4)</sup>. The lens has an inductance of 50 nH and at a current of 1.4 MA the magnetic field energy in the operating volume is about 50 kJ. For a pulse duration of  $100 \mu\text{s}$  the voltage on the lens is equal to 2.5 kV and for a transformation ratio of

4 GW. This generator has been constructed in IYaf SO AN and it is being tested at present. Diminishing a current frequency one can scale up a pulse duration. In this case the generator simplifies considerably. A  $Q$ -factor of the lens is high enough ( $Q \approx 50$ ). The active power losses in the contour at 10 Hz frequency are equal to 15–20 kW. In this case the maximum heat flux in the cone part of the lens is about 100 W/cm<sup>2</sup>.

#### 4. Parameters of $\pi^-$ -meson beam

Creation of focusing devices, collecting practically all  $\pi^-$ -mesons of a given momentum interval, produced in a target, will permit to have intensive meson beams not only from proton accelerators, but also from electron accelerators. First this question was discussed in ref. 5. From this work follows, that a pion flux in a focus of a special system will be only 30 times less for the electron conversion in comparison with the proton conversion at about 1 GeV energy and for the same collection conditions.

For the focusing system that we consider, geometrical conditions of the pion production are different for the proton and electron conversions. For an effective use of the proton beam the converter target should be about one inelastic nuclear interaction length long ( $\lambda_{in} \approx 10$  cm for tungsten at  $E_p \approx 1$  GeV). For the electron beam the target should be 2–3 times as long as  $r_{max}(E_\gamma > m_\pi)$ , where  $r_{max} \approx 1.5 X_0$  is the maximum position of the shower curve for photons of energy  $E_\gamma > m_\pi$  ( $m_\pi$ -pion mass) at  $E_e = 1$  GeV. For tungsten the radiation length is  $X_0 = 0.35$  cm. In the last case the pion source is more "bright". This slightly compensates a relatively low conversion efficiency for the electron beam.

In the given below calculations of the conversion efficiency for the electron beam we use the cylindrical tungsten target of  $L = 2$  cm length ( $5.7 X_0$  of  $W_0$ ). For this target the beam size in the focal plane given by dispersion of pion production points is equal to the dimension because of scattering in the walls of the lens (fig. 2). It was as-

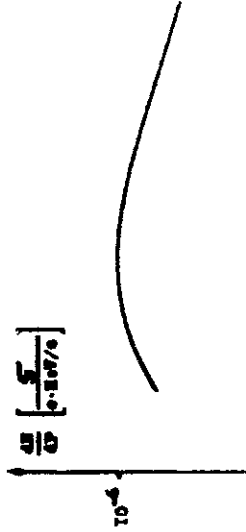
For the incident beam energy of  $E_e \lesssim 1$  GeV main input in a  $\pi^-$ -yield from the target is single photoproduction of pions from the nuclei by  $\gamma$ -quanta of the electron-photon in the converter. To estimate the  $\pi^-$ -momentum spectrum we used the experimental data on pion photoproduction from carbon and copper nuclei<sup>17,18</sup>. From ref. 18 follows that for the energy:  $300 \lesssim E_\gamma \lesssim 700$  MeV and  $\theta_{lab} \approx 2^\circ$  cross-section depends on  $A-Z$  as:

$$\frac{d\sigma}{d\Omega} \propto (A-Z)^{0.8},$$

where  $A$  - atomic weight,  $Z$  - atomic number, the data on the  $\pi^-$  photoproduction from protons<sup>19</sup> follows, that at  $E_\gamma \lesssim 1$  GeV the low pions emerge almost isotropically in the laboratory system ( $d\sigma/d\Omega \approx \text{const}$ ). Using this data we find for the  $\pi^-$ -yield from the target the following expression:

$$\frac{dN_\pi}{d\rho_\pi} \approx \frac{N_A}{A} \left( \frac{A-Z}{6} \right)^{0.8} \int_{E_{thr}}^{E_e} g(E_\gamma, E_e) dE_\gamma \int_0^\pi 2\pi \times \sin \alpha d\alpha \frac{d^2 \sigma_0(E_\gamma, P_\pi, \alpha)}{dP_\pi d\Omega},$$

where  $P_\pi$  - the momentum and  $E_\pi$  - the energy of pions,  $E_{thr} \approx E_\pi$  - the threshold energy of pion photoproduction,  $g(E_\gamma, E_e) = 0.57 X_0 E_e$  - the differential track length of photons<sup>20,21</sup>,  $E_e$  - the incident electron beam energy,  $E_\gamma$  - the pion energy,  $N_A$  - the Avogadro number,  $d^2 \sigma_0(E_\gamma, P_\pi, \alpha)/dP_\pi d\Omega$  - the twice different single  $\pi^-$ -mesons photoproduction cross-section from carbon nuclei<sup>17,18</sup>. A numerical integral of eq. (4) gives  $dN_\pi/d\rho_\pi$  in fig. 4. From this



follows that the spectrum does not change appreciably for  $P_\pi = 100$ – $150$  MeV/c and one can use for estimates:

$$\frac{dN_\pi}{dP_\pi} \approx 10^{-6} \pi^- \text{ MeV}^{-1} \text{ c (incident electron)}^{-1}. \quad (5)$$

The momentum spectra of  $\pi^-$ -mesons in the focal plane of the lens are represented in fig. 5. The histograms give pion spectra within circles of different radii  $R$  ( $1 - R = 2$  cm,  $2 - R = 4$  cm,  $3 - R = 8$  cm). The spectra are normalized to the total numbers of pions produced with angles  $30^\circ < \alpha < 150^\circ$  in the 5 MeV/c momentum intervals. Their maxima moved from  $P_\pi = 100$  MeV/c, for which the profile of the lens was computed, to  $P_\pi = 105$ – $110$  MeV/c. This shift is due to the scattering in the entrance surface of the lens. The scattering causes decreasing of the transverse in respect to the field momentum component, which is responsible for the focusing. The average density of  $\pi^-$ -meson flux within a circle of radius  $R$  per incident electron, as well as the expected flux densities of  $e^-$ ,  $\mu^-$ ,  $n$  contamination, is added in table 1.

The estimate of the  $\mu^-$  contamination from  $\mu^- - \mu^+$  pairs was done according to ref. 22.

The neutron contamination accounting the at-

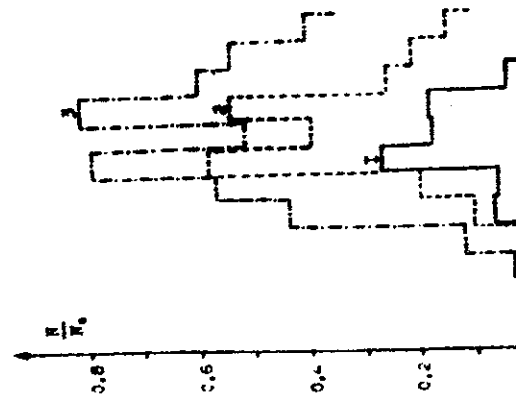


TABLE 1  
Particle flux densities (part./cm<sup>2</sup>)

Particle	$R = 2$ (cm)	$4$ (cm)	$8$ (cm)	Momentum interval (MeV/c)
$\pi^-$	$3 \times 10^{-7}$	$1.7 \times 10^{-7}$	$7 \times 10^{-8}$	$105 \pm 15$
$e^-$	$6 \times 10^{-6}$	$3.4 \times 10^{-6}$	$1.4 \times 10^{-6}$	$105 \pm 15$
$\mu^-$	$3 \times 10^{-10}$	$1.7 \times 10^{-10}$	$7 \times 10^{-11}$	$105 \pm 15$
$n$	$3 \times 10^{-8}$	$3 \times 10^{-8}$	$3 \times 10^{-8}$	-

tenuation of particles in the tungsten stopper, was estimated according to ref. 23.

The flux of electrons, leaving the converter, was computed with the help of the program in ref. 24. The major input in the electron contamination goes from the tails of angular distribution of electrons with  $P = 100$  MeV/c in the converter target. This contamination can be diminished by the increase of the angle occupied by the stopper. Some estimates show, that for the angle of  $40^\circ$  the contamination diminishes by a factor of 4.

For a comparison with this calculations, there were performed some estimates of the conversion efficiency for the proton beam of energy  $E_p = 730$  MeV. A tungsten target of 10 cm length was used in calculations. The center of target was placed in the point  $z = -15$  cm. The points of emission of pions were sampled from the distribution  $f(z) \propto \exp(-z/\lambda_{\text{int}})$ . To evaluate the pion yield from tungsten nuclei we used the experimental data<sup>15</sup> at 730 MeV proton energy (from lead nuclei). An extrapolation of this data to  $P_\pi = 100$  MeV/c gives:

$$\frac{dN_\pi}{dP_\pi} \approx 10^{-4} \pi^- \text{ MeV}^{-1} \text{ c} \quad (6)$$

per inelastic interaction. The average density of  $\pi^-$ -meson flux within a circle of radius  $R$  per incident proton in the focal plane of the system is given in table 2.

TABLE 2

It should be noted that in this case the momentum spectrum of pions is more wide than for the electron conversion. This is connected with the chromatic properties of the lens for extended sources.

In the case of the proton conversion an operation with the pion beam in the focus of the system will be difficult, apparently, because of very high proton and neutron fluxes. A local shield after the converter is not enough in this case, so it will be necessary to have a special channel to transport the meson beam in an area with the better radiation conditions.

### 5. Conclusions

The principal and technical possibility of creation of the focusing device, that can collect practically all low-energy pions produced in the converter, was shown in the paper. The described construction is a sketch project of one possible variant of such systems. We considered the limit parameters of the system (a field, a current, a heat loading). This parameters can be optimized and diminished for the concrete constructions. We have given the detailed description of some technical details of the focusing device to show, that the modern development of the strong pulsating magnetic fields technique ( $\beta > 100$  kOe) and the large pulsating currents technique ( $I > 1$  MA) allows to choose the parameters of such systems in the indicated range of fields and currents without any fear of the principal technical difficulties.

Unlike the considered system, the presently existing wide-angle focusing devices with the static magnetic fields<sup>4,5,7</sup> have two obvious failures: (a) a small in comparison with  $4\pi$  acceptance angle, (b) large longitudinal dimensions, so that the particle trajectory lengths are about the decay length for low-energy pions. Creation of systems with the large pulsating magnetic fields will allow to enlarge the acceptance angle by a factor of 10-20 and to decrease the lengths of trajectories up to

The authors are much indebted to valuable discussions with acad. A. N. Skrinsky, drs. T. A. Vsevolozskaya, V. I. Kupchik, V. I. Karasyuk, G. I. Villedwald, V. I. Zaicev, A. D. Chernyakin and B. Ya. Chudaev.

### References

- 1) V. P. Dzeleпов, V. P. Dmitrievsky and V. V. Gol'tsa, in *Problemy Yadernoy Fiziki i Fiziki Elementarnykh Chastits (Problems of nuclear physics and physics of elementary particles)* (Nauka, Moscow, 1975) in Russian.
- 2) V. I. Gol'dansky, *Trudy III Vsesoyuznogo Soveshchaniya po Uskoritelyam* (Proceedings of the III Soviet Particle Accelerators conference) vol. 1 (1973) p. 62, in Russian.
- 3) N. N. Blochin, *Ibid.*, 43.
- 4) V. M. Abazov, B. P. Dzeleпов, E. S. Kuz'min, G. A. Melokanov, O. V. Savchenko, G. P. Reshetnikov and E. P. Cherevatenko, *Preprints OIYaL P13-879*, in Russian.
- 5) *Particle Accelerators* 5 (1975) 57.
- 6) R. L. Burman, R. L. Fulton and M. Jakobson, *Nucl. Instr. and Meth.* 131 (1975) 29.
- 7) P. Kofod-Hansen, J. Lindhard and O. B. Nielsen, *Dokl. Danske Vidensk. Selskab., Math.-Fys. Medd.* 46 (1950) 25.
- 8) V. V. Vladimirov, E. K. Tarasov and Yu. V. Trebuchov, *Pribery i Technika Eksperimenta* (Soviet Journal on Measurements and Technique of Experiment) N 1 (1956) 13, in Russian.
- 9) L. L. Danilov, S. N. Rodionov and G. I. Sil'vestrov, *Jurnal Technicheskoy Fiziki* (Soviet Journal of Technical Physics) 37 (1967) 914, in Russian.
- 10) T. A. Vsevolozskaya, L. L. Danilov, V. N. Karasyuk and G. I. Sil'vestrov, *Trudy II Vsesoyuznogo soveschaniya po uskoritelyam*, vol. II (1972) 224, in Russian.
- 11) T. A. Vsevolozskaya and G. I. Sil'vestrov, *Jurnal Technicheskoy Fiziki* 43 (1973) 61, in Russian.
- 12) G. S. Villedwald, V. N. Karasyuk and G. I. Sil'vestrov, *Preprint IYaF SOAN 75-98*, in Russian.
- 13) D. G. Baratov, V. M. Valov, R. A. Rzeev, B. L. Rykov and I. M. Shalshov, *Priladnaya Mehanika i Technicheskaya Fizika* (Soviet Journal of Applied Mechanics and Technical Physics), N 3 (1974) 133, in Russian.
- 14) B. F. Baratov, A. V. Iljin, V. M. Pakin and G. I. Sil'vestrov, *Trudy I Vsesoyuznogo soveschaniya po uskoritelyam* 1 (1969) 283, in Russian.
- 15) D. F. R. Cothran, P. N. Dean, P. A. Gram, E. A. Kump, E. R. Martin, D. E. Nagle, R. B. Perkins, W. Y. Schlegel, H. A. Thiessen and E. D. Theriot, *Phys. Rev. D* 6 (1972) 3085.

and to decrease the length of hysteretic up to  
 into the acceptance angle by a factor of 10-50  
 make entering magnetic fields will show to en-  
 for low-speed hours. Creation of systems with the  
 these relatively lengths are about the same length  
 (b) make longitudinal dimensions so that the par-  
 a strength in combination with an acceptance angle  
 magnetic field. I have two options (listed (a)  
 using wide-angle focusing devices with the static  
 focus the consequent system, the practically ex-  
 less of the practical technical difficulties.

desired scale of fields and currents without sig-  
 increase the parameters of such systems in the in-  
 highest currents (up to 100 kG) and the tube  
 lower field techniques (2-100 kG) and the tube  
 magnetic development of the single magnetic mag-  
 details of the focusing device to show that the  
 their the detailed description of some technical  
 required for the concrete construction. We have  
 required. The parameters can be determined and di-  
 elements of the system (a) and a current of the  
 element of such systems. We considered the limit  
 construction of a group device of one possible  
 vector was shown in the paper. The described  
 field all low-current flows produced in the con-  
 line of the focusing device that can collect elec-  
 tron.

**2. Conclusions**

for operation conditions  
 namely, the most part of an area with the par-  
 will be necessary to have a special chamber to  
 for the convergence of not elongated in this case, so it  
 grid region and neutral fluxes. A local shield at  
 them will be difficult, especially, because of sev-  
 tion will the beam path in the focus of the sta-  
 in the case of the beam convergence in oblat-  
 device.

chromatic aberration of the lens for extended  
 section convergence. This is connected with the  
 that spectrum of beam is more wide than for the  
 it should be noted that in this case the magnetic

of the lens for extended section convergence  
 that spectrum of beam is more wide than for the  
 it should be noted that in this case the magnetic

H. A. Tikhonov and E. D. Zhurav, *Izv. Vuzov, Radiofizika*, 1968, 11, No. 1, p. 10.

E. K. Maslov, D. E. Naglo, B. B. Fedina, W. V. Serebrennikov, *Izv. Vuzov, Radiofizika*, 1968, 11, No. 1, p. 10.

D. E. K. Kostin, B. M. Dost, B. V. Gerasimov, E. V. Kozlov, *Izv. Vuzov, Radiofizika*, 1968, 11, No. 1, p. 10.

Sov. J. Tech. Phys., 1968, 38, No. 1, p. 10.

B. E. Maslov, A. V. Jilin, A. M. Petrov and G. I. Zhurav, *Izv. Vuzov, Radiofizika*, 1968, 11, No. 1, p. 10.

I. M. Gerasimov, *Izv. Vuzov, Radiofizika*, 1968, 11, No. 1, p. 10.

D. E. Kozlov, B. M. Dost, B. V. Gerasimov, E. V. Kozlov, *Izv. Vuzov, Radiofizika*, 1968, 11, No. 1, p. 10.

G. I. Zhurav, A. M. Petrov and G. I. Zhurav, *Izv. Vuzov, Radiofizika*, 1968, 11, No. 1, p. 10.

I. V. Maslov, A. V. Jilin, A. M. Petrov and G. I. Zhurav, *Izv. Vuzov, Radiofizika*, 1968, 11, No. 1, p. 10.

G. I. Zhurav, A. M. Petrov and G. I. Zhurav, *Izv. Vuzov, Radiofizika*, 1968, 11, No. 1, p. 10.

I. V. Maslov, A. V. Jilin, A. M. Petrov and G. I. Zhurav, *Izv. Vuzov, Radiofizika*, 1968, 11, No. 1, p. 10.

G. I. Zhurav, A. M. Petrov and G. I. Zhurav, *Izv. Vuzov, Radiofizika*, 1968, 11, No. 1, p. 10.

I. V. Maslov, A. V. Jilin, A. M. Petrov and G. I. Zhurav, *Izv. Vuzov, Radiofizika*, 1968, 11, No. 1, p. 10.

G. I. Zhurav, A. M. Petrov and G. I. Zhurav, *Izv. Vuzov, Radiofizika*, 1968, 11, No. 1, p. 10.

I. V. Maslov, A. V. Jilin, A. M. Petrov and G. I. Zhurav, *Izv. Vuzov, Radiofizika*, 1968, 11, No. 1, p. 10.

G. I. Zhurav, A. M. Petrov and G. I. Zhurav, *Izv. Vuzov, Radiofizika*, 1968, 11, No. 1, p. 10.

I. V. Maslov, A. V. Jilin, A. M. Petrov and G. I. Zhurav, *Izv. Vuzov, Radiofizika*, 1968, 11, No. 1, p. 10.

G. I. Zhurav, A. M. Petrov and G. I. Zhurav, *Izv. Vuzov, Radiofizika*, 1968, 11, No. 1, p. 10.

I. V. Maslov, A. V. Jilin, A. M. Petrov and G. I. Zhurav, *Izv. Vuzov, Radiofizika*, 1968, 11, No. 1, p. 10.

G. I. Zhurav, A. M. Petrov and G. I. Zhurav, *Izv. Vuzov, Radiofizika*, 1968, 11, No. 1, p. 10.

I. V. Maslov, A. V. Jilin, A. M. Petrov and G. I. Zhurav, *Izv. Vuzov, Radiofizika*, 1968, 11, No. 1, p. 10.

G. I. Zhurav, A. M. Petrov and G. I. Zhurav, *Izv. Vuzov, Radiofizika*, 1968, 11, No. 1, p. 10.

I. V. Maslov, A. V. Jilin, A. M. Petrov and G. I. Zhurav, *Izv. Vuzov, Radiofizika*, 1968, 11, No. 1, p. 10.

G. I. Zhurav, A. M. Petrov and G. I. Zhurav, *Izv. Vuzov, Radiofizika*, 1968, 11, No. 1, p. 10.

I. V. Maslov, A. V. Jilin, A. M. Petrov and G. I. Zhurav, *Izv. Vuzov, Radiofizika*, 1968, 11, No. 1, p. 10.

G. I. Zhurav, A. M. Petrov and G. I. Zhurav, *Izv. Vuzov, Radiofizika*, 1968, 11, No. 1, p. 10.

I. V. Maslov, A. V. Jilin, A. M. Petrov and G. I. Zhurav, *Izv. Vuzov, Radiofizika*, 1968, 11, No. 1, p. 10.

G. I. Zhurav, A. M. Petrov and G. I. Zhurav, *Izv. Vuzov, Radiofizika*, 1968, 11, No. 1, p. 10.

I. V. Maslov, A. V. Jilin, A. M. Petrov and G. I. Zhurav, *Izv. Vuzov, Radiofizika*, 1968, 11, No. 1, p. 10.

G. I. Zhurav, A. M. Petrov and G. I. Zhurav, *Izv. Vuzov, Radiofizika*, 1968, 11, No. 1, p. 10.

I. V. Maslov, A. V. Jilin, A. M. Petrov and G. I. Zhurav, *Izv. Vuzov, Radiofizika*, 1968, 11, No. 1, p. 10.

G. I. Zhurav, A. M. Petrov and G. I. Zhurav, *Izv. Vuzov, Radiofizika*, 1968, 11, No. 1, p. 10.

I. V. Maslov, A. V. Jilin, A. M. Petrov and G. I. Zhurav, *Izv. Vuzov, Radiofizika*, 1968, 11, No. 1, p. 10.

The employment of lithium lenses for antiproton collection has confirmed their high efficiency and the present antiproton target stations at FNAL and CERN are running on the basis of 2-cm-diam lenses working at magnetic fields roughly equal to 100 kOe [1, 2]. The current problem of the progress to the technology of lithium lenses is further extension of the range of their parameters: diameter up to 4-6 cm, frequency of the running cycle and ultimate magnetic field over 100 kOe. The analysis of heat removal regimes [3] and the stresses caused by thermal expansion of lithium [4] shows that when designing large-diameter lenses it is not advisable to merely enlarge the sizes, but it is necessary to search for the basically new designs. In the existing designs the heat is removed from the operating volume of a lens through a thin envelope confining a lithium cylinder and made from a material with low thermal conductivity—titanium or stainless steel, and the water passes over its outer surface. The time of heat removal, as a function of the envelope thickness  $\Delta$  and its radius  $r_0$ , may be estimated as  $\tau \approx \frac{\Delta r_0 c \gamma}{\lambda_{en}}$  where  $c$  and  $\gamma$  are the heat capacity of lithium and its density respectively, and  $\lambda_{en}$  is the thermal conductivity of the envelope. Simultaneously, the full energy released in the lithium volume grows as  $r_0^3$  because in addition to an increase of the lithium volume with increasing the radius, the duration of the current supplying the lens must increase also as  $r_0^3$  to conserve the ratio  $\sigma/r_0$  ( $\sigma$  is the thickness of the skin-layer) determining the degree of homogeneity of the current density; as a result, the lens cooling becomes a serious problem. At the same time, the maximum pressure in the lens, limiting the allowable magnetic field, is defined as

$$P_{max} = \frac{\alpha T}{\chi_L V_0 + \frac{2}{E_{en}} \Delta}$$

where  $T$  is the temperature of pulse heating proportional to  $H^2$ ,  $\alpha$  is coefficient of thermal expansion of lithium,  $\chi_L$  is its compressibility,  $E_{en}$  is the modulus of elasticity of the envelope,  $V_0$ —the total

the plastic deformation in solid lithium. At comparatively short cooling time this leads to a reduction of the pressure in the operating part of the lens below the initial level. For the pulse intervals shorter than the relaxation time, this can result to tear away of lithium from the wall and in violating the cooling conditions for the lens.

A cardinal change in the operational mode of the lens is the transition to the designs capable of working with liquid lithium which is pumped through the working volume of the lens and a heat exchanger. In this case, the pulse repetition frequency determined only by the time of lithium exchange in the lens, i. e. it will have no restrictions of principle. The amplitude of the pressure pulses will decrease substantially both due to bigger liquid lithium compressibility by a factor of about 5 and to the possibility to use effectively the large «buffer» volumes at the relaxation times in liquid lithium which are determined only the sound propagation in the system. When advancing the technology of liquid-lithium lenses we developed simultaneously two directions: the creation of small lenses at a pulse repetition frequency in hundreds of Hz for application to positron sources of linear accelerators the major problem for which is to remove the power in several kilowatts released in a volume of about 1 cm<sup>3</sup>, and the creating of large ones (4 cm and more in diameter) for an energy release in several tens of kilojoules [5, 6]. The development of the new lenses necessitates to eliminate the air-tight joints from the lithium volume for its reliability under high-temperature conditions and to create all-welded constructions. Below we will consider one of the recent designs of a 4-cm-diam lens satisfying the requirements for the operation at high radiation levels.

The lens (Fig. 1) is all-welded and much simpler in design owing to the absence of water cooling. The wall thickness of central tube 4, determining the cooling time in the former designs, is limited only by a permissible shunting of the current and can be increased, for the sake of reliability, up to several millimetres at the expense of a certain complication of the power supply system.

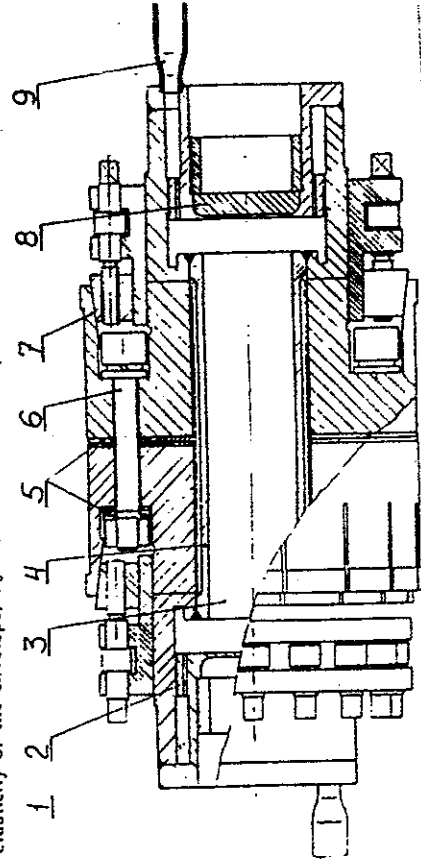


Fig. 1. Longitudinal section of the lens with circulating liquid lithium:

- 1—buffer volumes; 2—supply channels; 3—operating lithium volume; 4—thin-wall envelope of the operating lithium volume; 5—oxidized titanium insulators; 6—retaining bolts; 7—collet contacts; 8—beryllium windows; 9—supply tubes for liquid lithium.

The central tube is welded to the side cups soldered in turn to

In this design each primary turn is the section of toroidal lines, i.e. the rods passing in the axial direction through cylindrical

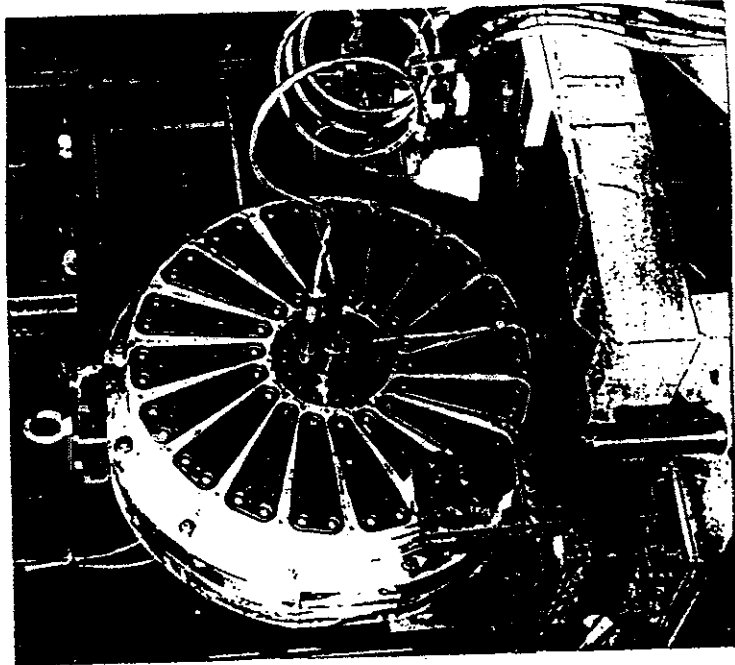


Fig. 3. Photograph of the lens-transformer and liquid lithium system.

holes in the body of the secondary turn; these are placed by one on the inner diameter and by two on the outlet. The rods are linked in the radial direction by flat wedge-like connectors being in the radial grooves on the faces of the secondary turn. The transformer faces are spanned by circular copper covers so that the equal gaps are formed above the planes of the wedge-like connectors, thus ensuring the equality of the magnetic fields on their surfaces and the complete winding balance. The collet clamps connect the cylindrical sections of the winding to the flat connectors. Each collet rests on ceramic insulators inserted into the cylindrical matches in the bottom of the body of the secondary turn, so that each turn proves to be aligned at several points on the ceramic insulators. The 3 mm air gaps being exactly filled. Such a transformer, the cross section of iron 180 cm<sup>2</sup> provides a current of 1 MA for a pulse duration of 3 ms. In this case, the induction inside steel core can achieve 3 T by its reversal of magnetization. It is the regime we obtained in our tests of a 3.6-cm-diam lens with solid lithium designed and manufactured in CERN. In service tests this lens carried half a million of pulses at 0.8 MA current. The largest toroidal lens of 4 cm diameter, manufactured at the ISEP, was tested at pulse duration of 1 ms.

Since the lens is a load with low Q factor when its powering by unipolar current pulses from the discharge of a bank of capacitors the back edge of the pulse turns out to be longer than that from front one so that the energy is mainly released in the lens after

because it makes it possible to create and control a preliminary pressure (0.30 atm) which guarantees the absence of any hollows; these can appear at lithium melting and hardening. It is a bellows with a welded bottom, which is filled with lithium and connected to the system. The bellows is placed in an air-tight cylinder filled with a gallium-indium alloy and connected in turn by a thin tube with a manometer and a piston pump.

The first experiments with liquid-lithium lenses of large diameter have shown that the basic problem is the shock waves in lithium arising in it at pulse heating and, as consequence, the units of the lithium circulation system should be reinforced additionally. Note that this determines the serviceability of the system as a whole. In this case, the whole lithium system serves as a buffer for lens operation. The holes of small diameter 2 at the lens faces through which lithium flows to its working volume attenuate these shocks partly. However, the cardinal solution is the mounting of locking valves at the exit and entrance of the lens which divide the lens volume from the whole system at the moment of a working pulse. The device is demonstrated in Fig. 2. Its massive central steel core 3 is in lower position between the working cycles thus allowing lithium to flow freely in the contour. Before triggering of the lens, the winding of the valve 2 is powered and the core is lifted to the upper position and switched to the circulation of lithium off. After a working cycle the valve winding ceases to be powered and the core sinks on the bottom of the body due to its own weight so that lithium continues to circulate.

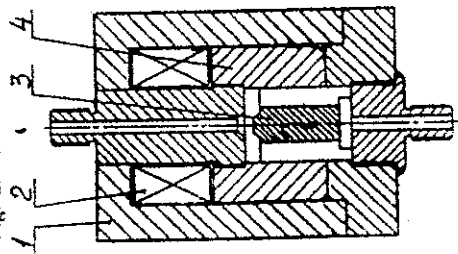


Fig. 2. Locking valve: 1—magnetic core; 2—coil; 3—steel core; 4—stainless steel cylinder.

As the lens diameter increases (>4 cm) the current necessary for its powering seems to be roughly equal to 1 MA and more and for the pulse duration increasing proportionally to  $t_0$  and equal to 0.1 ms, the power supply for the lens becomes rather a complicated problem. Note that as far as the power supply is concerned, there is one more advantage of liquid lithium, it offers the possibility of working at considerably shorter current pulses—in the ratio of the resistivity of liquid lithium to that of solid one  $\rho/\rho_s \approx 3-4$  for the same requirements to the field linearity, i.e. to the quantity  $\sigma/\tau_0$ . At the same energy release in the working section of the lens the ohmic losses in its current lines, transformer and the units of the pulse generator, usually equal to a half of the total energy release, will be correspondingly  $\rho/\rho_s$  times less.

The lens is a low-inductive load with  $L \approx 40$  nH and  $R \approx 5 \cdot 10^{-3} \Omega$ . It is powered by means of matching transformer, designed such that it has low scattering inductance with ceramic insulators, the latter determines its high radiation resistance. The transformation ratio is taken equal to 10-20, so that the load matches with minimal losses to a current feeder and the voltages in the radiation zone do not exceed 1-1.5 kV. The second transformer of conventional design with the coefficient 2-4 is assumed to be placed behind the radiation shielding for further matching with the pulse generator and for reducing the current being commuted down to several tens of kiloamperes; it is simply achieved

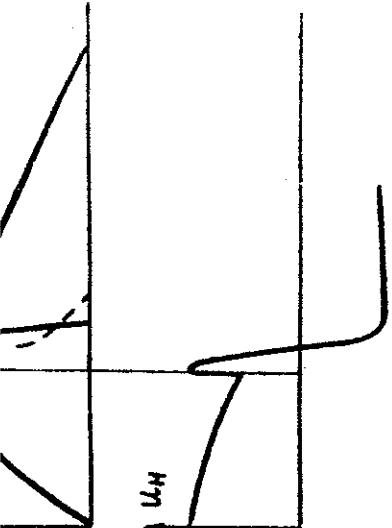
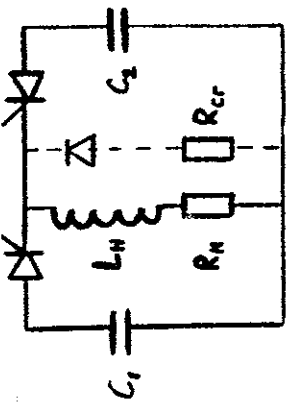


Fig. 4. Principal scheme of the pulse generator.

back front of the pulse becomes shorter the ratio  $(C_1/C_2)^{1/2}$ . This is achieved at the expense of the complication of the generator scheme since the requirements for the commutators  $T_1$  and  $T_2$  become considerably more stringent.  $T_1$  has to provide a minimal time of switching on, which determines the admissible rate of cut the back front of pulse, i. e. the quantity  $C_2$  and the maximum rate of increase of the direct voltage, while  $T_2$  is responsible for the maximum possible value of the derivative of the current increasing to the amplitude one for  $10-20 \mu s$  determined by the spurious parameters of the scheme. Modern thyristors satisfy these requirements and are capable of providing the formation of the back edge in several hundreds of  $\mu s$ . The dotted line shows a modification of this scheme which is more preferable from the point of view of the minimization of the energy release if the voltage, at which the capacitance  $C_2$  reverses its polarity, is the same.

Such a scheme was applied to the generator powering the liquid lithium lens at a current up to 0.6 MA.

References

1. G. Dugan. «P-bar Production and Collection of the FNAL Antiproton Sources». — XIII Intern. Conf. on High Energy Accelerators, Novosibirsk, 1986, v.2, p.264.
2. R. Bellone. et al. «The Results of Prototype Tests and Temperature and Field Computations of the CERN Lithium Lens». — XIII Intern. Conf. on High Energy Accelerators, Novosibirsk, 1986, v.2, p.272.
3. T.A. Vaevolozhskaya and G.J. Silvestrov. «Thermal Regime of Cylindrical Lenses». — Preprint INP 84-100, Novosibirsk, 1984.
4. B.F. Bayanov et al. «The Investigation and Design Development of Lithium Lenses with Large Operating Lithium Volume». — Proc. of 12-th Intern. Conf. on High Energy Accelerators, Fermilab, August 11-16, 1983, p.587.
5. B.F. Bayanov et al. «Multi-Hertz Conic Lenses with Liquid Lithium for the Focusing of Low-Energy Positrons». — Proc. of the 9-th National Accelerator Conf., Dubna, 1984, v.1, p.406.
6. B.F. Bayanov et al. «Cylindrical Large-Diameter Lenses with Liquid Lithium». — Proc. of the 9-th National Accelerator Conf., Dubna, 1984, v.1, p.402.





ИНСТИТУТ ЯДЕРНОЙ ФИЗИКИ СО АН С

G.I. Silvestrov

**PROBLEMS OF INTENSE SECONDARY  
PARTICLE BEAMS PRODUCTION**

PREPRINT



НОВОСИБИРСК

1986

---

**Institute of Nuclear Physics**

**G.I. Silvestrov**

**PROBLEMS OF INTENSE SECONDARY  
PARTICLE BEAMS PRODUCTION**

**PREPRINT 86-163**

**NOVOSIBIRSK  
1986**

---

Problems of Intense Secondary Particle  
Beams Production<sup>1)</sup>  
G.I. Silvestrov

ABSTRACT

Discussed are the production problems of intense beams of secondary particles: positrons, antiprotons,  $\pi$ - and  $K$ -mesons (to form the neutrino beams). Among these are the problems to provide the optimal focusing onto the target for primary beams and to collect the secondaries within a solid angle close to the production angle. At present the most effective methods for such a focusing are strong-focusing lenses based on solid and liquid lithium. Considered are the designs for the pumping of liquid lithium through the lenses which are intended for positron collection in a storage ring accelerator operating at a high repetition rate, as well as the parameters and the specialities of large diameter lenses used to collect the antiproton target particles. New problems dealing with the formation of neutrino parent beams at TeV-range accelerators (Fermilab, UNC) and the designs of large-diameter solid and liquid-lithium lenses intended for this purpose are considered as well.

The important problem one faces by the work with intense primary beam are the heat removal and the protection of the target against the thermal failure at high densities of energy release. To solve the problem of heat removal the creating of mobile solid and jet liquid metallic targets is suggested. To eliminate the target failure during the beam spill the scanning of the primary beam on a target, or rapid exchange of the target substance are considered.

In the optics of beams of secondary particles, three problems can be defined for which obtaining of a beam with maximum intensity is most urgent and requires the creation of focusing systems with extremely high magnetic fields. The first problem involves systems of electron-positron conversion in which the need has recently arisen to attain a conversion factor close to unity as, for example, in the projects of the positron source [1] and VLEPP [2] (in the latter case, a high degree of polarization,  $P \approx 0.6$ , of the electron and positron beams is required). The second kind of problem is associated with an effective focusing of antiprotons in the target stations of antiproton storage rings. In this case it is necessary to achieve the maximum brightness of the beam which provides a high phase space density of antiprotons within the limited acceptance of a storage ring. Finally, the most complex focusing apparatus is required for neutrino experiments, the main purpose is to ensure the most effective formation of a beam of neutrino «parents»,  $\pi$  and  $K$ -mesons, in a broad energy range.

In all the above cases the intensity of the primary beam is the determining factor. In view of this, its focusing on a target unavoidably leads to a heavy thermal load of the target, so that the optimization of the secondary beam generation turns out to be directly connected with the thermal target problems.

In the present report we treat a few variants of the solution of these problems, using lithium lenses and utilizing liquid metal in focusing elements and target devices.

<sup>1)</sup> Report presented at the XIII International Conference on High Energy Accelerators, Moscow, August 1966.

## SYSTEMS OF ELECTRON-POSITRON CONVERSION

Conventional scheme of generating intense positron beams using high-energy electrons into low-energy positrons, involves achieving a maximum output from a target, followed by additional acceleration in a linac with an accompanying longitudinal field, the basic problem is an effective quarter-wave transformer of the emittance of a positron beam, i. e. the transformation of a phase ellipse from small coordinate and a large angular spread to a large coordinate and a small angular spread. This is required for its matching to a focusing system accompanying the initial stage of acceleration. We should mention that the system of initial beam focusing must satisfy two conditions: a) to collect the positrons in a maximum angle of about  $\pm 0.6$  rad corresponding to the r.m.s. angle of the target at low energies and b) to transform the beam in a short distance from the target, to avoid an increase in the longitudinal size of the beam, which is due to a large divergence of the beam, for its successful additional acceleration in short-wave sections of a linac with a maximum rate of acceleration. These conditions can be satisfied only in systems with a strong magnetic field; for example, in the SLC project a solenoid with a longitudinal field equal to 6 T at the target and quadrupoles decreasing along the axis for a distance 10 cm. For the primary beam this provides a coefficient of positron collection of about 2, for the acceptance of the damping ring. To solve this problem, it has been proposed to employ, in the VLEPP conversion system, the most effective focusing system with a transverse-symmetric magnetic field — a short lithium lens of length 10 cm long with the gradient  $G=200$  kOe/cm placed directly in front of the conversion target. In the project under discussion the conversion of polarized electrons and positrons with a polarization of about 0.65, and a conversion factor of over unity, is to be performed by impinging, on a target, the polarized electron beam produced in a helical undulator of about 150 m long. The energy of the electron beam (positrons) with an energy of 20 MeV passes through this undulator and deflects from the target. After the target, the spectrum of positrons is cut off at 20 MeV and the appropriate angle of multiple scattering in a scattering substance,  $\sim 5 \cdot 10^{-2}$  rad, does not lead to a substantial increase in the beam emittance. The analysis in Ref. [3] of the aberration properties and the scattering shows that

similar lithium lenses can be efficiently used for the transformation of the beam emittances directly near the target within the 10–20 MeV range (corresponding to a high phase density of positrons) at collection angles up to 0.6 rad, unattainable in a linac with a longitudinal field.

To extend the possibilities of applying similar systems in electron sources of linear accelerators whose repetition rate reaches hundred Hz, we have solved the problem of heat removal from the lens by using liquid lithium pumped through it as a heat conductor. With a view to creating liquid lithium lenses operating in the real conditions of an accelerating installation has been initiated on the creation of a conversion system for a positron source of the Kharkov linear accelerator LUE-2. In this case, a 250 MeV primary electron beam at a frequency of 100 Hz and a cone-shaped lens has been used. For the same operating characteristics this allows the decrease of the current amplitude and the average released energy by a factor of 1.5 (Fig. 1) [3].

At an intensity of the LUE-2 electron beam of about  $10^{14}$  electrons per second, the pulse heating of the target is insignificant. To remove an average power of about 0.5 kW the target is cooled directly in the inner volume of the lens and is cooled by liquid lithium. The flow of lithium reaches symmetrically the operating volume of the lens, from the toroidal volumes on its faces. Liquid lithium circulates in a closed circuit consisting of the lens operating volume, two long tubes connected to it at one end to this volume and at the other end, to the electromagnetic pump outside the vacuum chamber. Current is supplied to the lens by a flat three-conductor line transforming into coaxial cylinders at the place of entrance into the vacuum chamber. Here there is a bellows connection, the lens is to be shifted in the transverse direction. The non-vacuum part of the lithium circuit, including the pump, is located on a movable plate connected to the current input. It is supplied by current pulses of 50  $\mu$ s duration with an amplitude up to 60 kA from a matching transformer located on the surface of the vacuum chamber. The initial heating of the lithium circuit is performed by a separate heating system. With the lithium melted in the whole volume it starts circulating, and at a frequency of 100 Hz and at the current the power of about 1 kW released in the operating volume of the lens is uniformly distributed throughout the system. An equilibrium temperature of about 230°C is established.

The construction is radiation resistant, the insulators are covered with ceramic and insulating oxide coatings.

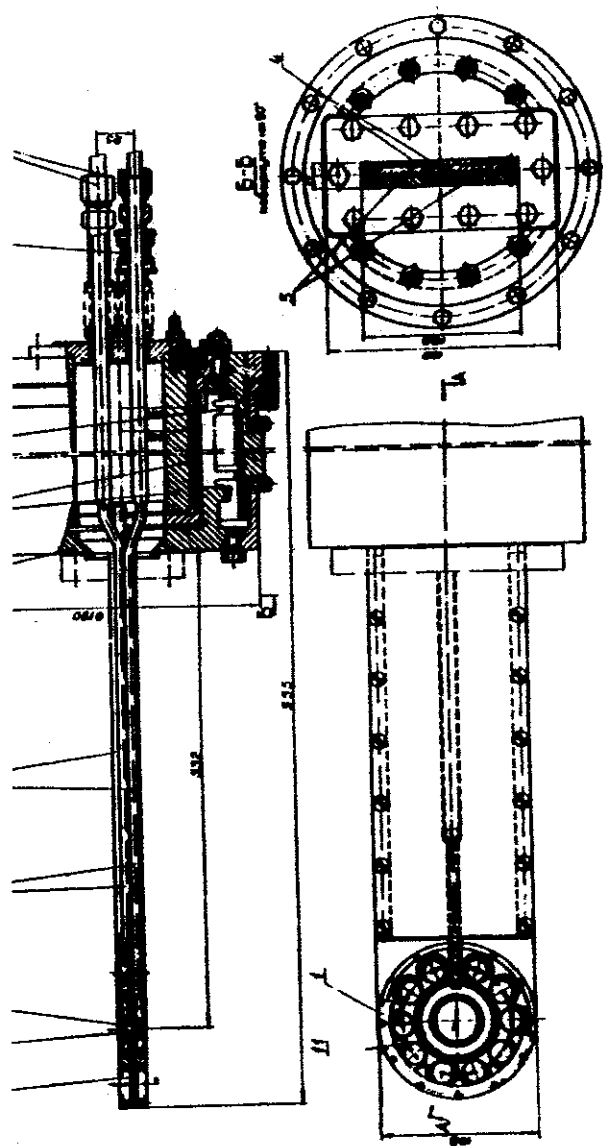


Fig. 1. A lens with liquid lithium:  
 1—cams of contact clamps; 2—conic lens; 3—W target; 4—titanium tubes for lithium supply; 5—flat current input; 6—vacuum chamber; 7—crossial section of the current input; 8—bellows; 9—ceramic insulators; 10—conic sealings; 11—case of eccentric clamps.

In the VLEPP conversion system the thermal regime of the target is determined by the specific features of the generation of a pure beam of  $\gamma$ -quanta, for which the density of energy grows practically linearly with the longitudinal coordinate of the target. Computer simulation [4] shows that with the following parameters: 150 GeV energy of the primary beam, 150-cm-lens with  $\lambda=0.7$  cm and  $P_1^2=0.1$ , the density of secondaries at the exit of a W target of 0.5 radiation length optical thickness constitutes about 5 pairs in the whole spectrum in a circle of 0.5 mm radius per one in the primary beam. At  $10^{12}$  pairs per pulse in the primary beam and at a frequency of 10 Hz of the pulse power, released in the target, is 50 W, while the energy of the exit achieves  $q=400$  J/g and the temperature is 500°C during one pulse; this exceeds the magnitude permissible for the operation of the target. The first step in the solution of the problem is to eliminate the possibility of multiple arrival of the beam at one place by shifting the target. In this case, the target can be made, for example, in the form of a disc. A similar solution of the rotating target with intense water cooling has been used for the SLC positron source, thereby solving the problem of a large (about 5 kW) average power, by spilling the beam onto the target.

We have another engineering solution. In our variant the target is cooled by liquid metal, the gallium-indium alloy, and it is not only a heat-transfer agent but it sets in rotation. The target is a freely-rotating disk about 50 mm diameter (Fig. 1). The target chamber is mounted on the input side of the lens; the target exit is at a distance of 1–2 mm from its edge. It is in the vacuum chamber with the lens and is connected to a vacuum pump through a long transport tube, the pump being connected to a vacuum system. If the target exit surface is destroyed during operation or from a single pulse (which will unavoidably occur with increasing energy of the primary beam), it is possible to change, without change of the construction, to a variant with the use of a liquid-metallic jet target (for example, a mercury target). In this case, the danger consists in splashes can be formed on the free exit mercury surface. These splashes may bombard the wall of the lens which contains the liquid-lithium volume. To prevent this, there are a protection titanium disk of about 0.3 mm thickness between the jet and the lens face, which is set into rotation with the mercury jet itself.

## 2. OBTAINING INTENSE ANTIPROTON BEAMS

Among the major problems concerning effective production of antiprotons for injection into storage rings, there are the focusing of the primary beam on a target, and the efficient collection of antiprotons up to angles close to the maximum product. The most effective optical systems for such problems are cylindrical lenses. The technology of their manufacture was developed at the INP in the late 70's and is being applied successfully at accelerator centres FNAL (USA) and CERN, where similar systems have been created for their application to antiproton targets of the Tevatron-I and AA-ACOL facilities.

The main characteristics of the lenses, which determine the efficiency of the collection of particles of r.m.s. product:

$$\langle \theta^2 \rangle = \frac{2mm_e c^2}{p^2} \approx \frac{\langle P_{\perp} \rangle^2}{p^2}, \text{ i. e. with transverse momentum}$$

$R_{\perp} \approx 0.5 \text{ GeV}/c$  for antiprotons, is the field integral over the length of a boundary particle, which gives the bending

$$\alpha_c = \frac{300}{p} \int_0^l H(l) dl. \text{ With the r.m.s. angle of collection } \alpha_c = \gamma$$

maximum field integral at the aperture boundary is

$$H_{\max} \cdot l = \frac{p_{\perp}}{300} = 1.7 \cdot 10^6 \text{ Oe cm, irrespective of the total energy of antiprotons.}$$

Since the storage ring acceptance,  $\epsilon_{st}$ , is somewhat smaller than the r.m.s. emittance of the antiproton beam,  $\epsilon_{st} < \epsilon_c$ ,

( $Z$  is the length of the target) and the optimal angle of collection into the acceptance  $\epsilon_{st}$  is equal to  $\alpha_c = 1.65 \left( \frac{\epsilon_{st} \langle \theta^2 \rangle}{\lambda_t} \right)^{1/4} \leq \gamma$

is the length of nuclear absorption of the target material) characteristic parameters of the lens will be  $H_{\max} \approx 10$

$l \approx 15 \text{ cm} \ll \lambda_t$ , for any energy of antiprotons. For the FNAL at  $P_p = 8.9 \text{ GeV}/c$  and  $\epsilon_{st} = 20 \pi \text{ mm} \cdot \text{mrad}$ , a lens with such parameters and aperture  $R = 1 \text{ cm}$  have an optimal angle of

$\alpha_c = 0.046 \text{ rad}$  ( $\sqrt{\langle \theta^2 \rangle} = 0.057$ ) and the total field integral  $F = R/\alpha_c = 22 \text{ cm}$ , while a lens for the CERN project

$\epsilon_{st} = 200 \pi \text{ mm} \cdot \text{mrad}$   $\alpha_c = 0.134$  ( $\sqrt{\langle \theta^2 \rangle} = 0.145$ ) and  $F = 7 \text{ cm}$   $P_p = 3.5 \text{ GeV}/c$ , i. e. in this case the source (target output) should be placed either near the entrance face of the lens, or

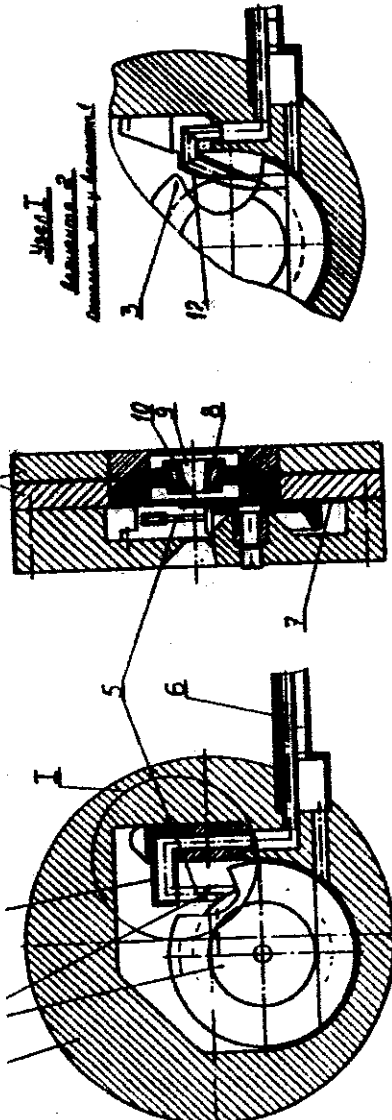


Fig. 2. Target of the VLEPP conversion system: variant 1: mercury jet; variant 2: tungsten disk;

- 1—body; 2—disk; 3—beam axis; 4—drain nozzle; 5—mercury jet target; 6—supply tubes; 7—guard titanium disk; 8—body of a lithium lens; 9—operating lithium volume; 10—entrance flange of the lens; 11—current input; 12—drain nozzle for the gallium jet.

a large aperture with the same field on its surface. or technical problems associated with the creation of re-diameter lenses with  $\sim 100$  kOe fields consists in the the pressure from the thermal expansion of lithium, ng to considerable stresses in the thin-wall envelope, and z adequate heat removal from lithium. At present there hods in manufacturing the lenses under discussion, from ion point of view. The lenses manufactured at the INP are elastic systems (Fig. 3a) where lithium in the art of the lens is limited by a thin-wall titanium cylinder

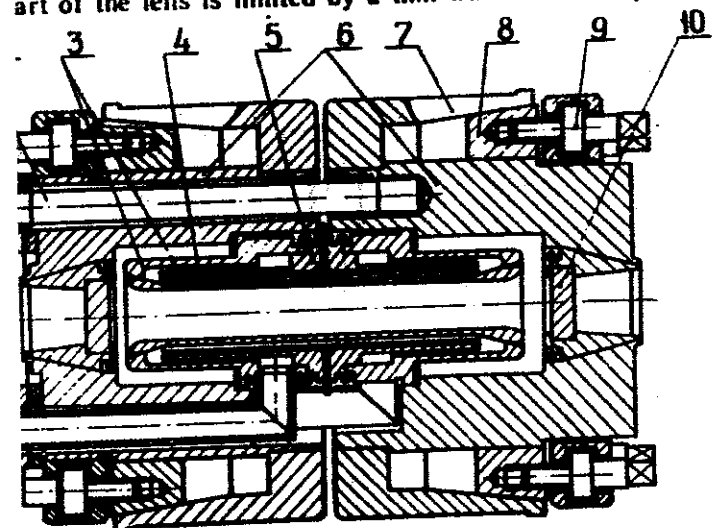


Fig. 3a. Lens with elastic wall:

1—water supply; 2—retaining bolts; 3—titanium body of the lens; 4—distribution pipes of the lens; 5—flanges of the distribution pipes; 6—steel body of the lens; 7—collet contact; 8—conic clamps; 9—bolts; 10—beryllium windows.

outer water-cooled surface. With increasing the lithium ring the pulse heating, the envelope expansion and the compressibility in the non-heated parts result in a decrease of stress in the system, while the stress in the envelope walls is as [5]:

$$\sigma = \frac{\alpha T}{\chi} \left( 1 + \frac{V_0}{V_1} \right) + \frac{2}{E_t}$$

Here  $\alpha$  is the factor of volumetric expansion of lithium,  $\chi$ —compressibility,  $\Delta$ —the wall thickness,  $R$ —the cylinder radius,  $E_t$ —modulus of titanium elasticity,  $V_1$ —the operating lithium volume being heated,  $V_0$ —the non-heated section of the lithium volume, current feeds, which is subjected to the pressure from the part of the lens. In the CERN lenses (Fig. 3b), the stai

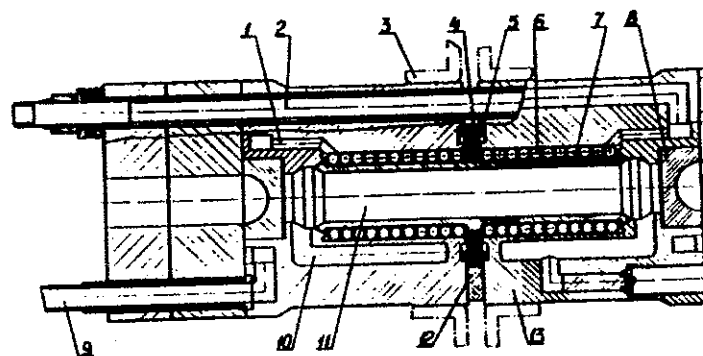


Fig. 3b. CERN lens:

1—water supply; 2—retaining bolts; 3—current input; 4—sealed insulator; 5—steel balls; 6—steel body of the lens; 7—titanium windows; 8—water supply tubes; 9—conic clamps; 10—beryllium windows; 11—operating lithium volumes; 12—insulator

envelope of the lithium is supported by a large number of balls. This lens is a rigid construction capable of withstanding maximum pressure close to  $p = \frac{\alpha}{\chi} T$ , in the given case; at  $p = 1200$  atm at  $T = 60^\circ$ .

With sufficiently durable construction, it will be reliable for lenses of large diameter, 4–6 cm, the development of such systems seems more promising. On this path the cardinal transition to the constructions with liquid lithium, which has a higher compressibility. In systems with flowing lithium the problem of heat removal is solved also, while in lenses with 50–100 kJ energy release this problem turns out to be practically insoluble with the use of water cooling.

The first experiments with the models of liquid-lithium lenses of large, 2–3 cm diameter, were performed in Novosibirsk and demonstrated that the main problems determining

of the system are associated with fluid shocks arising from pulse heating. This requires a proper strengthening of the elements: a pump, a heat exchanger and transport tubes. Figure 3c shows the working variant of a 4-cm-diameter lens under this construction we plan to test the system with stop valves located at the entrances to the buffer volumes (1). The latter is connected to the operating volume of the lens by the distribution

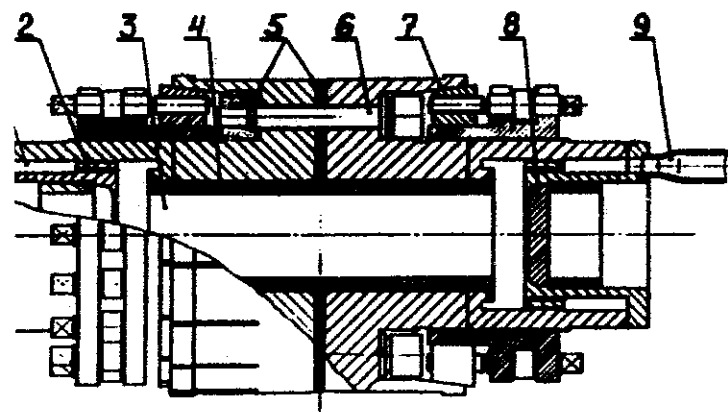


Fig. 3c. A lens with liquid lithium:

1—stop valves; 2—supply channels; 3—operating lithium volume; 4—thin-wall envelope of lithium volume; 5—oxidized titanium insulators; 6—retaining bolts; 7—collet contacts; 8—beryllium windows; 9—supply tubes for liquid lithium.

(2) and this is assumed to reduce the pulse pressure transmitted through the pumping system of the lithium. The lens power is provided through a toroidal matching transformer with radiation-resistant insulators and is intended for work with about 3 ms current pulses and with an amplitude up to 1 MA. The lens is cooled with a pump which is assumed to be placed behind the lens with shielding, using transfer tubes of about 4 m long. The purpose of studying stresses in the lens as well as the apparatus is to solve the technological problems associated with liquid lithium can be found in [5, 6].

The optimization of the focusing of a proton beam onto a target corresponds to obtaining its size  $r_p$ , smaller than the effective size of the proton source (which is determined by the target length  $l$ )

and the production angles as  $\sqrt{\langle r_p^2 \rangle} = \frac{z_0}{2\sqrt{3}}$ , under the

condition on the proton beam radius  $r_p^2 \ll \frac{8}{3} \frac{\epsilon_{eff}^2}{\langle \theta^2 \rangle}$ , for beam cap- ture the acceptance  $\epsilon_{eff}$  less than the effective emittance of the ions [7].

As the energy of antiprotons grows, the necessary proton beam size decreases down to fractions of a millimeter. For example, for Tevatron-I with  $P_p = 8.9 \text{ GeV/c}$  and  $\epsilon_{eff} = 2 \text{ mm}$  the optimal size of the beam has  $r_p \leq 0.2 \text{ mm}$ . At the peak intensity  $2 \cdot 10^{12} \text{ pp}$  the density of energy release will be  $0.8 \text{ kJ/g}$ . For a W target this corresponds to heating up and its destruction during one pulse. At highest densities of energy release which are expected, for example, in the targets of an antiproton source, in the variant under discussion corresponds to the generation of 15 GeV antiprotons by the 600 GeV proton source. A principal limitation in the work with small-size beams is the «massdepleting» of the target substance from the beam spot. A time considerably shorter than the time of its passage through the target surface is likely to be the only possibility for scanning the target surface to reduce the local energy release without a loss in phase space of the antiprotons. Such a scanning reduces the local energy release with an appropriate synchronous shift of the antiproton section of the focusing system. This method has been suggested in [8] and discussed in [9, 10] including versions of optical systems and calculated parameters of the system. At present we have completed the manufacturing of the first variant of the system which consists of four alternating magnets of vertical and horizontal deflection. The magnets are fed by phase-shifted sinusoidal current pulses with a period in order to achieve circular scanning of a 70 C beam, on the target stand of the Institute of High Energy [11] with a spill time of 5  $\mu\text{s}$ . The magnets have the length  $A_x = A_z = 1.6 \text{ cm}$  and, at a field of 20 kOe, provide beam scanning over a circle of 3 mm radius at the focal point of a lens whose focal distance is about 70 cm. The parameters and description of the system can be found in [10]. During the operation various systematic problems will have to be solved. Experiments will be performed to determine the ultimate densities

which do not result in a destruction of a targets during a spill under the scanning conditions. The data obtained provide the basis for the choice of the parameters of the operation of similar systems.

#### FORMATION OF THE BEAMS OF NEUTRINO «PARENTS» FOR NEUTRINO EXPERIMENTS

In consideration of projects of neutrino channels on TeV and the increasing requirements for the parameters of beams, the necessity arises to search for new methods of formation of the beams of neutrino parents. This is associated with the wide range of meson energies, 0.1–1 TeV, the angle of extraction from a target becomes very small ( $\theta \sim \frac{P_t}{P} \approx \frac{0.4}{P(\text{GeV})}$ ), the application of conventional focusing systems such as solenoids and parabolic lenses for their formation proves to be ineffective because of the connecting «neck» and the absence of the near-axis region. This gives rise to reduced particle flux and to generation of a high level of background caused by side-sign particles. Moreover, the growth of the amount of events in a detector necessitates working with millisecond pulses which in turn leads to complicated problems of cooling imposed by thin-wall envelopes, and to problems of stress caused by pulsed thermal expansion. To overcome these problems one can apply cylindrical lithium lenses with a large aperture which should be fed by long, several-millisecond pulses. In particular, a project has been accepted for the formation of neutrino channel for work with 3.6 TeV protons. Its focusing system includes a telescope composed of three lithium lenses with the following parameters:  $\varnothing$  1.8, 3.4 and 6 cm; length  $\sim$  15 cm; magnetic field 60 and 40 kOe; distances to the target of 10, 30 and 60 cm respectively. As has been demonstrated in [12], such lenses make it possible to reduce, by a factor of 2–3, the length of the focusing system in comparison with a similar variant based on parabolic lenses and reduce, by one order of magnitude, the background level. The mode of operation of the UNC is assumed to be the following:  $6 \cdot 10^{14}$  protons stored and their energy increased up to 3.6 TeV; separate portions of the beam, with  $5 \cdot 10^{13}$  particles in

each, will be extracted to the target with the 4 s inter-pulse cycle of extraction will last up to 1 ms. So the lenses will be supplied by current pulses with flat tops of about 1-ms and amplitude of up to 500 kA.

The major problems concerning the creation of lithium lenses with such parameters has been treated above and we will solve them of developing the technology of utilizing liquid lithium pumped through the system.

At the proton beam energy and intensity under consideration the thermal regimes of the targets become complicated and the energy release in them, depending on their substance and geometry, can achieve 100 kJ and higher. Using short-focus and small aperture lithium lenses to collect secondary particles requires a large proton beam on a target, to a small, about 1–2 mm diameter. A strong argument in favour of the work with a small-size target is connected with increasing the number of secondaries emerging from the side of the target which belong to a nuclear-electron cascade developed in it. These particles are responsible for the use of the total energy release; it can be decreased under conditions that as the size of the beam is reduced, a simultaneous increase of the transverse size  $h$  of the target can occur, the ratio  $h = 4\sigma$  being conserved. In the limiting case, at  $\sigma = 0.1$ –0.2 cm, the energy release will be only determined by ionization loss of the beam; the losses due to nuclear excitation of the primary beam are practically energy-irrespective. For example, in a lithium target about 150 cm long the energy release will be reduced to a value lower than 1 kJ. However, as the beam size decreases the energy release density grows fast, and a stationary target is destroyed only in an explosive regime. At a spill time of the order of about 1 ms this problem can be solved by a rapid exchange of the substance in the heating region, that is by using a flat lithium jet crossing the beam axis with a velocity of several kilometers per second, thereby offering simultaneously the possibility of solving the heat removal problem. This possibility has been discussed earlier [13, 14] and at present we start work on its realization.

To do this, an experimental device (Fig. 4) has been developed for a stationary freely-flowing jet of gallium-indium alloy. The jet is 20 cm wide (along the beam axis) and its transverse diameter  $h = 1 \div 2$  mm. The device is assumed to be mounted on a special target stand and we intend to investigate maximum admissible

energy release at which the substance density on the beam is not decrease, with the 76 GeV proton beam, focused to incident on it. This will give information about how many

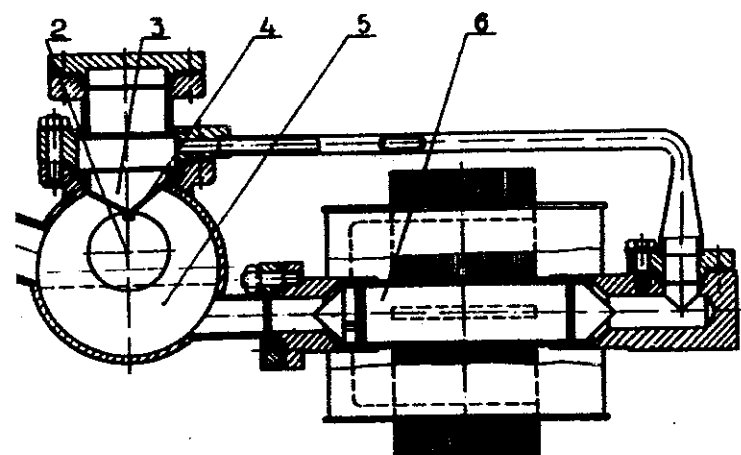


Fig. 4. A stationary jet target:

1—drain hole; 2—beam axis; 3—nozzle of the drain chamber; 4—liquid metal; 5—pump.

The substance should be exchanged in more intense UNC target about the required velocity of a jet. It is more rational to use liquid-metallic jet targets (the jet velocity is about 100 m/s) in pulse mode of operation, using for this purpose the electrostatic method of accelerating a liquid metal. To analyse these possibilities, a device has been designed in which a narrow, ~2-mm gap between two flat current 20-cm-wide conductors is short-circuited by a stationary flow of liquid metal. When passing through the gap under a current pulse of about 2 MA amplitude, the metal will be ejected from the gap under the pressure of the magnetic field whose magnitude is above 100 kOe. Using this device, the parameters of a liquid-metallic jet will be studied and the optimal regimes chosen, which provide the maximum velocity.

#### REFERENCES

1. Bulos F., De Staebler et al. Design of a High Yield Proton Target. SLAC-PUB-3635, April 1985.
2. Chernyakin A.D. et al. Development of the Conversion System for a Proton Beam. —Proc. of the 12th Intern. Conf. on High Energy Acc. Phys. 1985, p.131.
3. Bayanov B.F. et al. Multi-Hertz Conic Lenses with Liquid Lithium for Focusing of Low-Energy Positrons. —Proc. of the National Accelerator Conference, V.1, 1984, p.406.
4. Vsevolozhskaya T.A. et al. Helical Undulator of the VLE System. —Preprint INP 86-129. Novosibirsk, 1986.
5. Bayanov B.F. et al. Study of the Stresses in Cylindrical Lithium Targets. —Development of Their Design. Preprint INP 84-168. Novosibirsk, 1984.
6. Bayanov B.F. et al. The Investigation and Design Development of Targets with Large Operating Lithium Volume. —Proc. of the 12th High Energy Acc. Fermilab, August 11—16, 1983, p.587—591.
7. Vsevolozhskaya T.A. NIM, 190 (1981) 479—486.
8. Krienen F. and Mills F. Spreading the Hot Spot on the Target. —Proc. of the 1980, High Intensity Target Workshop, p.61.
9. Vsevolozhskaya T.A. et al. Scanning of the Proton Beam and the Study of Thermal-Destruction Effects of Targets in the Work with High Intensity Proton Beams. —Proc. of the 8th National Accelerator Conf., Protvino 1982. V.1, p.105.
10. Silvestrov G.I. and Chernyakin A.D. Sweeping—System for the Control of Secondary Beams of High Phase Density. Preprint INP 84-1984.
11. Alferov V.N. et al. A Device for Studying the Targets Irradiated by High Intensity Proton Beam. Preprint IHEP OP 85-132. Serpukhov, 1985.
12. Garkusha V.N. et al. Channel System for ASC Particles. —Proc. of the National Accelerator Conf. V.1, 1984, p.33.
13. Bayanov B.F. et al. Antiproton Target Station on the Basis of a Liquid Metal Jet. —Proc. of the XI Intern. Accelerator Conf., Geneva, CERN, 1980, p.105.
14. Vsevolozhskaya T.A. and Silvestrov G.I. Some Possibilities of Studying the Targets of High Phase Density Beams Using Accelerators with Several-TeV Energy. —Proc. of the National Accelerator Conf., Dubna 1980. V.1, p.105.



**Comments on Polarized Muons**

**Henry A. Thiessen**

**LANL**

At meson factory energies, the only significant source of muons is the decay:

$$\pi^{\pm} \rightarrow \mu^{\pm} + \nu$$

In the center of mass of the pion, the muon is produced with spin parallel (anti parallel) to its direction of motion. If the pion is in flight, the folding of the kinematics results in muons produced backwards in the center-of-mass appearing forwards in the lab. The resultant mixture of muons observed in the lab system then has nearly zero polarization.

To obtain polarized muons, we need to consider pions produced at rest or nearly at rest. Since the kinetic energy of the muon produced in the decay of a stopped pion is about 4 MeV, this necessarily means that we will be looking for very slow muons. This may be an advantage because these muons will have a smaller invariant phase space due to the small initial muon momentum.

It seems to me that it will pay to look at the technology developed at meson factories for producing low energy polarized muons.

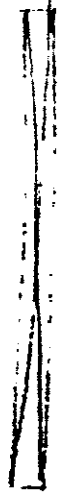
One good example is the so-called "surface" muon beam. In any production target, some pions will be produced that stop near the surface of the pion production target. When these pions decay, they result in a nearly monochromatic beam of 100% polarization. There are two serious difficulties with this approach. First, it works only for  $\pi^+$  ( $\mu^+$ ) as stopping  $\pi^-$  mostly interact before they decay. Second, any time structure of production of pions is washed out by the 26ns lifetime of the pion.

I hope that we at Los Alamos can evaluate some low energy muon sources as candidates for a muon collider. Since the technology is already well developed, we may be able to do this with only a small investment in time.

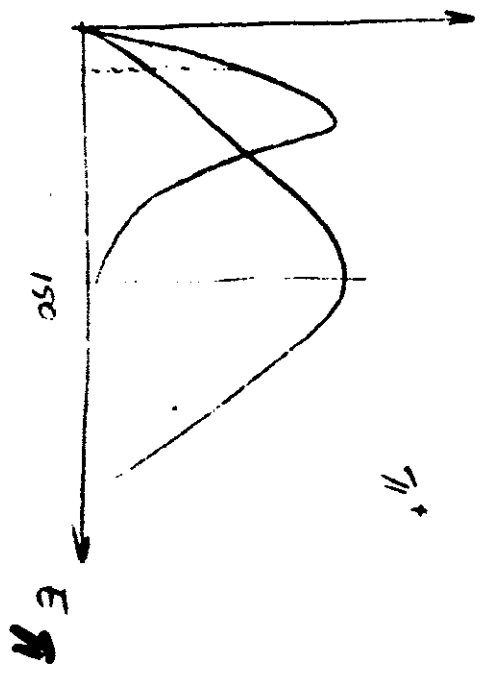
**Muon Source**

**Mikhail Grachev**

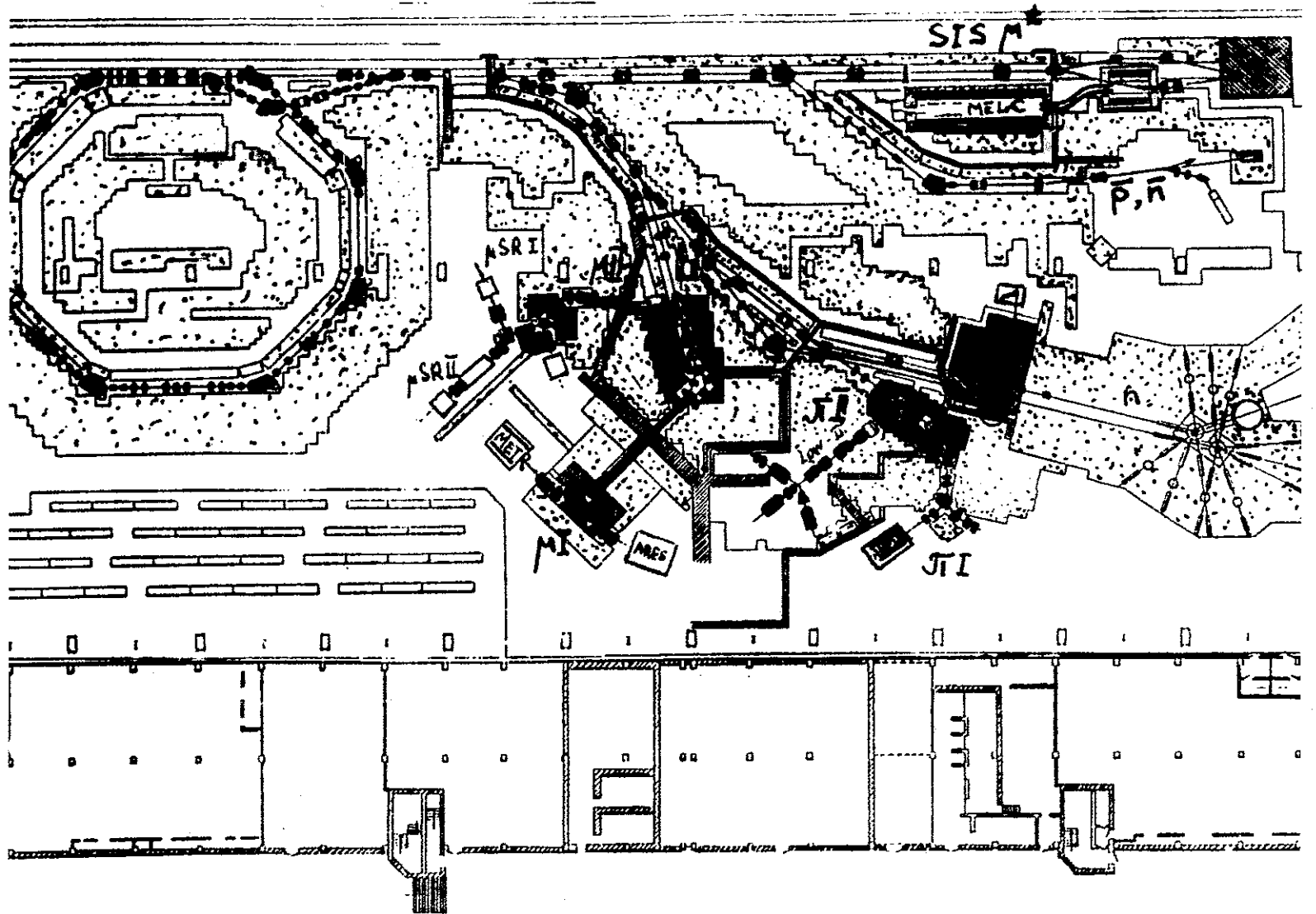
**INR**



$$\begin{aligned}
 I_p &= 100 \mu A \\
 E_p &= 600 \text{ MeV} \\
 \mu^- &= 0.7 \cdot 10^{11} \text{ s}^{-1} \\
 \mu^+ &= 10^{11} \text{ s}^{-1} \\
 E_n &= 1000 \text{ MeV}
 \end{aligned}$$



$$\begin{aligned}
 20 \text{ } \mu\text{m}^2 \\
 1.2 \cdot 10^{-4}
 \end{aligned}$$



Lay-out of the experimental hall of MMF.

